Contributions to the Improvement of Multiuser PLC Home Networks

Pierre Achaichia

N° d'ordre : 2012-17-TH

Thèse

présentée devant
SUPÉLEC

pour obtenir le grade de
Docteur de SUPÉLEC

Spécialité : *Télécommunications*

par

Pierre Achaichia

Équipe d'accueil : Wireless Access System Architecture / Connectivity REsearch and Modeling (WASA/CREM), Orange Labs Rennes & équipe SCEE Supélec, IETR
École doctorale : Mathématiques, Télécommunications, Informatique, Signal, Systèmes Electroniques (MATISSE)
Domaine : STIC

Contributions to the Improvement of Multiuser PLC Home Networks

Soutenue le 12 octobre 2012 devant la commission d'examen composée de :

Dr. Karine Cavalec-Amis	Télécom Bretagne, Brest, France	Examinatrice
Pr. François-Xavier Coudoux	University of Valenciennes, France	Rapporteur
M. Lorenzo Guerrieri	Dora, Aoste, Italie	Examinateur
Dr. Marie Le Bot	Orange Labs, Rennes, France	Encadrante
Pr. Jacques Palicot	Supélec, Rennes, France	Directeur de thèse
Pr. Daniel Roviras	CNAM, Paris, France	President & Rapporteur
Dr. Pierre Siohan	Orange Labs, Rennes, France	Co-directeur de thèse

À Rennes, le 5 novembre 2012.

Au terme de ces trois années passées chez Orange Labs, je tiens tout d'abord à exprimer ma profonde gratitude envers mes encadrants, Pierre Siohan et Marie Le Bot, qui ont largement contribué à la réussite de ces travaux. Leur disponibilité, leurs précieux conseils, et la confiance qu'ils m'ont accordée ont été autant d'éléments moteurs me permettant de traverser sereinement ces trois années, pour en faire une expérience d'une richesse incroyable, tant sur le plan des connaissances acquises que sur le plan humain.

Je tiens également à saluer tous les membres de l'URD CREM qui m'ont entouré, en ayant une pensée particulière pour son manager Jean-Christophe Rault, dont la gentillesse et la flexibilité m'ont permis de rapidement me sentir en confiance dans son équipe. Je tiens à remercier tout particulièrement Pascal Pagani et Philippe Christin pour leur aide.

J'exprime ma grande reconnaissance à mon directeur de thèse, le professeur Jacques Palicot, ainsi qu'à tous les membres de l'équipe SCEE de Supélec, pour l'accueil chaleureux qu'ils m'ont toujours réservé dans leur laboratoire.

Un grand merci également à tous les autres membres de mon jury de thèse: Pr. François-Xavier Coudoux, Pr. Daniel Roviras, Mme Karine Amis et M. Lorenzo Guerrieri.

Je remercie enfin mes parents, qui m'ont toujours encouragé tout au long de mes études en me laissant toujours la liberté de choix, et ma compagne Anne, pour son indéfectible soutien.

Contents

Acknowledgements **i**

Contents **iii**

List of Figures **vii**

List of Tables **xi**

Abstract **xiii**

Résumé **xv**

Acronyms **xvii**

Notations **xxiii**

1 Introduction **1**

2 Broadband Power Line Communications **5**
2.1 Introduction . . . 5
2.2 In-home PLC Environment Characterization . . . 7
2.2.1 PLC Channel Modeling . . . 7
2.2.2 Noise Sources . . . 8
2.3 Regulatory Authorities . . . 9
2.4 Broadband PLC Specifications . . . 10
2.5 Overview of HPAV-based Specifications . . . 12
2.5.1 PLC Network Overview . . . 12
2.5.2 Convergence Layer (CL) . . . 14
2.5.3 MAC Layer . . . 14
2.5.3.1 Channel Access Mechanisms . . . 14
2.5.3.2 Framing Processes . . . 17
2.5.3.3 MPDU Format . . . 20
2.5.4 Physical Layer . . . 21
2.5.4.1 Link Adaptation . . . 21
2.5.4.2 PPDU Format . . . 22
2.6 Conclusion . . . 23

3 Capacity Analysis in the HomePlug AV1 and AV2 contexts 25
3.1 Preliminary . . . 25
3.1.1 Context of this Study: the OMEGA Project . . . 25
3.1.2 What Modulation Scheme for Broadband PLC Networks? . . . 26
3.1.3 Transmission Capacity and Achievable Throughput . . . 27
3.2 Windowed OFDM: Study and Analysis of the HPAV Modulation Scheme . . . 28
3.2.1 OFDM Principle . . . 28
3.2.2 The Windowed OFDM Modulation . . . 31
3.2.3 Windowed OFDM Transmission over a Dispersive Channel . . . 32
3.3 HS-OQAM: Study and Analysis of an Alternative to windowed OFDM . . . 37
3.3.1 OFDM/OQAM Modulation Overview . . . 38
3.3.2 OFDM/OQAM Transmission over a Multipath Channel . . . 41
3.3.2.1 Channel Equalization for OFDM/OQAM . . . 41
3.3.2.2 Generalized Expression of HS-OQAM Interference Term . . . 42
3.3.2.3 Analytical Expression of the Noise Power at the ASCET Equalizer Output . . . 44
3.4 Windowed OFDM vs HS-OQAM: Transmission Capacity and Achievable Throughput . . . 47
3.4.1 Simulation Parameters . . . 47
3.4.2 Performance of Different Prototype Filters Following the HPAV Specification . . . 48
3.4.2.1 Set of Compared Prototype Filters . . . 48
3.4.2.2 Prototype Filter Selection . . . 51
3.4.3 Comparison Between windowed OFDM and HS-OQAM Associated with a Frequency Selective Filter . . . 54
3.4.3.1 HomePlug AV 1 Context . . . 54
3.4.3.2 HomePlug AV 2 Context . . . 57
3.4.4 Potential Impact of the CENELEC Mask on HPAV Networks . . . 60
3.4.4.1 Impact of the CENELEC Mask on the Number of HS-OQAM and Windowed OFDM Active Tones . . . 60
3.4.4.2 Impact of the CENELEC Mask on HPAV Networks Capacity: Comparison Between HS-OQAM and Windowed OFDM . . . 62
3.5 Conclusion . . . 67

4 Point-to-Multipoint Transmissions in Powerline Networks 69
4.1 Preliminary . . . 69
4.1.1 The Interest of FDM in PLC Networks . . . 69
4.1.2 Resource Allocation Problems . . . 70
4.1.3 Taking Advantage of the Frequency Diversity . . . 73
4.2 Problem Statement . . . 75
4.2.1 Problem Discretization . . . 75
4.2.2 Discrete Extension of the Theorem of Section 4.1.3 . . . 77
4.2.3 Mathematical Optimization . . . 78
4.3 Optimal OFDMA Resource Allocation: Geometrical Approach . . . 79
4.3.1 Optimal Capacity Region along Basis Vector $\vec{e}_1$ . . . 80
4.3.2 Optimal Capacity Region in the Plane $(\vec{e}_1, \vec{e}_2)$ . . . 80

4.3.3 Optimal Capacity Region in $(\vec{e}_1, \vec{e}_2, \vec{e}_3)$ . . . 82
4.3.3.1 Analysis of the Capacity Region in P_2 . . . 82
4.3.3.2 Allocation Process . . . 84
4.3.4 Optimal Resource Allocation for $K > 3$ . . . 89
4.4 Optimal OFDMA Resource Allocation: Study of a Particular Case . . . 91
4.5 Suboptimal OFDMA Resource Allocation: The Tone Maps Splitting Algorithm (TMSA) . . . 92
4.5.1 Algorithm Description . . . 92
4.5.2 Complexity Issue . . . 93
4.5.3 TMSA Performance . . . 93
4.6 Definition of an HPAV-compliant OFDMA Transmission Scheme . . . 97
4.6.1 Integration Challenges . . . 97
4.6.2 Comparison of the TDM and FDM Modes . . . 99
4.6.2.1 Simulation Parameters . . . 99
4.6.2.2 Simulation Results . . . 99
4.6.3 Hybridation of the TDM and FDM Mode. . . . 101
4.7 Conclusion . . . 103

5 Multicast Transmissions over Power Line Networks 105
5.1 Preliminary . . . 105
5.1.1 The Interest of Multicast in PLC Networks . . . 105
5.1.2 PLC Networks Multicast Issue . . . 107
5.2 The LCG Solution . . . 108
5.2.1 LCG: PHY Level Analysis . . . 108
5.2.1.1 PHY Rates Computation . . . 108
5.2.1.2 Unicast Conversion vs LCG: PHY Level comparison . . . 110
5.2.2 LCG: MAC level Analysis . . . 113
5.2.2.1 Definition of a Multicast Transmission Scheme . . . 113
5.2.2.2 MAC Rates Computation . . . 114
5.2.2.3 Unicast Conversion vs LCG: MAC Level Comparison . . . 115
5.3 Multicast Transmission Scheme Based on the Creation of Multiple Multicast Subsets . . . 116
5.3.1 LCG Limitations . . . 116
5.3.2 Smart Merging Approach . . . 117
5.3.2.1 Construction of a Fast Tone Map Merging Algorithm . . . 118
5.3.2.2 Simulation Results . . . 124
5.4 Conclusion . . . 125

6 Conclusion 127

Appendix 131

A The ns2-based PLC Network Simulator 133

B Transmission Masks **141**
B.1 North American excluded frequency ranges 141
B.2 CENELEC excluded frequency ranges 142

C Some Proofs **145**
C.1 Proof that $E\left[u^2_{m_0,n_0}\right]$ in (3.60) can be written as $(-1)^{n_0}F(m_0)$ 145
C.2 Proof that $\mathrm{Var}[u_{m_0,n_0}]$ in (3.60) does not depend on n_0 145

D Résumé Français du Mémoire de Thèse **147**
D.1 Chapitre 1: Introduction 147
D.2 Chapitre 2: La technologie des Courants Porteurs en Ligne pour les transmissions en Large Bande 149
D.3 Chapitre 3: Analyse de Capacités dans les Contextes des Spécifications HomePlug AV1 et AV2 151
D.4 Chapitre 4: Transmissions en Configuration Point-à-Multipoint dans les Réseaux CPL 155
D.5 Chapitre 5: Diffusion de Flux Multicast dans les Réseaux CPL 159
D.6 Chapitre 6: Conclusion 161

Contributions **167**

Bibliography **169**

List of Figures

2.1 Structure of a PLC access network [68] (M: Meter Unit). 6
2.2 3 realizations of PLC channels belonging to classes 1, 5 and 9, respectively. 8
2.3 One realization of the colored noise model. 9
2.4 HPAV Spectral mask. 10
2.5 Examples of Physical and logical Networks [7]. 13
2.6 HPAV system block diagram overview [4]. 14
2.7 HPAV Beacon period [87]. 15
2.8 Priority Resolution Period (PRP). 16
2.9 HPAV protocol layer architecture [87]. 18
2.10 MAC frame format [4] [7]. 19
2.11 MAC frame stream generation. 19
2.12 Construction of a MPDU. 20
2.13 520-byte and 136-byte PBs. 21
2.14 MPDU frame format: AV only mode on the left; Hybrid mode on the right [7]. 21
2.15 The HPAV transmission scheme (AV only mode). 23

3.1 CP-OFDM timing. 29
3.2 Efficient Implementation of CP-OFDM [82]. 29
3.3 Frequency Orthogonality of an OFDM Signal. 31
3.4 Windowed OFDM timing. 32
3.5 Windowed OFDM using HPAV tone map fits into the FCC Spectrum Mask. 33
3.6 Window and GI removal at the receiver side. 34
3.7 Comparison between the colored noise and the interference levels for a class 2 channel (cf section 2.2.1), in the HPAV band. 38
3.8 OFDM/OQAM in its analog form (continuous-time). 39
3.9 HS-OQAM general structure [84]. 40
3.10 OFDM/OQAM symbols overlapping [84]. 41
3.11 Structure of the per-carrier ASCET equalizer [84]. 41
3.12 Example of class 2 channel and colored noise realizations. 47
3.13 Compared PSD around a notch between windowed OFDM and HS-OQAM with FS4, using HPAV transmission mask. 49
3.14 Prototype filters: (a) in time (b) in frequency 50
3.15 Comparison of PHY data rates (D^{PHY}) between windowed OFDM and HS-OQAM using TFL1+ZF, $\sigma^2_{c,\mathrm{dB}} = -50$ dBm/Hz. 51

3.16 Comparison of PHY data rates (D^{PHY}) between windowed OFDM, HS-OQAM using TFL1+ASCET and HS-OQAM using FS4+ZF, $\sigma^2_{c,\mathrm{dB}} = -50$ dBm/Hz. 52
3.17 Transmission capacities ($D^{inf\ gran}$) comparison between FS4+ZF and MMB4+ZF.: (a) Class 9 channels (b) Class 2 channels. 53
3.18 Transmission capacities (dotted curves) and PHY data rates (continuous curves) in the HPAV 1 context on Class 9 channels. 55
3.19 Transmission capacities (dotted curves) and PHY data rates (continuous curves) in the HPAV 1 context on Class 5 channels. 55
3.20 Transmission capacities (dotted curves) and PHY data rates (continuous curves) in the HPAV 1 context on Class 2 channels. 56
3.21 HPAV Spectral mask and its extension in the upper band. 57
3.22 Achievable throughput (dotted curves) and PHY data rates (continuous curves) in the HPAV 2 context on Class 9 channels. 58
3.23 Achievable throughput (dotted curves) and PHY data rates (continuous curves) in the HPAV 2 context on Class 5 channels. 58
3.24 Achievable throughput (dotted curves) and PHY data rates (continuous curves) in the HPAV 2 context on Class 2 channels. 59
3.25 Compared PSD between HPAV windowed OFDM and HS-OQAM associated with a FS4 prototype filter, complying with CENELEC spectral mask: (a) permanently excluded frequencies only (b) permanently and dynamically excluded frequencies. 61
3.26 Magnified PSDs around the 18 MHz region of Fig. 3.25-(b). 62
3.27 Transmission capacities (dotted curves) and PHY data rates (continuous curves) on Class 9 channels, considering: (a) permanently excluded frequencies by CENELEC only (b) permanently and dynamically excluded frequencies by CENELEC. 63
3.28 Transmission capacities (dotted curves) and PHY data rates (continuous curves) on Class 5 channels, considering: (a) permanently excluded frequencies by CENELEC only (b) permanently and dynamically excluded frequencies by CENELEC. 65
3.29 Transmission capacities (dotted curves) and PHY data rates (continuous curves) on Class 2 channels, considering: (a) permanently excluded frequencies by CENELEC only (b) permanently and dynamically excluded frequencies by CENELEC. 66

4.1 Illustration of the Multiuser diversity among 4 measured PLC channels in the $[1.8, 100]$ MHz frequency range (provided by the HPAV working group). 70
4.2 Bit-loading performed in the $[1.8, 50]$ MHz frequency range, following the IEEE P1901 specification. 71
4.3 Multiple access and broadcast channels. 72
4.4 Point-to-multipoint transmission: (a) using TDMA (b) using FDMA. . . . 73
4.5 Splitting the frequency bandwidth into N subbands of equal capacity for each link. 74
4.6 Example of a sub-optimal and an optimal OFDMA capacity region for $K = 2$ ($\alpha_1 = 0.3$ and $\alpha_2 = 0.7$). 81

4.7 Impact of the reallocation of one subcarrier on the FDM capacity region around the F point. 83
4.8 Optimal OFDMA capacity region for $K = 3$: (a) Γ_2 and Γ_3 curves ($\alpha_1 = 0.5$, $\alpha_2 = 0.2$, $\alpha_3 = 0.3$) (b) Γ_2 curve after the N allocation steps on $\vec{e}_3$ ($\alpha_1 = 0.35$, $\alpha_2 = 0.15$, $\alpha_3 = 0.5$). 86
4.9 Representation of 50 optimal capacity regions for 50 different values of ϕ_2 ($= \arctan\left(\frac{\alpha_1}{\alpha_2}\right)$). 88
4.10 Representations of the $K-1$ planes containing the optimal capacity region between the K links 90
4.11 P1901 tone maps belonging to classes 2, 5 and 9 channels: (a) before orthogonalization (b) after orthogonalization with $\alpha_k = \frac{1}{K}$. 95
4.12 Evolution of G_{FDM} with the number of tone maps K using various orthogonalization techniques. 96
4.13 Comparison of the achieved values of G_{FDM} by TMSA to the optimal gain. 97
4.14 Modified P1901 payload and acknowledgment frames structures for FDM transmissions. 98
4.15 FDM and TDM transmission modes Hybridation ($K = 3$). 102

5.1 Possible configuration of the Orange multiscreen TV offer using 3 Orange *Liveplugs* (Picture downloaded from the Orange online support website). . 106
5.2 LCG applied among 4 HPAV 2 tone maps: (a) 4 unicast tone maps (b) Multicast tone map after applying LCG. 109
5.3 Static noise model used for the tone maps generation. 111
5.4 Cumulative Distribution Functions of the PHY rate improvement factor ($P(F > X)$), for $K = 2$, 3 and 4 stations to reach. 111
5.5 Averaged PHY data rate in each one of the 3 countries ($K = 4$). 112
5.6 Distribution of the PHY rate improvement factor each one of the 3 countries ($K = 4$). 113
5.7 Transmission schemes: (a) HPAV unicast [7] (b) HPAV-compliant multicast. 114
5.8 Cumulative Distribution Functions of the MAC rate improvement factor ($P(F > X)$), for $K = 2$, 3 and 4 stations to reach. 116
5.9 Averaged MAC data rate in each one of the 3 countries ($K = 4$). 117
5.10 Distribution of the MAC rate improvement factor in each one of the 3 countries ($K = 4$). 118
5.11 20000 bits broadcast to 5 stations: (a) by multiplexing 5 Unicast streams, (b) by merging all the tone maps (LCG solution), (c) by creating two merged tone maps. 119
5.12 Merging Algorithm. 123
5.13 Comparison of the rates improvement factor by the smart merging algorithm and by LCG, both at the PHY and MAC layers. 124

A.1 PLC network simulator Architecture. 134
A.2 Cumulative distribution functions of (a) HPAV and (b) IEEE P1901 tone maps capacities. 135
A.3 User interface screen capture. 137
A.4 Comparison between simulated (continuous curves) and measured data rates (dotted curves) for 1, 2, 3 and 4 uplink UDP flows. 138

A.5 Comparison between simulated (continuous curves) and measured data rates (dotted curves) for 1, 2, 3 and 4 uplink TCP flows. 139

B.1 HPAV Spectral mask. 144
B.2 CENELEC spectral Mask (permanent and dynamic notching). 144

D.1 Masque de transmission défini par la FCC (Amérique du Nord). 150
D.2 Pré-traitement effectué au niveau de récepteur avant de démoduler le signal windowed OFDM. 152
D.3 Recouvrement entre symboles OFDM/OQAM consécutifs [84]. 152
D.4 Représentation des 3 prototypes étudiés: (a) en temps (b) en fréquence. . . 154
D.5 Tone maps suivant la spécification IEEE P1901 générés sur des canaux de classes 2, 5 et 9, respectivement. 156
D.6 Région de capacité optimale pour $K = 3$ ($\alpha_1 = 0.5$, $\alpha_2 = 0.2$ and $\alpha_3 = 0.3$). 158
D.7 Modified P1901 payload and acknowledgment frames structures for FDM transmissions. 159
D.8 Fonction de répartition des facteurs de multiplication du débit au niveau de la couche physique($P(F > X)$), pour $K = 2$, 3 et 4 stations destinataires. 160
D.9 Comparaison des facteurs de multiplication des débits entre l'algorithme proposé et la solution LCG, aux niveaux des couches PHY et MAC. 161

List of Tables

2.1 CW and DC as a function of BPC and priority [17] 17

3.1 Coding scheme for OFDM/OQAM symbols 39

4.1 G_{FDM} (in %) in the case of 2 stations to reach (FEC rate $\frac{16}{21}$ / $\frac{1}{2}$). 100
4.2 G_{FDM} (in %) in the case of 3 stations to reach (FEC rate $\frac{16}{21}$ / $\frac{1}{2}$). 101

B.1 North America permanently excluded frequency ranges 141
B.2 Permanently excluded frequency ranges by CENELEC 142
B.3 Permanently or dynamically excluded frequency ranges by CENELEC . . . 143

Abstract

During the past few years, Power Line Communications (PLC) have become a popular connectivity solution to answer the growing need of home networks for bandwidth. As wireless technologies, this solution spares the user from cabling its Local Area Network (LAN), by directly using the home power grid as a transmission medium. While PLC generally offer a larger coverage than Wireless Local Area Networks (WLAN), the capacity offered by current systems is not sufficient to simultaneously support bandwidth intensive streams. In this thesis, we aim at exploring various solutions for future PLC networks. Firstly, we aim at improving the spectral efficiency of the current systems Physical (PHY) layer, where two modulation schemes are compared. On the one hand, we study the modulation deployed in current PLC networks, called windowed Orthogonal Frequency Division Multiplexing (OFDM), and we highlight the main limitation of this solution in the particular context of PLC. On the other hand, we show that and alternative solution, called OFDM/Offset Quadrature Amplitude Modulation (OQAM), offers some degrees of freedom which could highly benefit to PLC networks. Secondly, the study is oriented toward the Media Access Control (MAC) layer of PLC systems, considering a multiuser utilization of the network. In this second part, we aim at proposing allocation solutions that will allow a more efficient utilization of the limited and shared transmission resource. We firstly study the opportunity of defining an Orthogonal Frequency-Division Multiple Access (OFDMA) transmission scheme for point-to-multipoint transmissions, in order to increase data rates by taking advantage of the diversity between users' channels. Finally, the last chapter is dedicated to the study of broadcast and multicast communications in PLC networks, where we show that a smart aggregation of the set of users to reach could greatly improve the efficiency of multicast transmissions.

Résumé

Ces dernières années, la technologie des courants porteurs en ligne (CPL) a fait son apparition dans les réseaux domestiques afin de répondre au besoin grandissant de bande passante. Comme pour les solutions sans-fil, cette technologie présente l'avantage de ne pas nécessiter le déploiement de nouveaux câbles à l'intérieur de la maison, en utilisant directement le réseau électrique comme milieu de transmission. Offrant une zone de couverture plus importante que les réseaux Wi-Fi, les débits offerts par les équipements actuels ne sont néanmoins pas suffisants pour supporter simultanément des applications gourmandes en bande passante. Cette thèse vise donc à explorer différentes solutions pour les futurs réseaux domestiques basés sur cette technologie. L'étude a d'abord été menée au niveau de la couche Physique des systèmes, où deux solutions de transmission ont été comparées. D'un côté, la modulation windowed OFDM, déployée dans la grande majorité des réseaux actuels, est étudiée afin de mettre en avant ses limites dans le contexte particulier des réseaux sur courant porteur. Dans cette partie, nous montrons concrètement le gain en capacité que pourrait apporter une modulation alternative, l'OFDM/OQAM, présentant des degrés de liberté supplémentaires vis-à-vis de l'OFDM classique, et dont l'exploitation s'avère particulièrement intéressante. Dans un second temps, la problématique de la couche MAC a été abordée dans le contexte d'une utilisation multi-usager du réseau. L'objectif de cette seconde partie a été de proposer des solutions nouvelles pour l'allocation et le partage de la ressource entre les différents utilisateurs du réseau. Premièrement, nous étudions la possibilité de définir un nouveau mode d'accès, basé sur l'OFDMA, permettant de tirer efficacement parti de la diversité entre différents canaux de transmission, afin d'augmenter significativement les débits pour les transmissions point-à-multipoint. Enfin, le dernier chapitre aborde le problème de la transmission multicast inhérent aux réseaux PLC actuels, en proposant une méthode d'agrégation des utilisateurs permettant une augmentation significative des débits.

Acronyms

Here are the acronyms used in this document. The meaning of an acronym is usually indicated once, when it first occurs in the text.

AC Alternating Current

ACK Acknowledgment

ADSL Asynchronous Digital Subscriber Line

ARP Address Resolution Protocol

ARQ Automatic Repeat Request

ASCET Adaptive Sine/Cosine-modulated filter bank Equalizer for Transmultiplexer

ATS Arrival Time Stamp

AVB Audio Video Bridging

AVLN AV Logical Network

AWGN Additive White Gaussian Noise

BC Backoff Counter

BMMM Batch Mode Multicast MAC protocol

BPC Backoff Procedure event Counter

CAP Channel Access Priority

CCo Central Coordinator

CDF Cumulative Distribution Function

CDHN Convergent Digital Home Network

CENELEC Comité Européen de Normalisation

CIFS Contention Inter-Frame Space

CL Convergence Layer

CM Connection Manager

CP Cyclic Prefix

CSMA/CA Carrier Sense Multiple Access / Collision Avoidance

CTS Clear To Send

CW Contention Window

DAC Digital to Analog Converter

DC Deferral Counter

DHCP Dynamic Host Configuration Protocol

DTEI Destination TEI

EMC Electromagnetic Compatibility

EMI Electromagnetic Interference

FC Frame Control

FDM Frequency Division Multiplexing

FEC Forward Error Correction

FFT Fast Fourier Transform

FIR Finite Impulse Response

FM Frequency Modulation

FMT Filtered Multi Tone

FS Frequency Selectivity

FTTH Fiber-To-The-Home

GBN General Background Noise

GI Guard Interval

HD-PLC High-Definition Power Line Communications

HLE Higher Layer Entity

HP HomePlug

HPA HomePlug Powerline Alliance

HPAV HomePlug Audio/Video

HS-OQAM Hermitian Symmetric OQAM

ICI Inter-Carrier Interference

ICV Integrity Check Value

IEEE Institute of Electrical and Electronics Engineers

IFFT Inverse Fast Fourier Transform

IGMP Internet Group Management Protocol

IOTA Isotropic Orthogonal Transform Algorithm

IP Internet Protocol

IPTV IP Television

ISI Inter-Symbol Interference

ISP Internet Service Provider

ISPLC International Symposium on Power Line Communications and its applications

ITU International Telecommunication Union

LAN Local Area Network

LCG Lowest Channel Gain

LID Link Identifier

MAC Media Access Control

MCM Multi-Carrier Modulation

MIMO Multiple Input Multiple Output

MSDU MAC Service Data Unit

MPDU MAC Protocol Data Unit

MTL Multi conductor Transmission Lines

NEK Network Encryption Key

NPR Nearly Perfect Reconstruction

PAT Performance Analysis Tool

PB Physical Block

PBB PB Body

PBCS PB Check Sequence

PLC Power Line Communications

OFDM Orthogonal Frequency Division Multiplexing

OFDMA Orthogonal Frequency-Division Multiple Access

OQAM Offset Quadrature Amplitude Modulation

OSI Open Systems Interconnection

PHY Physical

PIM-SM Protocol-Independent Multicast - Sparse-Mode

PR Perfect Reconstruction

PRP Priority Resolution Period

PSD Power Spectral Density

PS-OFDM Pulse-Shaped OFDM

QoS Quality of Service

RI Roll-off Interval

RIFS Response Inter-Frame Spacing

ROBO Robust OFDM

RTS Request To Send

SAP Service Access Point

SACK Selective ACK

SER Symbol Error Rate

SINR Signal to Interference plus Noise Ratio

SNR Signal to Noise Ratio

TCP Transport Control Protocol

TFL Time-Frequency Localization

TDM Time Division Multiplexing

TDMA Time Division Multiple Access

TMSA Tone Maps Splitting Algorithm

TEI Terminal Equipment Identifier

UDP User Datagram Protocol

UPA Universal Powerline Association

UPnP Universal Plug and Play

VLC Visible Light Communication

VoD Video on Demand

VoIP Voice over IP

WPAN Wireless Personal Area Networks

WLAN Wireless Local Area Networks

ZF Zero Forcing

Notations

The notations used in this thesis are listed in below

x	scalar
$\|x\|$	norm of x
$(x)^*$	conjugate of x
$\delta(t)$	Dirac delta function
$\delta_{n,m}$	Kronecker delta
M	total number of carriers in both OFDM and OFDM/OQAM systems (in chapters 4 and 5, M is directly the number of active tones)
$\mathbb{M}$	set of subcarriers in both OFDM and OFDM/OQAM systems ($\text{Card}(\mathbb{M}) = M$)
$\mathbb{M}_u$	set of active subcarriers in both OFDM and OFDM/OQAM systems (in chapters 4 and 5, we set $\mathbb{M}_u = \mathbb{M}$)
T_s	sampling inteval
f_s	sampling frequency
T_0	useful OFDM symbol duration ($T_0 = MT_s$)
F_0	frequency spacing ($F_0T_0 = 1$)
τ_0	OFDM/OQAM system rate ($2\tau_0 = T_0$)
L_{GI}	guard interval length in samples
L_{RI}	roll-off interval length in samples
L_f	prototype filter length in samples
$\phi_{m,n}$	OFDM/OQAM phase term
$\text{E}[a]$	expectation of random variable a
$\text{Var}[a]$	variance of random variable a
$\mathbb{R}$	real field
$\mathbb{C}$	complex field
$\text{Re}\{a\}$	real part of a
$\text{Im}\{a\}$	imaginary part of a
j	$j^2 = -1$
Γ	SNR or SINR gap ($\Gamma = \frac{1}{3}\left[\mathbf{Q}^{-1}(\frac{\text{SER}}{4})\right]^2$)
$c_{m,n}$	complex QAM symbol located at subcarrier m of the n-th OFDM symbol
$a_{m,n}$	real or imaginary part of $c_{m,n}$
σ_n^2	variance of additive white noise
σ_c^2	variance of OFDM input complex-valued symbol

σ_a^2	variance of OFDM/OQAM input real-valued symbol ($2\sigma_a^2 = \sigma_c^2$)
$A_{g,f}[\tau, \mu]$	cross-ambiguity function between $g(t)$ and $f(t)$ at phase-space (τ, μ)
$A_p[\tau, \mu]$	ambiguity function of the prototype filter $p(t)$ at phase-space (τ, μ)
$\lceil a \rceil$	the smallest integer that is larger than a
$\lfloor a \rfloor$	the largest integer that is smaller than a
$T_k[m]$	tone map on link k
R_k	capacity of the tone map on link k
D_k^{PHY}	PHY data rate on link k
D_k^{MAC}	MAC data rate on link k

Chapter 1

Introduction

The intense competition between the French Internet Service Providers (ISPs) has led Orange to quickly expand its service offer during the last decade. This diversification resulted in the release of the well-known *triple play* offer, gathering broadband Internet Access, Internet Protocol Television (IPTV) and Voice over IP (VoIP) services. To differentiate from its competitors, Orange keeps improving the variety of services included in its Internet access offer. Moreover, Orange being the French historical operator, another fundamental component of its strategy lies in the customer service it provides. As the weakest link of the communication chain carrying the subscribed service is often the client home network, Orange has a deep interest in mastering existing home connectivity solutions. The past decade has seen the popularization of Asynchronous Digital Subscriber Line (ADSL) offers, allowing up to 20 Mbps Internet accesses. Nowadays, customers can obtain up to 100 Mbps Internet accesses with Fiber-To-The-Home (FTTH) offers. Consequently, Orange can offer numerous multimedia services to its customers, such as Internet Protocol Television (IPTV) or Video on Demand (VoD) services. Multimedia applications are so popular that, according to [1], 37% of the overall Internet bandwidth is dedicated to video applications. So, it appears that video streaming is one of the most popular application. Nevertheless, it is also one of the most critical in terms of admissible delay and requires high transmission capacity networks. So, in a context of multiple and heterogeneous streams circulating throughout the home, the LAN (Local Area Network) has to provide enough capacity and some prioritization mechanisms to ensure that Quality of Service (QoS) requirements are met.

Nowadays, the home connectivity market is dominated by two technologies. Firstly, there is the Ethernet, wired technology providing a short-delay and high-capacity transmission link [16]. However, this solution is mainly used to connect nearby devices because homes are generally not natively wired with Ethernet. Secondly, to connect stations located in separate rooms, 802.11-based wireless technologies [15] are generally preferred to Ethernet. The popularity of Wi-Fi solutions has resulted in a high concentration of wireless access points in urban areas [13], which drastically reduces the capacity and the reliability of these networks. Consequently, this technology does not answer all the use cases it may be subject to, especially when it comes to transmit services with strong QoS requirements, such as videos streaming. Moreover, the coverage of wireless networks is highly dependent on the walls thickness and on the distance between communicating stations, so that the whole home area may not be entirely covered. So, the current trend

in the home networking field is to diversify the connectivity solutions, as tends to show the ongoing IEEE P1905 standardization [40], which will result in the definition of a new layer above the Medium Allocation Control (MAC) in order to abstract the underlying connectivity solution.

In addition to WLAN technology, the PLC connectivity solution has appeared within the home networking area to answer this increasing demand for bandwidth. As wireless technologies, this solution spares the user from deploying new wires inside his home, while expanding the coverage of his home network. PLC technology basically allows to transform the home power grid into a wired Local Area Network (LAN). Current PLC devices allow to reach physical data rates comprised between 200 and 500 Mbits/s. However, the power line is a harsh transmission medium, such that the achieved data rates at the IP layer rarely exceed 80 Mbits/s. Since 2005, France Télécom has been selling PLC devices to its customers. They are generally sold by pairs and presented as a substitute to Ethernet, when the set-top box (IPTV decoder) and router are too far apart for cable connection. Yet, more than two PLC devices can be synchronized to allow the communications between multiple network hosts, transforming the electrical grid into a LAN. However, because of the opportunistic access technique implemented in existing devices and the lack of admission control policy, current PLC networks cannot always ensure that the QoS requirements for constrained services delivery are met.

Therefore, we can highlight two main issues regarding PLC for current home networks. Firstly, more efforts have to be made to increase their capacities: this issue is typically related to the Physical (PHY) layer of the system. Secondly, the simultaneous presence of heterogeneous data streams, with different bandwidth, delay or jitter requirements, makes necessary the definition of better prioritization mechanisms and resource allocation techniques. These functions are carried out by the Media Access Control (MAC) layer of the networking device. So, this thesis aims at investigating various solutions addressing the aforementioned problems. Firstly, this study is focused toward the PHY layer of current PLC systems. In chapter 3, we firstly highlight the limitations of the modulation scheme that is used in current PLC networks, called windowed Orthogonal Frequency Division Multiplexing (OFDM) modulation. Then, we compare this modulation to another Multi-Carrier Modulation (MCM) scheme, named OFDM Offset QAM (OFDM/OQAM), highlighting its benefits in the PLC context. This work contributed to a deliverable within the european FP7 project "OMEGA" [53], and resulted in the publication of three papers [28], [29], [32]. Then, in chapter 4, we aim at taking advantage of the frequency diversity between the channels of different users to reach, defining an OFDMA transmission scheme that can significantly improve data rates in the case of point-to-multipoint communications. In this part, we describe a method to optimally split the spectral resource between users in the case of quasi-static channels. Then, a suboptimal allocation algorithm is developed and compared to the optimum. The OFDMA transmission scheme is assessed using an ns-2 based PLC network simulator, which is described in Appendix A. This chapter resulted in several paper publications and technical contributions [30], [31]. Finally, chapter 5 addresses the broadcast/multicast issue inherent in all current PLC networks. A first analysis is conducted using measured PLC channels, which is then extended using simulated channels. In this fifth chapter, we describe an iterative method aiming at improving the multicast data rate by splitting the set of stations to reach into multiple multicast subsets. This chapter resulted in the publication of one paper [27] and several

technical contributions related to this study were presented to the HPAV Technical Working Group (all contributions are listed on page 167). Finally, a conclusion is drawn on this work, highlighting the issues left to address. In this final part, we also broaden the scope of this study by showing the important role that could play PLC in future Convergent Digital Home Networks (CDHNs).

Chapter 2

Broadband Power Line Communications

2.1 Introduction

Power Line Communications (PLC) refer to any solution using the power grid as a telecommunication medium. If this technology has been the subject of a growing interest over the last years, PLC is actually an old idea that dates back to the early 1900s, when the first patents were filed in this area [58]. Electric utilities around the world have been using this technology since then, using narrowband (NB) PLC solutions operating in the low frequency bands (from 9 to 140 kHz), achieving data rates ranging from few bps to a few kbps [105]. In this context, PLC is mainly used for remote metering and load control [98], [59]. The capability of remotely turning on/off appliances responsible for high energy consumption was an important driver for the original interest in PLC. Since the 1930s, Ripple Carrier Signaling has been used to control peak events at demand side by issuing control signals to switch off heavy duty appliances [58]. This solution has been quite successful, especially in Europe, and its use has been extended to include other applications such as day/night tariff switching, street light control, and control of the equipment on the power grid.

The revolution of digital comunications, combined with the deregulation of the telecommunications market initiated in 1998 in Europe, has renewed the interest in PLC over the last two decades. Indeed, according to [68], the traditional access networks represents approximately 50% of the investments in the total network infrastructures. PLC being a "no new wire" connectivity, this technology directly became a serious candidate for the so-called "last mile" connectivity, denoted as "access PLC". Access PLC networks can be realized using the medium and low-voltage power lines that feed homes as transmission medium (see Fig. 2.1). In such a case, end users are connected to the network via a PLC modem placed in the electrical power Meter unit (M, cf. Fig. 2.1) or connected to any socket in the internal electrical network. On the other hand, in-home electrical installations, that are naturally present in every home, can be used as a local area network (LAN). This last application of the PLC technology is referred to as "indoor PLC".

In spite of the main advantages inherent in this technology, easy to access and cost effective, PLC was not an immediate success. Actually, if we go several years back, this technology was far from reaching an unanimous support in the scientific community, es-

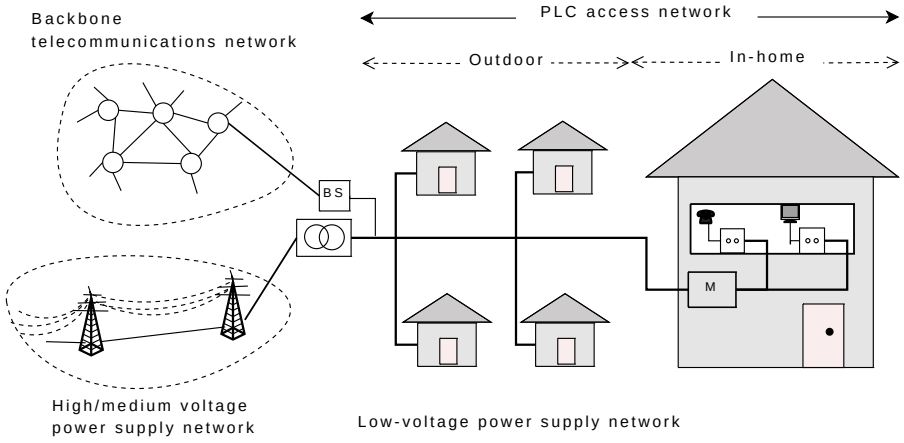

Figure 2.1: Structure of a PLC access network [68] (M: Meter Unit).

pecially as in this period wireless networks were also booming. Firstly, the power grid is a harsh transmission medium, and the frequency selective nature of the channel demands sophisticated technologies. Moreover, the PLC medium is subject to various forms of noise (background white/colored, impulsive noise periodic/aperiodic, narrowband interference) that require some special cares on signal processing. In addition to that, electrical wires are not shielded, resulting in Electromagnetic Interference (EMI) that strongly limits the maximum authorized power level for transmission, and making the medium also sensitive to external interference sources. Another afflicting worry is that the power grid cannot provide a dedicated link between transmitters. Since power line medium is shared within a set of users, the signal generated by one user may interfere with the others that appear in the same circuit, which makes the definition of efficient resource sharing policies of utmost importance.

The multiple challenges that broadband PLC were originally facing has made this study a hot topic in the communication area. More and more tracks concerning PLC have emerged in several well-known international electrical engineering conferences (International Conference on Communications, Global Communications Conference...). Moreover, an international symposium dedicated to PLC was created in 1997, as the International Symposium on Power Line Communications and its applications (ISPLC), that is now supported by the IEEE Communication Society. This illustrates the growing interest in PLC to provide high-rate data communications. Nowadays, a lot of applications may benefit from PLC advancements, from Internet Access [86], to indoor wired Local Area Networks (LANs) for residential and business premises, in-vehicle data communications [104] and smart grid applications [41], [5], [26] (advanced metering and control, realtime energy pricing, peak shaving, mains electricity monitoring, distributed energy generation, etc.).

In this Chapter, we provide an overview of broadband PLC networks. Firstly, the in-home PLC medium is characterized by introducing various models of PLC channels and noises that can be found in the litterature. Then, information related to regulatory issues about EMI is given. Finally, we describe the HomePlug Audio/Video (HPAV) specification for broadband in-home PLC networks, as it has been used as a baseline for this work.

2.2 In-home PLC Environment Characterization

2.2.1 PLC Channel Modeling

One of the first problem to tackle when designing a telecommunication system is to model the transmission channel. Consequently, many contributions in the field of broadband PLC were primarily focused on this topic. In litterature, PLC channels models are split into two categories. On the one hand, PLC channels can be modeled following a "bottom-up" approach, as it was done in [72], [62], [36] or [63]. This approach considers the power cables as two or Multi conductor Transmission Lines (MTL) [63], where the currents and the voltages vary in magnitude and phase along the cables. If this kind of models has the advantage of not requiring any field measurements, it needs a fine knowledge of the transmission environnement, such as the network topology, the cable characteristics, or the value of every terminating impedance at each network node. Consequently, a lack of knowledge in these characteristics may severely degrade the model accuracy [63].

The "top-down" approach is the other way to model PLC channels, and is the most widely used in the litterature [117], [95], [110], [61]. This approach firstly requires field measurements in order to fix various parameters of analytical expressions of the PLC channel. The "top-down" approach has the main advantage of not requiring knowledge of network characteristics. Among the models that can be found in litterature, the fundamental Zimmermann's model is one of the most famous. This model, originally proposed in [117], highlights the multipath nature of the powerline network. It considers that each cable derivation can be associated with a transmission and a reflection factors, and that impedance mismatches at outlets can be associated with a reflection factor. The general expression of the Zimmerman's channel frequency transfer function reads:

$$H(f) = \sum_{i=1}^{N_P} g_i(f) A(f, d_i) e^{-j2\pi f \tau_i} \tag{2.1}$$

where N_p is the number of signal paths, $g_i(f)$ is a complex and frequency dependent weighting factor, τ_i is the delay of path i that depends upon the dielectric constant of the conductor, and $A(f, d_i)$ is the attenuation encountered over path i of length d_i and at the frequency f. The attenuation in PLC actually corresponds to cable losses in the electrical network. It has been shown in [117] that $A(f, d)$ increases with frequency and cable length, and can be written in the following closed form:

$$A(f, d) = e^{-(a_0 + a_1 f^k)d}, \tag{2.2}$$

where parameters a_0, a_1 and k are the attenuation parameters that can be derived from measured transfer functions.

Zimmermann's model was used as a baseline to derive another PLC channel model by Tonello in [110]. This model adds some statistical properties to the Zimmermann one, by considering that some of its parameters can be modeled as random variables following specific distribution functions. For example, it considers that the reflection sources distribution over the power cables follows a Poisson law, and that the weighting factor g_i are complex random variables that are log-normally distributed in amplitude. On the other hand, a_0, a_1 and k parameters have still constant values, and are fixed such that the model fits with measured PLC channels.

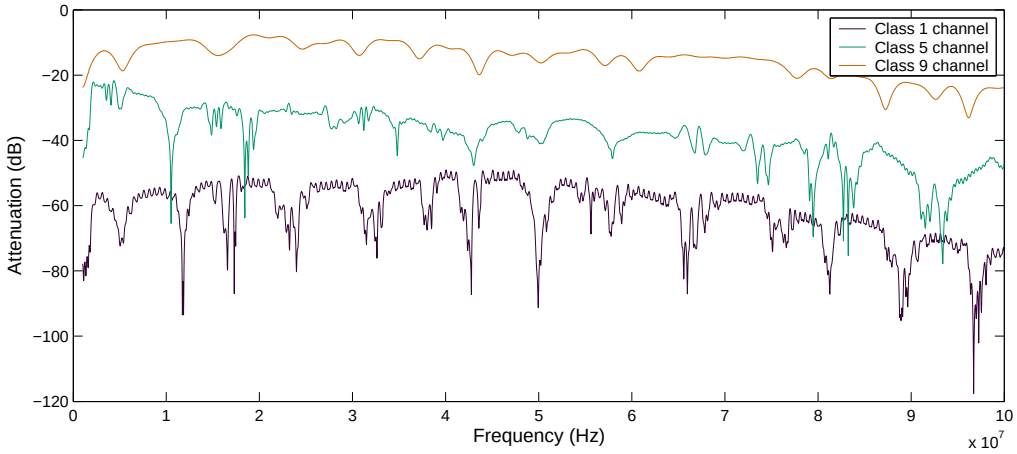

Figure 2.2: 3 realizations of PLC channels belonging to classes 1, 5 and 9, respectively.

In this thesis, we have used a third model of PLC channel model that also falls into the "top-down" approach. This model, proposed by France Télécom in [109], [107] has the peculiarity of being purely based upon field measurements. Based on a large set of measures in different types of PLC environments, from the recent house in the country to the old downtown apartment, a statistical analysis on these measures led to the classification of the PLC channels into 9 classes, class 1 corresponding to the most disturbed channels and class 9 covering the less disturbed ones. As the classification depends on the power line circuit topology and on realistic living environments [108], this model is considered as a fairly realistic in-home PLC model that truly captures the realistic channel features. From those measured PLC channels, an average magnitude and phase model is built for each class and multipath effects are introduced by means of a statistical-based channel generator [106]. According to the desired channel class and bandwidth, the corresponding channel realization is generated in frequency, as Fig. 2.2 illustrates.

2.2.2 Noise Sources

In addition to the multipath nature of the channel, various sources of noise combine, which results in a transmission medium that is sometimes qualified as "horrible" [39]. In [116], 5 PLC noise sources are distinguished, which can be classified into 2 general categories: the General Background Noise (GBN) and the impulsive noise.

The GBN is a combination of a colored background noise and narrowband interference. The GBN usually remains stationary as it varies very slowly in terms of seconds, minutes, and sometimes of hours. In [52], France Télécom developed a GBN model derived from a statistical analysis of several measures realized in domestic environments. In Fig. 2.3, the Power Spectral Density (PSD) representation of one realization of this GBN model shows that it can be described as a combination of a static component following an exponential decrease with frequency and a lot of narrowband interference components randomly distributed across the spectrum. This noise generator also models the Frequency Modulation (FM) broadcasting band.

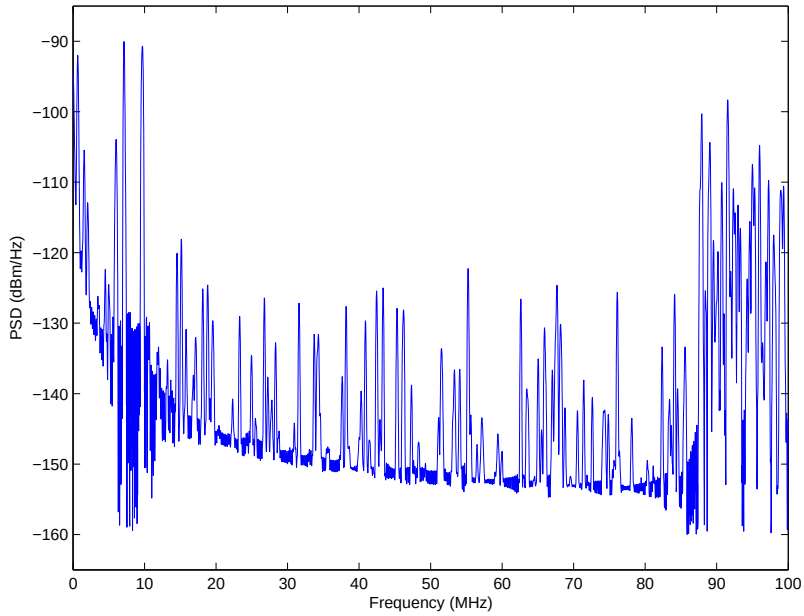

Figure 2.3: One realization of the colored noise model.

The second category gathers two kinds of impulsive noise that are highly time-dependent, and can consequently cause dramatic drop in the PLC network performance. Firstly, there is the periodic impulsive noise synchronous to the Alternating Current (AC) line cycle. This type of noise is typically caused by rectifier diodes in power supplies which operate synchronously with the network main frequencies (50 or 60 Hz). Some sources are thyristor- or triac-based electrical appliances such as light dimmers [67, 117] which creates impulses on every cycle or half cycle of the AC line period. However, the impulsive noise category is largely dominated by the asynchronous impulsive noise type, which is, at the same time, the most detrimental disturbance for data transmission. Indeed, because of its unpredictable nature and its peculiar high amount of energy, it can cause the simultaneous loss of multiple data segments in broadband PLC networks. In this thesis, the impulsive noise is not considered as all simulations assume static PLC channels, using the France Télécom's GBN generator described in [52]. For the interested reader, novel methods to mitigate the effect of impulsive noise in PLC networks were developed in [90] for instance.

2.3 Regulatory Authorities

Due to the lack of electromagnetic shielding of power lines, PLC are subject to severe restrictions concerning the transmitted power level. The transmission mask that has to be respected varies with the country. As our study used the HPAV specification as a baseline [20], we used the US mask which is the one described in this specification (see the Annex B.1 for more details about the protected applications). As we can see in Fig. 2.4, this mask limits the Power Spectral Density (PSD) to -50 dBm/Hz and imposes several notches in which the PSD is limited to -80 dBm/Hz to avoid interfering with other applications (such as amateur radio for instance). Considering the work conducted

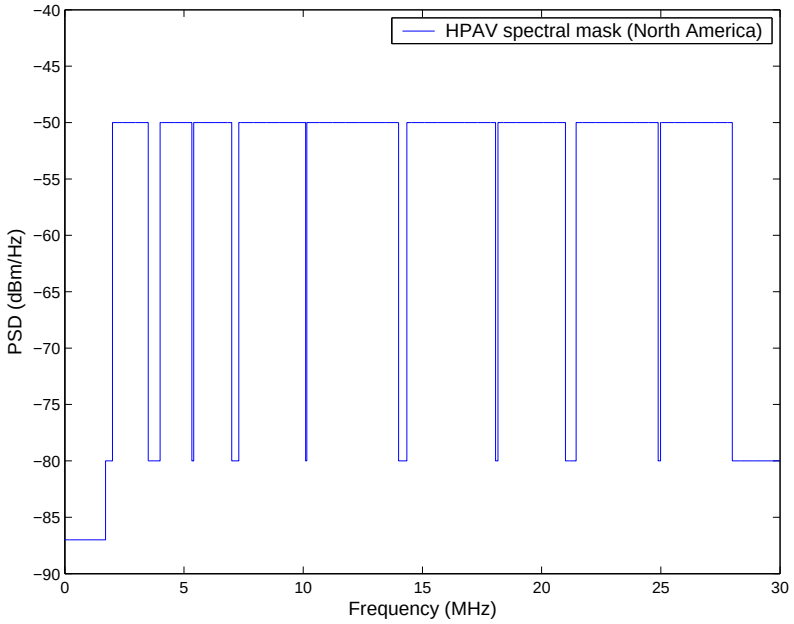

Figure 2.4: HPAV Spectral mask.

for the european FP7 "OMEGA" project [52], we extended this mask using frequencies higher than 30 MHz, limiting the PSD to −80 dBm/Hz for the carriers located beyond 28 MHz, and stopping the signal just below the FM band, starting at 87.5 MHz. This extended mask, presented in Fig. 3.21, is actually very similar to the mask defined by the HPAV 2 specification.

However, a new transmission mask imposed by the Comité Européen de Normalisation (CENELEC) is about to get released, and imposed to current PLC systems. This mask, described in Annex B.2, adds a lot more notches to the north american one for frequencies below 30 MHz, so that it may severely decrease the capacity of PLC networks located in Europe (the impact of this new transmission mask on HPAV networks capacity is assessed in the next Chapter).

2.4 Broadband PLC Specifications

The last decade has seen three industrial solution consortia competing to conquer the broadband in-home PLC market: the HomePlug Powerline Alliance (HPA) [6], the High-Definition Power Line Communications (HD-PLC) Alliance [3], and the Universal Powerline Association (UPA) [14]. Consequently, the PLC market has been fragmented for several years. Since 2010, when the UPA suspended its activities, the market has stabilized, thanks to the release of the P1901 standard [7] conducted by the Institute of Electrical and Electronics Engineers (IEEE).

In the attempt to define a standardized solution for broadband PLC networks, the HPA was a precursor, and is still the most active organization. The alliance is a trade organization, created in 2000 and gathering 60 member companies, from chip designers such as Qualcomm Atheros [12] or Maxim [9], to manufacturers such as Devolo [2] or

Lea [8], and also service providers like Orange. Twelve years ago, the alliance released the first specification for in-home broadband powerline communications: the HomePlug (HP) 1.0 specification [17]. These first broadband PLC systems directly showed their good performance when compared to 802.11 wireless systems [80], [81]. HP 1.0 allows PLC networks to reach data rates up to 14 Mbps in the $[4, 21]$ MHz frequency range, using an opportunistic channel access technique derived from the well-known Carrier Sense Multiple Access / Collision Avoidance (CSMA/CA) used in 802.11 networks. However, while HomePlug 1.0 enabled data networking throughout the home power grid, it was not suitable for multimedia applications [76]. Indeed, multimedia applications not only require significantly larger bandwidths, but also need Quality of Service (QoS) guarantees. To address this class of applications, a new generation of the HomePlug Standard, HomePlug AV (HPAV) [33], [4], was released by the alliance in 2005. HPAV-based PLC systems theoretically offer up to 200 Mbps throughput and operate in the frequency range of $[1.8, 30]$ MHz [59]. Furthermore, the specification introduces a centralized Time Division Multiple Access (TDMA) scheduling scheme for QoS provisioning. So, HPAV systems offer a reliable solution to support multimedia applications over the power grid. Actually, the success of HPAV-based PLC devices has made the specification a "de facto" standard. In 2010, broadband home communications over power line were officially standardized with the release of the IEEE P1901 standard [7]. P1901 uses HomePlug AV as baseline technology but extends the bandwidth up to 50 MHz, allowing up to 500 Mbps data rates at the physical layer. This standard has also the peculiarity of defining two different PHY (physical) layers [65]. In addition to the windowed OFDM (Orthogonal Division Frequency Multiplexing) scheme used in HPAV networks, P1901 defines an alternative modulation technique, called Wavelet OFDM, defended by the HD-PLC consortium led by Panasonic [64]. However, it seems that a large majority of P1901 systems only use the windowed OFDM transmission scheme, as it ensures backward compatibility with HPAV systems that are the most deployed PLC systems.

In 2009, the International Telecommunication Union (ITU) has issued the G.hn set of standards for home networking over existing wires [91]. Basically, a single G.hn device is able to network over any of the supported home wire types: telephone wiring, coaxial cables and power lines. There are great similarities with the IEEE solution, such that G.hn systems should provide about the same performance. If the two solutions can coexist, they are not compatible. G.hn developments are supported by a trade organization, the HomeGrid forum, which is also in charge of certifying G.hn products. It is likely that first HomeGrid certified products will appear this year. In comparison to HPAV, the major benefit of the G.hn solution comes from the multiple media on which it can work. Therefore, we could consider this standard as the most serious competitor to HPAV. However, the IEEE P1905 working group [40] excluded G.hn from its scope in 2011. As P1905 seems to be quite a success, considering that products implementing it are currently being launched on the market, G.hn could be definitely marginalized. Moreover, a new HomePlug standard, HPAV 2, was released in early 2012 [25]. Two main features differentiate HPAV 1 from HPAV 2. Firstly, a significant capacity improvement is made possible by extending the bandwidth up to 86 MHz. Secondly, it defines a Multiple Input Multiple Output (MIMO) OFDM transmission scheme, enabled by the Line-Neutral coupling and Line-Protective earth coupling used as two possible transmission paths. HPAV 2 networks should theoretically provide ten times higher data rates than HPAV ones. Now that actors

of the PLC industry are currently struggling to impose their solutions for the emerging smart grid market [66], it seems that the HPA has definitely conquered the in-home broadband PLC market. So, in the following of this thesis, we will always focus on HPAV-based PLC networks (AV1 and 2, and IEEE P1901).

2.5 Overview of HPAV-based Specifications

2.5.1 PLC Network Overview

The HPAV specification defines two network concepts: the Physical network and the Logical network. The Physical network is the set of stations that can directly communicate, meaning that its coverage depends on the characteristics of the transmission medium, as well as the transmitted power. Consequently, it is relative to a given station, and may even not be the same between two nearby PLC stations. Therefore, a first condition to be met for two HPAV stations to communicate will obviously be that they both belong to the same physical network. However, this condition is not sufficient to define an HPAV network. Stations able to communicate with each other must belong to the same AV Logical Network (AVLN), and possess a unique Terminal Equipment Identifier (TEI). The set of stations in the same AVLN possesses the same network identifier, and their communications are encrypted using the same encryption key. Moreover, the AVLN activity is coordinated by a specific station, called the Central Coordinator (CCo), which provides the network time basis, as well as optional QoS management services. Each node in an AV Logical Network must have a minimum functionality, denoted as mandatory features, which can be completed by optional features. The AVLN CCo is generally the station providing the most advanced functionalities. In Fig. 2.5-(a) is presented a network configuration where physical and logical networks are the same. In such a case, every station of the network is able to communicate with any other station (they are all linked with bidirectional arrows). Then, Fig. 2.5-(b) illustrates the case of two AVLNs where the two CCos can physically communicate with each other. In such case, HPAV defines optional coordination functions allowing the two CCos to negotiate the sharing of the transmission medium. Note that two stations belonging to the same logical network will not be able to communicate with each other if they are not in the same physical network, as it is shown in Fig. 2.5-(c). So, the specification defines advanced capabilities where an AV station can act as a repeater to retransmit data to hidden stations. As it remains an unlikely scenario to happen considering the home networking area, to our knowledge, this feature is not implemented in practice.

At the highest level of abstraction, an HomePlug AV system consists of the functional blocks described in Fig. 2.6. On the transmit side:

- The Convergence Layer (CL) performs bridging, classification of traffic into connections, and data delivery smoothing functions.
- The MAC determines the correct position of transmission, formats data frames into fixed-length entities for transmission on the channel and ensures timely and error-free delivery through Automatic Repeat Request (ARQ).
- The PHY layer performs error-control correction, mapping into OFDM symbols, and generation of time-domain waveforms.

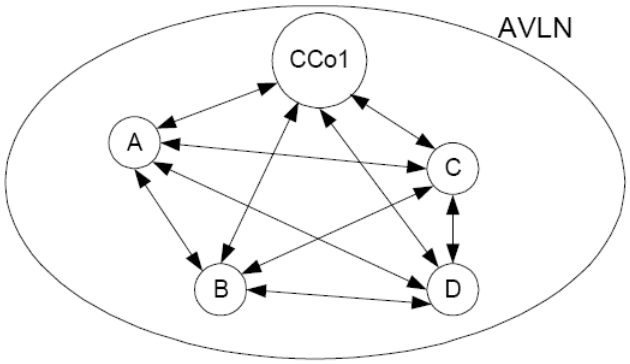

(a)

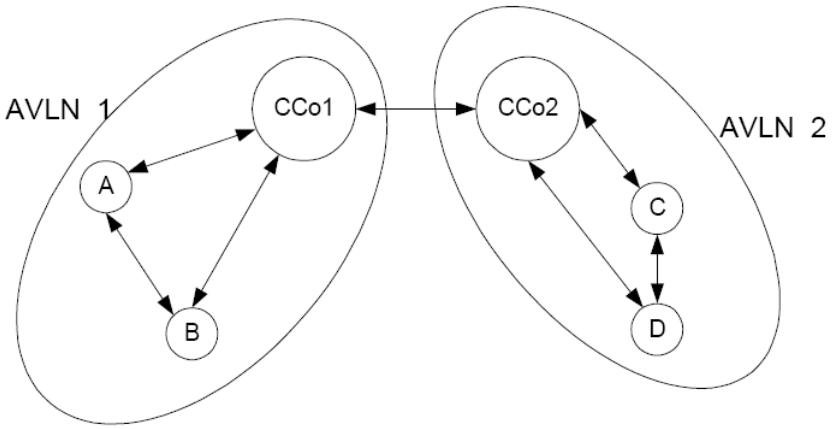

(b)

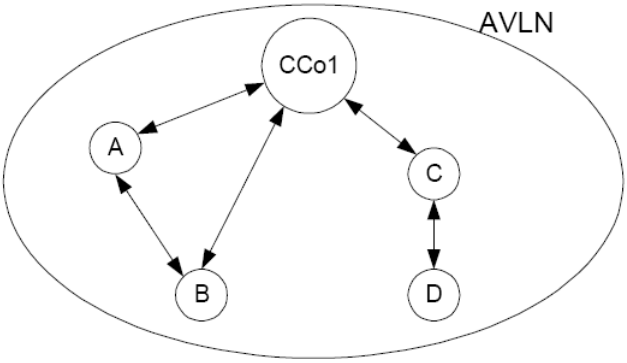

(c)

Figure 2.5: Examples of Physical and logical Networks [7].

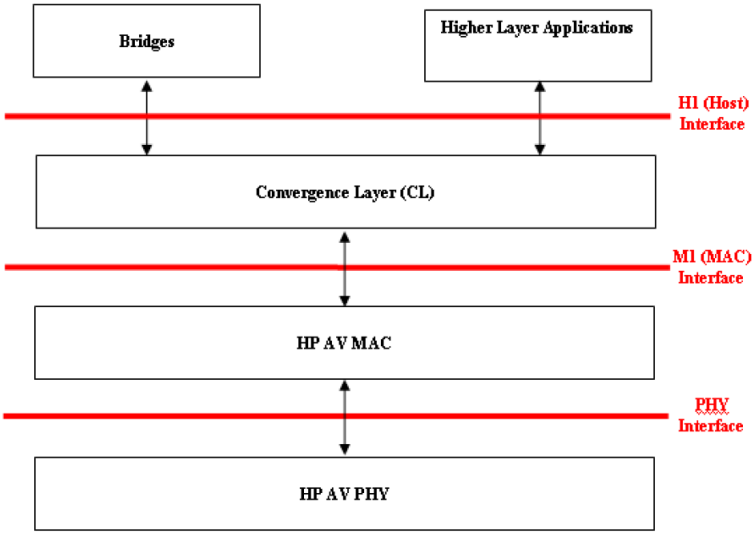

Figure 2.6: HPAV system block diagram overview [4].

On the receiver side, the corresponding functions are performed in reverse order.

2.5.2 Convergence Layer (CL)

The CL is the top portion of the HomePlug Data Link Layer (Layer 2). It is in charge of formatting packets originating from higher layers or corresponding layers of the bridged network (generally 802.3 LAN [16] or 802.11 WLAN [15]) before handing them to the MAC layer. At the receiver side, the CL performs the reverse operation. It also classifies incoming packets by matching them to established connections. A connection can be automatically initiated by the convergence layer through an automatic connection service. This may happen to ensure that QoS constraints are met for the delivery of time sensitive applications, such as video streaming for instance. In such a case, the CL establishes, maintains, and tears down connections for these flows. In addition, the CL monitors data traffic to ensure that the QoS guarantees of a connection are being met. Finally, it provides traffic smoothing services for jitter control.

2.5.3 MAC Layer

2.5.3.1 Channel Access Mechanisms

HPAV uses beacon-based periodic channel access mechanism. The beacon period can be split into three main intervals: the beacon region, the CSMA region, and the reserved region (cf. Fig. 2.7). The beacon region is reserved for the CCo to transmit the central beacon of the AVLN. Basically, the beacon is a short frame periodically broadcasted by the CCo that contains general information about the AVLN, such as its identifier or the terminal identifier of the CCo. The beacon optionally contains scheduling information for TDMA sessions within the beacon period. These sessions, associated to a unique connection identifier, are allocated time intervals within the reserved region. The duration of the

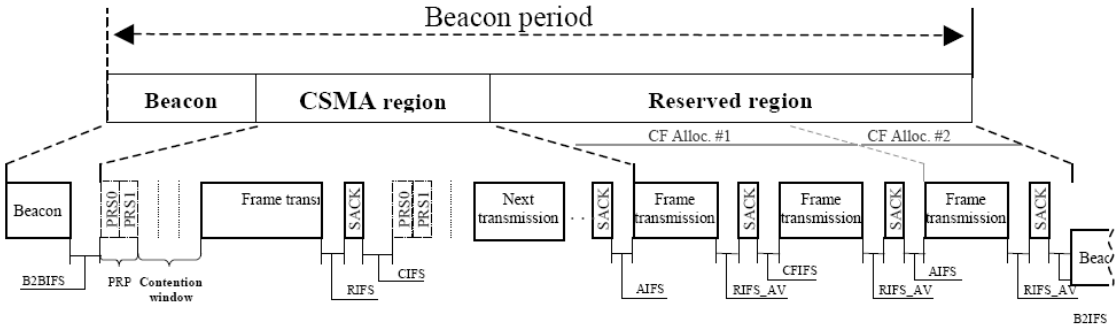

Figure 2.7: HPAV Beacon period [87].

beacon period is twice that of an AC line cycle. Thus, the US 60 Hz AC line cycle will result in a shorter beacon period (33.33 ms) than in Europe (50 Hz AC line cycle, resulting in a beacon period of 40 ms). To share the transmission medium between the stations, HPAV specification defines two channel access mechanisms, depending on the considered region: CSMA/CA and TDMA.

CSMA/CA Channel Access

Firstly, HomePlug systems implement a distributed and contention-based access procedure, which is mandatory since the release of the HomePlug 1.0 specification [17]. As in 802.11 WLAN, it is impossible to detect frame collisions in a PLC network. Therefore, the CSMA/CA (Carrier Sense Multiple Access/Collision Avoidance) opportunistic access technique, also used in 802.11 networks, was adopted by HomePlug standards [47]. Before contending for channel access, the transmitter must firstly listen to the state of the medium. For this purpose, HomePlug defines a two-level carrier sense mechanism. Firstly, the PHY layer realizes a Physical Carrier Sense (PCS) that detects priority resolution symbols and frame preambles. Secondly, the MAC layer realizes a Virtual Carrier Sense (VCS), by interpreting the frame control fields of detected frames to compute the expected duration of the channel occupancy. VCS can also infer frame collisions events by detecting the non-transmission of an expected acknowledgement. If the medium is busy (i.e. some other station is transmitting), the station defers its transmission until the medium becomes idle. On the other hand, if the medium is detected idle, the station will then attempt to transmit.

Before stations start contending for channel access, HomePlug CSMA/CA defines a Priority Resolution Period (PRP) for service differentiation purpose. This is the first difference with 802.11 CSMA/CA mechanism [15]. When a PLC station receives payload data from a Higher Layer Entity (HLE), packets are assigned a Channel Access Priority (CAP) among 4 possible values, from the lowest priority CAP0, to the highest priority CAP3. The priority allocation depends on the traffic type, and is based upon the 802.1D standard [19]. The PRP is composed of two Priority Resolution Slots, PRS0 and PRS1, corresponding to the transmission of two OFDM symbols (cf. CSMA region depicted in

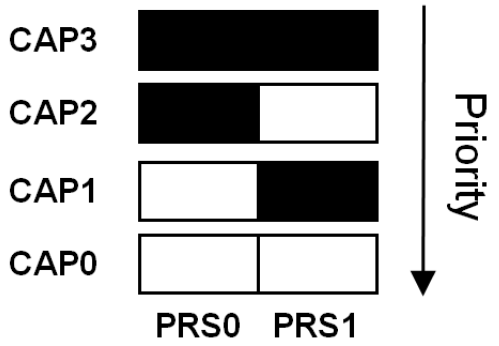

Figure 2.8: Priority Resolution Period (PRP).

Fig. 2.7). These two slots allow stations to assert their flow priorities on the medium, following the scheme depicted in Fig. 2.8. The first slot PRS0 is only filled by CAP2 and CAP3 contending stations. In such a case, CAP0 and CAP1 stations defer their access to a next transmission opportunity and the slot PRS1 will resolve priority accesses between CAP2 and CAP3 contending stations. If there is no CAP2 or CAP3 flow, the second slot PRS1 will resolve the priority access between stations contending at CAP0 and CAP1. Therefore, PRP ensures that only the stations with the highest priority traffic to send may contend for the medium in the contention period.

After the PRP comes the contention period, where a random backoff algorithm is used to disperse the times at which stations with queued frames attempt to transmit. This process allows to reduce the probability of collision between contending nodes, as each station determines a random time to wait before deciding to transmit. The second main difference between HomePlug and Wi-Fi CSMA/CA lies in their backoff algorithms, as HomePlug systems maintain three counters [73] instead of two, as the conventional IEEE 802.11 CSMA/CA [15]. The three counters are the Backoff Counter (BC), the Backoff Procedure event Counter (BPC) and, the new one, the Deferral Counter (DC). The BC corresponds to the number of contention slots the station has to wait, and it is set to any random value in the range [0, CW], where CW denotes the contention window size defined according to the transmission CAP and the number of transmission BPC (see Table 2.1). If the medium remains idle for a slot time, all contending stations decrement their BC while DC remains fixed. The first station whose BC reaches 0 gains access to the medium, and the transmission occurs. If the transmission is successful, BPC is reset to 0 for the next frame transmission. During the contention period, if the carrier sense reports that the medium state has become busy, the contending stations pause their BC and DC is decreased by one. Whenever a station experiences a collision, its BPC increases, and BC and DC are reset according to Table 2.1 schedule. The peculiarity of the HomePlug backoff procedure lies in the fact that BPC is also incremented by 1 if DC reaches 0. Thus, it allows to use the deferral information to reduce the collision probability (the higher is the number of contending stations, the more likely the DC will reach 0).

Table 2.1: CW and DC as a function of BPC and priority [17]

	CAP2 and CAP3	**CAP0 and CAP1**
BPC = 0	CW = 7, DC = 0	CW = 7, DC = 0
BPC = 1	CW = 15, DC = 1	CW = 15, DC = 1
BPC = 2	CW = 15, DC = 3	CW = 31, DC = 3
BPC = 3	CW = 31, DC = 15	CW = 63, DC = 15

TDMA in the Contention Free Period

If HomePlug CSMA/CA allows to differentiate applications using 4 different CAP values, there can never be QoS guarantees. Therefore, the HPAV specification introduced a contention free period using Time Division Multiple Access (TDMA) [59] (cf. Fig. 2.7). If a HLE or the CL wants to ensure a certain QoS level for a particular application, it requests the Connection Manager (CM) to establish a dedicated connection (the CM entity is presented in Fig. 2.9). Within an HPAV network, a connection corresponds to one or several links, depending on the unicast or multicast/broadcast nature of the flow, as well as the connection itself, which can be either unidirectional or bi-directional. Each link is uniquely identified in the AVLN thanks to its Link Identifier (LID), and can be either local or global. On the one hand, services using local links are directly monitored by the CM involved in the connection, and are transmitted in the CSMA region. On the other hand, global links are allocated by the CCo, at the source CM's request, which will then define a dedicated time interval for transmission within the Reserved Region. Based on the specifications of the requested connection, the CM can decide if a local or a global link should be used. TDMA sessions are directly monitored by the CCo, which announces TDMA schedules within the periodically transmitted beacon. As the CCo can retrieve information such as the number of pending packets left to transmit, as well as an estimation of the link data rate, it can adapt the TDMA interval length to maintain the desired level of QoS. Furthermore, HPAV introduced a persistent schedule technique allowing a station to still be able to precisely transmit in the slots it has been allocated by the CCo, even if it misses several beacons [74]. Within the home networking area, TDMA allocations are particularly suited to transport multicast video services, such as IPTV, as they need significant bandwidth and low latency delivery. However, TDMA channel access being an optional feature, most of current HPAV based systems only use CSMA/CA.

2.5.3.2 Framing Processes

Fig. 2.9 represents the protocol layer architecture of an HPAV system. The HPAV protocol stack can be split into two functional areas: the control plane and the data plane. Protocol entities that are involved in creating, managing and terminating the flow of data make up the control plane. The HPAV control plane is entirely contained in the CM entity. On the other hand, protocol entities involved in the transfer of user payload make up the data plane. The data plane defines the packets process chain, received from particular HLE at a dedicated Service Access Point (SAP), to the delivery of packets to the addressed HLE. Thus, it includes the HPAV MAC frame generation that will be part of a MAC frame stream, as well as the segmentation and encapsulation processes of this stream. In other

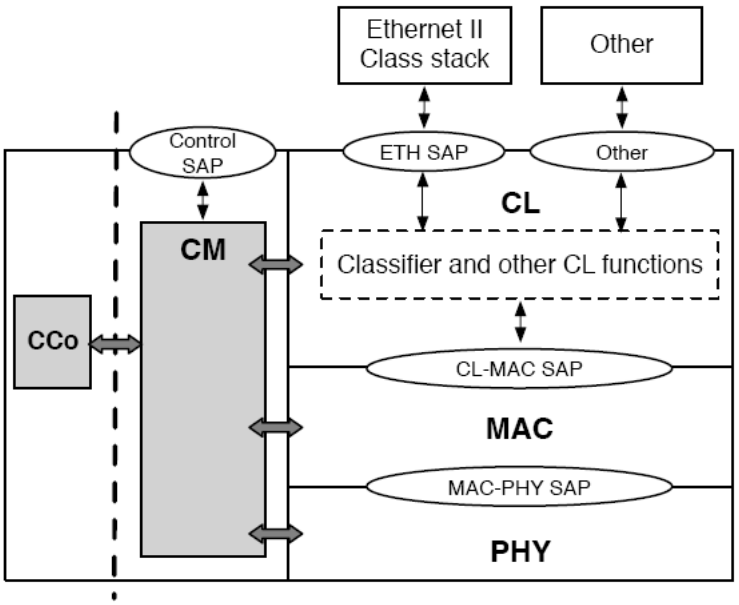

Figure 2.9: HPAV protocol layer architecture [87].

words, the data plane defines all functions that will process user data in the PLC network. These processes are detailed in the following.

HPAV MAC frame

HPAV distinguishes two types of MAC frames. On the one hand, there are MAC frames that encapsulate user payload, also called the MAC Service Data Unit (MSDU) payload. Note that a MSDU corresponds to data the overlying layer has requested the MAC to process, that is passed through the Data SAP at the M1 interface (see Fig. 2.6). On the other hand, MAC frames can encapsulate MSDUs that do not carry user payload: these are management messages, which come from the HPAV station itself (CM to CM communications, CM to CCo communications...). The MAC frame format is depicted in Fig. 2.10. It is prefixed by a 2-byte header, carrying information about the validity of the MAC frame, the presence or absence of an Arrival Time Stamp (ATS), and the length of the frame. An optional 4-byte ATS can be used by connection oriented transmissions, for jitter control purposes. In the case of management messages, the ATS is replaced by a random confounder that improves the encryption robustness against attacks. Then, the MAC frame either encapsulates MSDU payload or a management message, on which is computed a Integrity Check Value (ICV) that constitutes the last field of the MAC frame.

MAC Framing is a process by which MAC frames are enqueued in independent MAC frame streams (cf. Fig. 2.11). The HPAV MAC segregates MAC frames carrying MSDU payload based on the Destination TEI (DTEI), LID-tuple with which they are associated. MAC frames carrying MSDU payload and belonging to the same DTEI, LID are concate-

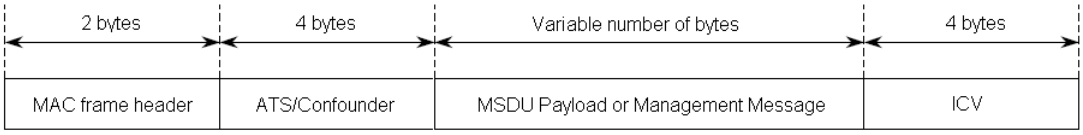

Figure 2.10: MAC frame format [4] [7].

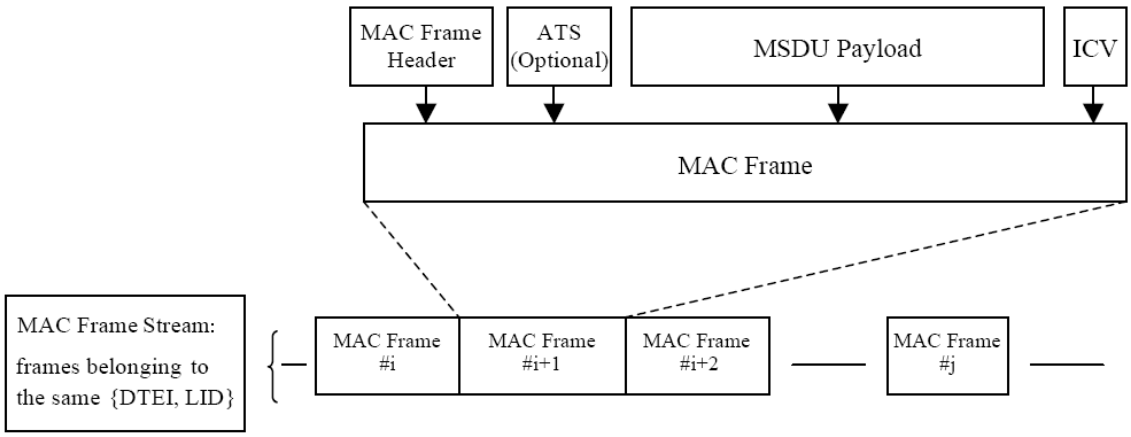

Figure 2.11: MAC frame stream generation.

nated to form a MAC frame stream, referred to as a "data stream". Concerning MAC frames carrying management messages, they are segregated simply using the DTEI with which they are associated. MAC frames carrying management messages and belonging to the same DTEI are also concatenated to form a MAC Frame Stream, but these streams are referred to as "Management Streams".

Segmentation

As it has been described in the previous section, using the MAC framing process, MAC frames are generated from MSDUs and multiple MAC frames that belong to the same stream are concatenated into MAC frame streams. The next step is to segment each MAC frame stream into 512-byte segments (cf. Fig. 2.12). These segments will be part of the MAC Protocol Data Unit (MPDU) payload. The segment can be considered as the basic transmitted entity, as each segment maps onto a single Forward Error Correction (FEC) block. Since PHY errors occur on a FEC block basis, segmentation ensures that only corrupted data will be retransmitted. Once a segment is generated from a MAC frame stream, it is firstly encrypted using the Network Encryption Key (NEK) of the AVLN. Then, it is encapsulated in Physical Block (PB), where it will constitute the PB

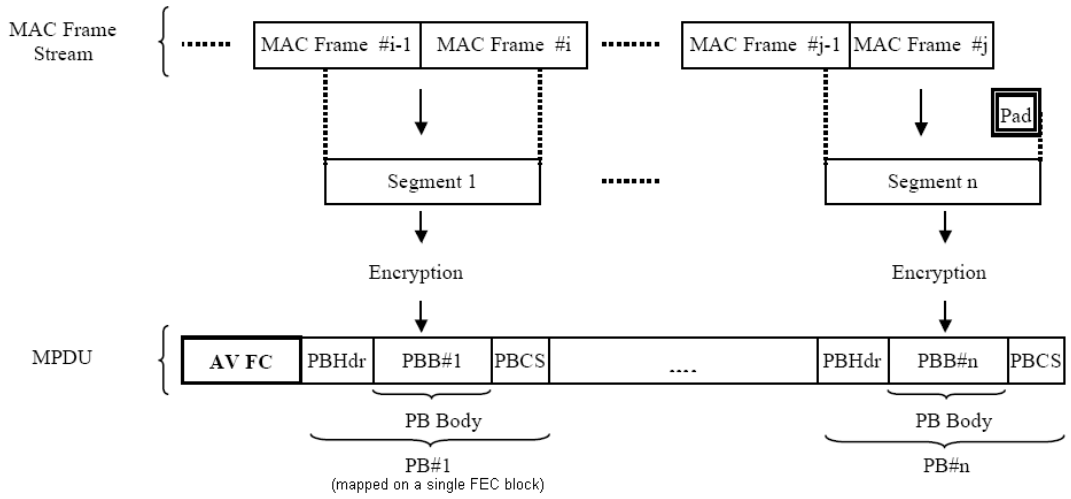

Figure 2.12: Construction of a MPDU.

Body (PBB). In Fig. 2.13 are presented the 520-byte and 136-byte PB (136-byte PBs can only be used for management purposes). The PB header contains the segment number, which is used for reassembly purposes, and the size of payload data it contains (the last segment may be padded). Finally, a PB Check Sequence (PBCS) is added to check data integrity at the receiver side.

Each time a station gains access to the channel, the number of transmitted segments is limited by the channel quality, the chosen FEC rate, and the maximum window of time the station is allowed to keep the channel (not the same in CSMA and TDMA regions). The segmentation process aims at improving the MAC efficiency, as it breaks dependency between the length of received MAC frame at M1 interface (see Fig. 2.6) and the transmission constraints inherent in the PLC network. Indeed, only part of MAC frames can be transported thanks to segmentation. However, segmentation increases complexity at the receiver side, where a reassembly process has to be performed to reconstruct the original MAC frame before handing it to the CL.

2.5.3.3 MPDU Format

The MPDU corresponds to the basic entity MAC layers of communicating stations will exchange. An MPDU is always prefixed by Frame Control (FC) information, and optionally followed by payload data containing segmented MSDUs. FC is used to communicate critical information to the receiver(s), such as the source and destination addresses, the frame duration, the tone map to use (cf. section 2.5.4.1)... HPAV defines four different MPDU frame formats [(1)], depicted in Fig. 2.14, depending on whether it carries MPDU payload or not, and if the AVLN is set in "AV only" or "Hybrid" mode. A short MPDU

[(1)]Note that HPAV 2 has added two new frame formats by defining a short delimiter used both for synchronization purposes and to transmit FC information. Therefore, it results in a reduced overhead, and can be used with both short and long MPDUs.

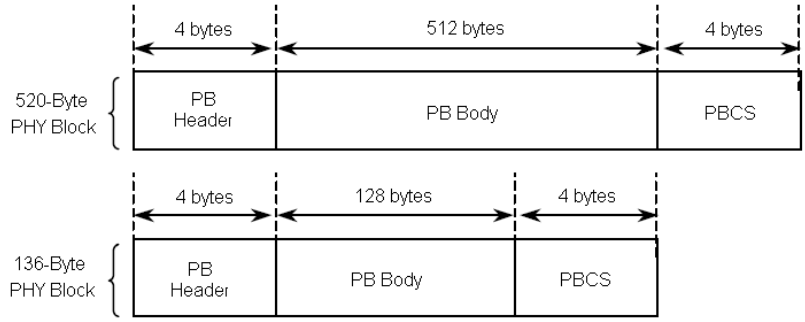

Figure 2.13: 520-byte and 136-byte PBs.

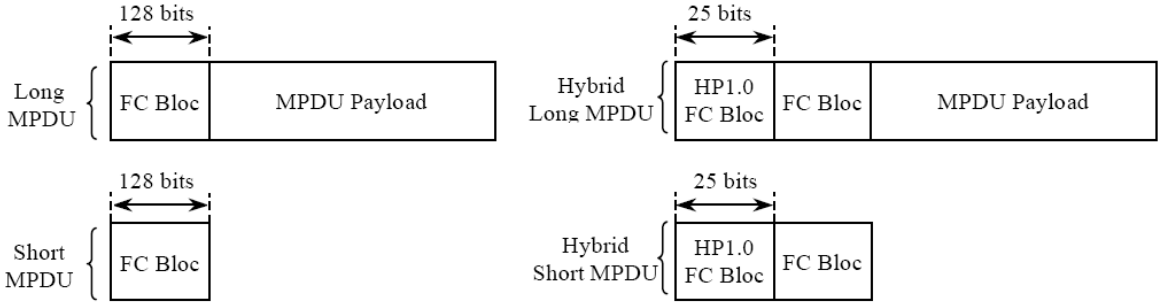

Figure 2.14: MPDU frame format: AV only mode on the left; Hybrid mode on the right [7].

only carries FC information. The Selective ACK (SACK) frames, communicating the correctness of the frame reception, and the Sounding (SOUND) frames, used for channel estimation purposes, use short MPDUs and therefore only carry FC information. On the other hand, a long MPDU also carries payload data. They are prefixed by FC information, followed by concatenated PBs, either carrying user or management data. If the AVLN is set in "AV only" mode, only HPAV-based stations are associated and authenticated in the network. If the AVLN is set in "Hybrid" mode, 25 bits of HomePlug 1.0.1 FC information are added to the HPAV FC, in order to be compatible with HP 1.0.1 legacy devices.

2.5.4 Physical Layer

2.5.4.1 Link Adaptation

The frequency selective nature of the PLC channel naturally led to choose Multicarrier Modulation (MCM) techniques, the most famous representant of this set being the Orthogonal Frequency Division Multiplexing (OFDM) modulation. However, the restrictive spectral mask imposed to PLC systems (cf. section 2.3) makes the classical OFDM, using a rectangular window, far from the optimal solution because of the bad spectral contain-

ment of the subcarriers[(2)]. So, HPAV uses a windowed OFDM modulation allowing to fit into the mask without losing too much spectral efficiency. In addition, the quasi-static nature of the PLC channel allows stations to adapt the transmitted signal to it [77]. Indeed, thanks to bit-loading algorithms, the number of bits transmitted on each active subcarrier is flexible and will depend upon the transmission environment. So, before two stations can start exchanging user data, the capacity of the link between the two nodes needs to be estimated. This process is performed at the receiver side, which computes the channel capacity thanks to specific "Sound" MPDUs, known by all HPAV stations. This stage results in the definition of a table describing the modulation orders to be used per subcarrier, also called a tone map, that the receiver will communicate to the transmitter. User data will then be transmitted by mapping the PBs on OFDM symbols following the dedicated tone map to the link. Note that the channel estimation procedure does not uniquely limit to the definition of a tone map. It is always associated with a FEC rate and a Guard Interval (see Chapter 3) to be used on the link.

While all active links of the AVLN are given a default tone map that can be used in any portion of the beacon period, HPAV allows the definition of mutiple tone maps per link. Indeed, channel and noise characteristics over powerlines tend to be periodic with respect to the underlying AC line cycle [70], [42], [49]. Therefore, it is possible for a tone map to be only made valid for a specific region of the beacon period. This feature is extremely useful in the case where short intervals of the AC line cycle are subject to periodic impulsive noise, as it avoids choosing the "worst case" PHY parameters within the considered period. However, if this adaptation to the channel capacity allows to approach the theoretical capacity of the channel at a given moment, there will obviously be a tradeoff involved in the choice of number of regions and the system performance/complexity, as it was shown in [75]. Moreover, the PB error rate is always monitored at the receiver side to adapt to unexpected variations of the channel, by communicating slight modifications of the current tone map to the transmitter.

2.5.4.2 PPDU Format

The PHY Protocol Data Unit (PPDU) corresponds to the physical entity that is exchanged between stations on the transmission medium. PPDUs are generated by the Physical (PHY) layer, which are then transmitted on the power line. Fig. 2.15 presents the transmission scheme that is used when an HPAV network is set in "HPAV only" mode. In this mode, the PPDU firstly consists of a preamble that is used by the receiver for detection and synchronization purposes. The preamble is followed by FC fields that are used by the MAC for management purposes. As FC contains critical information, it is transmitted using a Robust OFDM (ROBO) modulation scheme that ensures error free transmissions, by applying a low modulation order on every subcarrier of the OFDM symbol and by repeating information data several times. Note that the ROBO mode is also used for beacon transmissions, exchange of management messages and broadcast and multicast communication. FC is followed by the MPDU payload consisting of one or more forward error coded PBs. PBs are mapped on bit-loaded OFDM symbols, following the tone map dedicated to the link. When a station gains access to the medium, the maximum window that is allocated for transmission is limited. Considering the CSMA region, this

[(2)]Note that this section only gives a general overview of the frame formats exchanged between PHY layers. The windowed OFDM modulation is studied in Chapter 3.

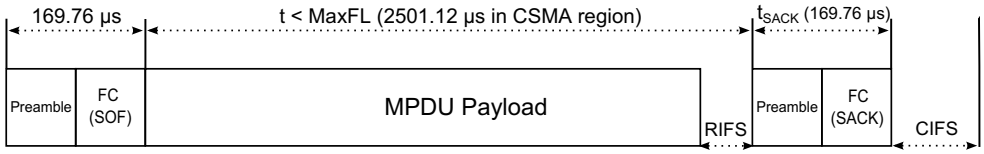

Figure 2.15: The HPAV transmission scheme (AV only mode).

window must not exceed 2.5 ms in order to limit the effect of collisions on the network (inside the TDMA region, this limit is extended to 5 ms). HomePlug AV uses Automatic Repeat reQuest (ARQ) at a segment level. As segments are numbered, corrupted PBs are identified at the receiver side. If errors occur during a transmission, the receiving station communicates which PBs must be retransmitted through the SACK frame that follows every point-to-point transmission. Finally, note that PLC networks may be subject to the hidden node problem, as the signal may be strongly attenuated. In such a case, it is possible to use a Request To Send (RTS)/Clear To Send (CTS) mechanism, as it is done in 802.11 networks. RTS and CTS frames offer a much better protection against collison. Before a payload transmission can occur, the transmitter sends a RTS frame and the station addressed responds with a CTS frame. Only then will the initiator send the data frame intended for the addressed station. With these two short and robust frames, all stations in the initiator and the replier's Phy networks are refrained from transmitting.

2.6 Conclusion

In this Chapter, an overview of the in-home PLC environment has been proposed. The multipath nature of the channel and the various sources of interference make it a very harsh transmission medium. Therefore, current broadband PLC networks, mostly following the HPAV specification, must implement advanced transmission techniques to ensure reliable message deliveries. On the Physical layer, an OFDM-based modulation scheme is used to fight interference caused by multipath propagation, and the MAC layer implements ARQ mechanisms allowing to efficiently react to unexpected events, such as asynchronous impulsive noise.

Nevertheless, HPAV networks cannot answer to all the use cases current home networks may be subject to, as the network capacity is easily reached as soon as multiple bandwidth-greedy streams are launched simultaneously (e.g. HD videos, file transfers...). So, increasing the capacity of PLC networks is still a high-priority necessity and that is why the HPAV 2 specification extends the current bandwidth used by HPAV.

In the following of this document, the France Télécom PLC channel generator [106] and the Omega GBN model proposed in [52] are used as reference models.

Chapter 3

Capacity Analysis in the HomePlug AV1 and AV2 contexts

3.1 Preliminary

3.1.1 Context of this Study: the OMEGA Project

The work presented in this Chapter was conducted for an FP7-supported project, called OMEGA [51], that Orange has led from January 2008 to December 2010. OMEGA is one of the roots of the current IEEE P1905 standardization effort that is mainly supported by Orange and Qualcomm. The goal of this project was to set a new standard for home networks that would take advantage of existing connectivity solutions present in the Home area, including Wi-Fi, Ethernet or PLC, as well as emerging technologies, such as Visible Light Communication (VLC) or 60 GHz Wireless Personal Area Networks (WPAN). The capacity target for OMEGA networks is to provide 1 Gbps LANs everywhere in the home by combining these various technologies. The core of this project concerns the definition of a so-called "inter-MAC", a layer 2.5 that allows to hide the heterogeneity of the underlying connectivity solutions to any HLE. This inter-MAC is in charge of forwarding incoming packets to the appropriate interface, depending on the destination to reach, as well as associating a packet to the appropriate service class from which it belongs to. OMEGA networks also define end-to-end QoS and security supports to deliver constrained services. Another benefit of this new layer concerns the home network area extension, thanks to inter-technology bridging. In addition, the reliability can be improved by taking advantage of path redundancy in the heterogeneous network. Broadband PLC was one of the studied connectivity solutions, and this Chapter presents part of the propositions made by Orange to improve the Physical layer of PLC networks [53]. This work led to publications in [28], [29] and [32]. When this study was conducted in 2009 and at the beginning of 2010, HPAV was undoubtedly the most implemented specification in broadband PLC systems. Therefore, this specification was naturally chosen as baseline technology to establish comparisons. Since the release of the HPAV specification in 2005, PLC has been considered as a viable solution to deliver multimedia services throughout the home. However, considering the maximum 200 Mbps that HPAV networks can provide at the physical layer, a significant effort had to be made to extend this capacity to reach OMEGA 1 Gbps target. So, the goal of this study was to firstly extend the useful bandwidth of PLC networks up

to 87.5 MHz, which corresponds pretty much to the maximum bandwidth that will use future HPAV 2 systems (up to 86 MHz). Secondly, we aim at investigating an alternate modulation solution, called OFDM/OQAM, that holds very interesting properties in the particular context of powerline communications.

3.1.2 What Modulation Scheme for Broadband PLC Networks?

While the potential benefits of the technology are well identified, PLC posed several challenges to the researchers community. Indeed, the power grid is clearly not designed to support broadband communications. On the one hand, the medium is strongly disturbed, being subject to different kinds of interference and, on the other hand, the electromagnetic radiations induced by power lines strongly limit the maximum authorized power level at the transmitter side. Moreover, protecting the multiple radio applications located in the [1.8; 30] MHz band resulted in the definition of a quite severe transmission mask (see section 2.4 on page 10). The frequency selective nature of the PLC channel makes MCM techniques a natural choice. However, the most famous representant of this set, known as the Orthogonal Frequency Division Multiplexing (OFDM) modulation, defines rectangularly shaped symbols, resulting in badly localized subcarriers in frequency. Consequently, this scheme is clearly not adapted to the restrictive spectral mask imposed to PLC systems because a large number of subcarriers would have to be switched off in order to generate a signal which PSD fits into the mask. So, HPAV defines a windowed OFDM modulation, derived from the CP-OFDM scheme (OFDM with Cyclic Prefix), allowing to fit into the transmission mask without losing too much spectral efficiency. However, with windowed OFDM, the effective protection against Inter-Symbol Interference (ISI) and Inter-Carrier Interference (ICI) is reduced in proportion of the Roll-off Interval (RI) length required for the windowing operation. Consequently, other solutions have been proposed. For example, Filtered Multi Tone (FMT) was studied in the scope of OMEGA as it can provide efficient notching in frequency [53], the counterpart of it being that it introduces an overhead because of the oversampling factor. Considering the IEEE P1901 standard [7], an alternative MCM scheme to the HPAV windowed OFDM was proposed: the Wavelet OFDM modulation. This solution can achieve deeper notches than traditional OFDM and does not require any guard interval. Wavelet OFDM is actually really close to the scheme we present in the following, called OFDM/OQAM, where OQAM stands for Offset Quadrature Amplitude Modulation [100], or Hermitian Symmetric OQAM (HS-OQAM) (Hermitian Symmetric version of OFDM/OQAM) [83]. In this chapter, we are going to show that this modulation offers a good response to PLC requirements by bringing major advantages compared to windowed OFDM. Since OFDM/OQAM relaxes the orthogonality condition in the real field, the shaping of the OQAM symbols is allowed so that a better selectivity in frequency can be obtained. So, it seems obvious that the degree of freedom offered by OFDM/OQAM in the pulse shaping can be easily exploited in the PLC context to perfectly fit into the spectral mask imposed by the authorities. Moreover, HS-OQAM does not use any CP, which naturally leads to a higher throughput, the counterpart of this being an increased sensitivity to ISI and ICI compared to windowed OFDM.

The benefit of OFDM/OQAM considering the spectral notching imposed to PLC systems was originally highlighted in [102]. Furthermore, this Chapter can be considered as an extension of the work presented in [84], in which a comparison between OFDM and HS-OQAM had been conducted. We extend this work by firstly comparing HS-OQAM to

the windowed OFDM scheme defined by the HPAV specification. We then compare the two modulation schemes in a useful bandwidth going up to 87.5 MHz, that will be referred to as the HPAV 2 context. But before interesting ourselves to the results of this comparison, we firstly present the windowed OFDM modulation used in HPAV networks, and we highlight the inherent limitations of this scheme. Then, we introduce the OFDM/OQAM modulation, presenting its main principle. A main advantage of this modulation comes from the latitude it gives in the shaping of the prototype filters. So, a section is dedicated to highlight the set of filters that are the most appropriate in the PLC context. We also evaluate the opportunity to associate OFDM/OQAM with a slightly more complex equalization technique than the 1-tap Zero Forcing (ZF) that is classically used with OFDM modulation. Finally, the comparison between the achievable throughput of the two modulation schemes is performed following the HPAV 1 and HPAV 2 specifications, considering various channel conditions.

3.1.3 Transmission Capacity and Achievable Throughput

The HPAV specification offers the possibility to finely adapt the transmitted signal to the channel. This process, performed at the receiver side after sounding the channel linking two communicating stations, consists in finding the optimal combination of the FEC rate, the Guard Interval (GI) length and, the appropriate QAM constellation for each subcarrier, according to a target error rate. In the following, we only consider this last process, called bit-loading. Applying a bit-loading algorithm on a particular channel results in the definition of a "tone map", that describes the number of carried bits per subcarrier on the frequency multiplex. To evaluate the quality of the m-*th* subchannel, the Signal to Interference plus Noise Ratio (SINR) needs to be evaluated after equalization. This metric depends upon the attenuation, the interference and the noise levels affecting the m-*th* subchannel $\forall m \in \mathbb{M}$, with $\mathbb{M} = \{1, .., M\}$. Assuming an OFDM system associated with a 1-tap ZF equalization, it can be approximated as [99], [92]:

$$\mathrm{SINR}[m] \approx \frac{\sigma_c^2}{\frac{\sigma_n^2[m]}{|H_m|^2} + \frac{P_{\mathrm{ISI+ICI}}[m]}{|H_m|^2}} \tag{3.1}$$

in which σ_c^2 denotes the variance of the transmitted symbols and H_m, $\sigma_n^2[m]$ and $P_{\mathrm{ISI+ICI}}[m]$ are the frequency channel coefficients, the colored noise level and the interference level at the m-*th* subcarrier, respectively. Concerning the interference term, it directly depends upon the considered modulation scheme. In section 3.2.3 [28], we highlight the interference that may be created because of the windowing process that is performed by HPAV systems. In section 3.3.2.2, we establish a generalized expression of the OFDM/OQAM interference term. Then, to evaluate the number of bits that can be transmitted in a given subchannel, we use the capacity formula (in bits/symbol) that reads, for the m-*th* subchannel:

$$C[m] = \log_2\left(1 + \frac{\mathrm{SINR}[m]}{\Gamma}\right) \tag{3.2}$$

where Γ is the SINR gap defined for a target Symbol Error Rate (SER) by [48]:

$$\Gamma = \frac{1}{3}\left[Q^{-1}\left(\frac{\mathrm{SER}}{4}\right)\right]^2 \tag{3.3}$$

in which $Q^{-1}(x)$ is the inverse tail probability of the standard normal distribution. Then the transmission capacity (in bits/second), assuming constellations of infinite granularity, meaning that each subcarrier can carry a fractional and unbounded number of bits, can be obtained with the following formula:

$$D^{inf\ gran} = \sum_{m \in \mathbb{M}_u} F_0 \frac{M}{M + L_{\mathrm{GI}}} C[m] \tag{3.4}$$

where $F_0 = 24.414$ kHz is the frequency spacing between two subcarriers, L_{GI} is the Guard Interval length in samples (cf. section 3.2.1), and $\mathbb{M}_u$ is the set of active tones (917 in HPAV using windowed OFDM). Note that this bit-loading algorithm only guarantees a peak SER condition per subcarrier. However, the choice of a given bit-loading algorithm will not significantly impact the comparison presented in this Chapter. Note also that the HPAV specification defines GI either lasting 5.56 μs, 7.56 μs or 47.12 μs corresponding to 417, 567 and 3534 samples, respectively. It has been shown that using a GI ensuring ISI-free transmissions does not necessarily lead to a maximization of the capacity [54]. According to our simulations, the smallest GI always provided better results in spite of an increased interference term. So, in all our simulations, we fixed L_{GI} to 417 samples not to penalize the windowed OFDM modulation, compared to OFDM/OQAM.

In practice, only an integer and bounded number of bits per subcarrier can be transmitted, such that the achievable throughput, also denoted as the PHY data rate, is expressed as follows:

$$D^{\mathrm{PHY}} = \sum_{m \in \mathbb{M}_u} F_0 \frac{M}{M + L_{\mathrm{GI}}} T[m], \tag{3.5}$$

where $T[m]$ is the tone map dedicated to the considered channel that gives the actual number of carried bits per subcarrier:

$$T[m] = \underset{b \in \mathrm{E}_{\mathrm{const}}}{\arg\max} \{b | b \leq C[m]\},\ \forall m \in \mathbb{M}_u, \tag{3.6}$$

where $\mathrm{E}_{\mathrm{const}}$ contains the actual number of bits a single subcarrier can carry. Considering HPAV specification, the possible constellations are BPSK, 4-QAM, 8-PSK, 16-QAM, 64-QAM, 256-QAM and 1024-QAM. So, we have $\mathbb{E}_{const} = \{1, 2, 3, 4, 6, 8, 10\}$, with $b_{max} = \max\{\mathbb{E}_{const}\} = 10$.

3.2 Windowed OFDM: Study and Analysis of the HPAV Modulation Scheme

3.2.1 OFDM Principle

The multipath nature of the PLC channel appears through frequency fadings that result from the combinations of the multiple received signal echoes. Depending on the considered frequency, the phase shift between the different paths may result in either destructive or constructive combinations. The channel delay spread, representing the time window during which an energy impulse is spread when passing through the channel, is directly related to the number of frequency fadings: a simple rule states that the periodicity of the frequency fadings is inversely proportional to the channel delay spread. The multipath

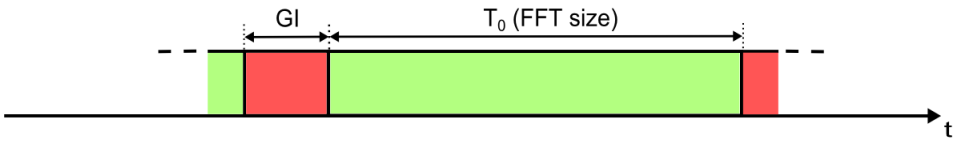

Figure 3.1: CP-OFDM timing.

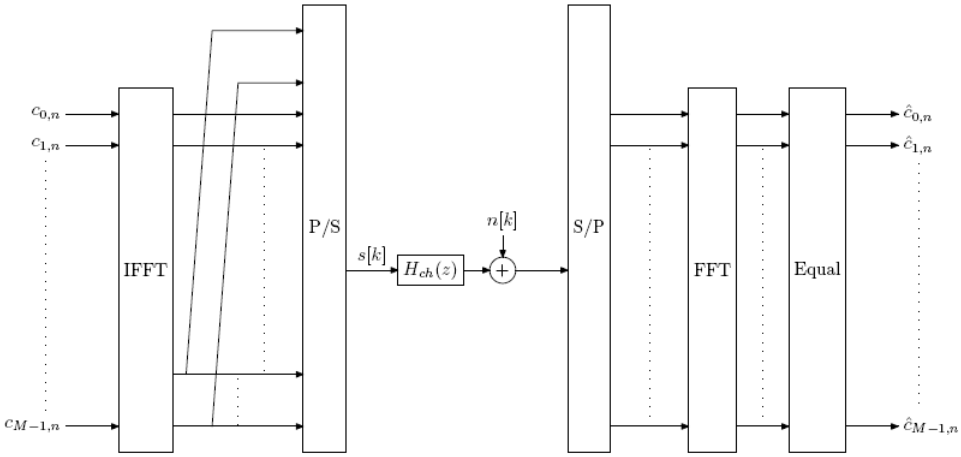

Figure 3.2: Efficient Implementation of CP-OFDM [82].

characteristic of the PLC channel has strong implications on the dimensioning of the transmitted signal. Indeed, if we use a single carrier modulation over a frequency selective channel, performant equalization techniques must be used to mitigate the signal distortion caused by the channel, as well as to cancel ISI caused by replicates of the previously transmitted symbols on the current symbol to estimate.

Instead of using single carrier modulations, the OFDM modulation can provide an efficient and simple alternative to provide broadband communication over frequency selective channels. The main concept of OFDM lies in the choice that is made of transmitting simultaneously M symbols over M slowly modulated subcarriers of frequency spacing $F_0 = \frac{1}{T_0}$, T_0 being the OFDM symbol duration. The idea behind OFDM modulation is that the wideband channel is divided into narrow band sub-channels so that each subchannel stream experiences a quasi flat frequency response. Moreover, as the interference is only located at the beginning of the transmitted symbol, it can be totally suppressed using a Guard Interval that will absorb all replicates of the previous OFDM symbol. Generally, the GI is constructed by prefixing each OFDM symbol with a so-called Cyclic-Prefix (CP), by adding the end of the transmitted symbol before its start to absorb the interference induced by the dispersive channel (ICI and ISI). In addition to isolating interference, the CP reduces the receiver sensitivity to time synchronization errors. Considering an interference-free transmission, CP-OFDM only needs a simple ZF equalization to be performed at the receiver side, multiplying each subcarrier by the inverse of the estimated

subchannel coefficient. Fig. 3.1 highlights the CP-OFDM timing, that includes the actual OFDM symbol of duration T_0, prefixed by its GI.

OFDM uses the principle of Fourier series decomposition allowing to express any periodic signal by projecting it on an orthogonal basis of sine and cosine functions. To generate an OFDM signal, an M-dimensional basis of orthogonal cosine and sine functions using a fundamental frequency of F_0 and the following overtones is needed. Then, the in-phase and quadrature components at each frequency can be used as independent subchannels to transmit complex symbols. Finally, the continuous time expression of a baseband OFDM signal can be simply written as the Inverse Fourier Transform of the M complex symbols simultaneously transmitted in the frequency multiplex:

$$s(t) = \sum_{m=0}^{M-1} \sum_{n\in\mathbb{Z}} c_{m,n} \Pi_{T_0}(t - nT_0)\, e^{j2\pi m F_0 t}, \tag{3.7}$$

where $c_{m,n} = c^R_{m,n} + j c^I_{m,n}$ is the complex-valued QAM symbol transmitted over the m-*th* subcarrier of the n-*th* OFDM symbol, and where $\Pi_{T_0}(t)$ is the rectangular function, equal to 1 for $t \in [0, T_0]$ and 0 elsewhere. However, as it was aforementioned, OFDM is classically associated with a CP, so that the CP-OFDM signal simply reads:

$$s(t) = \sum_{m=0}^{M-1} \sum_{n\in\mathbb{Z}} c_{m,n} \Pi_{T_0+\mathrm{GI}}(t - n(T_0 + \mathrm{GI}))\, e^{j2\pi m F_0 t}. \tag{3.8}$$

In practice, the OFDM signal is generated as depicted on Fig. 3.2, using the Inverse Fast Fourier Transform (IFFT) algorithm, resulting in a discrete time signal composed of M samples. The last L_{GI} samples are then copied before the first sample, resulting in the discrete CP-OFDM signal that reads:

$$s[k] = \sum_{m=0}^{M-1} \sum_{n\in\mathbb{Z}} c_{m,n} \Pi_{M+L_{\mathrm{GI}}}[k - n(M + L_{\mathrm{GI}})]\, e^{j2\pi \frac{km}{M}}, \tag{3.9}$$

where $\Pi_{M+L_{\mathrm{GI}}}[k - n(M + L_{\mathrm{GI}})]$ corresponds to the discrete rectangular function, equal to 1 for $k \in \{1, .., M + L_{\mathrm{GI}}\}$ and 0 elsewhere. After a parallel to serial conversion, the $M + L_{\mathrm{GI}}$ samples are passed through a Digital to Analog Converter (DAC) to generate the continuous signal. At the receiver side, the inverse operation is performed, by firstly removing the GI and computing an M-point Fast Fourier Transform (FFT) with the M remaining samples. Note that, if we consider the general case, (3.8) is a complex-valued signal as it is not hermitian symmetric. In order to directly generate a real baseband signal, the IFFT size is generally doubled to impose the following condition at the IFFT input:

$$\begin{cases} c_{m,n} = c^*_{M-m,n} \\ c_{0,n} = c_{M/2,n} = 0 \end{cases} \tag{3.10}$$

If we take a closer look to each subcarrier signal spectrum around a subset of subcarriers, as Fig. 3.3 shows, we easily verify the orthogonality in frequency. Indeed, at each subcarrier frequency (dot on the peak), all other subcarriers do not contribute to the overall waveform (dot at zero). The spectral efficiency of OFDM directly comes from this orthogonality condition being verified between the M adjacent subcarriers. On the other

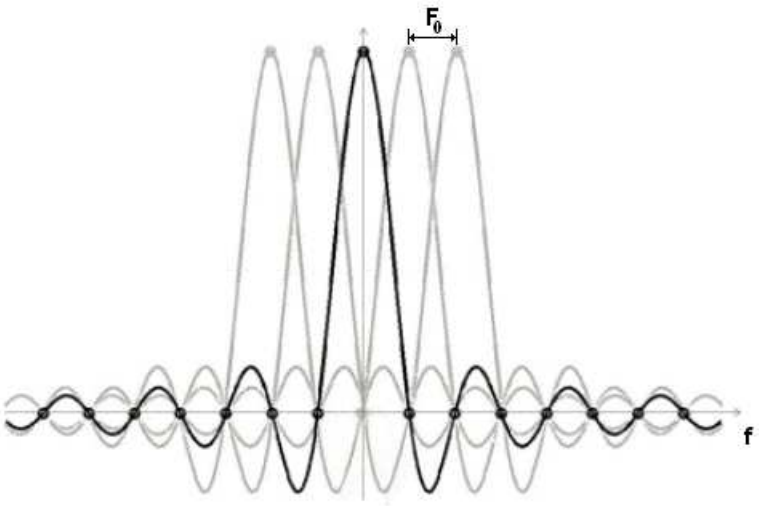

Figure 3.3: Frequency Orthogonality of an OFDM Signal.

hand, Fig. 3.3 also highlights two main drawbacks of this modulation. Firstly, OFDM is sensitive to frequency shifts, which cause Inter Carrier Interference. ICI is classically caused by frequency synchronisation offset between transmitters, or by the presence of Doppler effect causing frequency spreading of the energy. Secondly, if the OFDM symbols are well localized in time using periodic rectangular windows, ensuring the time orthogonality between consecutive symbols, this results in badly contained subcarriers following a sinc function in frequency. As we will see in the following, this constitutes a main limitation for the classical OFDM modulation in the context of PLC.

3.2.2 The Windowed OFDM Modulation

The radiated power induced by the power lines resulted in the definition of a quite severe transmission mask imposed to HPAV devices, limiting the transmitted power to -50 dBm/Hz, and imposing several notches in which the transmitted power has to be reduced under -80 dBm/Hz to protect other applications, such as amateur radio. The classical CP-OFDM modulation, with its rectangularly shaped symbols, cannot provide a frequency containment of its subcarriers good enough to simultaneously get a suitable spectral efficiency and respect the transmission mask. So, the HPAV specification defines a windowed OFDM (also denoted as Pulse-Shaped OFDM, PS-OFDM [101]) scheme whereby the symbols are softened on their borders on a Roll-off Interval (RI) [33], thus limiting the number of subcarriers that have to be switched off at the edges of the notches. This modulation is directly derived from the CP-OFDM technique, but the windowed OFDM scheme differs from CP-OFDM by adding a stage after the prefix addition where the symbols are filtered. Fig. 3.4 describes the windowing scheme, where it can be seen that unlike conventional CP-OFDM, the CP length is equal to GI+RI, in which GI $= L_{\mathrm{GI}}T_s$ denotes the conventional CP length and RI $= L_{\mathrm{RI}}T_s$ denotes the roll-off interval, T_s being the sampling period. After GI+RI addition, each OFDM symbol is filtered to soften its borders, on a time interval corresponding to RI. The discrete-time expression of the transmitted

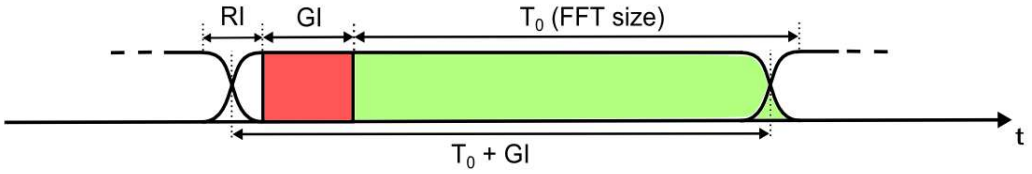

Figure 3.4: Windowed OFDM timing.

windowed OFDM symbols reads:

$$s[k] = \sum_{m=0}^{M-1} \sum_{n \in \mathbb{Z}} c_{m,n} g\left[k - n\left(M + L_{\mathrm{GI}}\right)\right] e^{j2\pi \frac{km}{M}}, \tag{3.11}$$

where M is the IFFT size, L_{GI} the Guard Interval length in samples, g is the symbol window of length $M + L_{\mathrm{GI}} + L_{\mathrm{RI}}$ and $c_{m,n}$ is the complex QAM symbol located at the m-*th* subcarrier of the n-*th* OFDM symbol. Note that the window shape in the roll-off interval defined by HPAV actually corresponds to a piecewise linear function [33]. This interval also corresponds to the overlapping duration between two consecutive symbols. This windowing operation allows the modulated signal PSD to exactly fit into the tone mask (see Fig. 3.5). Considering the HPAV specification, the real valued discrete-time baseband signal is provided at a sampling rate of 75 MHz and using a 3072-point IFFT. 1155 carriers are employed in the range from 1.8 MHz to 30 MHz. The default HPAV tone map includes 917 active carriers among the 1155 ones, the remaining carriers being switched off. Also, note that the subcarriers are separated by a frequency spacing $F_0 = 24.414$ kHz, corresponding to a symbol duration $T_0 = 40.96\ \mu s$, that the Roll-off interval $RI = 4.96\ \mu s$ and that the Guard Interval GI can take three different values: 5.56 μs, 7.56 μs, 47.12 μs. At the receiver side, before applying the classical FFT demodulation, each symbol is processed as follows (cf. Fig. 3.6):

- Serial to parallel conversion for each block of size $M + L_{\mathrm{GI}}$;
- Remove the first L_{GI} samples of each block;
- Move the first L_{RI} samples to the end for each block.

3.2.3 Windowed OFDM Transmission over a Dispersive Channel

In this Chapter, we aim at evaluating the achievable throughput of the windowed OFDM transmission scheme, and compare it to the achievable throughput of the OFDM/OQAM modulation (introduced in section 3.3). The computation of the capacity needs the knowledge of the Signal to Interference plus Noise Ratio (SINR) at the receiver that will be computed on a subcarrier basis to perform bit-loading (see section 3.1.3). As it is commonly done for CP-OFDM, a simple Zero-Forcing (ZF) equalization is performed at the receiver side. With that assumption, the SINR at the m-*th* subcarrier reads:

$$\mathrm{SINR}[m] \approx \frac{\sigma_c^2[m]}{\frac{\sigma_n^2[m]}{|H_m|^2} + \frac{P_{\mathrm{ISI+ICI}}^{\mathrm{Win}}[m]}{|H_m|^2}} \tag{3.12}$$

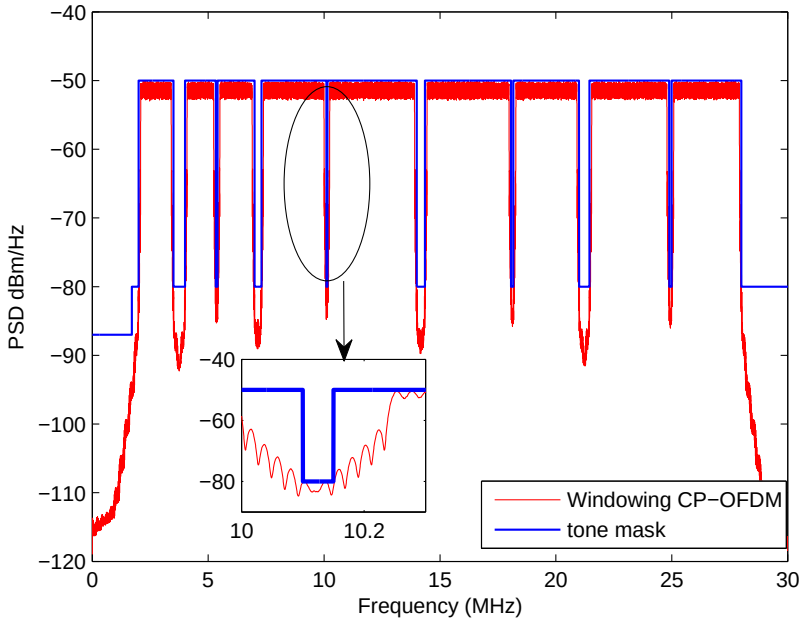

Figure 3.5: Windowed OFDM using HPAV tone map fits into the FCC Spectrum Mask.

in which $\sigma_c^2[m]$ denotes the variance of the transmitted symbols and H_m, $\sigma_n^2[m]$ and $P_{\text{ISI+ICI}}^{\text{Win}}[m]$ are, respectively, the frequency channel coefficient, the colored noise level and the interference level at the m-*th* subcarrier.

If the windowing scheme introduced by HPAV allows to keep the same transmission efficiency as the equivalent CP-OFDM scheme while fitting into the transmission mask, Fig. 3.6 clearly highlights that the L_{RI} samples that are directly copied from the GI to demodulate the OFDM signal may result in an increase of the interference level. Indeed, an interference occurs as soon as the channel impulse response length L_h becomes longer than $^{(1)}L_{\text{GI}} - L_{\text{RI}}$. A way to deduce the interference power for windowed OFDM was firstly presented in [54]. In the following, we present a direct calculation to obtain the analytical expression of this interference term. Firstly, let us introduce the main parameters for this calculation:

- $c_{m,n}$: Complex QAM, 8-PSK or BPSK symbol located at the m-*th* subcarrier of the n-*th* OFDM symbol, which variance $\sigma_c^2[m]$ depends upon the transmission mask;
- T_s: Sampling period;
- $GI = L_{\text{GI}}T_s$: Guard Interval;
- $RI = L_{\text{RI}}T_s$: Roll-off interval;
- $T_0 = MT_s$: FFT window;
- $F_0 = \frac{1}{T_0}$: frequency spacing between adjacent carriers;

(1) We chose to conserve the terminology used in the specification but it has to be underlined that the time interval designated by *GI* in HPAV does not define, strictly speaking, a *Guard Interval*.

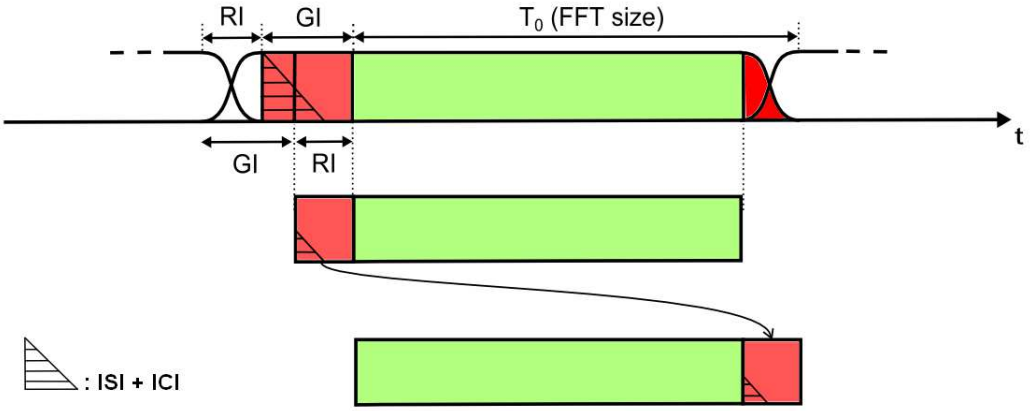

Figure 3.6: Window and GI removal at the receiver side.

- $T = (L_{\text{GI}} + M)T_s$: symbol period;
- $g(t)$: OFDM symbol window (of length $RI + GI + T_0$);
- $f(t)$: FFT window (of length T_0);
- $h(t) = \sum_{i=0}^{P-1} h_i \delta(\tau - \tau_i)$: multipath channel impulse response.

Then, the continuous time expression of the transmitted windowed OFDM symbols is given by:

$$s(t) = \sum_{m=0}^{M-1} \sum_{n=-\infty}^{+\infty} c_{m,n} g(t - nT) e^{j2\pi m F_0 t}, \tag{3.13}$$

in which the $c_{m,n}$ must be hermitian symmetric in order to generate a real baseband signal, meaning that:

$$\begin{cases} c_{m,n} = c^*_{M-m,n} \\ c_{0,n} = c_{M/2,n} = 0 \end{cases}. \tag{3.14}$$

Noise taken apart, the received signal $y(t) = h(t) * s(t)$ reads:

$$y(t) = \sum_{i=0}^{P-1} h_i \sum_{m=0}^{M-1} \sum_{n=-\infty}^{+\infty} c_{m,n} g(t - nT - \tau_i) e^{j2\pi m F_0 (t-\tau_i)}. \tag{3.15}$$

Windowed OFDM demodulation:

To recover the QAM symbol c_{m_0,n_0}, we first compute the demodulated signal as follows

$$y_{m_0,n_0} = \int_{-\infty}^{+\infty} y(t) f^*_{m_0,n_0}(t) dt \tag{3.16}$$

with $f^*_{m_0,n_0}(t) = f(t - n_0T)e^{-j2\pi m_0F_0t}$, which leads to

$$y_{m_0,n_0} = \sum_{m=0}^{M-1}\sum_{n=-\infty}^{+\infty} c_{m,n}\sum_{i=0}^{P-1} h_i e^{-j2\pi mF_0\tau_i} \times \int_{-\infty}^{+\infty} g(t - nT - \tau_i)f(t - n_0T)e^{j2\pi(m-m_0)F_0t}dt \tag{3.17}$$

where $f(t) = \Pi_{T_0}(t - \frac{GI-RI}{2})$ and corresponds to the FFT window. Note that we introduce this $\frac{(GI-RI)}{2}$ delay because we consider $g(t)$ centered at the time origin. Then, to obtain a more tractable expression, we proceed to a change of variables by setting:

$$\begin{cases} t - nT - \tau_i = \mu + \frac{\tau'}{2} \\ t - n_0T = \mu - \frac{\tau'}{2} \end{cases}. \tag{3.18}$$

Then (3.17) can be rewritten as

$$\begin{aligned} y_{m_0,n_0} = &\sum_{m=0}^{M-1}\sum_{n=-\infty}^{+\infty} c_{m,n}\sum_{i=0}^{P-1} h_i e^{-j2\pi mF_0\tau_i} \\ &\times \int_{-\infty}^{+\infty} g(\mu + \frac{\tau'}{2})f(\mu - \frac{\tau'}{2})e^{j2\pi(m-m_0)F_0\mu}d\mu \\ &\times e^{j2\pi(m-m_0)F_0(\frac{(n+n_0)}{2}T + \frac{\tau_i}{2})} \end{aligned}$$

Setting $\nu = -(m - m_0)F_0$, we get:

$$\begin{aligned} y_{m_0,n_0} = &\sum_{m=0}^{M-1}\sum_{n=-\infty}^{+\infty} c_{m,n}\sum_{i=0}^{P-1} h_i e^{-j2\pi mF_0\tau_i} \\ &\times \underbrace{\int_{-\infty}^{+\infty} g(\mu + \frac{\tau'}{2})f(\mu - \frac{\tau'}{2})e^{-j2\pi\nu\mu}d\mu}_{A_{g,f}(\tau',\nu)} \\ &\times e^{j2\pi(m-m_0)F_0(\frac{(n+n_0)}{2}T + \frac{\tau_i}{2})} \end{aligned} \tag{3.19}$$

where $A_{g,f}(\tau, \nu)$ is the cross-ambiguity function between $g(t)$ and $f(t)$ and is defined as follows:

$$A_{g,f}(\tau, \nu) = \int_{-\infty}^{+\infty} g(\mu + \frac{\tau}{2})f(\mu - \frac{\tau}{2})e^{-j2\pi\nu\mu}d\mu \tag{3.20}$$

with:

$$\begin{cases} \tau' = (n_0 - n)T - \tau_i \\ \nu = -(m - m_0)F_0 \end{cases}, \tag{3.21}$$

so that (3.19) can be rewritten in:

$$\begin{aligned} y_{m_0,n_0} = &\sum_{m=0}^{M-1}\sum_{n=-\infty}^{+\infty} c_{m,n}\sum_{i=0}^{P-1} h_i e^{-j2\pi mF_0\tau_i} \\ &\times A_{g,f}(\tau', \nu)e^{j2\pi(m-m_0)F_0(\frac{(n+n_0)}{2}T + \frac{\tau_i}{2})}. \end{aligned} \tag{3.22}$$

Rearranging (3.22), we finally express the demodulated signal in its analog version as:

$$y_{m_0,n_0} = \sum_{m=0}^{M-1} \sum_{n=-\infty}^{+\infty} c_{m,n} e^{j\pi(m-m_0)(n+n_0)F_0T} \times \sum_{i=0}^{P-1} h_i A_{g,f}(\tau', \nu) e^{-j\pi(m+m_0)F_0\tau_i} \tag{3.23}$$

Discretization step:

Of course, in a practical case, the demodulated signal is obtained in discrete-time. So let us rewrite the channel impulse response as:

$$h[k] = \sum_{l=0}^{L_h-1} h_l \delta[k-l] \tag{3.24}$$

where we define that

$$h_l = \begin{cases} h_i, \ l = \lceil \frac{\tau_i}{T_s} \rceil \\ \\ 0, \ \text{otherwise.} \end{cases} \tag{3.25}$$

where $\lceil a \rceil$ denotes the smallest integer greater or equal to a. Then, setting $p = m - m_0$ and $q = n - n_0$, corresponding to the relative frequency and time indexes, respectively, with $0 \leq m_0 + p \leq M - 1$, and $A_{g,f}[q,p] = A_{g,f}(qT_s, pF_0)$, we express the discretized demodulated signal (3.23) as follows:

$$y_{m_0,n_0} = \sum_{(p,q)} c_{m_0+p,n_0+q} e^{j\pi p(2n_0+q)\frac{M+L_{\text{GI}}}{M}} \times \begin{pmatrix} \sum_{l=0}^{L_h-1} h_l \ A_{g,f}[-q(M+L_{\text{GI}})-l,-p] \\ \times e^{-j\pi(2m_0+p)\frac{l}{M}} \end{pmatrix}$$

Finally, we can split (3.26) into two parts, corresponding to the useful part and an interference part, respectively:

$$\begin{aligned} y_{m_0,n_0} &= \underbrace{\sum_{l=0}^{L_h-1} h_l A_{g,f}[-l,0] e^{-j\pi 2m_0\frac{l}{M}}}_{\text{distortion: } \alpha_{m_0}} c_{m_0,n_0} \\ &+ \underbrace{\begin{pmatrix} \sum_{(p,q)\neq(0,0)} c_{m_0+p,n_0+q} e^{j\pi p(2n_0+q)\frac{M+L_{\text{GI}}}{M}} \\ (\sum_{l=0}^{L_h-1} h_l A_{g,f}[-q(M+L_{\text{GI}})-l,-p] \\ \times e^{-j\pi(2m_0+p)\frac{l}{M}}) \end{pmatrix}}_{\text{ISI+ICI}: J_{m_0,n_0}} \\ &= \alpha_{m_0} c_{m_0,n_0} + J_{m_0,n_0} \end{aligned}$$

Calculation of the interference power (before equalization):

$$J_{m_0,n_0} = \sum_{(p,q)\neq(0,0)} c_{m_0+p,n_0+q} e^{j\pi p(2n_0+q)\frac{M+L_{\mathrm{GI}}}{M}} \times \underbrace{\left(\begin{array}{l} \sum_{l=0}^{L_h-1} h_l A_{g,f}[-q(M+L_{\mathrm{GI}})-l,-p] \\ \times e^{-j\pi(2m_0+p)\frac{l}{M}} \end{array} \right)}_{H_{m_0}^{(p,q)}}$$

$$H_{m_0}^{(p,q)} = \sum_{l=0}^{L_h-1} h_l A_{g,f}[-q(M+L_{\mathrm{GI}})-l,-p] e^{-j\pi(2m_0+p)\frac{l}{M}} \tag{3.26}$$

The interference term being isolated, we compute the interference power as follows:

$$\begin{aligned} P_{\mathrm{ISI+ICI}}^{\mathrm{Win}}(m_0,n_0) &= \mathrm{E}\left[|J_{m_0,n_0}|^2\right] \\ &= \sum_{(p^0,q^0)} \sum_{(p'^0,q'^0)} \mathrm{E}\left[c_{m_0+p,n_0+q} c_{m_0+p',n_0+q'}\right] \\ &\quad \times \left(\begin{array}{l} e^{j\pi p(2n_0+q)\frac{M+L_{\mathrm{GI}}}{M}} \\ \times e^{-j\pi p'(2n_0+q')\frac{M+L_{\mathrm{GI}}}{M}} \\ \times H_{m_0}^{(p,q)} H_{m_0}^{(p',q')^*} \end{array} \right) \end{aligned}$$

in which (p^0,q^0) stands for $(p,q)\neq(0,0)$. Finally, assuming that the $c_{m,n}$ are independent and identically distributed for $0 \leq m \leq M/2-1$, we obtain an interference power only dependent upon the frequency index m_0:

$$P_{\mathrm{ISI+ICI}}^{\mathrm{Win}}(m_0) = \sum_{(p^0,q^0)} \sigma_c^2(m_0+p) \left| H_{m_0}^{(p,q)} \right|^2 \tag{3.27}$$

We remind that in HPAV, the GI can have three different durations: 5.56 μs or 7.56 μs or 47.12 μs. In the following, the chosen GI was always the shortest one not to penalize windowed OFDM. In Fig. 3.7, the interference level (before ZF) in a channel belonging to class 2 [108] (cf. section 2.2.1) is compared to the static colored noise level introduced in section 2.2.2 (see Fig. 2.3), assuming a -50 dBm/Hz transmitted PSD. From this graph, we can reasonably assume that in severe channels, the remaining interference of windowed OFDM has to be taken into account to obtain accurate throughput calculations.

3.3 HS-OQAM: Study and Analysis of an Alternative to windowed OFDM

Considering the very restrictive transmission mask imposed to PLC systems, it clearly appears that the classical CP-OFDM scheme is not appropriate in this context. Moreover, if the windowing solution allows to improve the subcarriers localization, this technique is quickly limited by the interference term that will arise as the RI increases relatively to the GI. We are going to see in the following that the OFDM/OQAM modulation possesses strong assets to provide spectrally efficient transmissions over the power grid.

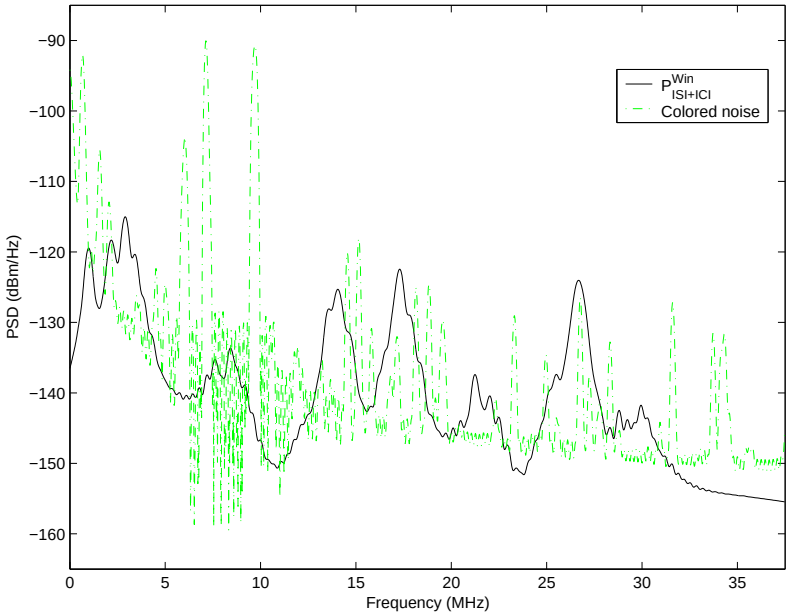

Figure 3.7: Comparison between the colored noise and the interference levels for a class 2 channel (cf section 2.2.1), in the HPAV band.

3.3.1 OFDM/OQAM Modulation Overview

The first multicarrier modulation systems based on QAM constellations including a time-offset, i.e. Offset QAM (OQAM), date back to the sixties [97]. This initial scheme was based on continuous-time filters. A discrete-time FFT-based was then proposed in 1981 [71]. The acronym OFDM/OQAM only appeared in 1995 for a continuous-time system [79]. The peculiarity of OFDM/OQAM lies in the fact that instead of transmitting complex-valued QAM symbols $c_{m,n} = c^R_{m,n} + jc^I_{m,n}$ over each subcarrier at a given rate T_0, the real and imaginary parts are transmitted separately, with a time-offset $\frac{T_0}{2}$. It means that either the real or the imaginary part is delayed of one half-symbol duration. The constraint is to keep a phase difference of $\frac{\pi}{2}$ between adjacent symbols in time and frequency. The Offset QAM (OQAM) coding rule introduced in [97] is given in Tab. 3.1. In this Table, T_0 is the complex symbol duration, $T_0/2$ the time-offset and $F_0 = 1/T_0$ the frequency spacing. Based on these construction rules, we get the modulator depicted in Fig. 3.8. From this figure it can be seen that the baseband OFDM/OQAM signal $s(t)$ is obtained as the combination of 4 signals that are shifted in time by $\frac{T_0}{2}$, the duration of one real symbol, and in frequency by F_0, the spacing between two successive sub-carriers. Thus $s(t)$ is obtained as a summation in time and frequency of 4 terms that can also be written in the concise form proposed in [79], leading to a continuous baseband OFDM/OQAM signal that reads:

$$s(t) = \sum_{m=0}^{M-1} \sum_{n=-\infty}^{+\infty} a_{m,n} p_{m,n}(t) \tag{3.28}$$

Table 3.1: Coding scheme for OFDM/OQAM symbols

	$(2m-1)F_0$	$(2m)F_0$	$(2m+1)F_0$
$nT_0 - \frac{T_0}{2}$	$c^R_{2m-1,n-1}$	$jc^I_{2m,n-1}$	$c^R_{2m+1,n-1}$
nT_0	$jc^I_{2m-1,n}$	$c^R_{2m,n}$	$jc^I_{2m+1,n}$
$nT_0 + \frac{T_0}{2}$	$c^R_{2m-1,n}$	$jc^I_{2m,n}$	$c^R_{2m+1,n}$

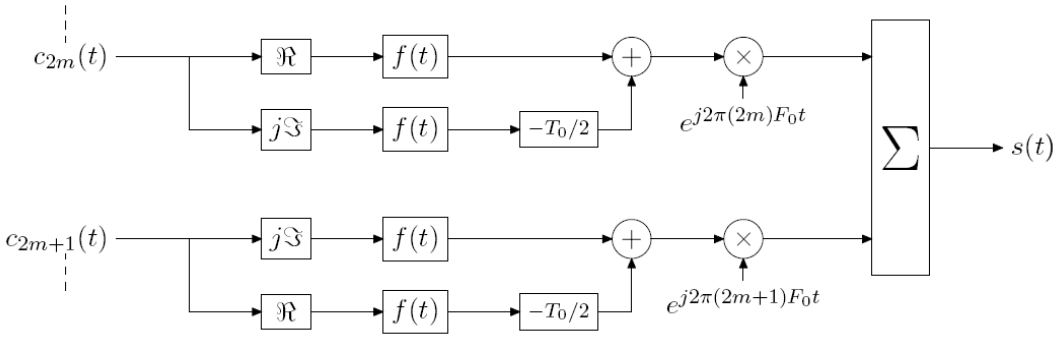

Figure 3.8: OFDM/OQAM in its analog form (continuous-time).

where the $a_{m,n}$ are the real-valued numbers derived from the decomposition of the complex symbols $c_{m,n}$ and where the base of modulation can be expressed as follows:

$$p_{m,n}(t) = e^{j\phi(m,n)} e^{j2\pi m F_0 t} p(t - n\tau_0) \tag{3.29}$$

in which $p(t)$ is the prototype filter, $\tau_0 = \frac{T_0}{2}$ and $\phi(m,n) = \frac{\pi}{2}(n+m) + \phi_0(m,n)$ is an additional phase term where $\phi_0(m,n)$ can be arbitrarily chosen. $\phi(m,n)$ ensures a phase shift of $\frac{\pi}{2}$ between two adjacent symbols in time and in frequency.

In practice, OFDM/OQAM modulation can be realized by means of FFT-based implementation, such that the discrete-time OFDM/OQAM signal can be expressed as follows [100]:

$$s[k] = \sum_{m=0}^{M-1} \sum_{n\in\mathbb{Z}} a_{m,n} \underbrace{p[k - nN] e^{j\frac{2\pi}{M} m(k - \frac{L_p - 1}{2})} e^{j\phi_{m,n}}}_{p_{m,n}[k]} \tag{3.30}$$

where L_p is the filter length, M is the IFFT size and $N = \frac{M}{2}$ is the discrete-time offset. Note that the added complexity of this modulation compared to the classical OFDM scheme mainly comes from the fact that transmitting separately the real and imaginary parts imposes the IFFT to run twice as fast [100]. However, as shown recently in [56], this drawback has been solved at the transmitter side. Concerning the pulse shaping implementation, its extra computational cost remains limited using efficient polyphase implementations and relatively short prototype filters. At this point, it is important to highlight the main difference between OFDM/OQAM and the classical OFDM modulation. In the general case, OFDM multiplexes complex QAM symbols, such that a complex orthogonality must be verified at the receiver to retrieve interference-free symbols. On the other hand, OFDM/OQAM relaxes the orthogonality condition by imposing it only in

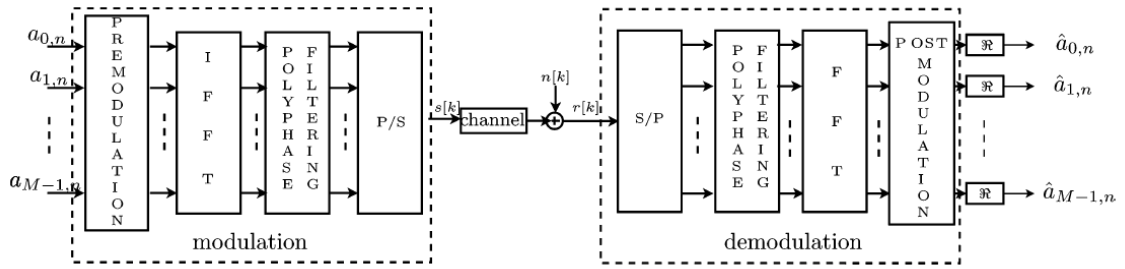

Figure 3.9: HS-OQAM general structure [84].

the real field, because only real symbols are transmitted at a given time. Therefore, the orthogonality can be checked with the following relation:

$$\mathrm{Re}\{\langle p_{m,n}[k], p_{m',n'}[k]\rangle\} = \mathrm{Re}\{\sum_{k\in\mathbb{N}} p_{m,n}[k]\, p^*_{m',n'}[k]\} = \delta_{m,m'}\delta_{n,n'} \tag{3.31}$$

where $\delta_{m,m'} = 1$ if $m = m'$ and $\delta_{m,m'} = 0$ if $m \neq m'$.

An alternative version of OFDM/OQAM, called HS-OQAM (for Hermitian Symmetric), was proposed in [83] to directly obtain a real signal at the output of the IFFT. The HS-OQAM scheme is simply obtained by imposing the following condition:

$$\begin{cases} a_{0,n} = a_{N,n} = 0 \\ a_{m,n} = a_{M-m,n}(-1)^{L_p-1-N-n} \end{cases} \tag{3.32}$$

The general HS-OQAM structure (without equalization) is depicted in Fig. 3.9. Even if the modulation and demodulation process of HS-OQAM system executes two times faster than that of the equivalent CP-OFDM system, the overall symbol rate of HS-OQAM remains the same as the equivalent CP-OFDM scheme because only half of the information is transmitted at a given time. However, the staggering rule imposed by OQAM means that the transmitted signal always carries an intrinsic interference. Indeed, if CP-OFDM ensures an orthogonality in time between two consecutive symbols, the modulated HS-OQAM symbols are overlapped with each other. Moreover, the overlapping degree depends on the length of the prototype filter. Fig. 3.10 gives a clear view of this situation, where we assume that the prototype filter is of length M (in samples). In this example, the present HS-OQAM symbol interferes both with the previous and the following HS-OQAM symbols. Fortunately, in an ideal channel case, this interference is limited to pure imaginary-valued term, thanks to the real-field orthogonal condition given by (3.31). In other words, it means that HS-OQAM achieves an interference-free transmission if we only consider the useful part of the signal, that is either located on the in-phase or on the quadrature component.

Relaxing the orthogonality condition to the real field gives much more latitude to design the prototype filter $p[k]$ in comparison to the classical OFDM modulation. We will see in section 3.4.2.1 how we can efficiently exploit this degree of freedom with the restrictive transmission mask imposed to PLC systems. Moreover, the HS-OQAM modulation does not use any CP, which provides a direct gain in the transmission efficiency. However, the absence of CP also means that there will always remain ISI and ICI in a dispersive channel.

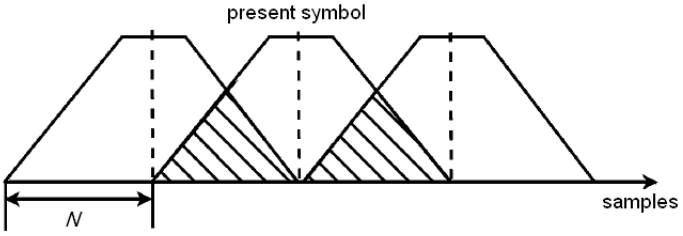

Figure 3.10: OFDM/OQAM symbols overlapping [84].

3.3.2 OFDM/OQAM Transmission over a Multipath Channel

3.3.2.1 Channel Equalization for OFDM/OQAM

As HS-OQAM modulation does not define any *GI* prefixing its symbols, the transmission capacity is naturally improved, the counterpart of this being an increased sensitivity to ISI and ICI. The remaining interference varies with the chosen prototype filter but also with the equalization technique applied at the receiver. Classically, OFDM modulation is associated with a simple 1-tap ZF equalization. Considering HS-OQAM, a slightly more complex equalizer can be chosen to limit the interference. In [84], the Adaptive Sine/Cosine-modulated filter bank Equalizer for Transmultiplexer (ASCET) [35] has been adapted to the OFDM/OQAM modulation. ASCET is a point-wise equalizer generally involving 3-tap per subcarrier, and can be seen as a 3-tap ZF equalizer. The 3-tap ASCET structure is depicted for the sub-carrier of index m in Fig. 3.11. At frequency index m, the equalizer Finite Impulse Response (FIR) filter writes $E_m^{\text{ASCET}}(z) = e_{0m}z + e_{1m} + e_{2m}z^{-1}$. Assuming that the OQAM phase term is defined as $\phi(m,n) = \frac{\pi}{2}(n+m)$, the equalizer coefficients e_{im} read [84]:

$$\begin{cases} e_{0m} = -\frac{1}{2}\left(\frac{\eta_{-1m}-\eta_{1m}}{2} - j\left(\eta_{0m} - \frac{\eta_{-1m}+\eta_{1m}}{2}\right)\right) \\ e_{1m} = \frac{\eta_{-1m}+\eta_{1m}}{2} \\ e_{2m} = -\frac{1}{2}\left(\frac{\eta_{-1m}-\eta_{1m}}{2} + j\left(\eta_{0m} - \frac{\eta_{-1m}+\eta_{1m}}{2}\right)\right) \end{cases}, \tag{3.33}$$

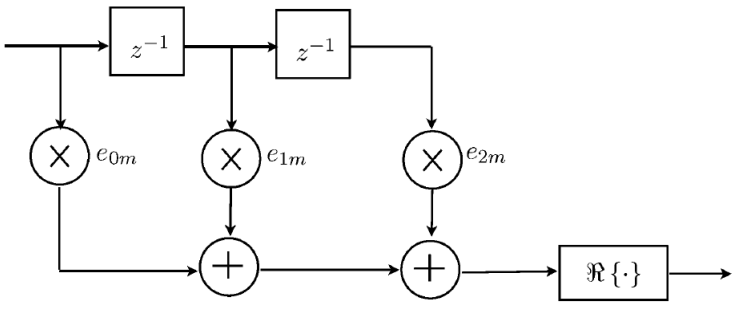

Figure 3.11: Structure of the per-carrier ASCET equalizer [84].

where η_{im} compensates the channel distortion at a chosen frequency following the ZF criterion, such that it is equal to the inverse of the channel response at this particular frequency point. So, the e_{im} can be calculated by simply evaluating the channel transfer function at chosen frequency points, wherein half of the chosen frequencies are nothing else than the central carrier frequencies and the rest half can be chosen in the transition band. Generally, these points will be chosen as the middle frequency between two consecutive subcarriers. Therefore, the ICI on the chosen frequencies can be perfectly compensated by this method. As ASCET is a linear equalizer, it has the advantage to permit further analytical computations, such as the capacity, which will be presented in section 3.1.3. Moreover, with only 3 coefficients per carrier, ASCET is relatively simple to implement and, as we will show in subsection 6.5.4, it allows getting significant improvements w.r.t. ZF. However, using a 3-tap ASCET equalizer modifies the noise PSD. In section 3.3.2.3, we conduct an analysis on the noise power after the equalization stage.

3.3.2.2 Generalized Expression of HS-OQAM Interference Term

Some expressions of the interference power have been provided in [84] for the 1-tap Zero Forcing and the 3-tap ASCET equalizers. In this section, we provide a simpler expression of the interference power in the case of an arbitrary length ASCET, for which the 1-tap ZF equalizer appears as a particular case. The parameters reused in this part keep the same significations as in section 3.2.3. However, differently from windowed OFDM, with HS-OQAM we have the same window, a prototype function $p(t)$, at the transmitter and the receiver sides. Then, for concision, its ambiguity function will be denoted $A_p(\tau, \nu)$, with $A_p(\tau, \nu) = A_{p,p}(\tau, \nu)$. We assume the HS-OQAM signal, derived from (3.30) and (3.32), uses a real-valued and symmetrical prototype function. Therefore, its ambiguity function is also real valued. Furthermore, as p is orthogonal, i.e. satisfies (3.31), its ambiguity function is such that

$$A_p(nT_0, 2mF_0) = \delta(n)\delta(m). \tag{3.34}$$

Knowing that $T_0 = MT_s$, this orthogonality condition can be expressed in a discrete-time formalism:

$$A_p[nM, 2m] = \delta(n)\delta(m). \tag{3.35}$$

Received signal:

For a P-path time invariant channel (see subsection 3.2.3), the received HS-OQAM signal is given by $y(t) = h(t) * s(t)$, so that:

$$y(t) = \sum_{i=0}^{P-1} h_i \sum_{m=0}^{M-1} \sum_{n=-\infty}^{+\infty} a_{m,n} p_{m,n}(t - \tau_i). \tag{3.36}$$

HS-OQAM demodulation:

For the subcarrier of index m_0 and at time index n_0, the demodulated signal is

$$y_{m_0,n_0} = \int_{-\infty}^{+\infty} y(t) p^*_{m_0,n_0}(t) dt. \tag{3.37}$$

As seen in [84] the discretized demodulated signal can be written, with $0 \leq m_0+p \leq M-1$, as

$$y_{m_0,n_0} = \sum_{(p,q)} a_{m_0+p,n_0+q} e^{j\Phi^{(p,q)}_{m_0,n_0}} H^{(p,q)}_{m_0} \tag{3.38}$$

with

$$H^{(p,q)}_{m_0} = \sum_{l=0}^{L_h-1} h_l e^{-j\pi(2m_0+p)l/M} A_p[-l-qM/2,-p] \tag{3.39}$$

and

$$\Phi^{(p,q)}_{m_0,n_0} = \begin{cases} \frac{\pi}{2}(p+q+pq)+\pi p n_0 \text{ if } \phi_0(m,n)=0 \\ \frac{\pi}{2}(p+q-pq)-\pi q m_0 \text{ if } \phi_0(m,n)=-\pi mn \end{cases} \tag{3.40}$$

Equalization step:

Denoting by $e^{(r)}_{m_0}$ the $2K_e+1$ coefficients of the ASCET equalizer, the target estimated symbol being a_{m_0,n_0}, the central coefficient is $e^{(0)}_{m_0}$ and the output of the equalizer is defined by

$$\hat{a}_{m_0,n_0} = \mathrm{Re}\{ \sum_{r=-K_e}^{K_e} e^{(r)}_{m_0} y_{m_0,n_0+r} \}. \tag{3.41}$$

Note that the 3-tap ASCET equalizer presented in [84] did not use this symmetric indexation. Note also that the ZF equalizer can be viewed as a particular case of 1-tap ASCET, with $K_e = 0$ and one coefficient defined by

$$e^{(0)}_{m_0} = \frac{1}{H_{m_0}}. \tag{3.42}$$

Inserting the expression (3.38) of y_{m_0,n_0} we have

$$\hat{a}_{m_0,n_0} = \mathrm{Re}\left\{ \sum_{r=-K_e}^{K_e} e^{(r)}_{m_0} \sum_{(p,q)} a_{m_0+p,n_0+r+q} \times e^{j\Phi^{(p,q)}_{m_0,n_0+r}} H^{(p,q)}_{m_0} \right\} \tag{3.43}$$

that we rewrite in

$$\hat{a}_{m_0,n_0} = \sum_{(p,q)} a_{m_0+p,n_0+q} \mathrm{Re}\left\{ \sum_{r=-K_e}^{K_e} e^{(r)}_{m_0} \times e^{j\Phi^{(p,q-r)}_{m_0,n_0+r}} H^{(p,q-r)}_{m_0} \right\}. \tag{3.44}$$

Noticing that the phase term can be written as (3.40)

$$\Phi^{(p,q-r)}_{m_0,n_0+r} = \Phi^{(p,q)}_{m_0,n_0} + \frac{\pi}{2} r(p-1) + \begin{cases} 0 \text{ if } \phi_0(m,n)=0 \\ \pi r m_0 \text{ if } \phi_0(m,n)=-\pi mn \end{cases} \tag{3.45}$$

we define

$$F_\phi(k) = \begin{cases} 1 \text{ if } \phi_0(m,n)=0 \\ (-1)^k \text{ if } \phi_0(m,n)=-\pi mn \end{cases} \tag{3.46}$$

and

$$A^{(p,q)}_{m_0} = \sum_{r=-K_e}^{K_e} e^{(r)}_{m_0} F_\phi(r m_0) e^{j\frac{\pi}{2}r(p-1)} H^{(p,q-r)}_{m_0}. \tag{3.47}$$

Then we have

$$\hat{a}_{m_0,n_0} = \sum_{(p,q)} a_{m_0+p,n_0+q} \mathrm{Re}\{e^{j\Phi_{m_0,n_0}^{(p,q)}} A_{m_0}^{(p,q)}\}. \tag{3.48}$$

The output of the equalizer can be split into the useful part and the interference part as follows

$$\hat{a}_{m_0,n_0} = \beta_{m_0} a_{m_0,n_0} + I_{m_0,n_0} \tag{3.49}$$

where the expression of the distortion β_{m_0} is

$$\beta_{m_0} = \mathrm{Re}\{A_{m_0}^{(0,0)}\}. \tag{3.50}$$

Therefore, as the QAM symbol estimates are defined by

$$\begin{array}{lcl} \hat{c}_{2m_0,n_0} & = & \hat{a}_{2m_0,2n_0} + j\hat{a}_{2m_0,2n_0+1} \\ \hat{c}_{2m_0+1,n_0} & = & \hat{a}_{2m_0+1,2n_0+1} + j\hat{a}_{2m_0+1,2n_0} \end{array} \tag{3.51}$$

the useful power of $\hat{c}_{m_0,n_0}$ is

$$P_{\text{useful}}(m_0) = \sigma_c^2(m_0) \left[\mathrm{Re}\{A_{m_0}^{(0,0)}\}\right]^2 \tag{3.52}$$

and the total power of $\hat{c}_{m_0,n_0}$ is:

$$P_{\text{TOT}}(m_0) = E\left[|\hat{a}(m_0, 2n_0)|^2\right] + E\left[|\hat{a}(m_0, 2n_0+1)|^2\right] \tag{3.53}$$

After some computations, assuming that the $a_{m,n}$ are independent and identically distributed for $0 \leq m \leq M/2-1$, we have:

$$P_{\text{TOT}}(m_0) = \sum_{(p,q)} \sigma_c^2(m_0+p) \left[\mathrm{Re}\{e^{j\frac{\pi}{2}(p+q+pq)} A_{m_0}^{(p,q)}\}\right]^2 \tag{3.54}$$

so that the interference power is:

$$P_{\text{ISI+ICI}}(m_0) = \sum_{(p^0,q^0)} \sigma_c^2(m_0+p) \left[\mathrm{Re}\{e^{j\frac{\pi}{2}(p+q+pq)} A_{m_0}^{(p,q)}\}\right]^2 \tag{3.55}$$

3.3.2.3 Analytical Expression of the Noise Power at the ASCET Equalizer Output

A simplified expression of the noise power has been provided in [84]. Although this expression is valid in most of the PLC environments, we provide in this section the full expression in order to get a comprehensive survey.

HS-OQAM demodulator output:

The noise $n(t)$ at the receiver output is assumed to be a Additive White Gaussian Noise (AWGN), with variance σ_n^2, so that the noise at the HS-OQAM demodulator output is expressed as

$$b_{m_0,n_0} = \int n(t) p_{m_0,n_0}^*(t) dt \tag{3.56}$$

with variance σ_n^2.

Equalizer output:

If v_{m_0,n_0} and v'_{m_0,n_0} refer to the noise term at the output of the equalizer and at the output of the $a_{m,n}$ to $c_{m,n}$ symbol converter (3.51), respectively, the noise power is given by

$$P_{\text{noise}}(m_0) = \text{Var}[v'_{m_0,n_0}] = \text{Var}[v_{m_0,2n_0}] + \text{Var}[v_{m_0,2n_0+1}] \tag{3.57}$$

In the next paragraph, we detail the expression of $\text{Var}[v_{m_0,n_0}]$, showing that the noise power P_{noise} only depends on the frequency carrier index m_0.

ASCET equalizer:

The noise at the output of the ASCET equalizer is

$$v_{m_0,n_0} = \text{Re}\{u_{m_0,n_0}\} \tag{3.58}$$

where

$$u_{m_0,n_0} = \sum_{r=-K_e}^{K_e} e_{m_0}^{(r)} b_{m_0,n_0+r} \tag{3.59}$$

The variance of v_{m_0,n_0} can be computed from u_{m_0,n_0} thanks to the following relation

$$\text{Var}[v_{m_0,n_0}] = \frac{1}{2}\left(\text{Var}[u_{m_0,n_0}] + \text{Re}\{E\left[u_{m_0,n_0}^2\right]\}\right) \tag{3.60}$$

We can easily show that $\text{Var}[u_{m_0,n_0}]$ does not depend on n_0 and that $E\left[u_{m_0,n_0}^2\right]$ can be written as $(-1)^{n_0}F(m_0)$, where F is a function that only depends on m_0. Proofs are given in Annex C. Therefore, inserting (3.60) in (3.57) leads to the following expression of the noise power

$$P_{\text{noise}}(m_0) = \text{Var}[u_{m_0,n_0}] \tag{3.61}$$

Expression of the noise power:

The power of the noise at the output of the symbol estimator is finally expressed as

$$\begin{aligned} P_{\text{noise}}(m_0) &= \text{Var}[u_{m_0,n_0}] \\ &= \sigma_n^2 \sum_{r=-K_e}^{K_e} \sum_{r'=-K_e}^{K_e} e_{m_0}^{(r)} e_{m_0}^{(r')*} e^{j\Phi_{m_0,0}^{(0,r'-r)}} A_p[(r'-r)M/2, 0] \end{aligned}$$

The ambiguity function $A_p[qM/2, 0]$ being null if q is even and different from 0, the noise power becomes

$$P_{\text{noise}}(m_0) = \sigma_n^2 \sum_{r=-K_e}^{K_e} |e_{m_0}^{(r)}|^2 A_p[0,0] + \underbrace{\sigma_n^2 \sum_{\substack{-K_e \le r \le K_e \\ -K_e \le r' \le K_e \\ (r'-r) \text{ odd}}} e_{m_0}^{(r)} e_{m_0}^{(r')*} e^{j\Phi_{m_0,0}^{(0,r'-r)}} A_p[(r'-r)M/2, 0]}_{T(m_0)} \tag{3.62}$$

Note that the second term $T(m_0)$ of this expression, that only accounts for odd $(r'-r)$ indexes, is negligible for most of the classical PLC channel profiles. We nevertheless detail it in order to be exhaustive.
$(r'-r)$ is odd if and only if r and r' have different parities. Therefore, noticing that $\Phi_{m_0,0}^{(0,r-r')} = -\Phi_{m_0,0}^{(0,r'-r)}$ and recalling that the ambiguity function is real and symmetrical in time, we have

$$T(m_0) = \sum_{\substack{r \text{ odd} \\ r' \text{even}}} 2\text{Re}\{e_{m_0}^{(r)} e_{m_0}^{(r')*} e^{j\Phi_{m_0,0}^{(0,r'-r)}}\} A_p[(r'-r)M/2, 0] \tag{3.63}$$

Setting $r = 2k+1$ and $r' = 2k$, the phase term can be written

$$\Phi_{m_0,0}^{(0,r'-r)} = -\frac{\pi}{2} + \pi(k'-k) + \begin{cases} 0 \text{if } \phi_0(m,n) = 0 \\ \pi m_0 \text{if } \phi_0(m,n) = -\pi mn \end{cases} \tag{3.64}$$

Then, using the function F_ϕ defined in (3.46), we have

$$T(m_0) = 2F_\phi(m_0) \sum_{\substack{-K_e \le 2k+1 \le K_e \\ -K_e \le 2k' \le K_e}} \text{Im}\{e_{m_0}^{(2k+1)} e_{m_0}^{(2k')*}\} \times (-1)^{k'-k} A_p[(k'-k-1/2)M, 0]$$

In the case of a 3-tap ASCET ($K_e = 1$), this term corresponds to $k \in \{-1, 0\}$ and $k' = 0$, and is equal to

$$T(m_0) = 2F_\phi(m_0)\text{Im}\{(e_{m_0}^{(1)} - e_{m_0}^{(-1)}) e_{m_0}^{(0)*}\} A_p[M/2, 0] \tag{3.65}$$

Therefore, the noise power is finally expressed as

$$P_{\text{noise}}(m_0) = \sigma_n^2 \sum_{r=-1}^{1} |e_{m_0}^{(r)}|^2 A_p[0,0] + 2\sigma_n^2 F_\phi(m_0)\text{Im}\{(e_{m_0}^{(1)} - e_{m_0}^{(-1)}) e_{m_0}^{(0)*}\} A_p[M/2, 0] \tag{3.66}$$

Zero Forcing equalizer:

The ZF equalizer being viewed as a particular case of a 1-tap ASCET with $K_e = 0$ and one coefficient (3.42), the noise power (3.62) is simply expressed as

$$P_{\text{noise}}(m_0) = \frac{\sigma_n^2}{|H_{m_0}|^2}. \tag{3.67}$$

3.4 Windowed OFDM vs HS-OQAM: Transmission Capacity and Achievable Throughput

3.4.1 Simulation Parameters

In this section, results are presented in terms of transmission capacity (see (3.4)) or achievable throughput, also denoted as the PHY data rate (see (3.5)). For both of these metrics, the SINR achieved per subcarrier has to be computed (see (3.1)). A first parameter to fix concerns the channel frequency response. To obtain realistic PLC channels, we use the PLC channels generator developed by Orange Labs and described in [106]. In short, this generator is based on a statistical analysis of PLC channels measured in several indoor environments, more or less appropriate for PLC. This analysis led to the classification of PLC channels into 9 classes, class 1 corresponding to the worst channels while class 9 includes the less disturbed ones [107]. So, to generate a PLC channel, the inputs needed by the tool are limited to the desired class and frequency bandwidth. As class 2 channels were found to be one of the most encountered channels in realistic conditions, according to [107], we naturally use this class in our simulations. Then, to compare achievable

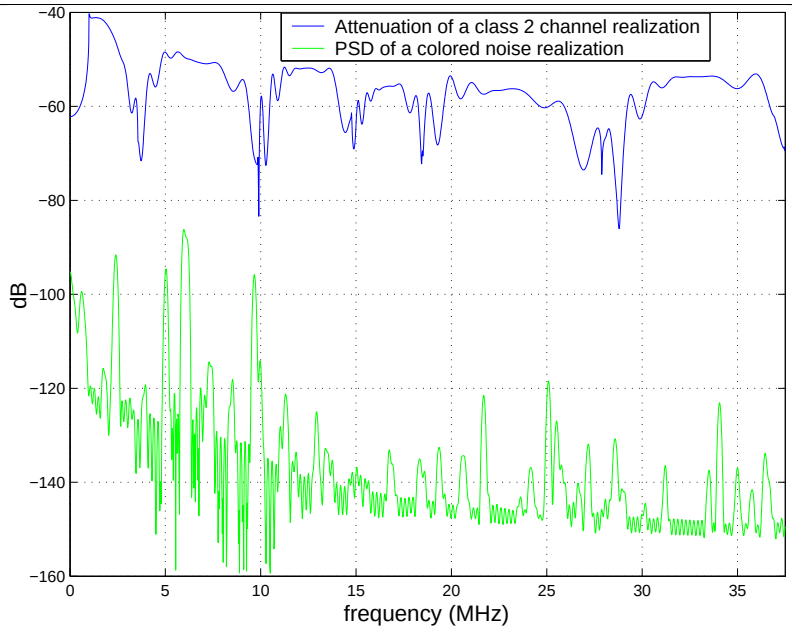

Figure 3.12: Example of class 2 channel and colored noise realizations.

throughputs in less disturbed environments, we used classes 5 and 9 channels. To generate the noise, we also used a software developed by Orange Labs that generates a realistic indoor colored noise Power Spectral Density (PSD) [52]. This model presents an exponential decrease with frequency as well as randomly distributed narrow-band noises, as it can be seen in Fig. 3.12. To finely compute the SINR achieved per subcarrier, we use the interference terms (3.27) and (3.55), derived in sections 3.2.3 and 3.2.3 for windowed OFDM and HS-OQAM, respectively, with respect to the selected equalization technique (see (3.1) for a 1-tap ZF equalizer). When ASCET equalizer is used, we also take into account the impact on the noise power using the expression (3.66) that was established in section 3.3.2.3. Each result presented in the following is computed by averaging over 100 channel and noise realizations, with a target SER fixed to 10^{-2}, so that the SINR gap $\Gamma_{\text{dB}} = 6$ dB (cf. (3.3)).

3.4.2 Performance of Different Prototype Filters Following the HPAV Specification

3.4.2.1 Set of Compared Prototype Filters

The main benefit of OFDM/OQAM comes from the latitude it gives in the design of the prototype filter. This degree of freedom can be exploited to optimize one or several criteria, depending on the target application. In this study, we only use prototype filters with real coefficients and satisfying the property of phase linearity. To work properly, a prototype filter must satisfy an orthogonality condition. However, two classes of filters need to be distinguished because the orthogonality condition can be perfectly or approximately met. Indeed, a filter either belongs to the Perfect Reconstruction (PR) or Nearly Perfect Reconstruction (NPR) class of filters. Of course, the PR feature only holds in ideal conditions, i.e. no channel distortion and no noise. Ideally, the prototype filter should always be the one that maximizes the throughput. However, adapting in real-time the prototype filter is a nearly untractable optimization problem. So, here, we only compare design methods that do not reach this goal but can be run off-line.

Note also that different approaches can be used in the design of prototype filters. Indeed, we can firstly distinguish filters that are designed using a continuous-time formalism. The main drawback of the continuous-time formalism comes from the fact that in a practical implementation case, the prototype filters have to be discretized and truncated and, therefore, lose their orthogonality property. Nevertheless, they can still satisfy a NPR condition. On the other hand, prototype filters can be designed in discrete-time. In this case, the design problem is directly stated as an optimization problem upon the chosen criterion, for the finite number of taps of the prototype filter. A design method of PR prototypes, called "compact representation method" [96], has been validated for the Frequency Selectivity (FS) criterion, with a minimization of the out-of-band energy, and for the Time-Frequency Localization (TFL) criterion, which minimizes the product of second order moments in time and frequency [57].

In the following, we select 3 prototype filters to run our simulations. Firstly, we choose to use a prototype filter optimized upon the TFL criterion. A famous representant of this set is the Isotropic Orthogonal Transform Algorithm (IOTA) filter [34], which has the peculiarity of having the same degree of spreading over time and frequency. Therefore, it is well suited in both time and frequency dispersive channels. However, if it was shown

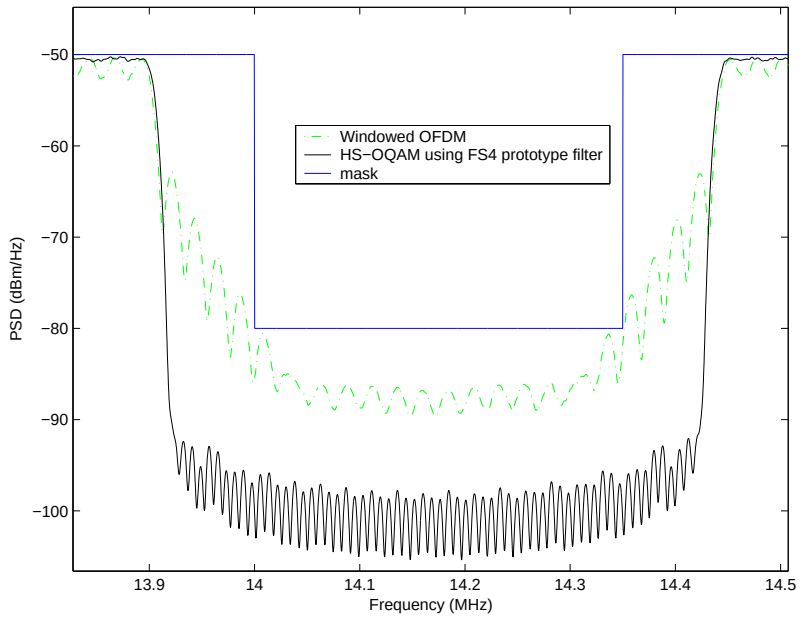

Figure 3.13: Compared PSD around a notch between windowed OFDM and HS-OQAM with FS4, using HPAV transmission mask.

that the PLC channel can be dispersive over frequency in [42], it clearly is a negligible effect when compared to the impact of the channel delay spread. So, here we limit to the utilization of a single prototype filter optimized upon the TFL criterion, which is the TFL1 filter. The postfix 1 means that the prototype length is one time the symbol duration. Thus TFL1 is a relatively short PR prototype filter directly optimized in discrete time upon the TFL criterion, lasting only T_0 (or M samples in a discrete-time formalism), while to be nearly isotropic IOTA requires to be at least of length $4T_0$. Interestingly, it was shown in [82] that for transmission over time-invariant frequency selective channel, ICI is the predominant factor that limits the overall performance, when compared to ISI. Therefore, it was highlighted in the same study that in the PLC field, prototype filters optimized upon the FS criterion lead to better performance than other filters, such as IOTA for instance. Moreover, the restricting transmission mask clearly highlights the necessity to optimize the spectral containment of the subcarriers, as it may give the opportunity of activating more subcarriers around mask notches. However, a good frequency selectivity can only be attained with a sufficient number of taps, that is why a length of $4T_0$ is a minimum duration for that kind of filters. A great advantage, in the PLC context, of using prototype filters with good spectral containment is that it allows to use more subcarriers than the 917 active tones defined in HPAV, using windowed OFDM. This point is clearly illustrated in Fig. 3.13 where we see that windowed OFDM just fits into the mask while HS-OQAM using FS4 filter offers the possibility to still satisfy the mask with more subcarriers on. Moreover, we will see in section 3.4.4 that this great advantage of OFDM/OQAM will become even more predominant when imposing a much more restrictive transmission mask, such as the one that the CENELEC is currently defining and might be imposed to PLC systems in a near future. A last filter, also with a good stopband behavior but satisfying a NPR condition, was chosen in our simulation. This filter, independently proposed in [88]

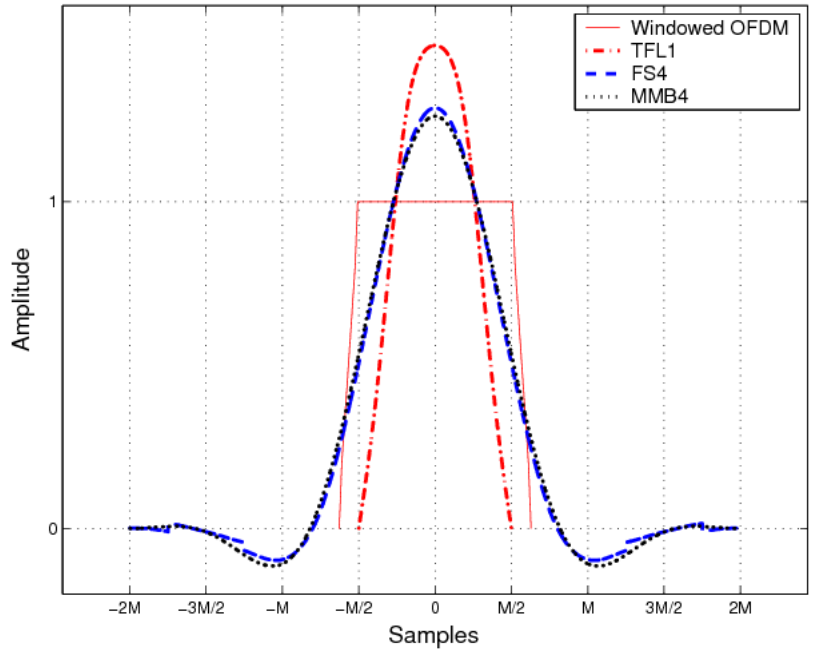

(a)

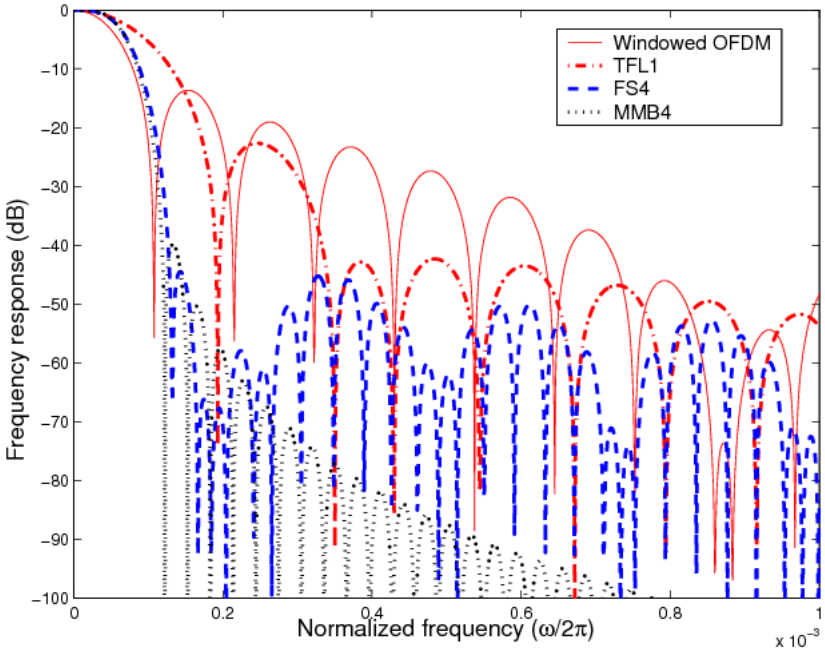

(b)

Figure 3.14: Prototype filters: (a) in time (b) in frequency

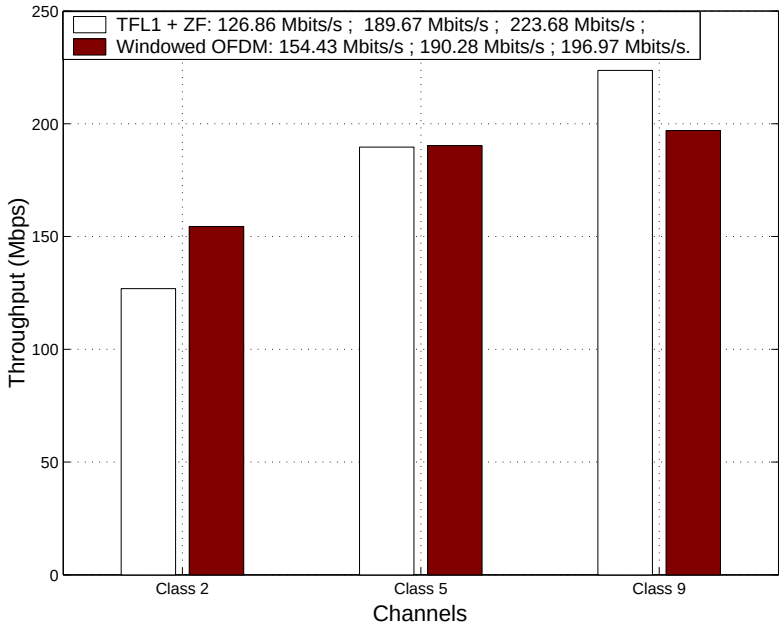

Figure 3.15: Comparison of PHY data rates (D^{PHY}) between windowed OFDM and HS-OQAM using TFL1+ZF, $\sigma^2_{c,\mathrm{dB}} = -50$ dBm/Hz.

and [37], is named in short MMB, using the names of its promoters. This MMB4 prototype filter is also known as PHYDYAS, in relation with a recent FP7 project [11]. The MMB4 prototype filter lasts $4T_0$. In Fig. 3.14 are plotted the time and frequency representations of the three prototype filters, as well as the window defined in HPAV. Note that this window spreads over $M + L_{\mathrm{GI}} + L_{\mathrm{RI}}$ samples, where L_{RI} is the roll-off interval length. Two consecutive symbols are overlapped during this interval that lasts 4.96 μs (372 samples considering the 75 MHz sampling frequency). Also, we see that TFL1 is represented with M samples while the two frequency selective filters spread over $4M$ samples. A quick look at the frequency representations of the prototype filters confirms the frequency selectivity of FS4 and MMB4.

3.4.2.2 Prototype Filter Selection

Let us firstly show the performance of a low complexity HS-OQAM system compared to the one of windowed OFDM, following the HPAV 1 specification, i.e. with $\mathrm{Card}(\mathbb{M}_u) = 917$ and $M = 3072$. So, we compute both the achievable throughput and the transmission capacity of HS-OQAM using TFL1 prototype filter together with a simple 1-tap ZF equalizer. Fig. 3.15 shows that if HS-OQAM provides similar and better PHY data rates compared to windowed OFDM in classes 5 and 9 channels, respectively, HS-OQAM is surpassed in class 2 channels. This result can be easily explained by the fact that if HS-OQAM takes advantage of the absence of GI in good channels, this advantage is lost in the worst channels because of a much higher interference term. So, we see that associating a short filter with a simple equalizer leads to mixed results, when compared to the ones provided by windowed OFDM.

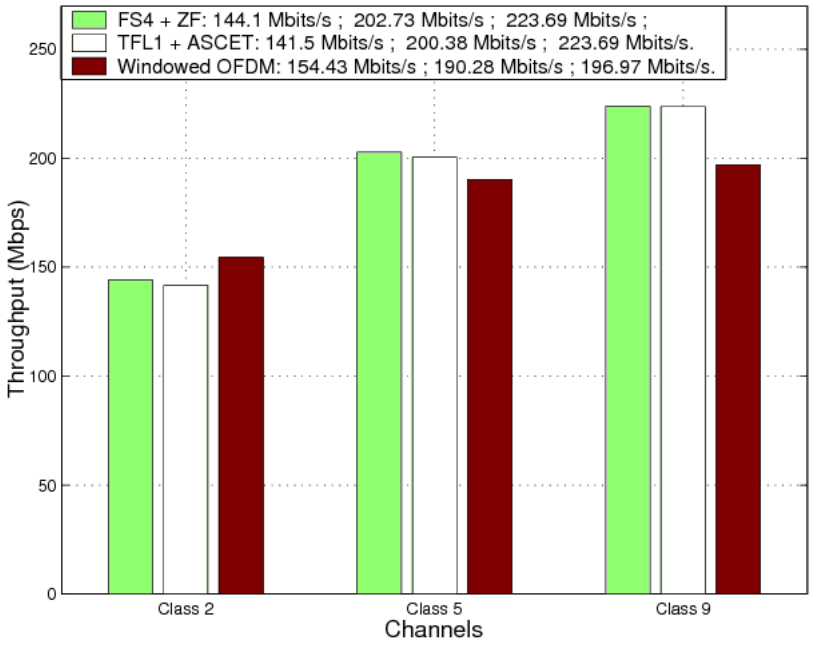

Figure 3.16: Comparison of PHY data rates (D^{PHY}) between windowed OFDM, HS-OQAM using TFL1+ASCET and HS-OQAM using FS4+ZF, $\sigma^2_{c,\text{dB}} = -50$ dBm/Hz.

Next, we propose to increase the complexity either in the prototype filter or in the equalization technique. So, on one side, we simulate HS-OQAM keeping TFL1 to shape the transmitted symbol but using the 3-tap ASCET equalizer, which is slightly more complex than a 1-tap ZF. On the other side, we keep the ZF equalizer but we use the FS4 prototype filter which, we recall, lasts $4T_0$. Fig. 3.16 naturally shows a general improvement in the achieved throughputs compared to the *TFL1+ZF* case. An interesting remark that can be made about this result is that the two different combinations lead to similar results. But if we consider the remark made in the previous section, a frequency selective filter offers a degree of freedom that can be exploited to add more subcarriers around the notches of the imposed transmission mask (see Fig. 3.13). So, exploiting this advantage, as shown later on, will put the *FS4+ZF* association ahead of the *TFL1+ASCET* solution.

In the two previously presented cases, both filters satisfy the PR condition. Now, we study the influence of the orthogonality or pseudo-orthogonality nature of the filter. To this end, we use FS4 and MMB4 filters, which possess about the same qualities in terms of frequency selectivity, MMB4 being a NPR prototype filter and FS4 a PR one. We compute the transmission capacity (3.4) versus the achieved Signal to Noise Ratio (SNR) at the receiver side, by increasing the signal power with a maximum imposed by the -50 dBm/Hz limitation. The SNR_{RX} is computed as follows:

$$\text{SNR}_{RX} = 10\log_{10}\left(\frac{1}{\text{Card}(\mathbb{M}_u)}\sum_{m\in\mathbb{M}_u}\frac{|H_m|^2\sigma_c^2}{\sigma_n[m]^2}\right) \tag{3.68}$$

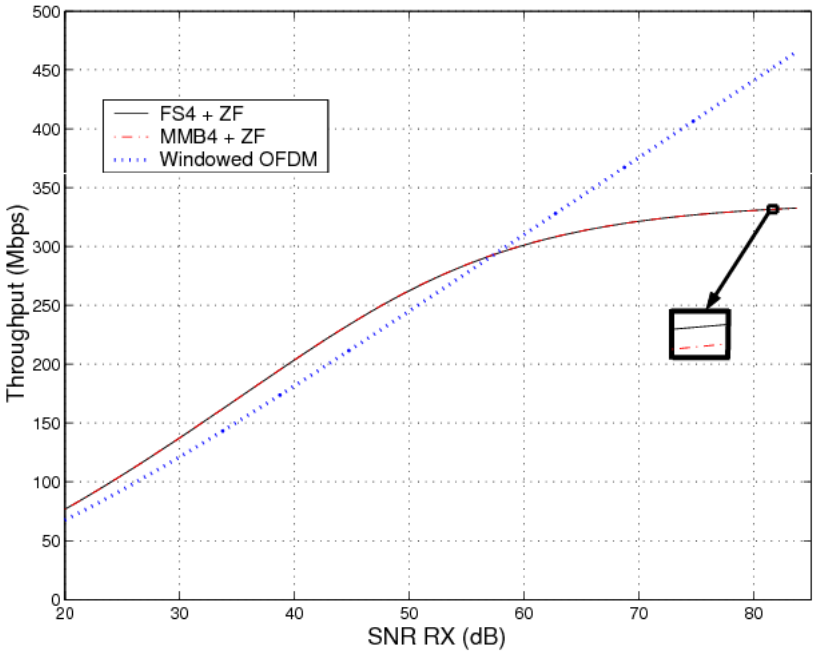

(a)

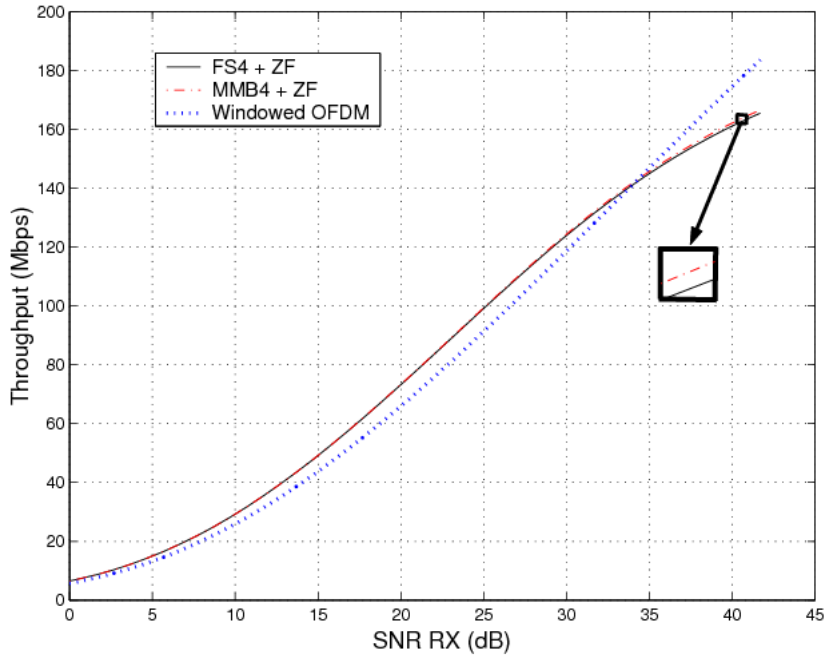

(b)

Figure 3.17: Transmission capacities ($D^{inf\ gran}$) comparison between FS4+ZF and MMB4+ZF.: (a) Class 9 channels (b) Class 2 channels.

In Fig. 3.17, we observe similar results for all channels classes but looking at the asymptotical behaviors of the transmission capacities curves, we see that MMB4 provides higher throughputs in class 2 channels than FS4, tendency that is reversed in class 9 channels. In fact, in good channels, as the interference caused by the time spreading of the impulse response is really low, the perfect orthogonality nature of FS4 leads to better SINR while the NPR nature of MMB4 always creates interference even if the channel is perfect. However, in class 2 channels, in which the interference is much more higher, the slight advantage brought by the perfect orthogonality is lost and the slightly better frequency selectivity of MMB4 (see Fig. 3.14-(b)) leads to an higher throughput. Concerning windowed OFDM, as there is no interference in class 9 channels thanks to the GI, the transmission capacity linearly increases with the SNR. From the results shown in this section, we can expect HS-OQAM, associated with frequency selective filters, to achieve better throughput than windowed OFDM once we will have exploited the possibility to add additional subcarriers around the notches. However, considering that class 2 channels correspond to a more often encountered environment than class 9 ones, the ASCET equalizer should always be preferred than the 1-tap ZF when using HS-OQAM.

3.4.3 Comparison Between windowed OFDM and HS-OQAM Associated with a Frequency Selective Filter

In this section, we compute both the achievable throughput and the transmission capacity using firstly the HPAV bandwidth and secondly, an "extended" HPAV band, that will be denoted as HPAV 2, as it is really similar to the transmission mask that will be imposed to systems following this new specification. For all the results of this section, presented in terms of transmission capacity ($D^{inf\ gran}$) and achievable throughput (D^{PHY}), windowed OFDM is associated with a 1-tap ZF equalizer while HS-OQAM is associated with a 3-tap ASCET equalizer. Moreover, here we exploit the possibility to add subcarriers around notches thanks to the good spectral containment of the FS4 prototype filter.

3.4.3.1 HomePlug AV 1 Context

First of all, we used the HPAV 1 specification as the referential of our simulations, meaning that we started this study by limiting our comparisons using windowed OFDM, defined in HPAV with $\mathrm{Card}(\mathbb{M}_u) = 917$ active carriers in the $[1.8, 30]$ MHz band with $\mathbb{E}_{const} = \{1, 2, 3, 4, 6, 8, 10\}$, and an FFT size of $M = 3072$. Concerning HS-OQAM, some subcarriers can be added while still satisfying the specification (see Fig. 3.30). Using the FS4 prototype filter, it appears that compared to the windowed OFDM defined in HPAV, we can add 53 extra subcarriers, setting the last two ones at a -80 dBm/Hz level. Therefore, with HS-OQAM, we can have 970 subcarriers on instead of 917. Figs. 3.18, 3.19, 3.20 present the achievable throughput versus the averaged SNR at the receiver for classes 9, 5 and 2 channels, respectively. We remind that all the presented curves result from an average over 100 channels realizations, with a unique colored noise generation per channel realization. To obtain these curves, the signal PSD is increased from -120 dBm/Hz to -50 dBm/Hz. So, for each curve, the last point on the right corresponds to the maximum authorized PSD by the spectral mask (see Fig. 3.21). The averaged SNR is computed as in (3.68). However, as $\mathbb{M}_u$ of windowed OFDM differs from $\mathbb{M}_u$ of HS-OQAM, the resulting SNR_{RX} will vary slightly between the two modulations. In Fig. 3.18, a significant gap

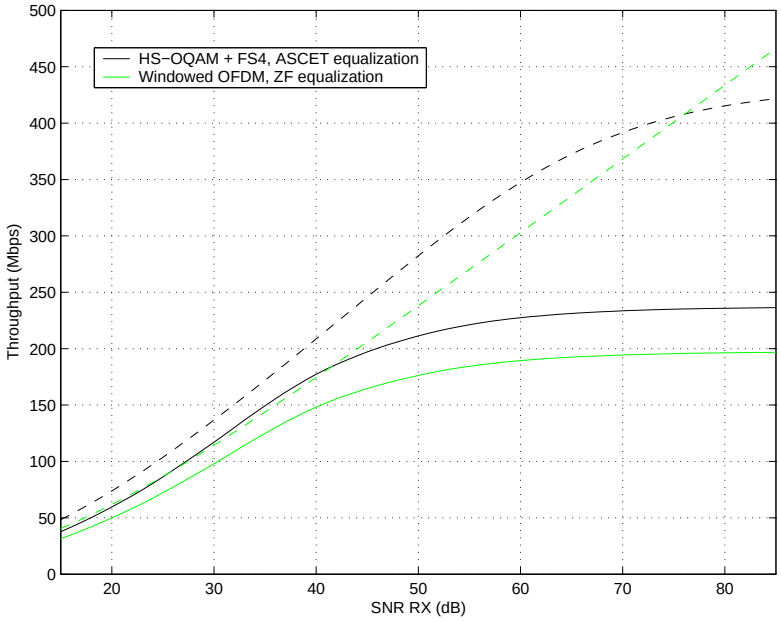

Figure 3.18: Transmission capacities (dotted curves) and PHY data rates (continuous curves) in the HPAV 1 context on Class 9 channels.

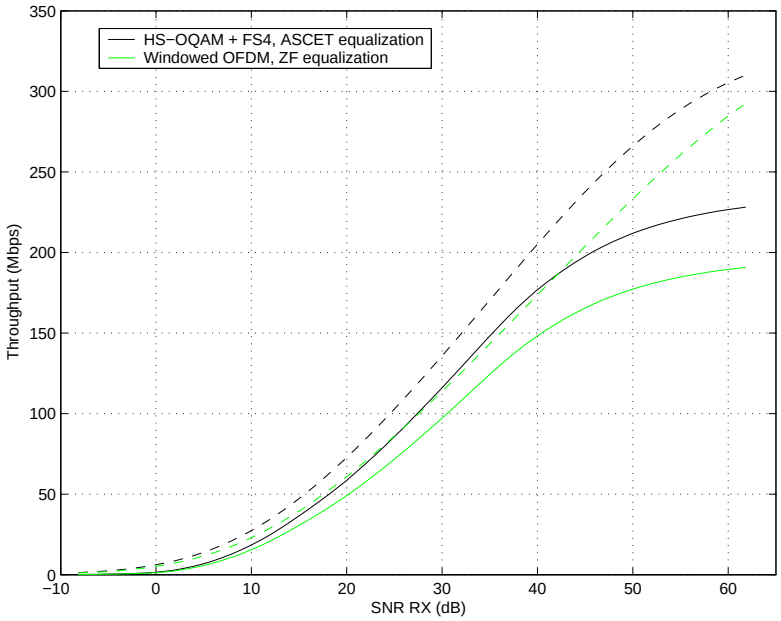

Figure 3.19: Transmission capacities (dotted curves) and PHY data rates (continuous curves) in the HPAV 1 context on Class 5 channels.

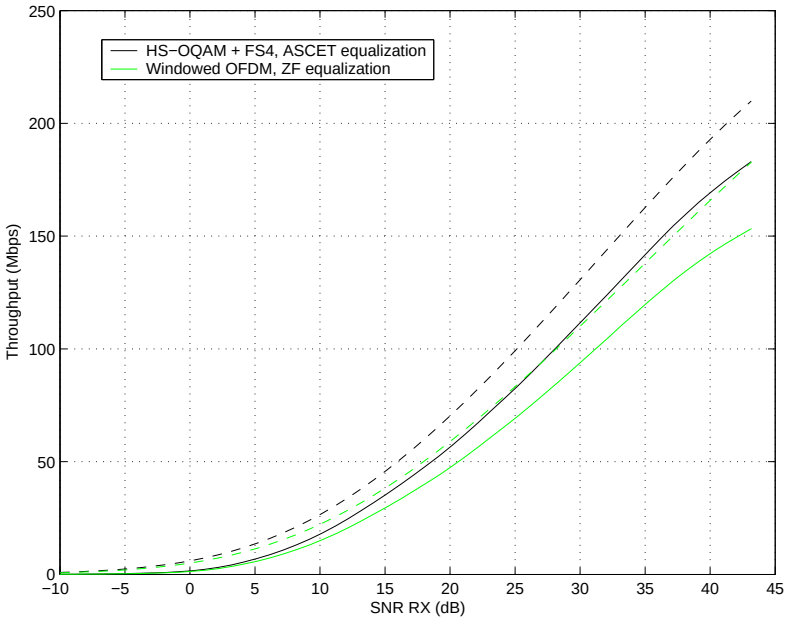

Figure 3.20: Transmission capacities (dotted curves) and PHY data rates (continuous curves) in the HPAV 1 context on Class 2 channels.

can be observed between the results presenting the transmission capacity (dotted curves) and the ones presenting the achievable throughput (continuous curves). Actually, as these results were established using class 9 channels, the SINR per subcarrier is very high and for that reason, the capacity reached per subcarrier theoretically (see (3.2)) allows to carry much more bits than b_{max} (see (3.6)). In the same figure, we can also note that from a certain SNR_{RX}, the transmission capacity of HS-OQAM bends and finally becomes lower than the one reached by windowed OFDM. This can be easily explained by the remaining interference inherent in HS-OQAM whenever the channel is not perfect, while the short delay spread of class 9 channels does not affect windowed OFDM, which is practically noticed by the linear increase of its transmission capacity. Note that for channels belonging to classes 5 and 2, this crossing cannot be seen because the maximum SNR_{RX} is much lower than the 85 dB reached with class 9 channels. The three figures also present the achievable throughput, also denoted as the PHY data rate, for classes 2, 5 and 9 channels. In these three cases, for any value of the SNR_{RX}, HS-OQAM provides better performance than windowed OFDM. Actually, at the maximum transmitting power, the bit-rate provided by HS-OQAM is at least 19% higher compared to the one provided by windowed OFDM. Indeed, for class 2 channels, HS-OQAM outperforms windowed OFDM with an averaged data rate being 19.3% higher than the one provided by OFDM. Moreover, it can be noticed that the gap between the data rates reached by the two modulations increases with the channel class, as the remaining interference decreases. Indeed, for class 5 channels, the improvement reaches 19.6% while for class 9 channels, the averaged data rate is 20.1% higher than for windowed OFDM. So, in spite of a bigger interference term for HS-OQAM, the advantages of having a guard interval reduced to zero and using more subcarriers are still predominant and allow this modulation to be ahead of windowed OFDM in terms of bit-rate. However, this advantage could be partly lost if the PLC system could operate at

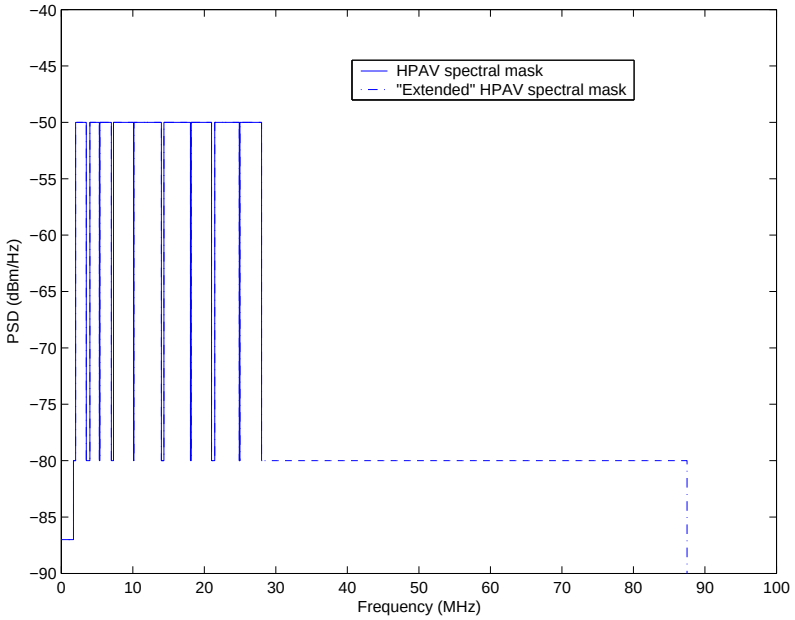

Figure 3.21: HPAV Spectral mask and its extension in the upper band.

still higher SNR, which is not envisioned in any specification nor standard, or if the bit limitation could be significantly increased. Now, let us look at the results achieved in the context of HPAV 2 networks.

3.4.3.2 HomePlug AV 2 Context

In this part, we extend the HPAV bandwidth up to 87.5 MHz, just below the FM broadcasting band. As for future HPAV 2 systems, we now consider a sampling frequency $F_s = 200$ MHz, and all previous length parameters (M, L_{GI}, L_{RI}) are simply multiplied by an $8/3$ factor. So, the window keeps its initial shape, only its length in samples is increased using an 8192-point FFT, still with a subcarrier spacing unchanged at $F_0 = 24.414$ kHz. The window function is modified in order to take into account the new IFFT size. Thus the roll-off interval (RI) is increased going from 372 samples in the HPAV band to $372 \times \frac{8}{3} = 992$ samples. As it can be seen in Fig. 3.21, the transmitted PSD is limited to -80 dBm/Hz beyond 28 MHz. Now, keeping the 917 active sub-carriers in the HPAV band and because of its secondary lobes, windowed OFDM does not respect the spectral mask if the subcarriers located just beyond the 28 MHz limit are switched on. So, for windowed OFDM, the 10 first subcarriers are not used in order to still satisfy the HPAV requirement together with the -80 dBm/Hz limitation. Concerning HS-OQAM using FS4 prototype filter, these subcarriers can be active while still satisfying the mask. To summarize, the number of usable subcarriers according to the different modulations is as follows:

- windowed OFDM: $\mathrm{Card}(\mathbb{M}_u) = 917$ (HPAV) $+ 2428 = 3345$
- HS-OQAM/FS4: $\mathrm{Card}(\mathbb{M}_u) = 970$ (HPAV) $+ 2438 = 3408$

Moreover, HPAV 2 specification, as the IEEE P1901 standard, allows to carry a maximum of 12 bits per subcarrier. So, in these simulations, we set $b_{max} = 12$ (see subsection

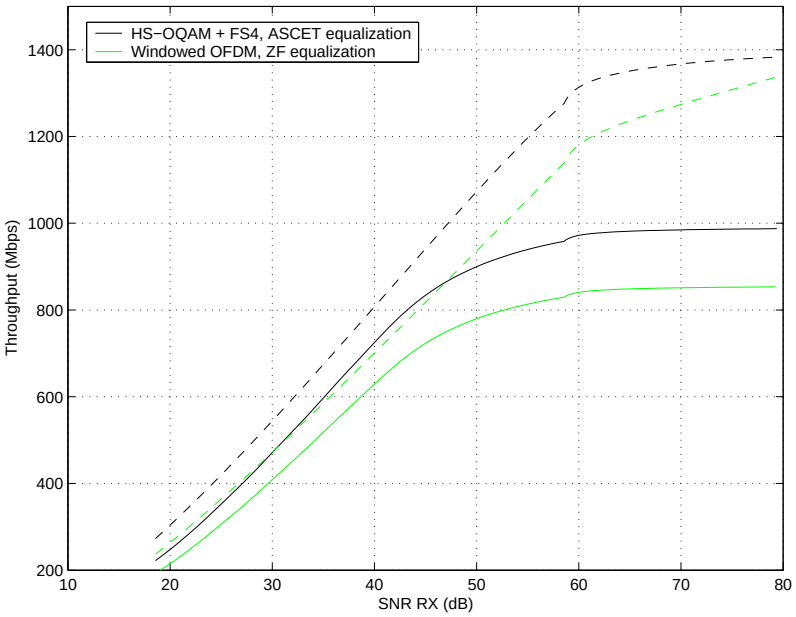

Figure 3.22: Achievable throughput (dotted curves) and PHY data rates (continuous curves) in the HPAV 2 context on Class 9 channels.

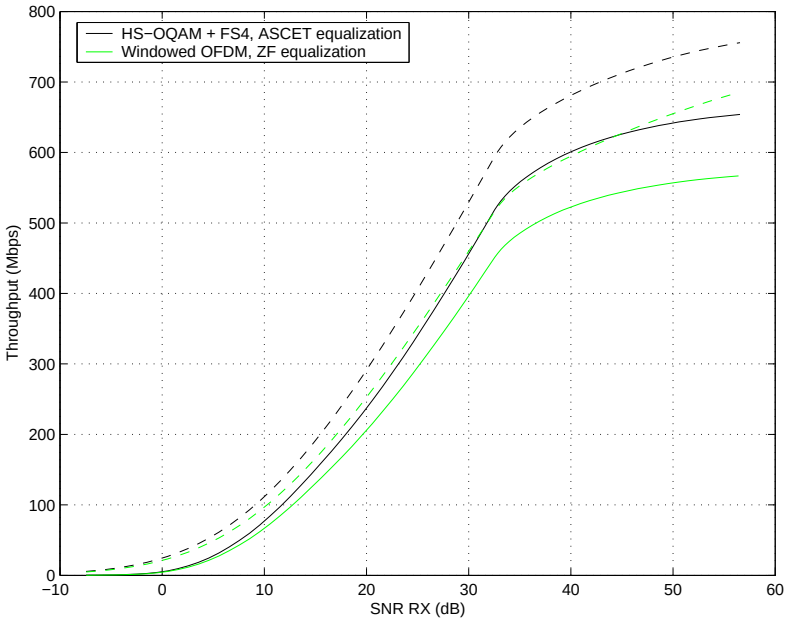

Figure 3.23: Achievable throughput (dotted curves) and PHY data rates (continuous curves) in the HPAV 2 context on Class 5 channels.

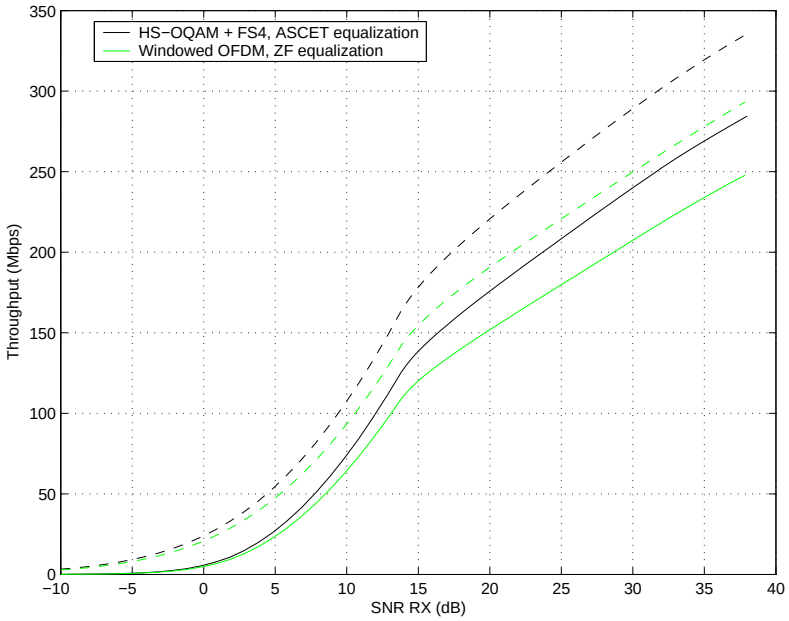

Figure 3.24: Achievable throughput (dotted curves) and PHY data rates (continuous curves) in the HPAV 2 context on Class 2 channels.

3.1.3). The results on the three classes of channels are presented in Figs. 3.22, 3.23 and 3.24. As for Fig. 3.18, 3.19 and 3.20, the transmitted PSD is linearly increased starting from −120 dBm/Hz for all the active subcarriers but as soon as it reaches −80 dBm/Hz, the transmitted PSD is only increased for the subcarriers located below 28 MHz until it reaches −50 dBm/Hz. The point from which the PSD is saturated in the upper band can be easily noticed in the figure. The first remark that can be made on the results is that HS-OQAM always shows better performance than windowed OFDM, for the achievable throughput as for the transmission capacity. Nevertheless, we can notice that the gains in the data rates, for all channels classes, are lower than the ones observed for the simulations in the HPAV band only. Actually, the achievable throughputs provided by HS-OQAM are 14.8%, 15.4% and 15.7% higher for channels belonging to classes 2, 5 and 9, respectively. These lower gains can be easily explained by the fact that, by extending the bandwidth, the ratio of subcarriers added exclusively for HS-OQAM modulation is lower than the same ratio observed in the HPAV band only. One can also notice that the crossing between the transmission capacity curves is no more present. Indeed, because of the limitation to −80 dBm/Hz in the upper band, the maximum SNR_{RX} reached in the *extended* HPAV context is, for each class, lower than the one attained in the HPAV context. Nevertheless, for the simulations in classes 5 and 9 channels, we really take advantage of the extension in the bandwidth, by reaching data rates up to 1 Gbps using HS-OQAM over class 9 channels for instance. Now, these good results have to be mitigated for class 2 channels, in which the gain in the achievable throughput is much lower. Obviously, with the limitation to -80 dBm/Hz, the achievable SINRs per subcarrier are too low to really take advantage of the new bandwidth, considering its relatively large increase. Finally, these simulations in an *extended* HPAV context show that HS-OQAM can provide an important improvement in the achievable throughput, realizing data rates about 15% higher than windowed OFDM.

3.4.4 Potential Impact of the CENELEC Mask on HPAV Networks

While the FCC clearly defines a spectral mask that PLC systems must comply with in North America, the regulatory environment remains uncertain in the EU. Indeed, it appears that more applications have to be protected from the radiated power by PLC equipments in Europe (see Appendix B.2) than in the US. Consequently, the european committee in charge of Electromagnetic Compatibility (EMC) regulations, the CENELEC, proposed a new EMC standard in 2011 for broadband PLC systems. The first version of the document was firstly rejected by a majority of the national standard committees of the EU countries, but a new vote will occur in early 2013 to approve or reject the standard. This document defines a first set of frequency ranges that must always be safe from PLC EMI, and a second set of frequencies that might be necessary to dynamically notch, depending on the location where the PLC system is in use. However, regardless of the considered CENELEC spectral mask, either including permanently only or permanently and dynamically excluded frequency ranges, the mask remains much more restrictive than the FCC one. In the case where this standard would be ratified in its current version, it would have a dramatic impact on the capacity of current PLC networks. In this section, we firstly aim at assessing the potential decrease in the capacity of HPAV networks that would be caused by the introduction of this new spectral mask. Secondly, we highlight the increased performance gap between HS-OQAM and windowed OFDM caused by the introduction of the CENELEC mask.

3.4.4.1 Impact of the CENELEC Mask on the Number of HS-OQAM and Windowed OFDM Active Tones

In Fig. 3.25, we present the PSDs of windowed OFDM and HS-OQAM using the FS4 prototype filter. It clearly appears that both CENELEC masks define a lot more notches than the North American one (see Fig. 3.5), which results in a severe decrease of the number of active subcarriers. While HPAV 1 allows to use 917 subcarriers following the FCC spectral mask, this number drops to 767 in order to fit into the CENELEC mask that only includes permanently excluded frequencies, such that about 16 % of the original bandwidth is lost. Moreover, if we also consider all dynamic notches, only 503 subcarriers can be activated, meaning that more than 45 % of the frequency resource is lost! On the other hand, the excellent spectral containment of the FS4 prototype filter allows HS-OQAM to keep 871 active tones while still complying with the first CENELEC mask, which represents a significant gap when compared to the 767 active subcarriers of the equivalent windowed OFDM scheme. Considering the most restrictive CENELEC mask, HS-OQAM still allows 632 subcarriers to be used, meaning that HS-OQAM would provide more than 25 % additional subcarriers than windowed OFDM in such a scenario. As we have already highlighted in this chapter, using a frequency selective filter allows to activate more subcarriers at the notch edges. Consequently, the more notches there are, the bigger will be the gap between HS-OQAM and windowed OFDM. Moreover, the gap becomes even more important considering the closeness of some notches, which is highlighted in Fig. 3.26, where it appears that it is sometimes not possible to insert any subcarrier between two consecutive notches using windowed OFDM, while HS-OQAM with FS4 can activate several ones.

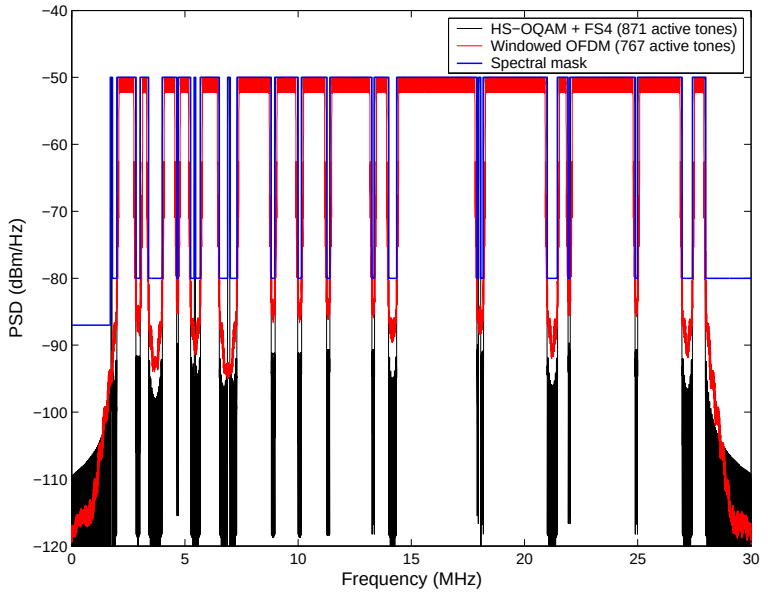

(a)

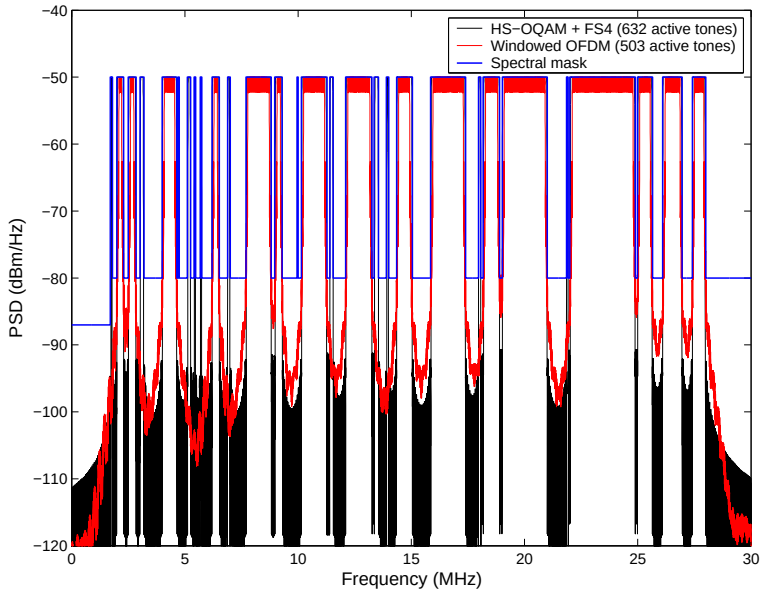

(b)

Figure 3.25: Compared PSD between HPAV windowed OFDM and HS-OQAM associated with a FS4 prototype filter, complying with CENELEC spectral mask: (a) permanently excluded frequencies only (b) permanently and dynamically excluded frequencies.

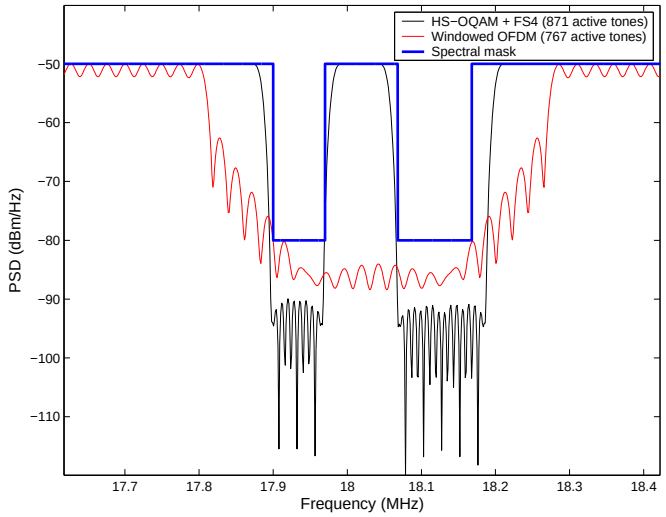

Figure 3.26: Magnified PSDs around the 18 MHz region of Fig. 3.25-(b).

3.4.4.2 Impact of the CENELEC Mask on HPAV Networks Capacity: Comparison Between HS-OQAM and Windowed OFDM

As in section 3.4.3, all the results are presented here both in terms of transmission capacity ($D^{inf\ gran}$) and achievable throughput (D^{PHY}). The HPAV 1 specification is followed, such that a maximum of 10 bits can be carried with a single subcarrier. Windowed OFDM is still associated with a 1-tap ZF equalizer, and the number of active subcarriers is either equal to 767 or 503, depending on whether dynamic notching is used or not. Considering HS-OQAM, we exploit the possibility to add subcarriers using the FS4 prototype filter, such that 871 and 632 tones are active, this number also depending on the applied CENELEC mask. However, as the relative difference in the number of active tones between the two modulations is significantly higher than in section 3.4.3, in addition to ASCET equalization, we also associate HS-OQAM with a 1-tap ZF to see if the higher interference term can be compensated by the additional bandwidth. The curves depicted in Fig. 3.27, Fig. 3.28 and Fig. 3.29, are computed by averaging simulation results over 100 channels realizations, using a unique colored noise generation per channel realization. To obtain these curves, the signal PSD is increased from -120 dBm/Hz to -50 dBm/Hz. So, for each curve, the last point on the right corresponds to the maximum authorized PSD by the spectral mask. The averaged SNR is computed as in (3.68). However, as $\mathbb{M}_u$ of windowed OFDM differs from $\mathbb{M}_u$ of HS-OQAM, the resulting SNR_{RX} will vary slightly between the two modulations. Let us firstly look at Fig. 3.27, where the results are presented on class 9 channels for both masks. The significant gap between the transmission capacity (dotted curves) and the achievable throughput (continuous curves) has already been explained in 3.4.3.1: on class 9 channels, the SINR per subcarrier is very high and for that reason, the capacity reached per subcarrier (see (3.2)) allows to carry much more bits than b_{max}. Consequently, the achieved PHY data rates by HS-OQAM on class 9 channels will not depend upon the chosen equalizer, so that both curves (continuous black and purple ones) are overlapping. It is also interesting to notice that the association of HS-OQAM and ASCET allows to reach a maximum capacity higher than windowed OFDM when

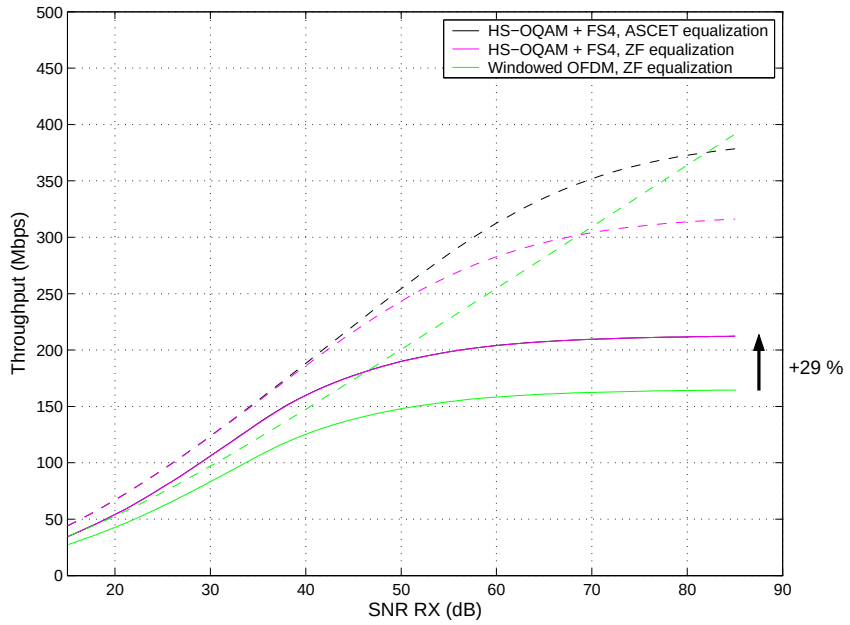

(a)

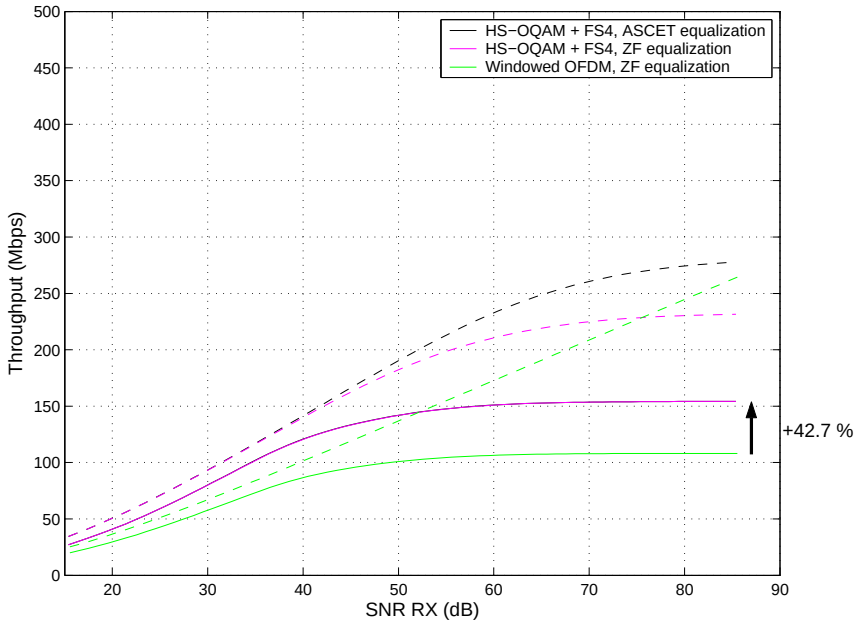

(b)

Figure 3.27: Transmission capacities (dotted curves) and PHY data rates (continuous curves) on Class 9 channels, considering: (a) permanently excluded frequencies by CENELEC only (b) permanently and dynamically excluded frequencies by CENELEC.

the most restrictive mask is applied (Fig. 3.27-(b)), which was not the case in Fig. 3.18. Concerning the PHY rates shown in 3.27-(a), HS-OQAM allows to keep about the same capacity of 200 Mbps as current HPAV networks that use the North American mask (see Fig. 3.18). Moreover, it appears that if the most restrictive CENELEC mask were to be imposed to current systems, it would lead to almost dividing by 2 the overall capacity of HPAV networks! On the other hand, thanks to the additional subcarriers, HS-OQAM significantly limits the impact of the bandwidth reduction, by achieving saturated PHY data rates 29 % and 42.7 % higher than windowed OFDM in Fig. 3.27-(a) and Fig. 3.27-(b), respectively. In Fig. 3.28 where the simulations were performed on class 5 channels, the two curves presenting the achieved PHY data rates of HS-OQAM either using an ASCET or a 1-tap ZF can now be discriminated because of the higher interference term. However, we can notice on both graphs that using the 1-tap ZF still allows HS-OQAM to significantly outperform windowed OFDM in terms of bit rates. Considering the most efficient equalization method, HS-OQAM can increase PHY data rates by 28.4 % and 41.6 %, respectively. These gains are slightly lower than the ones achieved on class 9 channels, due to the higher interference level of HS-OQAM. This term is even higher in class 2 PLC channels, so that PHY rates are improved by 27.7 % and 40.3 % in Fig. 3.29. Looking at the dotted curves on both plots, we can also notice that HS-OQAM always provides an higher transmission capacity than windowed OFDM. It is finally important to highlight the fact that the association of HS-OQAM with a 1-tap ZF always outperforms the HPAV modulation scheme, whatever channel class being considered. While this short study clearly highlights the dreadful effect of this new regulation policy, it also confirms the benefits of a highly spectrally efficient modulation such as HS-OQAM.

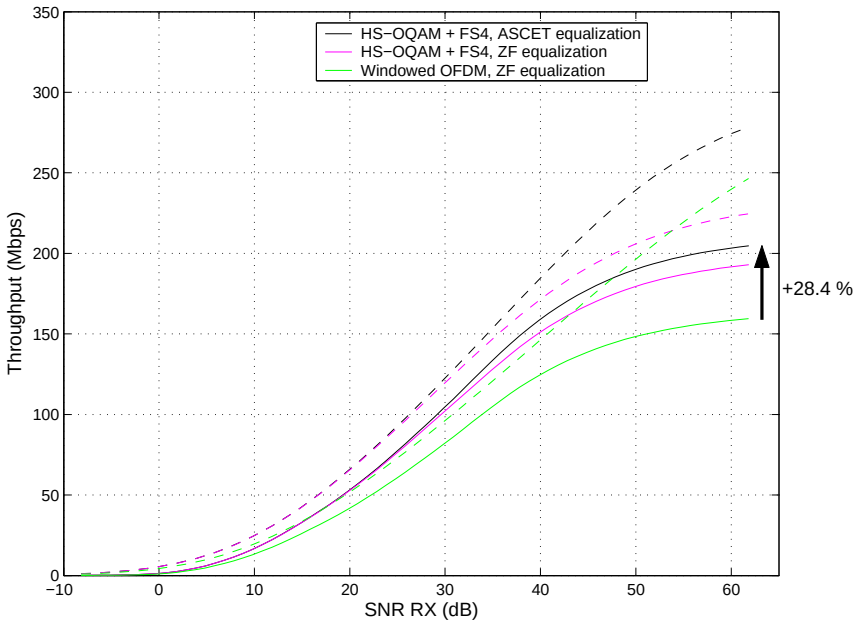

(a)

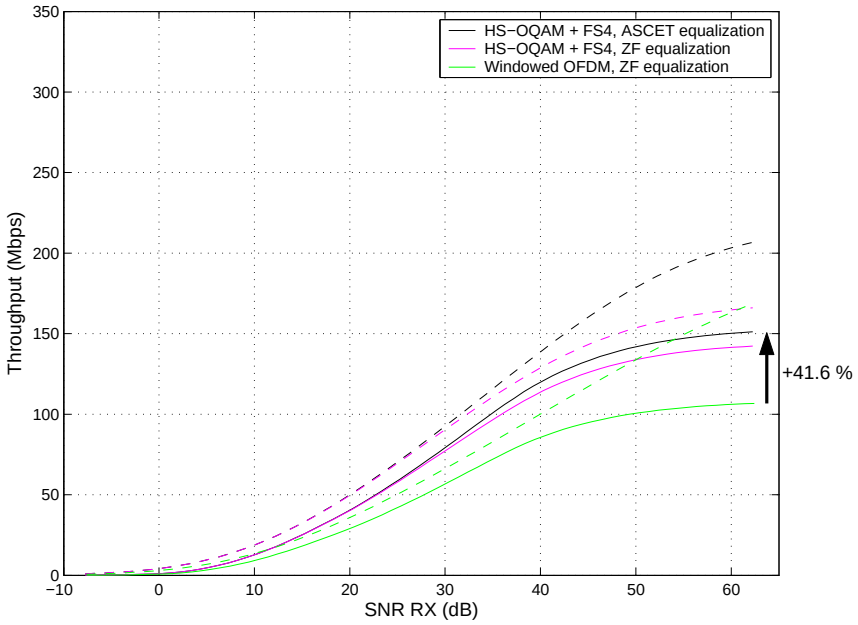

(b)

Figure 3.28: Transmission capacities (dotted curves) and PHY data rates (continuous curves) on Class 5 channels, considering: (a) permanently excluded frequencies by CENELEC only (b) permanently and dynamically excluded frequencies by CENELEC.

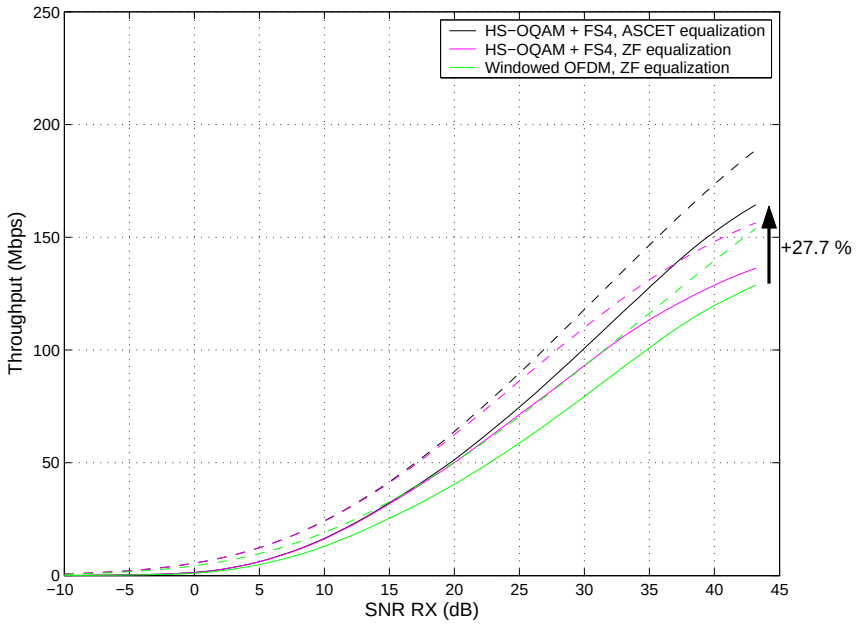

(a)

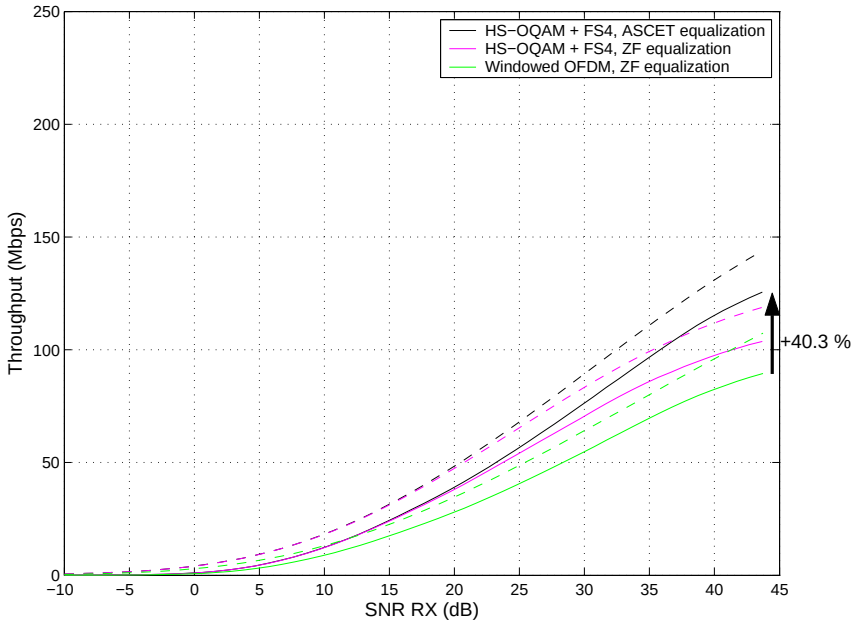

(b)

Figure 3.29: Transmission capacities (dotted curves) and PHY data rates (continuous curves) on Class 2 channels, considering: (a) permanently excluded frequencies by CENELEC only (b) permanently and dynamically excluded frequencies by CENELEC.

3.5 Conclusion

The main purpose of this Chapter was to study HS-OQAM performance in a realistic scenario and compare it to windowed OFDM, the modulation scheme used by HPAV systems. We have shown that a significant improvement in the data rates can be achieved using this alternative modulation scheme, when associated to a frequency selective prototype filter with a length of at least 4 times the IFFT size, together with a 3-tap equalizer per subcarrier. Indeed, the flexibility offered by HS-OQAM in the pulse shaping allows the design of prototype filters well adapted both to the frequency selective channel and to the transmission mask. Thus, we show that HS-OQAM using an FS4 prototype filter and associated to an ASCET equalizer always outperforms windowed OFDM, with a minimum improvement of 15% in the data rates. It is important to notice that the 3-tap ASCET equalizer only induces a slight complexity augmentation when considering the whole system complexity and, above all reasons, when considering the potential benefit brought by HS-OQAM in this particular context. Moreover, the gap between the two compared schemes could be even more important if the spectral mask defines more notches in the $[0, 100]$ MHz bandwidth. If the CENELEC spectral mask is eventually imposed to every HPAV system sold in the European Union, the capacity of HPAV networks would be then drastically reduced. It clearly highlights the need for more spectrally efficient modulations schemes, such as OFDM/OQAM. Finally, we emphasize on the fact that a drawback of OFDM/OQAM, concerning the time spread of frequency selective prototype filters that can be an issue when transmitting frames on a shared medium, can be now totally avoided for short prototype filters, e.g. TFL1, [55], and strongly attenuated for longer ones [38]. In the following of this document, we are going to consider PLC networks working in a multiuser context, and we will show how the link adaptation that is realized through the definition of tone maps could be much more efficiently exploited by the MAC layer. The tone maps we will use in the following were generated using the windowed OFDM modulation defined by HPAV. Nevertheless, for every solution presented in Chapters 4 and 5, the OFDM/OQAM modulation could have been used to generate tone maps.

Chapter 4

Point-to-Multipoint Transmissions in Powerline Networks

4.1 Preliminary

4.1.1 The Interest of FDM in PLC Networks

Broadband Internet accesses allow customers to simultaneously access a lot of distant services. Considering the fact that PLC stations are often requesting distant services, the network activity is often centralized around the PLC station in charge of forwarding these services throughout the PLC network, i.e. the one directly connected to the Internet access point (in the following, this station is referred to as the "access point" of the PLC network). So, it appears that point-to-multipoint communication is a common use case considering home networking applications. Also, as current PLC networks only define point-to-point transmissions, the transmission of multiple services in a point-to-multipoint scenario is currently handled only using a Time Division Multiplexing (TDM) transmission scheme, by the means of CSMA/CA or TDMA access techniques.

Now, we have seen that the quasi static nature of the PLC transmission channel allows the use of bit-loading techniques, resulting in the definition of dedicated tone maps. Moreover, it has been widely shown in literature that the frequency fading nature of the PLC channel mainly comes from multiple signal reflections due to impedance mismatches at the outlets [94], [115]. So, it is highly likely that the transmission channels between the access point, and all the other stations of the network, will provide a multiuser diversity that will appear through the K tone maps exclusively created to reach the K stations the central node will be communicating with. In Fig. 4.1, 4 measured point-to-multipoint channels illustrate this multiuser diversity in frequency in the range $[1.8, 100]$ MHz. Actually, the frequency selective nature of the PLC channel is not the only source of diversity. Indeed, in the previous Chapter, we have introduced the transmission mask imposed to all PLC systems, where it appears that above 30 MHz, the transmitted power must be drastically reduced. From a -50 dBm/Hz PSD limitation in the lower band, the maximum transmitted PSD beyond this limit must drop to -80 dBm/Hz. Consequently, if we consider the case where the access point communicates with one station with a low channel attenuation on the one hand and, on the other hand, with another station for which the transmission channel is strongly attenuated, thanks to this power limitation, the diversity will be even

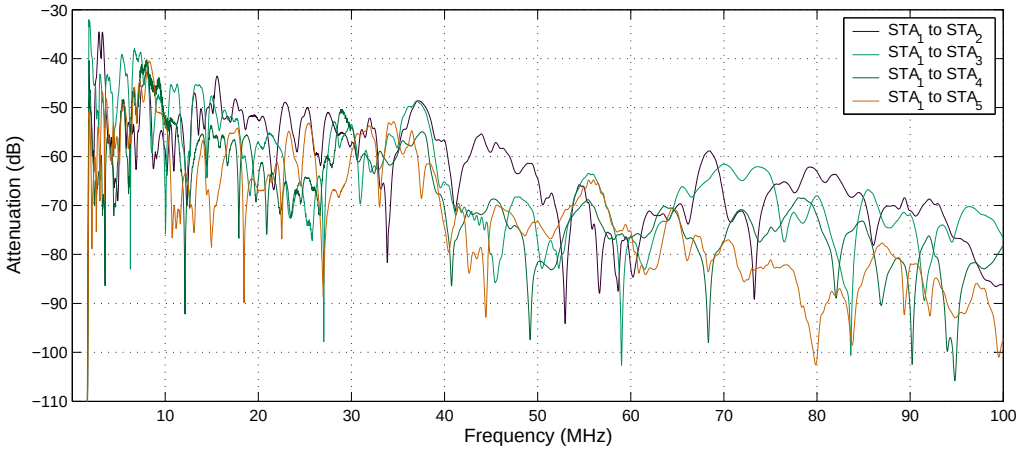

Figure 4.1: Illustration of the Multiuser diversity among 4 measured PLC channels in the $[1.8, 100]$ MHz frequency range (provided by the HPAV working group).

more important between these two transmission paths. Indeed, as it is illustrated by the two tone maps of Fig. 4.2, a severely attenuated channel will achieve most of its transmission capacity below 30 MHz, meaning that the the frequency resource beyond this limit is wasted. On the other hand, considering the low attenuated channel, the achieved capacity in the upper band may be important. So, in this particular but common case, it is obvious that the PLC network would greatly benefit from the definition of an OFDMA transmission scheme.

However, it appears that this multiuser diversity is not exploited by current PLC systems, as only TDM is used. So, in this Chapter, we aim at defining a Frequency Division Multiplexing (FDM) access mode for point-to-multipoint transmissions, by orthogonalizing the K tone maps respectively defined on each of the K active links. Firstly, we study the tone maps orthogonalization problem and we develop a geometrical method for solving it. Then, we propose a low-cost algorithm to efficiently split tone maps. This solution is compared to another tone map splitting algorithm that was proposed in [69]. Finally, we define an HPAV compliant OFDMA transmission scheme which performance is tested using the PLC network simulator described in Appendix A. In the following, we only consider quasi-static channels, meaning that their evolutions in time are really slow compared to the duration of an OFDM symbol. Then, obviously, the tone maps are also considered time-invariant. To ease notations, we now assume that $\mathbb{M} = \mathbb{M}_u = \{1, .., M\}$, as we will only work with the set of active tones.

4.1.2 Resource Allocation Problems

The capacity of multiuser channels has been extensively studied in the literature. If a limited resource has to be allocated among K users, a K-dimensional capacity region can be computed to evaluate every possible partition of the resource among the K users. In a multiuser context, two different scenarios are generally studied, which are presented in Fig. 4.3 in which $H_k(\omega)$ and n_k denote the channel frequency response and the noise source on link k, respectively. Firstly, there is the well-known broadcast channel, introduced

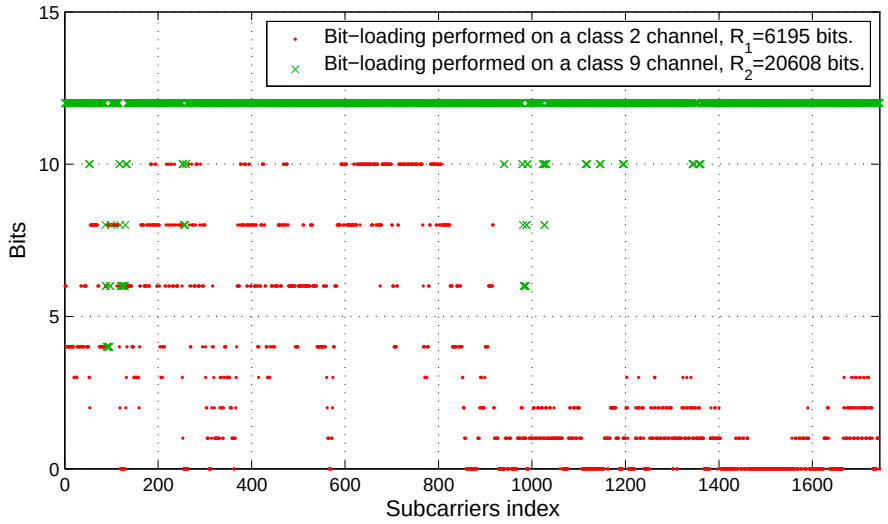

Figure 4.2: Bit-loading performed in the [1.8, 50] MHz frequency range, following the IEEE P1901 specification.

in [50], and modeling downlink transmissions from the "access point" to multiple nodes of the network. Secondly, there is the multiple access channel [46], corresponding to the uplink transmission scenario, where all users can access the medium to communicate with the Base Station, also corresponding to the access point of the network. Considering in-home PLC, the network has a bus topology and each station can access the channel to directly communicate with any station of the network. So, multiuser PLC networks can be modeled using the two aforementioned models and the particular case of point-to-multipoint transmissions is modeled using the broadcast channel. The balanced capacity of a multiuser system is defined as the distribution of maximum simultaneously achievable bit rates that are in proportion with the single-user rates. It is a specific point of the boundary of the capacity region for which the coexistence with the other users has the same relative cost for every user. In the past, many studies have been conducted to maximize the capacity under fixed power constraints [112]. In other approaches, the resource allocation strategy aims at minimizing the consumed power to satisfy a fixed bit rate by a particular application [111].

In our approach, we consider the transmissions to be already established using a time division multiplexing scheme that is actually the current mode of operation of PLC networks. Secondly, and this a key point to put in perspective previous works, the bit-loading is done at the receiver side, meaning that the access point has only knowledge of the tone maps associated to the K links it is using. Consequently, the classical degrees of freedom of resource allocation problems, such as power allocation or QoS, are fixed. This also means that most of the sub-optimal allocation algorithms developed in the literature cannot directly be applied in the considered context. Basically, the tone maps orthogonalization problem comes down to distribute M active subcarriers among K links, where the m-th subcarrier of the k-th link is associated with a fixed number of carried bits. Now, solving this problem is far from being straightforward as the optimal allocation solution

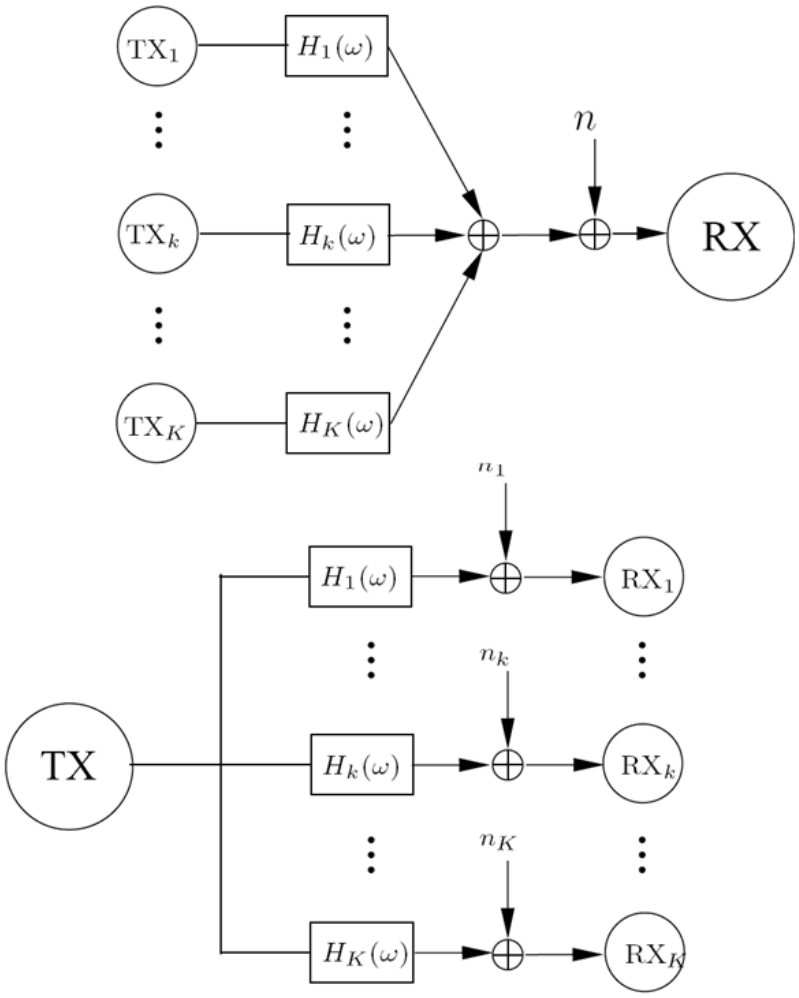

Figure 4.3: Multiple access and broadcast channels.

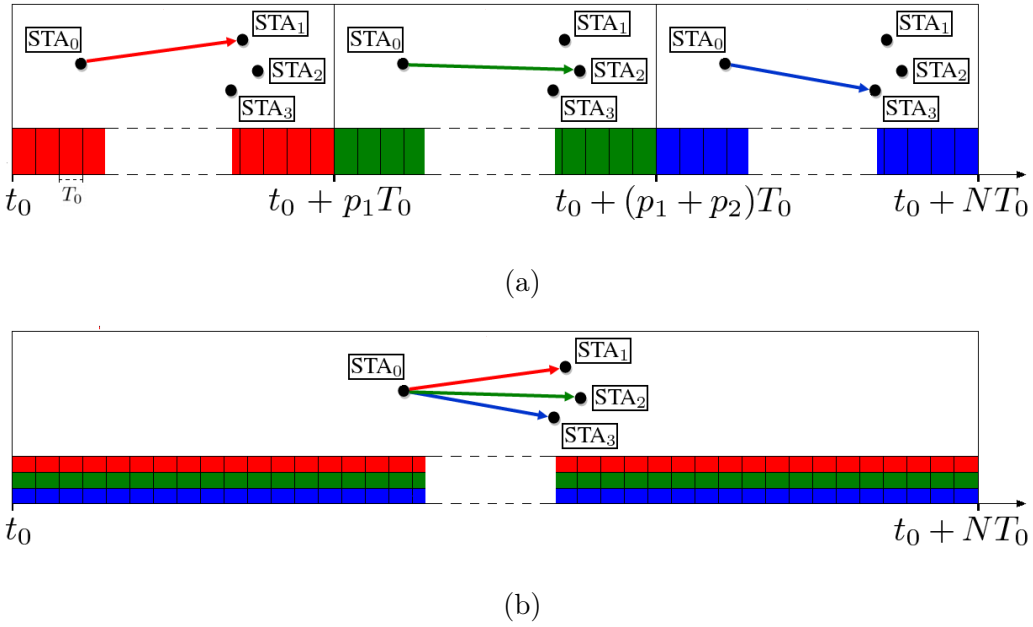

Figure 4.4: Point-to-multipoint transmission: (a) using TDMA (b) using FDMA.

is not necessarily to assign a user the best subcarriers seen by that user. Actually, the complexity of this problem can be foreseen considering the case where the best subcarrier of a user is also the best subcarrier of another user who happens to have no other good subcarriers.

4.1.3 Taking Advantage of the Frequency Diversity

Before putting down the tone maps orthogonalization problem, let us prove that FDMA improves point-to-multipoint transmissions, considering quasi-static links. We consider the case of K stations to reach: STA_1, STA_2,..., STA_K. The communication channel between STA_0, the transmitter, and the station STA_k is characterized by its transmission capacity C_k, computed inside the bandwidth $B = [f_{\min}, f_{\max}]$, $B \subseteq \mathbb{R}^+$:

$$C_k = \int_{f_{\min}}^{f_{\max}} b_k(f) df, \tag{4.1}$$

with $b_k(f) = \log_2(1 + \frac{\text{SINR}_k(f)}{\Gamma})$, a continuous and differentiable function in $\mathbb{R}^+$, $\forall k \in \mathbb{K} = \{1, ..., K\}$, where $\text{SINR}_k(f)$ stands for the Signal to Interference plus Noise Ratio at frequency f. Γ, the SINR gap, is set to the same value for the K links and is defined for a target symbol error rate (SER) by [48]:

$$\Gamma = \frac{1}{3}\left[Q^{-1}\left(\frac{\text{SER}}{4}\right)\right]^2 \tag{4.2}$$

in which $Q^{-1}(x)$ is the inverse tail probability of the standard normal distribution.

The studied problem is illustrated in Fig. 4.4 and we make the following assumptions: only useful information is transmitted, so that no overhead is taken into account. Also,

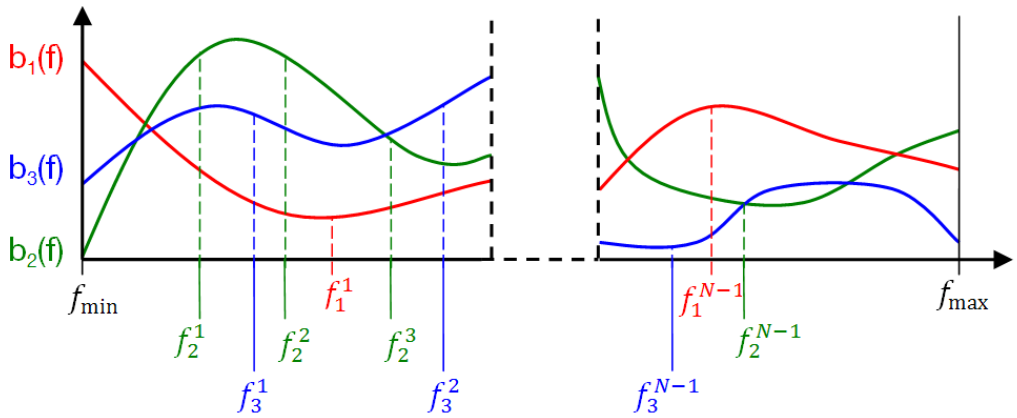

Figure 4.5: Splitting the frequency bandwidth into N subbands of equal capacity for each link.

the considered time interval exactly corresponds to the transmission of N OFDM symbols of duration T_0. Here, we recall that the channels are supposed to be static during NT_0. Considering TDMA, p_k OFDM symbols are transmitted to STA_k, so that $\sum_{k=1}^{K} p_k = N$. Note that all values of p_k can be different, in order to take into account the fact that data rates may vary on every link, that each link possesses its own transmission capacity and also that the streams may be prioritized by STA_0. The averaged transmission capacity during NT_0 using TDMA can be computed as:

$$C_{\text{av}}^{\text{TDMA}} = \frac{\sum_{k=1}^{K} p_k C_k}{N}. \tag{4.3}$$

Now, considering FDMA, the K transmissions occur simultaneously, so that:

$$C_{\text{av}}^{\text{FDMA}} = \sum_{k=1}^{K} C_k^{\perp} \tag{4.4}$$

with

$$C_k^{\perp} = \int_{B_k} b_k(f)df,\ B_p \cap B_q = \varnothing,\ \forall\ (p,q) \in \mathbb{K}^2. \tag{4.5}$$

Theorem. *Considering* $p_k | p_k \in \mathbb{N}$ *and* $\sum_{k\in\mathbb{K}} p_k = N$ *in which* $\mathbb{K} = \{1,..,K\}$, C_k *and* $C_k^{\perp}$ *following the definitions given in* (4.1) *and* (4.5), *respectively,* $\exists\ \{B_k | B_k \in B,\ B \subseteq \mathbb{R}^+\}$ *so that:*

$$\begin{cases} \bigcup_{k=1}^{K} B_k \subseteq B \\ \bigcap_{k=1}^{K} B_k = \varnothing \\ C_k^{\perp} \geq \frac{p_k C_k}{N},\ \forall k \in \mathbb{K} \end{cases} \tag{4.6}$$

Proof. For each link k, the bandwidth B is divided into N sub-bands $\Delta B_k^n = \left[f_k^{n-1}, f_k^n\right[$, $n \in \{1,..,N\}$, $f_k^0 = f_{\min}$ and $f_k^N = f_{\max}$, $\forall k \in \mathbb{K}$, so that:

$$\int_{\Delta B_k^n} b_k(f)df = \frac{C_k}{N}. \tag{4.7}$$

In the following, N sub-bands ΔB^n are iteratively distributed among the K links, so that $B_k = \bigcup_{i \in F_k} \Delta B^i$, $F_k \subseteq \{1, .., N\}$. The number of allocations to the link k is saved in a_k, $a_k = \text{Card}(F_k)$, initialized to 0, and $p_k > 2$, $\forall k \in \mathbb{K}$. This principle, which is illustrated on Fig. 4.5, leads to the iterative algorithm which is described in the following for any value of K:

$\underline{\mathbf{n = 1}}$: the first sub-band is allocated to the link q, with $f_q^1 \leq f_k^1$, $\forall k \in \mathbb{K}$, so that $\Delta B^1 = \Delta B_q^1$. a_q is incremented so that $\sum_{k \in \mathbb{K}} a_k = 1$, $C_q^{\perp} = \frac{C_q}{N}$ and is null on any other link. Also, $\forall k \in \mathbb{K}$, the remaining capacity beyond f_q^1 is greater or equal than $\frac{(N-1)C_k}{N}$.

$\underline{\mathbf{n = 2}}$: the second sub-band is allocated to the link r, with $f_r^2 \leq f_k^2$, $\forall k \in \mathbb{K}$, so that $\Delta B^2 = \Delta B_r^2$. From the previous iteration, we know that $f_r^2 \geq f_q^1$, so that $\Delta B^1 \cap \Delta B^2 = \varnothing$. a_r is incremented so that $\sum_{k \in \mathbb{K}} a_k = 2$ and $C_r^{\perp} = \frac{a_r C_r}{N}$. Also, $\forall k \in \mathbb{K}$, the remaining capacity beyond f_r^2 is greater or equal than $\frac{(N-2)C_k}{N}$.
...
$\underline{\mathbf{n = A_1}}$: proceeding in a same manner as for the previous iterations, let us suppose that the A_1^{th} allocation is for the benefit of the link 1 and that a_1 reaches the value of p_1, while $a_k < p_k$, $\forall k \in \mathbb{K} \setminus \{1\}$. From the previous iterations, we have $\bigcap_{n=1}^{A_1} \Delta B^n = \varnothing$. The link 1 has reached the targeted transmission capacity, so that $C_1^{\perp} = \frac{p_1 C_1}{N}$ (no more bandwidth will be allocated to it) and $\sum_{k \in \mathbb{K}} a_k = A_1$. Also, $\forall k \in \mathbb{K}$, the remaining capacity beyond $f_1^{A_1}$ is greater or equal than $\frac{(N-A_1)C_k}{N}$.
...
$\underline{\mathbf{n = A_{K-1}}}$: again, let us suppose that the A_{K-1}^{th} allocation is for the benefit of the link $(K-1)$ and that a_{K-1} reaches the value of p_{K-1}, so that only $a_K < p_K$. From the previous iterations, we have $\bigcap_{n=1}^{A_{K-1}} \Delta B^n = \varnothing$. The link $K-1$ has reached the targeted transmission capacity, so that $C_{K-1}^{\perp} = \frac{p_{K-1} C_{K-1}}{N}$ and $\sum_{k \in \mathbb{K}} a_k = A_{K-1}$. Also, $\forall k \in \mathbb{K} \setminus \{1, .., K-2\}$, the remaining capacity beyond $f_1^{A_{K-1}}$ is greater or equal than $\frac{(N-A_{K-1})C_k}{N}$. As the $N - A_{K-1}$ null-intersected sub-bands left can be allocated to the link K, its current capacity $\frac{a_K C_K}{N}$ increases by $\frac{(N-A_{K-1})C_K}{N}$. As $N - A_{K-1} = p_K - a_K$, we get $C_K^{\perp} = \frac{p_K C_K}{N}$.

Finally, N null-intersected sub-bands ΔB^n have been allocated, allowing every link to reach one $\frac{p_k}{N}^{\text{th}}$ of their own transmission capacities. In other words, it means that FDMA allows to transmit the same quantity of information as TDMA, while using a total bandwidth lower than B. By extension, we prove that FDMA potentially provides a better transmission capacity than TDMA, as it is always possible to obtain $C_k^{\perp} \geq \frac{p_k C_k}{N}$, $\forall k \in \mathbb{K}$, using the same bandwidth B. □

In the following, we set $\frac{p_k}{N} = \alpha_k$, with $\sum_{k \in \mathbb{K}} \alpha_k = 1$, which will be referred to as a *priority coefficient*.

4.2 Problem Statement

4.2.1 Problem Discretization

In Section 4.1.3, the demonstration of the superiority of FDMA over TDMA has been done using a continuous-variable formalism. If we now consider K tone maps, defined on each

one of the K links, it confers a finite granularity to this resource allocation problem as the frequency bandwidth is divided into M sub-bands, corresponding to the M subcarriers of the OFDM signal. As there are M subcarriers to allocate among the K links, we easily infer that the number of allocation solutions is equal to K^M.

On the subcarrier m of the link k, $(k,m) \in \mathbb{K} \times \mathbb{M}$ where $\mathbb{M} = \{1,..,M\}$, the associated capacity reads:

$$C_k[m] = \int_{f_{m-1}}^{f_m} b_k(f)df, \text{ with } \begin{cases} f_0 = f_{\min} \\ f_M = f_{\max} \end{cases}. \tag{4.8}$$

At this point, we underline the fact that imposing the same value of Γ (see (4.1)) for the M subcarriers is essential to ensure the OFDM symbol error rate to remain lower than the target error rate on the K links after proceeding to the tone maps orthogonalization. Finally, the k^{th} transmission channel is associated with a unique tone map $T_k[m]$, obtained by proceeding to a quantization of $C_k[m]$, such that:

$$T_k[m] = \underset{b \in \mathrm{E}_{\text{const}}}{\arg\max}\{b | b \leq C_k[m]\}, \forall (k,m) \in \mathbb{K} \times \mathbb{M}, \tag{4.9}$$

where $\mathrm{E}_{\text{const}}$ contains the actual number of bits a single subcarrier can carry. As an example, if we consider the IEEE P1901 specification [7], we have $\mathrm{E}_{\text{const}} = \{0,1,2,3,4,6,8,10,12\}$.

So, a tone map can be seen as a vector with M components, each of them belonging to a finite and discrete set $\mathrm{E}_{\text{const}}$, the m^{th} component corresponding to the actual number of bits carried by the m^{th} subcarrier. Also, we define the tone map capacity R_k, $R_k < C_k$:

$$R_k = \sum_{m \in \mathbb{M}} T_k[m], \forall k \in \mathbb{K}. \tag{4.10}$$

In the following we mainly work with normalized versions of tone maps, defined as:

$$t_k[m] = \frac{T_k[m]}{R_k}, \forall (k,m) \in \mathbb{K} \times \mathbb{M}, \tag{4.11}$$

and associated to the unitarian capacity:

$$r_k = \sum_{m \in \mathbb{M}} t_k[m] = 1. \tag{4.12}$$

The definition of an FDMA mode using tone maps comes down to distribute the M subcarriers among the K links to create an OFDMA scheme, so that K orthogonal tone maps $t_k^{\perp}[m]$ are constructed:

$$t_k^{\perp}[m] = \begin{cases} t_k[m], \text{ if } m \in \mathbb{S}_k, \text{ with } S_k \subseteq \mathbb{M} \text{ and } \bigcap_{k \in \mathbb{K}} \mathbb{S}_k = \varnothing \\ 0, \text{ otherwise.} \end{cases}, \tag{4.13}$$

and associated to their normalized capacities:

$$r_k^{\perp} = \sum_{m \in \mathbb{M}} t_k^{\perp}[m] = \sum_{m \in \mathbb{S}_k} t_k[m]. \tag{4.14}$$

The orthogonality between the newly defined tone maps can be verified using the scalar product. Recalling that their components are never negative, the orthogonality condition is reached if $t_p^{\perp}[m] t_q^{\perp}[m] = 0$, with $p \neq q$ and $\forall\ m \in \mathbb{M}$.

4.2.2 Discrete Extension of the Theorem of Section 4.1.3

If FDMA can always provide at least an equivalent capacity than TDMA in the continuous case, this cannot be assumed anymore after having discretized the problem. In the following, we are going to establish a sufficient condition to ensure the existence of K null-intersected $\mathbb{S}_k$ subsets, so that:

$$r_k^{\perp} = \sum_{m \in \mathbb{S}_k} t_k[m] > \alpha_k, \forall k \in \mathbb{K}. \tag{4.15}$$

As $\sum_{m \in \mathbb{M}} t_k[m] = 1$, we can firstly notice that:

$$(4.15) \Rightarrow \sum_{m \in \mathbb{M} \setminus (\mathbb{S}_k)} t_k[m] < 1 - \alpha_k. \tag{4.16}$$

$$\Leftrightarrow \sum_{k \in \mathbb{K}} \sum_{m \in \mathbb{M} \setminus (\mathbb{S}_k)} t_k[m] < \sum_{k \in \mathbb{K}} (1 - \alpha_k). \tag{4.17}$$

Assuming that $\bigcup_{k \in \mathbb{K}} S_k = \mathbb{M}$ and $\bigcap_{k \in \mathbb{K}} S_k = \varnothing$, we have $\sum_{m \in \mathbb{M} \setminus (\mathbb{S}_k)} = \sum_{p \in \mathbb{K} \setminus \{k\}} \sum_{m \in \mathbb{S}_p}$, so that:

$$\sum_{k \in \mathbb{K}} \sum_{p \in \mathbb{K} \setminus \{k\}} \sum_{m \in \mathbb{S}_p} t_p[m] < K - 1 \tag{4.18}$$

$$\Leftrightarrow \sum_{k \in \mathbb{K}} \sum_{m \in \mathbb{S}_k} \sum_{p \in \mathbb{K} \setminus \{k\}} t_p[m] < K - 1 \tag{4.19}$$

$$\Leftrightarrow \sum_{k \in \mathbb{K}} \sum_{m \in \mathbb{S}_k} \frac{1}{K-1} \sum_{p \in \mathbb{K} \setminus \{k\}} t_p[m] < 1. \tag{4.20}$$

Here, we have computed an equivalent tone maps on each $\mathbb{S}_k$ subset, by averaging the $(K-1)$ tone maps $t_p[m]$ verifying $p \neq k$. In the following, we set:

$$\bar{t}_k[m] = \frac{1}{K-1} \sum_{p \in \mathbb{K} \setminus \{k\}} t_p[m]. \tag{4.21}$$

At this point, we have demonstrated that satisfying (4.15) implies the capacity of this equivalent tone map to be lower than 1. From (4.15) and (4.20), we can write that:

$$\sum_{k \in \mathbb{K}} \sum_{m \in \mathbb{S}_k} (t_k[m] - \bar{t}_k[m]) > 0. \tag{4.22}$$

A sufficient condition to verify (4.22) is:

$$\sum_{m \in \mathbb{S}_k} (t_k[m] - \bar{t}_k[m]) > 0, \tag{4.23}$$

which is met if at least 1 subcarrier $m_k \in \mathbb{S}_k$ verifies $t_k[m_k] > \bar{t}_k[m_k]$. Moreover, as $\sum_{m \in \mathbb{S}_k} (t_k[m] - \bar{t}_k[m]) = -\sum_{m \in \mathbb{M} \setminus \mathbb{S}_k} (t_k[m] - \bar{t}_k[m])$, there must be at least 2 subcarriers, $m_k^1 \in \mathbb{S}_k$ and $m_k^2 \in \mathbb{M} \setminus S_k$, on which the two tone maps take different values. Now, if only 2 subcarriers verify $t_k[m] \neq t_k^{\perp}[m]$, it only ensures the existence of only one $\mathbb{S}_k$ so that (4.23) be satisfied. So, to ensure the existence of K null-intersected $\mathbb{S}_k$, a sufficient condition is

that $t_k[m]$ and $\bar{t}_k[m]$ take different values on $2K$ subcarriers, which is necessarily ensured if the following condition is met:

$$\sum_{m\in\mathbb{M}} |t_k[m] - \bar{t}_k[m]| > 4K\phi,\ \forall k \in \mathbb{S}_k, \tag{4.24}$$

where ϕ overestimates the coarsest capacity granularity and is defined as follows:

$$\phi = \max_{(k,m)\in\mathbb{K}\times\mathbb{M}} (t_k[m])\,. \tag{4.25}$$

(4.24) guarantees that there are at least K subcarriers where $t_k[m] > \bar{t}_k[m]$, $\forall k \in \mathbb{K}$, meaning that for each $k \in \mathbb{K}$, there are at least K different solutions ($\mathbb{S}_k$ subsets) ensuring $r_k^{\perp} > \alpha_k$, a final condition being that $\alpha_k < 1 - K\phi$, $\forall k \in \mathbb{K}$. Finally, we can extend the formulation of the theorem stated in section 4.5 to the discrete case.

Theorem. *We consider* $\{\alpha_k | \alpha_k \in \mathbb{R}^+,\ \alpha_k < 1 - K\phi$ *and* $\sum_{k\in\mathbb{K}} \alpha_k = 1\}$ *with* $\mathbb{K} = \{1, .., K\}$, $t_k[m]$, $r_k^{\perp}$, $\bar{t}_k[m]$ *and* ϕ *following the definitions given in* (4.11), (4.14), (4.21) *and* (4.25), *respectively. If* $\sum_{m\in\mathbb{M}} |t_k[m] - \bar{t}_k[m]| > 4K\phi$, $\forall k \in \mathbb{S}_k$, $\exists\ \{S_k | S_k \subseteq \mathbb{M} \subseteq \mathbb{N}\}$ *so that:*

$$\begin{cases} \bigcup_{k\in\mathbb{K}} S_k \subseteq \mathbb{M} \\ \bigcap_{k\in\mathbb{K}} S_k = \varnothing \\ r_k^{\perp} > \alpha_k,\ \forall k \in \mathbb{K} \end{cases}, \tag{4.26}$$

4.2.3 Mathematical Optimization

As we want to equally share the frequency diversity among the K links, the FDM gain maximization problem comes down to:

$$\text{Maximize:} \quad \min_{k\in\mathbb{K}} \sum_{m\in\mathbb{S}_k} \frac{t_k[m]}{\alpha_k}$$

$$\text{subject to:} \quad \{S_k | \bigcup_{k\in\mathbb{K}} S_k \subseteq \mathbb{M} \text{ and } \bigcap_{k\in\mathbb{K}} S_k = \varnothing\}$$

In this case, each subcarrier is exclusively allocated to only one link. According to [112], this resource allocation problem belongs to the class of integer programming problems, for which an exact solution usually involves an exhaustive search. As there are M subcarriers to assign among K stations, the number of possible partitions of the spectrum is equal to K^M, making an exhaustive search not even thinkable. To solve this problem, a possible method is to enlarge the constraint set using a continuous formalism. In other words, it comes down to allow a subcarrier to be fractionally allocated among the K links. In [111], the fractional allocation of a subcarrier is interpreted as the possibility to subdivide each tone allocation in time, allowing a subcarrier to be shared among several stations. So, instead of dealing with a discrete set of solutions, we are now dealing with a continuous set, implying that an infinite number of partitions is possible. Relaxing the problem results in the following optimization problem statement:

$$\text{Maximize:} \quad \sum_{k\in\mathbb{K}} \sum_{m\in\mathbb{M}} w_{k,m} \frac{t_k[m]}{\alpha_k}$$

$$\begin{aligned}\text{subject to: } & - \sum_{m\in\mathbb{M}}\{w_{i,m}\frac{t_i[m]}{\alpha_i} - w_{j,m}\frac{t_j[m]}{\alpha_j}\} = 0,\ \forall\ (i,j)\in\mathbb{K}^2,\ \forall\ m\in\mathbb{M}\\ & - \sum_{k\in\mathbb{K}} w_{k,m} = 1,\ \forall\ m\in\mathbb{M}\\ & - w_{k,m}\geq 0,\ \forall\ (k,m)\in\mathbb{K}\times\mathbb{M}\end{aligned}$$

where $0 \leq w_{k,m} \leq 1$ represents the fractional allocation value of the subcarrier m to the link k. This problem belongs to the convex programming problem family, which can be solved using the Karush-Kuhn-Tucker (KKT) conditions. To do so, we define the modified Lagrangian as follows:

$$\begin{aligned}M(w_{k,m},\lambda_{k,j},\nu_m) = & \sum_{k\in\mathbb{K}}\sum_{m\in\mathbb{M}} w_{k,m}\frac{t_k[m]}{\alpha_k}\\ & - \sum_{i=1}^{K}\sum_{j=i+1}^{K}\lambda_{i,j}\sum_{m\in\mathbb{M}}\{w_{i,m}\frac{t_i[m]}{\alpha_i} - w_{j,m}\frac{t_j[m]}{\alpha_j}\}\\ & - \sum_{m\in\mathbb{M}}\nu_m\{\sum_{k\in\mathbb{K}} w_{k,m} - 1\}.\end{aligned} \tag{4.27}$$

The solution of this problem can be found by solving the following system (KKT first order conditions):

$$\begin{cases}\frac{\partial M}{\partial w_{k,m}} \leq 0,\ \forall\ (k,m)\in\mathbb{K}\times\mathbb{M}\\ w_{k,m}\geq 0,\ \forall\ (k,m)\in\mathbb{K}\times\mathbb{M}\\ w_{k,m}\frac{\partial M}{\partial w_{k,m}} = 0,\ \forall\ (k,m)\in\mathbb{K}\times\mathbb{M}\\ \frac{\partial M}{\partial \lambda_{i,j}} = 0,\ \forall\ (i,j)\in\mathbb{K}\times\mathbb{K}\setminus\{1,..,i\}\\ \frac{\partial M}{\partial \nu_m} = 0,\ \forall\ m\in\mathbb{M}\end{cases} \tag{4.28}$$

Now, it clearly appears that the computational complexity of this system may remain prohibitive as the numbers of subcarriers and links increase. In the following, we develop a geometrical approach of the tone maps splitting problem, allowing to directly converge to the optimal allocation solution.

4.3 Optimal OFDMA Resource Allocation: Geometrical Approach

The continuous relaxation of the tone maps splitting problem is kept, s.t. the orthogonalized tone maps are associated to the following capacity:

$$r_k^{\perp} = \sum_{m\in\mathbb{M}} w_{k,m}t_k[m],\ \forall k\in\mathbb{K}, \tag{4.29}$$

the orthogonality condition being ensured by the following condition:

$$\sum_{k\in\mathbb{K}} w_{k,m} = 1,\ \forall m\in\mathbb{M}. \tag{4.30}$$

Then, as we want to equally share the diversity among the K links, we define the FDM gain, w.r.t. TDM, as follows:

$$G_{\text{FDM}} = \frac{r_k^{\perp}}{\alpha_k},\ \forall k \in \mathbb{K}. \tag{4.31}$$

Then, in a K-dimensional Euclidean space of basis vectors $\{\vec{e}_k : 1 \leq k \leq K\}$, where $\vec{e}_k$ denotes the vector with a 1 in the *k-th* coordinate and 0's elsewhere, we define:

$$\vec{R} = \left[r_1^{\perp}, r_2^{\perp}, .., r_K^{\perp}\right]^{\text{T}}, \tag{4.32}$$

a K-dimensional vector which *k-th* component corresponds to the achieved capacity on link k. Then, based on (4.31), we can write:

$$\vec{R} = G_{\text{FDM}} \left[\alpha_1, \alpha_2, .., \alpha_K\right]^{\text{T}}, \tag{4.33}$$

so that the norm of $\vec{R}$ simply reads:

$$||\vec{R}|| = G_{\text{FDM}} \sqrt{\sum_{k \in \mathbb{K}} \alpha_k^2}. \tag{4.34}$$

So, for a fixed K-tuple $(\alpha_1, \alpha_2, .., \alpha_K)$, solving the maximization problem stated in the previous section comes down to maximize the norm of a K-dimensional vector $\vec{R}$, which components correspond to the achieved capacities by the K orthogonal tone maps, and which directions are given by $(\alpha_1, \alpha_2, .., \alpha_K)$. In the following, starting from a 1-dimensional space and progressively extending the dimensions, we iteratively construct the optimal vector $\vec{R}_{\text{opt}}$, i.e. maximizing G_{FDM}.

4.3.1 Optimal Capacity Region along Basis Vector $\vec{e}_1$

If we consider the maximization of G_{FDM} on link 1 only, assuming that $\alpha_1 \neq 0$, maximizing $||\vec{R}||$ is done by allocating the M subcarriers to the first link, so that $\vec{R} = G_{\text{FDM}} \alpha_1 \vec{e}_1 = \vec{e}_1$.

4.3.2 Optimal Capacity Region in the Plane $(\vec{e}_1, \vec{e}_2)$

At this point, we have $\sum_{m \in \mathbb{M}} w_{1,m} = M$ and $w_{k,m} = 0,\ \forall k \in \mathbb{K} \setminus \{1\}$. Without loss of generality, we consider the study of the capacity region between links 1 and 2, i.e. in the plane generated by basis vectors $\vec{e}_1$ and $\vec{e}_2$. The two tone maps to process are associated with two priority coefficients (α_1, α_2), respectively. We also associate the tone map $t_k[m]$ to $c_k[m]$, representing the realized fractional capacity on its first m subcarriers, $m \leq M$, and expressed as follows:

$$c_k[m] = \begin{cases} 0, \text{ if } m = 0 \\ \sum_{p=1}^{m} t_k[p],\ \forall m \in \mathbb{M} \end{cases}. \tag{4.35}$$

Then, assuming the first $(m-1)$-*th* subcarriers are allocated to link 2, the last $(M-m)$ remaining allocated to link 1, while the *m-th* subcarrier is shared between the two, we can express the capacity allocated to the first link as a function of the capacity allocated to the second link, by defining a piecewise function parameterized as follows:

$$\Gamma_2 : \begin{cases} r_2^{\perp}[m] = c_2[m-1] + w_{2,m} t_2[m] \\ r_1^{\perp}[m] = 1 - c_1[m-1] - w_{2,m} t_1[m] \end{cases}, \tag{4.36}$$

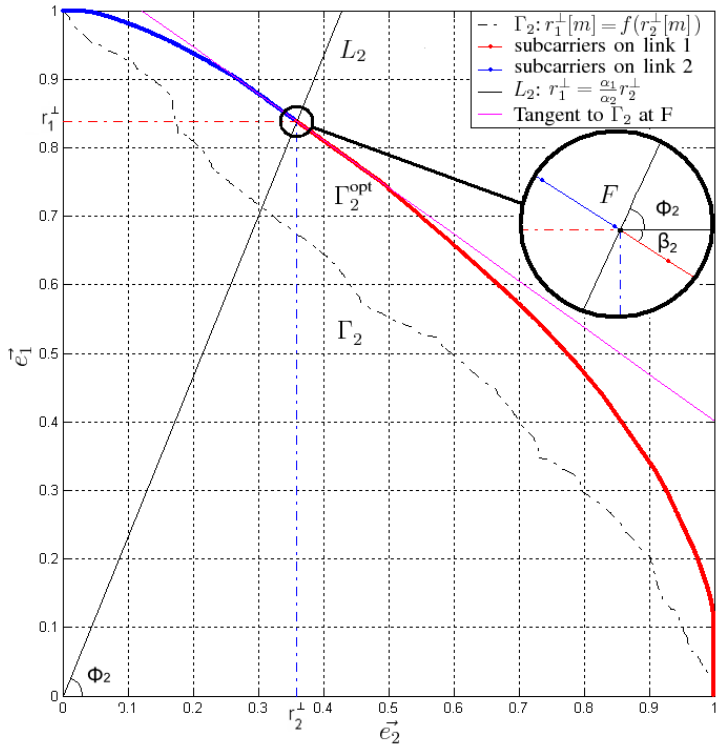

Figure 4.6: Example of a sub-optimal and an optimal OFDMA capacity region for $K = 2$ ($\alpha_1 = 0.3$ and $\alpha_2 = 0.7$).

---

from which we get:

$$w_{2,m} = \frac{r_2^\perp[m] - c_2[m-1]}{t_2[m]}, \tag{4.37}$$

leading to the following expression:

$$r_1^\perp[m] = -\frac{t_1[m]}{t_2[m]} r_2^\perp[m] + 1 + \frac{t_1[m]}{t_2[m]} c_2[m-1] - c_1[m-1] \tag{4.38}$$

which is plotted in Fig. 4.6 as the Γ_2 curve, continuously decreasing on $[0, 1]$.

Noticing that $\frac{\mathrm{d}r_1^\perp[m]}{\mathrm{d}r_2^\perp[m]} = -\frac{t_1[m]}{t_2[m]}$, we define a σ permutation, so that the new sequencing follows the increasing value of the $\frac{t_1[m]}{t_2[m]}$ ratio, i.e.:

$$\frac{t_1[\sigma(m+1)]}{t_2[\sigma(m+1)]} \geq \frac{t_1[\sigma(m)]}{t_2[\sigma(m)]}, \ \forall m \in \mathbb{M} \setminus \{M\}. \tag{4.39}$$

Then, if we reorder the subcarriers contained in $\mathbb{M}$ following the σ permutation, the resulting capacity region, denoted as Γ_2^{opt} (see Fig. 4.6), appears to be concave. So, this simple operation leads directly to the optimal OFDMA capacity region, as a maximization of the capacities on both links is obtained for any (α_1, α_2) combination. As the projection of $\vec{R}$ onto the plane P_2, containing Γ_2^{opt}, corresponds to an $\vec{R}_2$ vector of directions (α_1, α_2),

an optimal orthogonalization is achieved by separating the capacity region into two halves at the point F, crossing of the curve Γ_2^{opt} and the line L_2 of equation $r_1^{\perp} = (\tan(\phi_2))r_2^{\perp} = \frac{\alpha_1}{\alpha_2} r_2^{\perp}$. The set of subcarriers verifying $r_1^{\perp}[\sigma(m)] - \frac{\alpha_1}{\alpha_2} r_2^{\perp}[\sigma(m)] > 0$ are allocated to the second link, while all the others remain allocated to link 1. At this point, it clearly appears that the optimal partitioning of two tone maps only needs one subcarrier at most to be shared among the two links. This subcarrier is the one associated to the part of the piecewise linear function containing the F point. In the following, in order to simplify the notations and without loss of generality, we consider that the natural order of the subcarriers follows the increasing value of the $\frac{t_1[m]}{t_2[m]}$ ratio, so that Γ_2 is naturally concave.

4.3.3 Optimal Capacity Region in $(\vec{e}_1, \vec{e}_2, \vec{e}_3)$

In the previous section, we managed to maximize the norm of $\vec{R}_2$, projection of $\vec{R}$ on P_2. In this third stage, we are going to release subcarriers allocated to links 1 and 2 to the benefit of the third link, in order to construct an $\vec{R}_3$ vector, projection of $\vec{R}$ on the $\mathbb{R}^3$ basis $(\vec{e}_1, \vec{e}_2, \vec{e}_3)$, and directed by $(\alpha_1, \alpha_2, \alpha_3)$. Obviously, each subcarrier reallocation will result in a decrease of $||\vec{R}_2||$. So, maximizing $||\vec{R}_3||$ comes down to find the set of subcarriers which reallocations will result in a maximization of the capacity gain on $\vec{e}_3$, while minimizing the loss on $||\vec{R}_2||$. At each reallocation step i, $r_1^{\perp,(i)}$ and $r_2^{\perp,(i)}$ decrease while $r_3^{\perp,(i)}$ increases, and the F point slides along L_2 in the plane P_2 (cf. Fig. 4.7). Actually, the plane P_2, containing the OFDMA capacity region between the links 1 and 2, will be translated by $\epsilon_i \vec{e}_3$ at each reallocation step, while a piecewise linear function, representing the loss on $\left\|\vec{R}_2\right\|$ as a function of $r_3^{\perp}$, will be generated in a plane P_3, containing vectors $\vec{R}_2$ and $\vec{e}_3$ (see Fig. 4.8). So, maximizing $\left\|\vec{R}_3\right\|$ comes down to minimize the distance covered by F along $\vec{R}_2$ before $\frac{r_3^{\perp}}{\alpha_3}$ reaches the value of $\frac{r_k^{\perp}}{\alpha_k}$, $k \in \{1, 2\}$, s.t. (4.31) be satisfied. In the following, $\text{F}^{(i)}$ denotes the translated F point at the *i-th* reallocation step.

4.3.3.1 Analysis of the Capacity Region in P_2

Let us firstly define a cost function computing the covered distance by F if we allocate on $\vec{e}_3$ a fractional capacity $\epsilon^{(i)}$ at the *i-th* allocation step. Firstly, we can notice that the portion of the *m-th* subcarrier needed to allocate a capacity $\epsilon^{(i)}$ directly depends upon the tone map of link 3, so that this fractional subcarrier is defined as follows:

$$\delta_{3,m}^{(i)} = \frac{\epsilon^{(i)}}{t_3[m]}. \tag{4.40}$$

In Fig. 4.7, we have magnified the region where Γ_2^{opt} and L_2 intersect. The red continuous and dotted curves present Γ_2^{opt} before and after the release of $\delta_{3,m}^{(i)}$, respectively. We can notice that the impact of this reallocation on Γ_2^{opt} comes down to apply two translations. Firstly, the part of the Γ_2^{opt} curve located on the left hand side of the released capacity region is translated by $-\delta_{3,m}^{(i)} t_1[m]\vec{e}_1$. Secondly, the part of the curve located on the right hand side of the released capacity region is translated by $-\delta_{3,m}^{(i)} t_2[m]\vec{e}_2$. Looking at Fig.

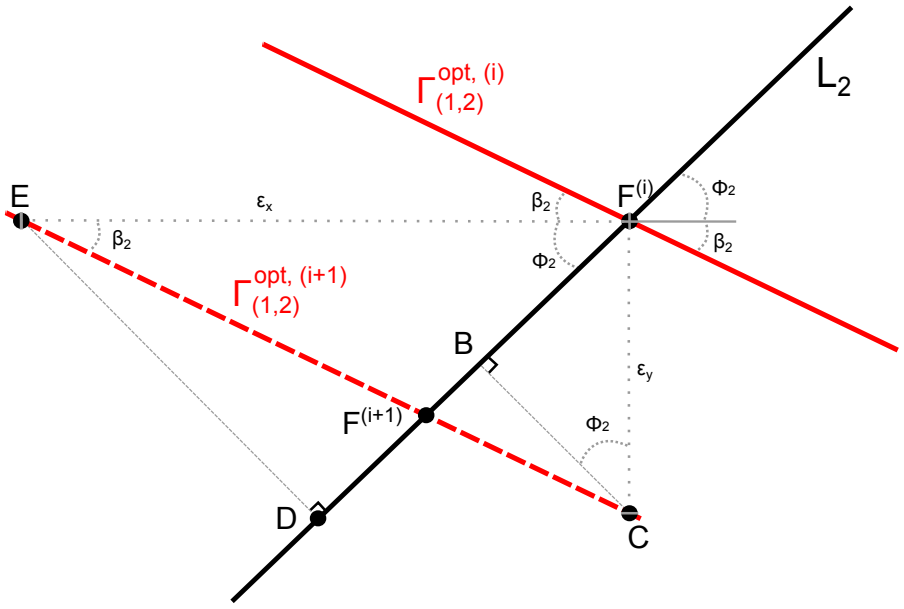

Figure 4.7: Impact of the reallocation of one subcarrier on the FDM capacity region around the F point.

4.7, we then deduct that:

$$\begin{cases} \epsilon_x = \delta_{3,m}^{(i)} t_2[m], \text{ if } w_{2,m} > 0 \\ \epsilon_y = \delta_{3,m}^{(i)} t_1[m], \text{ if } w_{1,m} > 0. \end{cases}, \tag{4.41}$$

which means that if the chosen subcarrier to be released is currently allocated to link 1, the local impact on Γ_2^{opt} around the $\text{F}^{(i)}$ point will be a translation of $-\delta_{3,m}^{(i)} t_1[m]\vec{e}_1$. On the other hand, if the chosen subcarrier is currently allocated to link 2, the local impact on Γ_2^{opt} around the $\text{F}^{(i)}$ point will be a translation of $-\delta_{3,m}^{(i)} t_2[m]\vec{e}_2$. However, Γ_2^{opt} being a continuous piecewise linear curve, it is necessary to discriminate the left hand side and the right hand side values of β_2 w.r.t. F, denoted as $\beta_{2,l}$ and $\beta_{2,r}$, respectively. In order to compute the translation of the F point at the i-*th* iteration $\left\|\text{F}^{(i)}\text{F}^{(i+1)}\right\|$ for any subcarrier m, two cases need to be considered:

- If the released subcarrier is currently allocated to link 1, then we have $\epsilon_y = \delta_{3,m}^{(i)} t_1[m]$. In such a case, assuming that the value of $\beta_{2,l}$ remains unchanged after $\epsilon^{(i)}$ has been allocated to link 3, we express $\left\|\text{F}^{(i)}\text{F}^{(i+1)}\right\|$ as a function of ϵ_y:

$$\left\|\text{F}^{(i)}\text{F}^{(i+1)}\right\| = \left\|\text{F}^{(i)}\text{B}\right\| + \left\|\text{B}\text{F}^{(i+1)}\right\| \tag{4.42}$$

$$\Leftrightarrow \left\|\text{F}^{(i)}\text{F}^{(i+1)}\right\| = \epsilon_y \sin(\phi_2) + \|\text{BC}\| \tan\left(\frac{\pi}{2} - \beta_{2,l} - \phi_2\right) \tag{4.43}$$

$$\Leftrightarrow \left\|\text{F}^{(i)}\text{F}^{(i+1)}\right\| = \epsilon_y \left[\sin(\phi_2) + \cos(\phi_2) \tan\left(\frac{\pi}{2} - \beta_{2,l} - \phi_2\right)\right]. \tag{4.44}$$

- If the released subcarrier is currently allocated to link 2, then we have $\epsilon_x = \delta_{3,m}^{(i)} t_2[m]$. In such a case, assuming that the value of $\beta_{2,r}$ remains unchanged after $\epsilon^{(i)}$ has been allocated to link 3, we express $\left\|\mathrm{F}^{(i)}\mathrm{F}^{(i+1)}\right\|$ as a function of ϵ_x:

$$\left\|\mathrm{F}^{(i)}\mathrm{F}^{(i+1)}\right\| = \left\|\mathrm{DF}^{(i)}\right\| - \left\|\mathrm{DF}^{(i+1)}\right\| \tag{4.45}$$

$$\Leftrightarrow \left\|\mathrm{F}^{(i)}\mathrm{F}^{(i+1)}\right\| = \epsilon_x \cos(\phi_2) - \|\mathrm{ED}\| \tan\left(\frac{\pi}{2} - \beta_{2,r} - \phi_2\right) \tag{4.46}$$

$$\Leftrightarrow \left\|\mathrm{F}^{(i)}\mathrm{F}^{(i+1)}\right\| = \epsilon_x \left[\cos(\phi_2) - \sin(\phi_2) \tan\left(\frac{\pi}{2} - \beta_{2,r} - \phi_2\right)\right] \tag{4.47}$$

Thus, we can define for both links an exclusive cost function allowing us to assess the value $\left\|\mathrm{F}^{(i)}\mathrm{F}^{(i+1)}\right\|$ $\forall m \in \mathbb{M}$:

$$\begin{cases} C_1^{(i)}[m] = \frac{t_1[m]}{t_3[m]} \left[\sin(\phi_2) + \cos(\phi_2) \tan\left(\frac{\pi}{2} - \beta_{2,l}^{(i)} - \phi_2\right)\right], \text{ if } w_{1,m} > 0 \\ C_2^{(i)}[m] = \frac{t_2[m]}{t_3[m]} \left[\cos(\phi_2) - \sin(\phi_2) \tan\left(\frac{\pi}{2} - \beta_{2,r}^{(i)} - \phi_2\right)\right], \text{ if } w_{2,m} > 0 \end{cases}, \tag{4.48}$$

Finally, the translation of the F point after the release from link k of a capacity $\epsilon^{(i)}$ on the subcarrier m of the link 3 simply reads:

$$\left\|\mathrm{F}^{(i)}\mathrm{F}^{(i+1)}\right\| = \epsilon^{(i)} C_k^{(i)}[m]. \tag{4.49}$$

In the following, we assume that the value of $\delta_{3,m}^{(i)}$ is always set such that the following constraint on β_2 is met: if the chosen subcarrier to be released was originally allocated to link 1, then $\beta_{2,l}^{(i)} = \beta_{2,l}^{(i+1)}$, while if it was originally allocated to link 2, then $\beta_{2,r}^{(i)} = \beta_{2,r}^{(i+1)}$. In the following, a fine analysis will be conducted to consider the case where F is located on a singularity point of Γ_2, i.e. when $\beta_{2,l} \neq \beta_{2,r}$.

Remark: It is important to notice that the value of $C_k^{(i)}[m]$ is actually dependent upon the $(i-1)$-*th* previous allocation steps. In order to ease the reading, we choose not to make this dependency explicitly appear in the expression of the cost function defined in (4.48).

4.3.3.2 Allocation Process

In this stage, we are going to describe the step-by-step allocation process on $\vec{e}_3$, and we will simultaneously prove that this method leads to a maximization of $\left\|\vec{R}_3\right\|$. To understand the basic idea of the following analysis, it is helpful to see this problem as a directed graph where, at each node, M possible paths can be chosen, each one corresponding to a subcarrier of the frequency multiplex. Every subcarrier for which $w_{3,m} = 1$, i.e. that is entirely allocated on link 3, is associated with an infinite weighting value, while subcarriers still allocated to links 1 and 2 are associated with weighting values equal to $C_1^{(i)}[m]$ and $C_2^{(i)}[m]$, respectively. Now, what we want to demonstrate here is that if we choose the minimal weighted edge at each iteration, we will necessarily follow the path minimizing $\left\|\mathrm{F}^{(0)}\mathrm{F}^{(N)}\right\|$, where N would be the number of allocations steps to satisfy the fairness constraint $\frac{r_1^{\perp}}{\alpha_1} = \frac{r_2^{\perp}}{\alpha_2} = \frac{r_3^{\perp}}{\alpha_3}$. Actually, it can be proved that, if we do not choose the minimal

weighted path at the *i-th* iteration, it will not be possible to find another path leading to a better solution. As we will see in the following, the veracity of the previous statement lies in the concavity of the capacity region. Let us now study the only two possible scenarios of the allocation process.

- $\beta_2 = \beta_{2,l} = \beta_{2,r}$ remains constant during the allocation process:

  In this particular case, the modification of the capacity region does not lead to a modification in the value of β_2, such that the demonstration of the optimality is straightforward. Indeed, in such a scenario, the cost function is unchanged during all the allocation process, apart from the set of subcarriers that were entirely allocated on $\vec{e}_3$. So, at any considered allocation step, the weighting factors associated to the available subcarriers keep the same values. It is therefore obvious that choosing to allocate on link 3 the subcarriers minimizing the cost at each one of the N iteration steps results in a maximization of $\left\|\vec{R}_3\right\|$. Moreover, as $\left\|\mathrm{F}^{(i-1)}\mathrm{F}^{(i)}\right\| \leq \left\|\mathrm{F}^{(i)}\mathrm{F}^{(i+1)}\right\|$ $\forall i \in \{1,..,N\}$, the curve Γ_3, representing the loss on $\left\|\vec{R}_2\right\|$ as a function of the capacity allocated to $\vec{e}_3$ in the plane P_3 (see Fig. 4.8), is also concave.

- The value of β_2 changes during the allocation process:

  This is the general case. According to (4.48), the values of the cost function will change with β_2, as $C_2[m]$ increases while $C_1[m]$ decreases with the value of this angle. Now, let us assume that for the $(i-1)th$ first allocation steps, we were in the previous scenario, i.e. $\beta_2 = \beta_{2,l} = \beta_{2,r}$, so that, according to the previous analysis, $\left\|\mathrm{F}^{(0)}\mathrm{F}^{(i-1)}\right\|$ has been minimized. Without loss of generality, let us now assume that at the $(i-1)th$ allocation step:

  $$\underset{k\in\{1,2\}}{\arg\min}\{C_k^{(i-1)}[m]\} = 2, \tag{4.50}$$

  meaning that the link 2 was chosen at the previous iteration, and this has resulted in the F point to be located on a discontinuity point of Γ_2^{opt}. Thanks to the concavity of the capacity region and according to the analysis made in the previous stage, we can write:

  $$\begin{cases} \beta_{2,l}^{(i)} = \beta_{2,l}^{(i-1)} \\ \beta_{2,r}^{(i)} > \beta_{2,r}^{(i-1)} \end{cases} \Rightarrow \begin{cases} C^{(i)}_{1,\beta_{2,l}^{(i)}}[m] = C^{(i-1)}_{1,\beta_{2,l}^{(i-1)}}[m] \\ C^{(i)}_{2,\beta_{2,r}^{(i)}}[m] > C^{(i-1)}_{2,\beta_{2,r}^{(i-1)}}[m] \end{cases} \tag{4.51}$$

  Then, if the following property is verified:

  $$\underset{m\in\mathbb{M}}{\arg\min}\{C^{(i)}_{1,\beta_2=\beta_{2,l}^{(i)}}[m], C^{(i)}_{2,\beta_2=\beta_{2,l}^{(i)}}[m]\} = \underset{m\in\mathbb{M}}{\arg\min}\{C^{(i)}_{1,\beta_2=\beta_{2,r}^{(i)}}[m], C^{(i)}_{2,\beta_2=\beta_{2,r}^{(i)}}[m]\}, \tag{4.52}$$

  it means that the two cost functions, either computed with the left or right value of β_2 indicate the same subcarrier to be released, so that we can be sure of the path minimizing the loss on $\left\|\vec{R}_2\right\|$ and, in the next iteration, we will be back in the case where $\beta_2 = \beta_{2,l} = \beta_{2,r}$. However, if (4.52) is not verified, it means that a singular point has been reached, where choosing the minimal cost at each allocation step would make the F point to oscillate around the edges of the two line segments

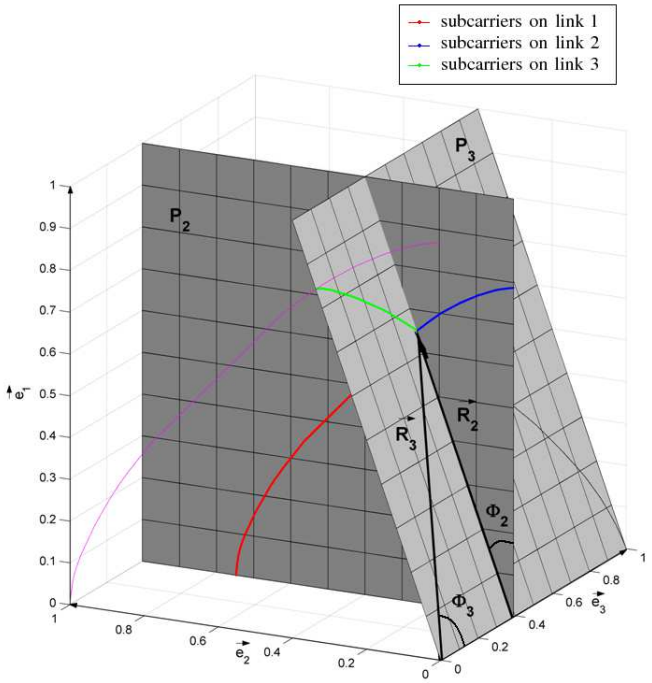

(a)

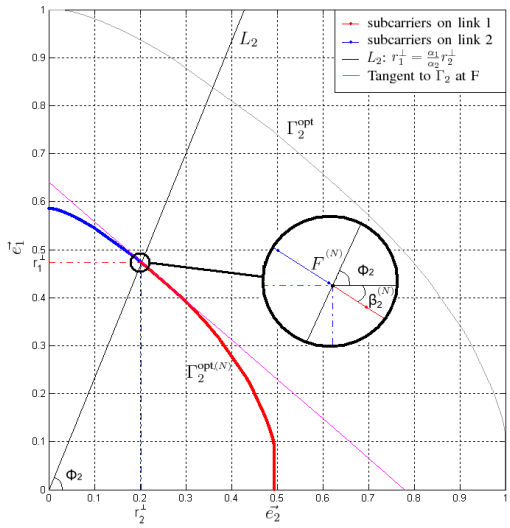

(b)

Figure 4.8: Optimal OFDMA capacity region for $K = 3$: (a) Γ_2 and Γ_3 curves ($\alpha_1 = 0.5$, $\alpha_2 = 0.2$, $\alpha_3 = 0.3$) (b) Γ_2 curve after the N allocation steps on $\vec{e}_3$ ($\alpha_1 = 0.35$, $\alpha_2 = 0.15$, $\alpha_3 = 0.5$).

of different slopes, while (4.52) is not verified. To interpret this phenomenon, we have to underline the fact that until now, we have not considered that the optimal reallocation solution could be a simultaneous transfer of two subcarriers from tone maps 1 and 2, and that is exactly what is highlighted if (4.52) is not verified. In such a case, minimizing the reallocation cost on $\left\|\vec{R}_2\right\|$ is achieved by combining two capacity reallocations from two subcarriers m_1 and m_2 selected as follows:

$$\begin{cases} m_1 = \arg\min_{m\in\mathbb{M}}\{C^{(i)}_{1,\beta^{(i)}_{2,l}}[m]\} \\ m_2 = \arg\min_{m\in\mathbb{M}}\{C^{(i)}_{2,\beta^{(i-1)}_{2,r}}[m]\} \end{cases}, \tag{4.53}$$

where m_1 and m_2 are obviously allocated to $\vec{e}_1$ and $\vec{e}_2$, respectively. While (4.52) is not verified, we must ensure that the F point remains at the edges of the two line segments of different slopes. Firstly, we set:

$$\epsilon^{(i)} = \epsilon^{(i)}_1 + \epsilon^{(i)}_2, \tag{4.54}$$

where $\epsilon^{(i)}_1 = \delta^{(i)}_{3,m_1} t_3[m_1]$ and $\epsilon^{(i)}_2 = \delta^{(i)}_{3,m_2} t_3[m_2]$. Then, to ensure $\mathrm{F}^{(i+1)}$ to still be located on the discontinuity point of the capacity region after the *i-th* allocation, as

$$\overrightarrow{\mathrm{F}^{(i)}\mathrm{F}^{(i+1)}} = -\delta^{(i)}_{3,m_1}.t_1[m_1]\vec{e}_1 - \delta^{(i)}_{3,m_2}.t_2[m_2]\vec{e}_2, \tag{4.55}$$

$\delta^{(i)}_{3,m_1}$ and $\delta^{(i)}_{3,m_2}$ are set s.t.:

$$\frac{\delta_{3,m_1}.t_1[m_1]}{\delta_{3,m_2}.t_2[m_2]} = \tan(\phi_2) = \frac{\alpha_1}{\alpha_2}, \tag{4.56}$$

resulting in a minimized loss on $\left\|\vec{R}_2\right\|$ for the allocation of $\epsilon^{(i)}$ that simply reads

$$\left\|\mathrm{F}^{(i)}\mathrm{F}^{(i+1)}\right\| = \epsilon^{(i)}_1 C^{(i)}_{1,\beta^{(i)}_{2,l}}[m_1] + \epsilon^{(i)}_2 C^{(i)}_{2,\beta^{(i)}_{2,r}}[m_2]. \tag{4.57}$$

with

$$\begin{cases} \epsilon^{(i)}_1 = \frac{\alpha_1 t_2[m_2] t_3[m_1]}{\alpha_1 t_2[m_2] t_3[m_1] + \alpha_2 t_1[m_1] t_3[m_2]} \epsilon^{(i)} \\ \epsilon^{(i)}_2 = \frac{\alpha_2 t_1[m_1] t_3[m_2]}{\alpha_1 t_2[m_2] t_3[m_1] + \alpha_2 t_1[m_1] t_3[m_2]} \epsilon^{(i)} \end{cases}. \tag{4.58}$$

Remark: according to (4.50), in the previous iteration, the loss on $\left\|\vec{R}_2\right\|$ was:

$$\left\|\mathrm{F}^{(i-1)}\mathrm{F}^{(i)}\right\| = \epsilon^{(i-1)} \min_{m\in\mathbb{M}}\{C^{(i-1)}_2[m]\}. \tag{4.59}$$

According to (4.51), we firstly have:

$$C^{(i-1)}_2[m_2] \leq C^{(i-1)}_1[m_1] = C^{(i)}_1[m_1] \tag{4.60}$$

$$\Leftrightarrow \epsilon^{(i)}_1 C^{(i-1)}_2[m_2] \leq \epsilon^{(i)}_1 C^{(i)}_1[m_1]. \tag{4.61}$$

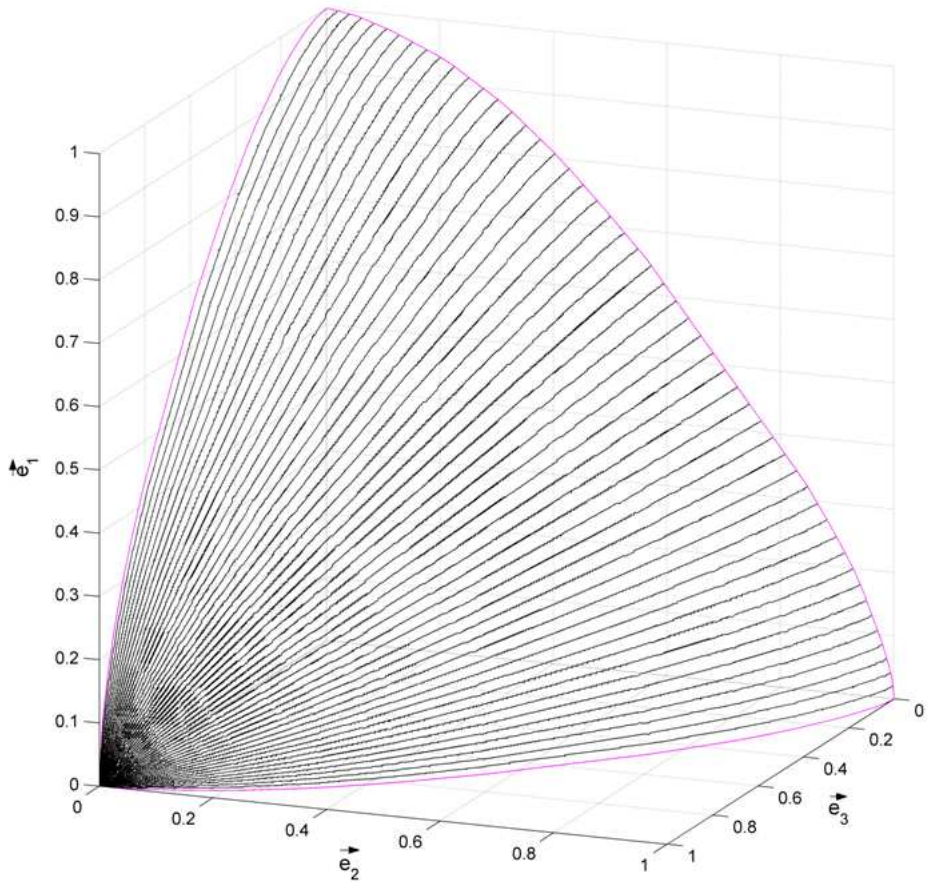

Figure 4.9: Representation of 50 optimal capacity regions for 50 different values of ϕ_2 ($= \arctan\left(\frac{\alpha_1}{\alpha_2}\right)$).

and, secondly:

$$C_2^{(i-1)}[m_2] < C_2^{(i)}[m_2] \tag{4.62}$$

$$\Leftrightarrow \epsilon_2^{(i)} C_2^{(i-1)}[m_2] < \epsilon_2^{(i)} C_2^{(i)}[m_2]. \tag{4.63}$$

Summing (4.63) and (4.61) finally leads to:

$$\epsilon^{(i)} C_2^{(i-1)}[m_2] \leq \epsilon_1^{(i)} C_1^{(i)}[m_1] + \epsilon_2^{(i)} C_2^{(i)}[m_2], \tag{4.64}$$

which means that it is always possible to find a path on which the minimal cost is increasing with i, so that the piecewise linear function representing the loss on $\left\|\vec{R}_2\right\|$ as a function of the capacity allocated to $\vec{e}_3$ in the plane P_3, which is represented in Fig. 4.8, is also concave. In Fig. 4.9, we present several optimal capacity regions, obtained

for different values of Φ_2: all these capacity regions are concave and are contained in a plane P_3, which is fully defined once the value of Φ_2 is fixed. Concavity is the key property for solving the tone map splitting problem when K is higher than 3. Actually, this is the concave nature of the capacity region in P_2 that ensures that, even if we had chosen another subcarrier to be released than the one providing the minimal cost at the $(i-1)$-th iteration, there would not be any new minima to be discovered others than the one discovered following the minimal cost path. So, choosing the minimal cost path at each allocation step always provides a global optimum.

4.3.4 Optimal Resource Allocation for $K > 3$

At this point we have managed to prove the optimality of the geometrical approach for the case of 3 tone maps to orthogonalize, but is it possible to apply the same process for higher values of K? For the $K = 4$ case, a geometrical analysis of the 3-dimensional capacity region represented in Fig. 4.8 leads to establish the 3 following cost functions, each one being exclusively associated with one of the first 3 links:

$$\begin{cases} C_1^{(i)}[m] = \frac{t_1[m]}{t_4[m]} f^-(\beta_{2,l})\, f^-(\beta_{3,l}), \text{ if } w_{1,m} > 0 \\ C_2^{(i)}[m] = \frac{t_2[m]}{t_4[m]} f^+(\beta_{2,r})\, f^-(\beta_{3,l}), \text{ if } w_{2,m} > 0 \\ C_3^{(i)}[m] = \frac{t_3[m]}{t_4[m]} f^+(\beta_{3,r}), \text{ if } w_{3,m} > 0 \end{cases} \tag{4.65}$$

with:

$$\begin{cases} f^-(\beta_{k,l}) = \sin(\phi_k) + \cos(\phi_k) \tan\left(\frac{\pi}{2} - \beta_{k,l} - \phi_k\right) \\ f^+(\beta_{k,r}) = \cos(\phi_k) - \sin(\phi_k) \tan\left(\frac{\pi}{2} - \beta_{k,r} - \phi_k\right) \end{cases} \tag{4.66}$$

where $f^-(\beta_{k,l})$ decreases with $\beta_{k,l}$ and $f^+(\beta_{k,r})$ increases with $\beta_{k,r}$, β_k being the absolute value of the slope of Γ_k in the plane P_k, and $\phi_k = \arctan\left(\frac{\sqrt{\sum_{n=1}^{k-1} \alpha_n^2}}{\alpha_k}\right)$ is the value of the angle between $\vec{R}_k$ and $\vec{e}_k$ in the plane P_k. With the equivalent assumptions made in the previous section on the value of β_k to perform the allocation of a capacity $\epsilon^{(i)}$ on $\vec{e}_4$, we can also demonstrate that choosing the minimal cost allows to generate a concave capacity region in a plane P_4, containing vector $\vec{R}_4$ directed by $(\alpha_1, \alpha_2, \alpha_3, \alpha_4)$. Then, we can easily generalize the expression of the cost function on link n as follows:

$$C_n^{(i)}[m] = \frac{t_n[m]}{t_K[m]} f^+(\beta_{n,r}) \prod_{k=n+1}^{K-1} f^-(\beta_{k,l}), \text{ if } w_{n,m} > 0,\ \forall n \in \{1, .., K-1\}, \tag{4.67}$$

setting $f^+(\beta_{1,r}) = 1$.

Thus, for $K > 3$, the logic remains the same as it is always possible to compute the cost of any carrier reallocation on $\left\|\vec{R}_{k-1}\right\|$. However, the optimality of the process lies in the concavity of the generated capacity region in any of the $(K-1)$ plane containing $\vec{R}_K$. In order to meet this condition, the allocation step $\epsilon^{(i)}$ may have to be more and more reduced as the dimension increases, because the probability that F reaches a singular point of the capacity region becomes more and more likely. Indeed, if in the previous case,

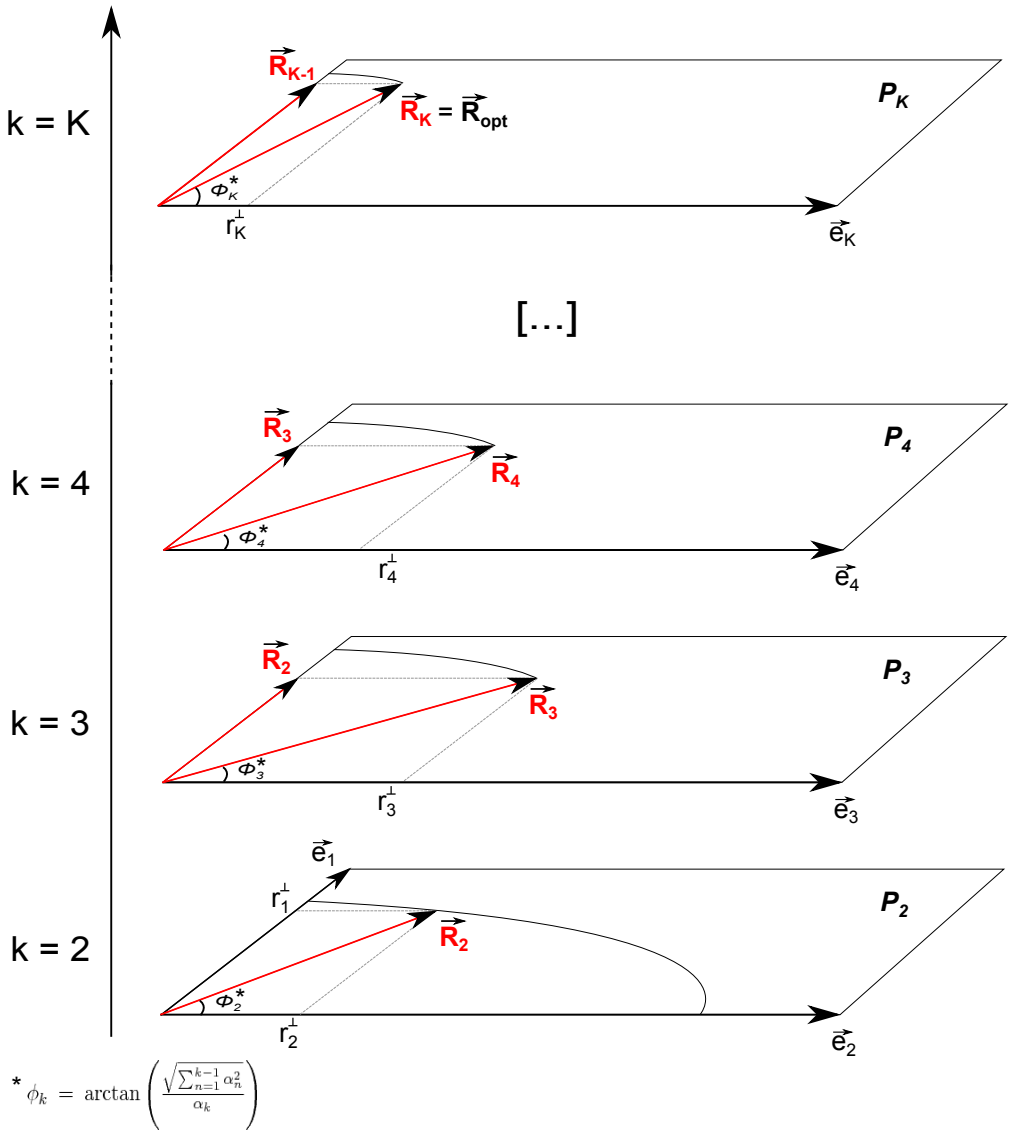

Figure 4.10: Representations of the $K-1$ planes containing the optimal capacity region between the K links

there were only 3 possibilities of reallocation (from $\vec{e}_1$, $\vec{e}_2$ or both), there are 7 different possible sources of reallocation for the construction of $\vec{R}_4$. Actually, for the construction of $\vec{R}_K$, we can easily compute the number of reallocation possibilities, which is equal to $\sum_{p=1}^{K-1} \binom{K-1}{p} = 2^{K-1} - 1$. Moreover, each $\epsilon^{(i)}$ reallocation implies to balance capacities between the $(k-1)$ links that were previously processed, in order to always satisfy the fairness constraint. In other words, the computational complexity may rapidly become quite high as M and K increase.

4.4 Optimal OFDMA Resource Allocation: Study of a Particular Case

We have previously described a method to solve the problem in the general case. Yet, the computational complexity of this method increases with M and K and may be too high to rapidly converge to a solution when using real tone maps (e.g. P1901 specification defines more than 1700 active subcarriers). So, here we study a particular case that will happen to be useful to assess the performance of the allocation algorithm described in section 4.5. Firstly, let us recall that the problem statement is to maximize G_{FDM}, while satisfying a fixed combination of the priority coefficients $(\alpha_1, \alpha_2, .., \alpha_K)$:

$$G_{\text{FDM}} = \frac{r_k^{\perp}}{\alpha_k}, \forall k \in \mathbb{K} \tag{4.68}$$

$$\Leftrightarrow \alpha_k G_{\text{FDM}} = r_k^{\perp}, \forall k \in \mathbb{K}. \tag{4.69}$$

Then, the summation of the K terms of (4.69) gives:

$$G_{\text{FDM}} \sum_{k \in \mathbb{K}} \alpha_k = \sum_{k \in \mathbb{K}} r_k^{\perp}. \tag{4.70}$$

Noticing that $\sum_{k \in \mathbb{K}} \alpha_k = 1$, we finally obtain an expression of the FDM gain, independently of any priority coefficients combination:

$$G_{\text{FDM}} = \sum_{k \in \mathbb{K}} r_k^{\perp}. \tag{4.71}$$

This constraint being released, we are going to maximize G_{FDM}. Recalling the definitions of $t_k^{\perp}[m]$ and $r_k^{\perp}$ given in (4.13) and (4.14), respectively, we can write:

$$G_{\text{FDM}} = \sum_{k \in \mathbb{K}} \sum_{m \in \mathbb{S}_k} t_k^{\perp}[m]. \tag{4.72}$$

From (4.72), it clearly appears that the maximization of the gain is simply obtained by allocating each subcarrier to the link reaching the maximal fractional capacity among the K ones. So, we define the K $\mathbb{S}_p^{\max}$ sets satisfying:

$$\forall p \in \mathbb{K} \text{ and } \forall m \in \mathbb{M},\ m \in \mathbb{S}_p^{\max} \Leftrightarrow t_p[m] = \max_{k \in \mathbb{K}} \left(t_k[m] \right) \tag{4.73}$$

Finally, we have:

$$G_{\text{FDM}}^{\max} = \sum_{m \in \mathbb{M}} \max_{k \in \mathbb{K}} \left(t_k[m] \right), \tag{4.74}$$

from which we easily deduce the associated priority coefficients:

$$\alpha_k^{\max} = \frac{r_k^{\perp}}{G_{\text{FDM}}^{\max}}, \text{ with } r_k^{\perp} = \sum_{m \in \mathbb{S}_k^{\max}} t_k[m], \forall k \in \mathbb{K}. \tag{4.75}$$

So, it appears that the priority coefficients combination maximizing G_{FDM} can easily be found. Fixing the priority coefficients based on the FDM gain may appear to be useless in practice. However, this particular case will be useful to assess the performance of the suboptimal allocation algorithm described in the next section for values of K higher than 3.

Remark: In fig. 4.6 the (α_1, α_2) combination maximizing the FDM gain can easily be inferred. This optimum corresponds to the point from which β_2 becomes greater than $\pi/4$, i.e. from which Γ starts drawing closer to the linear function of equation $y = 1 - x$.

4.5 Suboptimal OFDMA Resource Allocation: The Tone Maps Splitting Algorithm (TMSA)

4.5.1 Algorithm Description

In this section, we describe a fast allocation algorithm, originally proposed in [31], converging to suboptimal partitions of the frequency bandwidth (optimal in the $K = 2$ case).

Step 1: Pre-processing. The first step of the algorithm is to define a strategy by which only one partition solution will be tested, being as close as possible to the optimum one. A subcarrier assignment needs two choices to be made, as we need to choose which subcarrier to allocate and which link will benefit from this allocation. To answer the former question, K decision functions are defined:

$$\Delta_k[m] = \begin{cases} \frac{T_k[m]}{\sum_{p \neq k} T_p[m]}, \text{ if } \sum_{p \neq k} T_p[m] \neq 0 \\ \\ T_k[m] + (b_{\max}/b_{\min}), \text{ otherwise.} \end{cases}, \tag{4.76}$$

where $b_{\min} = \arg\min_{b \in \mathbb{E}_{\text{const}}} \{b | b > 0\}$ and $b_{\max}$ is the largest element in $\mathbb{E}_{\text{const}}$. $\Delta_k[m]$ is the ratio of the capacity of the tone map $T_k[m]$ to the summed capacities of the other tone maps. In another way, it means that for each transmission path k, the denominator of $\Delta_k[m]$ corresponds to an equivalent tone map constructed by adding up all the tone maps of the other links. The purpose of this criterion is to directly isolate the subcarriers that have to be allocated for each link, by taking into account its own capacity, but also the impact of its allocation on the other links. Note that the decision criterion could be easily improved by working with normalized tone maps, replacing $T_k[m]$ by $t_k[m] = \frac{T_k[m]}{R_k}$. Because of the increase in the complexity and the low improvement brought by this alternative, which was verified in numerous simulations, we chose not to define (4.76) that way.

Step 2: Tone maps splitting processing. The algorithm consists in a M-iteration loop by which the M subcarriers will be distributed among the K links. At the initializa-

tion stage, we set:

$$\begin{cases} \mathbb{S}_k = \varnothing, \forall k \in \mathbb{K} \\ \mathbb{M} = \{1, .., M\}. \end{cases} \tag{4.77}$$

While $(\mathbb{M} \neq \varnothing)$

- *Selection of one of the links l verifying:*
  $l = \arg\min_{k \in \mathbb{K}} \{\frac{r_k^{\perp}}{\alpha_k}\}$.
- *Selection of one of the subcarriers s verifying:*
  $s = \arg\max_{m \in \mathbb{M}} \{\Delta_l[m]\}$.
- *Update parameters:*
  - $\mathbb{S}_l = \mathbb{S}_l \cup \{s\}$;
  - $\mathbb{M} = \mathbb{M} \setminus \{s\}$;

end

So, an iteration comes down to firstly choose the link l that has the lowest $\frac{R_k^{\perp}}{\alpha_k R_k}$ and, secondly, by allocating to l an available subcarrier for which $\Delta_l[m]$ reaches its maximum. Proceeding that way, the algorithm naturally converges to a partition which is close to satisfy the fairness constraint $\frac{R_p^{\perp}}{\alpha_p R_p} = \frac{R_q^{\perp}}{\alpha_q R_q}$, $\forall (p, q) \in \mathbb{K}^2$.

4.5.2 Complexity Issue

At first sight, the $\Delta_k[m]$ computation can be seen as a the main drawback of the proposed algorithm, as this metric needs $K \times M$ divisions and $K \times (K-1) \times M$ additions. Another solution would be to compute it off-line, but this implementation is less flexible and can be really costly in terms of memory usage. Now, it can be noticed that the algorithm does not need all values of $\Delta_k[m]$ to be computed, so that the complexity can be drastically reduced. Indeed, $\Delta_k[m]$ is only used to find the subcarrier for which it reaches its maximum. As this function is the ratio of two integer values $\frac{y}{x}$, its maximum, reached with the couple $(x_{\min}, y_{\max})$, can be easily found following this procedure: firstly, all couples satisfying $y = y_{\max}$ are saved in a set S_1. From this list, the subcarrier s_1 is selected, which is associated to the couple $(x_1, y_{\max})$, verifying $x_1 \leq x$, $\forall x \in S_1$. If $x_{\min} = 0$, the maximum is found and s_1 is selected. If not, all the couples satisfying $x = x_{\min}$ are saved in a set S_2. From this second list, the subcarrier s_2 is selected, which is associated to the couple $(x_{\min}, y_2)$, verifying $y_2 \geq y$, $\forall y \in S_2$. If $s_1 = s_2$, the maximum is found and the subcarrier can be allocated. If $s_1 \neq s_2$, the two values of $\Delta_k[s_1]$ and $\Delta_k[s_2]$ still need to be compared, which needs 2 divisions. So, at worst, as there are M subcarriers to allocate, $2M$ divisions will have to be computed. For that reason, we infer that the complexity, both in terms of computational resource and memory usage, can be well contained. Of course, as always, only an hardware implementation will draw a final conclusion about the complexity issue.

4.5.3 TMSA Performance

In this section, we present the performance of the algorithm in the PLC context. Following the IEEE P1901 specification, the tone maps consist of $M = 1744$ subcarriers, each

subcarrier carrying a number of bits taking its value in $\mathbb{E}_{\text{const}} = \{0, 1, 2, 3, 4, 6, 8, 10, 12\}$. The mapping is realized using a bit-loading algorithm, based on a peak SER target as it is defined in section 3.1.3 on page 27. Then, to run the splitting algorithm, K tone maps are randomly chosen in a data base, in order to ensure the singularity of each simulation run and the diversity of the situations. This data base contains 300 uncorrelated tone maps, generated using 300 simulated static PLC channels realizations belonging either to classes 2, 5 or 9 [107], [106]. In Fig. 4.11-(a), we give 3 randomly generated tone maps, each one belonging to a different class. Note that all dots cannot be seen, as some subcarriers carry the same number of bits on several links. Also, we underline the fact that the general decrease in the right half of the figure can be explained by the imposed limitation on the transmitted power beyond 30 MHz (which goes from -50 dBm/Hz to -80 dBm/Hz). On average, class 2 tone maps capacity is around one half of class 5 one and one third of class 9 one. Then, in Fig. 4.11-(b), we show the obtained tone maps after running the splitting algorithm, setting the priority coefficients $\alpha_k = \frac{1}{K}$, $\forall\ k \in \mathbb{K}$, so that the K links are equally prioritized. Comparing figures 4.11-(a) and 4.11-(b), we clearly see that most of the low-capacity subcarriers of the channel 2 tone map have been allocated to the other 2, so that the achieved gain $G_{\text{FDM}} = 1.48$.

In Fig. 4.12, we give an averaged value of G_{FDM} using various splitting algorithms. To obtain a relevant mean value using the 3 different channel classes, we ensure that each K-tuple combination is tested 100 times. To do so, we use the K-combination with repetitions formula, given by $\binom{n+K-1}{K}$, with $n = 3$ as there 3 channel classes. In other words, it means that the $K = 2$ case needs 600 simulation runs and the $K = 15$ case needs 13600 simulation runs. Also, as in Fig. 4.11, the K links are equally prioritized. In this figure, we can firstly notice that the proposed algorithm (circles) converges to the optimal solution (squares) for the $K = 2$ case. With $K = 3$, the algorithm reaches an averaged G_{FDM} slightly lower than the optimum. Above $K = 3$, the gain keeps increasing until $K = 10$ and finally levels off for higher values of K. The increase can be interpreted by firstly noticing that the case where the K tone maps belong to class 9 channels reduces the averaged G_{FDM}, as these tone maps are quasi-constant. Also, as the weight of this case decreases with K, the frequency diversity increases and so is the FDM gain. Above $K = 10$, we converge to splitting solutions where orthogonalized tone maps are ensured to keep their best subcarriers, so that G_{FDM} levels off. Even if it cannot be seen on the figure as the gain is averaged, it has to be underlined that for all the simulation runs, $G_{\text{FDM}} > 1$, which tends to confirm the demonstration made in section 4.1.3. On this figure, we also represent the performance of a reference solution [69] (stars). As this method targets a fixed capacity $R_k^{\perp}$ for every link, our algorithm is firstly executed. Then, based on the $R_k^{\perp}$ provided by the TMSA, the capacity to be reached on each link k for the reference solution is fixed. As it can be seen on the figure, this method provides a gain from $K = 2$ to $K = 9$. Above this value, OFDMA degrades the transmission efficiency, compared to TDMA. Even if it cannot be seen on the figure, it has to be underlined that for all the simulation runs, the G_{FDM} gain reached by the reference solution never beats the proposed algorithm. Finally, we examined a simplified version of our orthogonalization method (crosses), where the definition of $\Delta_k[m]$ is changed, while the core of the algorithm remains the same as in section 4.5.1. Instead of defining $\Delta_k[m]$ as the ratio of the tone map k to the addition of the others, we define $\Delta_k[m]$ as the difference between the two aforementioned values. The new definition does not change the variation of $\Delta_k[m]$, but

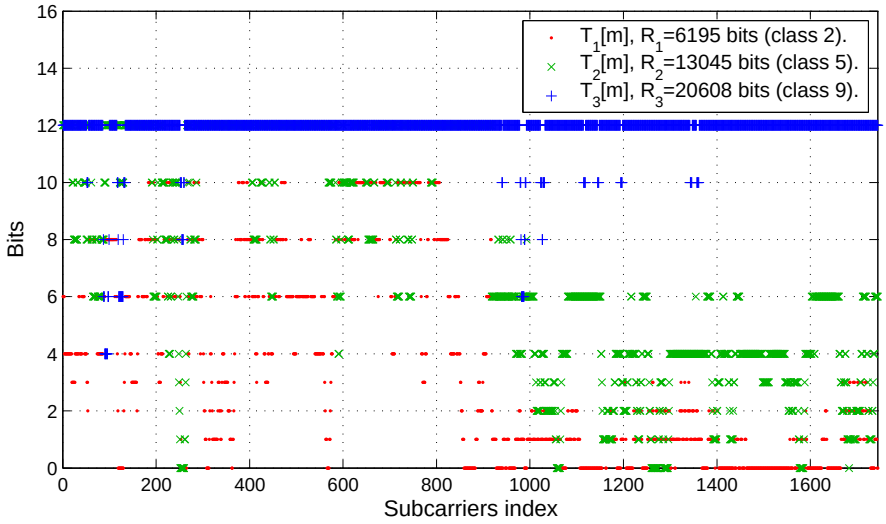

(a)

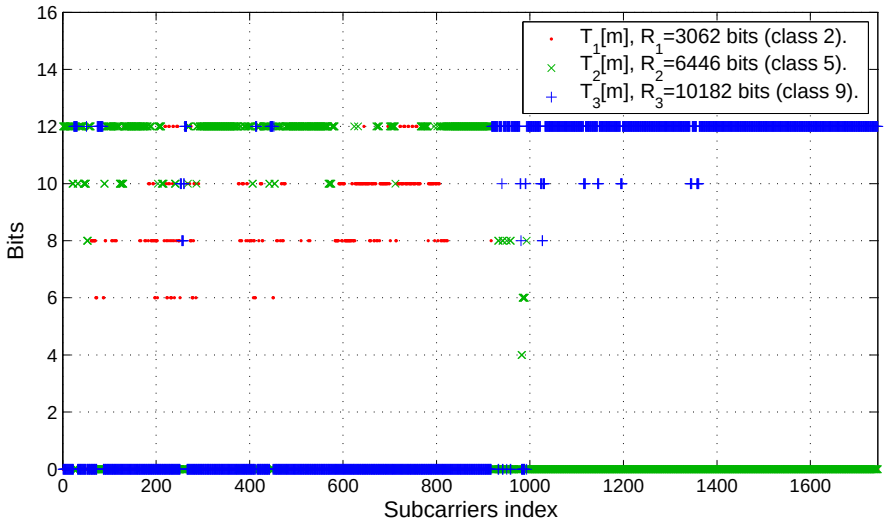

(b)

Figure 4.11: P1901 tone maps belonging to classes 2, 5 and 9 channels: (a) before orthogonalization (b) after orthogonalization with $\alpha_k = \frac{1}{K}$.

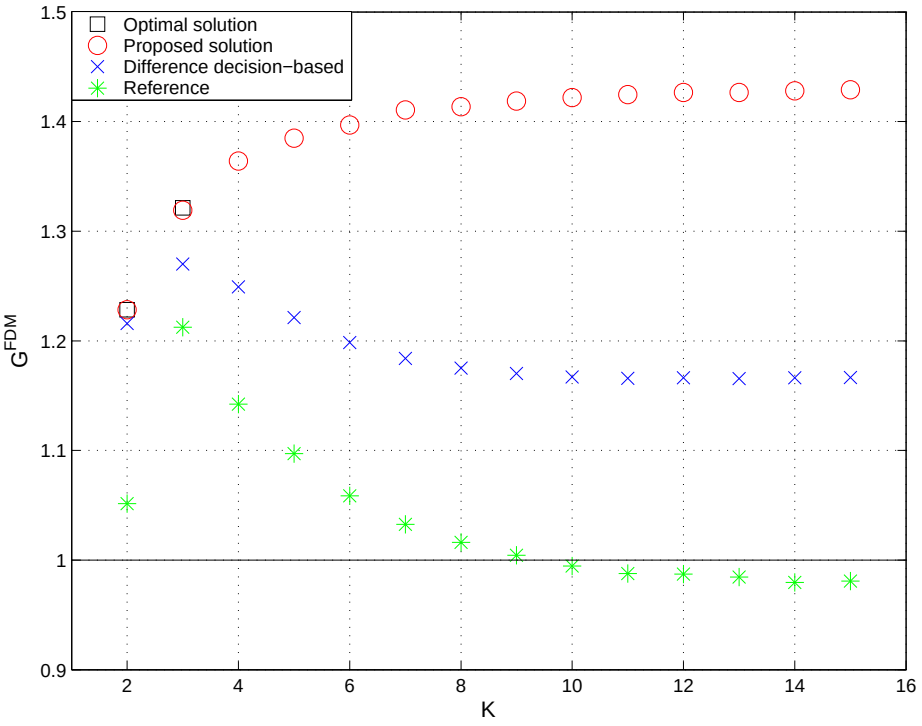

Figure 4.12: Evolution of G_{FDM} with the number of tone maps K using various orthogonalization techniques.

the maxima are not reached on the same subcarriers. As we can see in Fig. 4.12, if this alternative always leads to a gain, it is much lower than the one provided by the original algorithm. Indeed, as the gain provided by the proposed solution always increases, the alternative one decreases above $K = 3$ to finally level off for values of K higher than 8.

As it was previously mentioned, the complexity of the geometrical method for solving the tone maps orthogonalization problem becomes quite important when K is higher than 3. So, to assess the performance of TMSA for higher values of K, a comparison is made in Fig. 4.13 using the particular case described in section 4.3.4, resulting in the computation of $G_{\text{FDM}}^{\max}$. So, the averaged values of the gain presented in Fig. 4.13 are obtained by firstly computing the priority coefficients associated to the achieved value of $G_{\text{FDM}}^{\max}$, which are then used as input values of TMSA. Note that the number of tested cases is exactly the same as for the simulations of Fig. 4.12. According to these results, it seems that the proposed algorithm provides solutions really close to the optimum. Moreover, as we are going to see in section 4.6.1, if we take into account the overhead generated at the MAC layer of realistic PLC systems, the effective increase in the data rates that is achieved using TMSA is generally strictly equal to the gain that would be obtained by optimally orthogonalizing the tone maps.

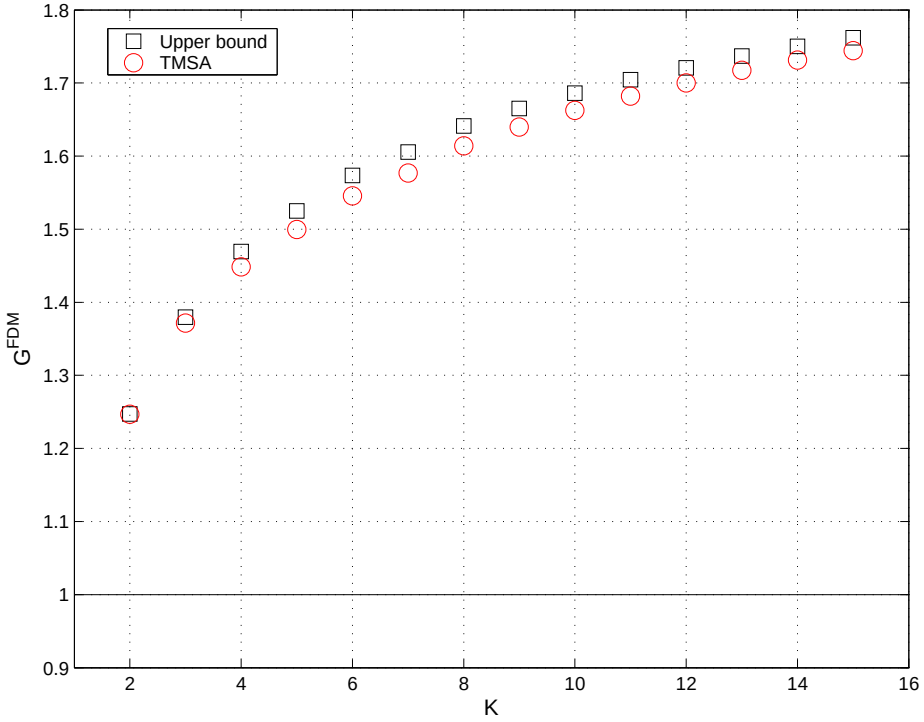

Figure 4.13: Comparison of the achieved values of G_{FDM} by TMSA to the optimal gain.

4.6 Definition of an HPAV-compliant OFDMA Transmission Scheme

This work originally described in [30].

4.6.1 Integration Challenges

To ensure the compatibility with current PLC systems, this new access mode has to comply with several requirements. First of all, the use of the FDM mode has to be exclusively used for point-to-multipoint transmissions, because only one station at a time can access the medium. Moreover, this new mode imposes that the same value of guard interval is used for the K multiplexed flows, as they are synchronously transmitted. Here, we also remind that the tone map is established by the receiver which communicates it to the transmitter. So, we assume that a new management frame has been defined in order to communicate the tone allocation to the K receivers.

In Fig. 4.14, a possible integration of the FDM transmission mode is presented. After the preamble, on which all stations simultaneously synchronize, comes a modified FC field where the *SOF* (Start Of Frame) delimiter has been replaced by a new *FDM_SOF* delimiter. The modified FC gathers all the information needed by the receiving stations to decode the packets transmitted on their own subchannel. Currently, the *FDM_SOF* FC is a concatenation of K *SOF* FC. As this part of the integration is not optimized and, as probably, the massive amount of redundant information will be drastically reduced in a near future, the assumption of an unchanged number of FC Symbols per FDM frame is

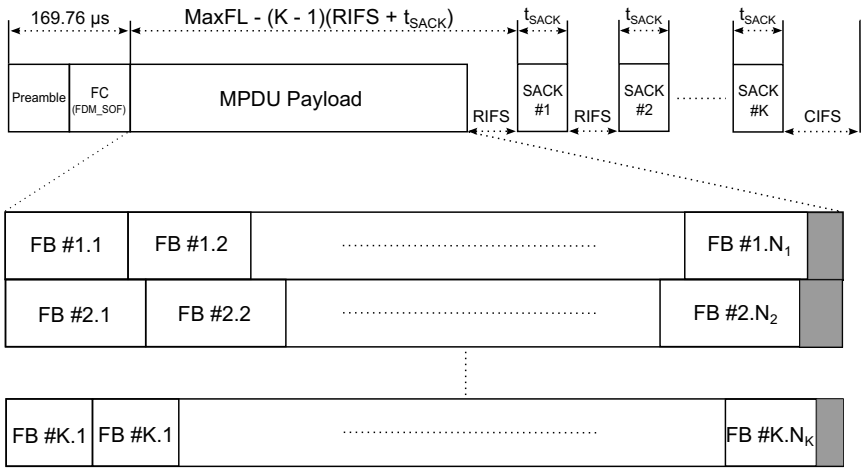

Figure 4.14: Modified P1901 payload and acknowledgment frames structures for FDM transmissions.

made. To acknowledge the K frequency-multiplexed data flows, we use the same method as proposed for the 802.11ac Wi-Fi specification [24] for beam-forming purposes (allowing simultaneous space-multiplexed transmissions). Applying this method comes down to sequence all the receiving stations in a specific order, explicitly specified in the *FDM_SOF* FC, so that the FDM frame is acknowledged by the stations one after the other. Remarking that the less segments to acknowledge there are, the more important the overhead constituted by the acknowledgement frame is, a first drawback of defining a P1901-compliant FDM mode arises. Indeed, in the introduction Chapter, we underlined the fact that the time during which a station can access the medium is limited by the *MaxFL* parameter (see Fig. 2.15 on page 23). Theoretically, keeping a *MaxFL* of 2501.12 μs for FDM frames complies with P1901 specification. Nevertheless, the $(K-1)$ additional acknowledgement frames are part of the whole transmission, so that we decide to reduce the FDM frame duration by $(K-1)(RIFS + t_{\text{SACK}})$. That way, we ensure that the FDM transmission mode does not worsen the effects of collisions on the network performance (cf. section 2.5.4.2). However, it obviously appears that the number of frequency-multiplexed flows will have to be limited in order to reach a good effective value of G_{FDM}.

Because of segmentation, another drawback can be anticipated concerning this new transmission mode. Indeed, as the payload is made of FEC blocks of fixed size, the last OFDM symbol has to be padded (see Fig. 4.14). Now, using the FDM transmission mode, K independently padded flows are transmitted in parallel, so that the padding on a specific link can potentially extend across several OFDM symbols. Also, because of segmentation and the padding of the last OFDM symbol, the slight differences that could be observed between the gains provided by TMSA and the upper bound in Fig. 4.13 will vanish in most cases. Finally, it is important to underline that the encryption and encoding functions in charge of processing segments to be sent do not need to be parallelized. Indeed, the FDM frame construction still needs less computational resource than a TDM frame transmitted on an ideal channel, i.e. at the maximum transmission capacity allowed by the system.

4.6.2 Comparison of the TDM and FDM Modes

4.6.2.1 Simulation Parameters

To assess the performance of the FDM transmission mode in realistic PLC networks (P1901 based), we have modified the MAC layer of the ns-2 based PLC network simulator, that is described in Appendix A. To ensure the diversity of the simulated scenarios, transmission paths may be assigned 4 different channel classes: $1, 3, 6$ and 9. In order to obtain an averaged value of G_{FDM}, each classes combination is tested varying 1000 times the tone maps combination.

STA_0 is supposed to be the only station of the P1901 network with pending packets to transmit. Also, point-to-multipoint transmissions are limited to 2 or 3 parallel data flows, each one being addressed to a unique station of the network. Also, as we aim at assessing the packet-level performance of the FDM mode, only User Datagram Protocol (UDP) flows are used. The simulated flows are set so that the network capacity is always reached. In other words, we ensure that the queues in STA_0 are always filled with packets waiting to be sent. Also, all data flows are assigned the same priority, so that $\alpha_k = \frac{1}{K}$. Concerning the Response Inter-Frame Spacing (RIFS) parameter setting, it normally depends on the processing time at the receiver. Obviously, as FDM reduces the peak data rates on each link and as the acknowledgements are deferred for $(K-1)$ stations, it seems highly likely that the RIFS will be reduced using this transmission mode. Now, as this assumption cannot be assessed, the RIFS parameter is set to 30 μs for both transmission modes, which is the minimal value allowed by the specification. Finally, only 1/2 and 16/21 FEC rates are used, the 18/21 one being an optional feature of the P1901 standard.

4.6.2.2 Simulation Results

Table 4.1 presents the improvement brought by the FDM mode, G_{FDM}, as an averaged percentage of the data rates increases on both links. First of all, it can be noticed that using the FDM mode in the case where the two links are assigned class 9 channels (which can be assumed as ideal) reduces by 5% the achievable throughput. This behavior had been foreseen in section 4.6.1, where it was underlined that, because of segmentation, the FDM mode would increase the overhead caused by the padding. Moreover, the access time dedicated to transmit useful information is reduced by 0.2 ms ($RIFS + t_{\text{SACK}}$). As the frequency diversity is null on class 9 channels (see Fig. 4.11-(a)), using FDM is not profitable in that case. Now, if we look at the results on the diagonal of Table I, we can see that the gain increases as the channel class reduces. This improvement is a direct product of an increase in the frequency diversity of the tone maps to split, that TMSA perfectly exploits when $K = 2$ [31]. So, when both channels belong to class 1, the data rates are increased by more than 20% for both FEC rates, even if the overhead is at its highest. Considering this parameter, note that the gains are generally slightly better when using the 16/21 rate. Indeed, the highest the FEC rate is, the lower the FEC block size is, and so is the average overhead caused by the padding of the last OFDM symbol.

Another important remark that can be made about Table 4.1 concerns the general increase of the gain that seems to converge toward the right up corner of the table, where a 30% improvement of the data rates is reached by associating classes 1 and 9 channels. Actually, this tendency is not entirely due to the natural frequency diversity brought by the PLC channels. Indeed, the limitation of transmitted power above 30 MHz (see Fig.

3.21 on page 57) produces a "virtual" frequency diversity that is at its highest when combining classes 9 and 1 channels. Now, we have to mitigate this last remark by the fact that the association of classes 1 and 3 gives results that seem to contradict this tendency. Actually, in its current version, the simulator processes each link independently, meaning that the number of scheduled OFDM symbols to be transmitted is only dependent upon the tone map associated to the link it is currently processing. So, once the simulator has processed the K parallel flows, the number of scheduled OFDM symbols to transmit can potentially be of K different values. Of course, using the FDM transmission mode, the number of transmitted symbols is the same on the K links, so that the simulator selects the greatest value among the different ones that have been computed. Considering the combination of classes 1 and 3 tone maps, we have noticed that the padding made on the class 1 link generally extends on a number of OFDM symbols higher than for the other classes combinations, which explains these odd results. Obviously, if the cumulated overhead on the K links was considered, the number of transmitted OFDM symbols could be optimized. So, this an issue that could be addressed in a future release of the simulator.

On Table 4.2, a third flow is added, so that the PLC network is now composed of 4 stations. It can be firstly noticed that the FDM mode reduces the data rates for four different combinations of channel classes. Moreover, the case where transmission channels are ideal now decreases the achievable throughput by more than 10%. Indeed, as the overhead caused by the padding and the reduction of the useful access time has been worsened when increasing K, the degradation is accentuated. Still, in a large majority of the tested cases, the FDM mode brings a noticeable gain, reaching a maximum of 26.6% with the $(9, 1, 1)$ classes combination. Now, this maximum remains lower than the 30% reached in Table 4.1, which seems a bit odd considering the fact that G_{FDM} should increase with K. At this point, we can see that defining a P1901-compliant FDM mode gives performance far from an optimized system (cf. the 48% improvement shown in the example of Fig. 4.11). Indeed, using segments of fixed size (8320 bits in the case of a 1/2 FEC rate) advantages channels with high capacity tone maps whereas splitting them naturally results in a reduction of their capacities. Also, it has to be underlined that P1901 specification defines short segments of 136 bytes but these segments are not intended to carry payload data. Yet, we think that using these short segments with the FDM transmission mode could improve the results shown here.

Table 4.1: G_{FDM} (in %) in the case of 2 stations to reach (FEC rate $\frac{16}{21}$ / $\frac{1}{2}$).

Class \ Class	9	6	3	1
9	-4.9 / -5.2	2.4 / 2.1	19.1 / 18.9	29.9 / 29.1
6	...	1.4 / 1.2	14.2 / 14.1	24.2 / 23.8
3	...	...	11.4 / 11.5	17.5 / 18.5
1	...	...	...	20.6 / 20.1

Table 4.2: G_{FDM} (in %) in the case of 3 stations to reach (FEC rate $\frac{16}{21}$ / $\frac{1}{2}$).

Classes \ Class	9	6	3	1
(9,9)	-10.8 / -11	-5.7 / -5.9	5.2 / 4.2	10.5 / 9.2
(9,6)	...	-3.9 / -4.1	7.0 / 5.1	11.3 / 9.1
(6,6)	...	-2.7 / -2.7	7.0 / 5.5	12.1 / 10.4
(9,3)	...	...	16.7 / 14.0	20.8 / 18.2
(6,3)	...	...	11.5 / 9.2	15.1 / 12.9
(3,3)	...	...	11.6 / 10.7	14.1 / 14.8
(9,1)	...	...	...	26.6 / 26.2
(6,1)	...	...	...	19.6 / 19.8
(3,1)	...	...	...	13.2 / 17.1
(1,1)	...	...	...	23.4 / 22.2

4.6.3 Hybridation of the TDM and FDM Mode.

The results shown in section 4.6.2.2 have raised the following paradox: on the one hand, increasing the number of parallel flows improves the diversity, which should improve G_{FDM} but, on the other hand, it simultaneously worsens the overhead caused by the padding at the end of the frame and reduces the part of access time used for the transmission of payload data. Now, as there is not a transmission mode always better than the other, we aim at defining a metric that the transmitter may use to switch between the two modes. Note that we always assume a saturated throughput scenario, meaning that the transmitter has always pending packets to transmit in its K queues, so that the duration of the transmission is as close as possible to the maximum allowed. Also, we decide to use FDM only if data rates are increased on all active links. Knowing N_{pay}, the greatest number of OFDM symbols carrying payload data, we compute N_k^{TDM}, the maximum number of 520 bytes segments carried by a single TDM frame on link k, weighted by its priority coefficient α_k:

$$N_k^{\text{TDM}} = \alpha_k \lfloor \frac{r_{\text{FEC}} N_{pay} R_k}{8 \times 520} \rfloor, \tag{4.78}$$

with $\lfloor a \rfloor$ denoting the greatest integer less or equal than a, remembering that R_k denotes the capacity of the tone maps on link k. Then, we compute N_k^{FDM}, the maximum number of 520 bytes segments carried by a single FDM frame on link k:

$$N_k^{\text{FDM}} = \lfloor \frac{r_{\text{FEC}} \left(N_{pay} - \lfloor (K-1) \frac{\text{RIFS}+t_{\text{SACK}}}{T_0+T_{GI}} \rfloor \right) R_k^{\perp}}{8 \times 520} \rfloor, \tag{4.79}$$

in which $R_k^{\perp}$ is the capacity of the tone map on link k after orthogonalization. We can notice that N_{pay} is reduced in order to comply with the transmission window limitation we

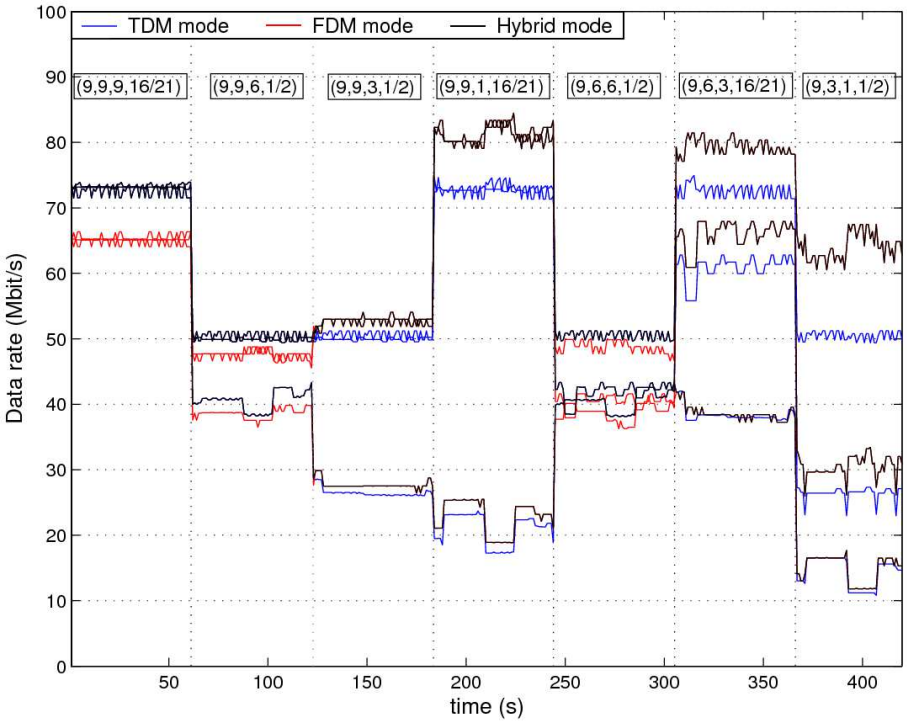

Figure 4.15: FDM and TDM transmission modes Hybridation ($K = 3$).

imposed in section 4.6.1. Also, we remind here that the priority coefficient α_k is directly taken into account by TMSA to compute the FDM tone map of capacity $R_k^{\perp}$. Finally, we define the Δ_k metric, which is computed on each of the K active links, as:

$$\Delta_k = N_k^{\mathrm{FDM}} - N_k^{\mathrm{TDM}}. \tag{4.80}$$

Before starting the FEC block construction, the transmitter computes the K values of Δ_k and, if it is positive $\forall k$, the FDM transmission mode is activated.

In Fig. 4.15, the achieved data rates for 3 different simulations are presented, setting $K = 3$. The blue curves present the results only using the TDM transmission mode, while the red ones present the results only using FDM. Finally, the black curves present the achieved data rates when both modes can be used, the switching between the two modes being enabled by the computation of the Δ_k metric. Each second, one tone map among the three ones is changed and each minute, the channel classes and/or the FEC rate are changed. Looking at the FDM results during the last minute of the simulation, It is interesting to note how low capacity channels are penalized by the segmentation process. Indeed, even if TMSA provides the same relative gain to the capacities of the K orthogonal tone maps, the effective gain is always less important as the channel class is low. Nevertheless, these results show that the switching metric always chooses the best transmission mode.

4.7 Conclusion

This Chapter has shown that current PLC networks could really take advantage of defining a new transmission mode enabling the frequency multiplexing of multiple flows in a point-to-multipoint scenario. Also, this study tends to demonstrate that this new feature could already be integrated in current PLC networks, even if complying with current specifications implies an increased overhead. Moreover, we have highlighted that the currently applied segmentation process may appear to be pretty unfair on severely attenuated channels. Indeed, if the MAC efficiency is naturally degraded as the tone map capacity is low, this effect becomes even more important because of the fixed 520-byte segment size that are not small enough to efficiently use the transmission window. Obviously, this drawback is increased when flows are frequency multiplexed. So, it could be useful to enable the use of shorter segments, or to increase the maximum transmission window when using the FDM mode. In the future, complementary studies remain to be done. For instance, the flow-level performance of this transmission scheme must be studied, using Transport Control Protocol (TCP) data transmissions. Also, the comparison between TDM and FDM still needs to be assessed in a non-saturated throughput scenario.

Considering the HPAV 2 specification [25] that will extend the useful bandwidth up to 86 Mhz, and will enable the utilization of MIMO, the number of active subcarriers will possibly be multiplied by 4 in comparison to P1901 systems. So, considering next generation PLC systems, the frequency diversity will be increased while the impact of segmentation on overhead will be reduced, so that better gains have to be expected using this OFDMA transmission scheme. To avoid a significant decrease of the MAC efficiency, note that we could also limit the number of frequency multiplexed flows. If this limitation is imposed, an interesting study would be to develop a method that would create subsets of tone maps which orthogonalization brings the highest FDM gain.

Chapter 5

Multicast Transmissions over Power Line Networks

5.1 Preliminary

5.1.1 The Interest of Multicast in PLC Networks

Multicast refers to the delivery of the same message to a group of network hosts, all of them being connected to the source transmitting the message. Multicast differs from Broadcast in the sense that a broadcast message is addressed to any station able to decode it. Also, while broadcast transmissions are generally limited at layer 2, typically by the mean of "Ethernet broadcast", multicast commonly refers to layer 3 of the Open Systems Interconnection (OSI) model with IP multicast. As broadcast can be seen as a particular multicast where every network host has subscribed to the service, only the term "multicast" is used in the following. In practice, IP multicast is realized by means of specific IP multicast adresses which must be subscribed by any user who wants to access the service. The subscription mechanism allows the routing of multicast messages, and can be practically realized using the Internet Group Management Protocol (IGMP) [18] at a LAN level, and the Protocol-Independent Multicast - Sparse-Mode (PIM-SM) [21] protocol in large scale networks. As the PLC connectivity we are studying is located in the home network, let us take a closer look at IGMP. Basically, the integration of this protocol allows a level-2 network equipment (switch) to intercept multicast messages, so that this equipment be aware on which interface is connected the host that subscribed the multicast service. Consequently, multicast messages will only be routed on this interface. On the other hand, if the switch does not implement IGMP, it cannot know where is located the subscriber, such that multicast messages will be broadcast on every interface. From a network topology point of view, a PLC network bridges two or more Ethernet networks throughout the electrical grid of the home, so that it can be seen as a switch. Current PLC devices implement the IGMP stack, so that multicast streams are only sent to stations directly connected to the subscribers. Yet, if multiple stations must receive the same multicast message, the transmission is far from being optimized.

Considering home networking, multicast applications are mostly represented by IPTV streaming services. Nowadays, all french ISPs offer multiscreen television services allowing the customer to install more than one IPTV decoder inside his home network (see Fig.

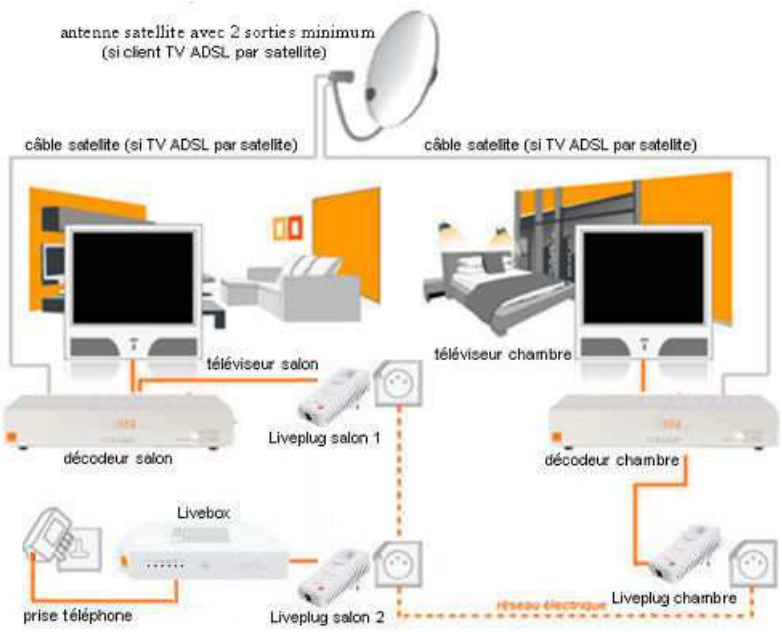

Figure 5.1: Possible configuration of the Orange multiscreen TV offer using 3 Orange *Liveplugs* (Picture downloaded from the Orange online support website).

5.1). If the second decoder is mostly used to watch another program than the first one, multicast over the PLC network may happen if the user is moving inside his home while watching live sport on TV, so that his two decoders subscribe to the same multicast stream. In that particular case, the user could benefit from a PLC network optimizing multicast transmissions. Apart from user-level applications, some management messages, either generated from the bridged or the PLC network, may also need to be broadcast inside the home network (ex: Address Resolution Protocol (ARP) and Dynamic Host Configuration Protocol (DHCP) requests, Universal Plug and Play (UPnP) announcement messages...). Also, the recent release of the 802.1 Audio Video Bridging (AVB) standard [23] may increase multicast traffic in a near future. This standard aims at replacing any application specific cable by a simple Ethernet cable, by providing new features to current LAN so that time sensitive audio and/or video data streams will be successfully supported. For this purpose, AVB devices will be able to be finely synchronized, in order to play multi-channel audio tracks for instance. However, to work properly, AVB networks will need frequent transmissions of time-synchronization broadcast messages between playing devices. So, it is possible that the apparition of AVB devices will increase the need for efficient multicast transmissions. Nevertheless, it obviously appears that multicast use cases are not so common considering current home networking applications, but PLC devices can be used for other purposes than home networking. In public places particularly, several PLC-based solutions have already been deployed for video streaming purposes. For instance, in Beijing subway has been deployed an in-train video broadcasting system using broadband PLC modems [85]. Also, several plasma TVs have been installed in Paris subway to display animated advertisements, also connected to the IP backbone through PLC. We can

easily think of a similar system to be used for live sport or news broadcasting in subway hallways. It clearly appears that all these use cases would benefit from efficient multicast transmissions over powerline networks. Apart from public spaces, office environments may also support frequent multicast transmissions. Indeed, it was shown in [93] that 5% to 10% of the payload bytes traffic were transmitted in multicast streaming in enterprise private networks. This is also the case considering campus networks, where a course may be broadcast in several classrooms simultaneously. So, if PLC technology becomes an ubiquitous connectivity solution such as Wi-Fi, addressing the PLC multicast issue will become necessary.

5.1.2 PLC Networks Multicast Issue

As it was described in previous chapters, the quasi-static nature of the PLC channel allows to dynamically adapt the transmitted signal to the channel, using bit-loading techniques. This process, based on an accurate knowledge of the communication channel at the transmitter side, consists in applying independently, for each subcarrier, the appropriate QAM constellation based on the quality of the subchannel on which it is transmitted, resulting in the definition of a dedicated tone map. In this Chapter, we will refer to such tone map as "unicast", as it is defined for a particular transmission path linking two stations of the PLC network. However, if bit-loading allows to efficiently optimize the point-to-point transmissions by approaching the theoretical capacity of the link, it naturally partitions all the receivers from one another. Indeed, as OFDM symbols are mapped following the tone map dedicated to the unique channel linking two communicating stations, it naturally makes other stations of the network unable to decode these symbols. Consequently, if a multicast stream is subscribed by several hosts located beyond different PLC stations of the network, the multicast transmission delivery may become a problem.

In 2007, when the HomePlug AV (HPAV) specification was released [20], this problem was not addressed at all. Actually, this can be imputed to the fact that a lot of the PLC MAC functionalities are derived from 802.11 Wi-Fi standards. As the 802.11 protocol does not require any Acknowledgment (ACK) for a multicast transmission, some of the receivers can experience high loss rate. Consequently, several studies were conducted to improve multicast transmissions over Wi-Fi networks [43], [45]. In [78] and [44], an interesting leader based mechanism is proposed to improve the reliability of multicast transmissions, where only one station in the multicast group acknowledges the transmission. On erroneous reception of the packet at receivers other than the leader, the proposed protocol allows negative acknowledgements from these receivers to collide with the acknowledgement from the leader, thus destroying the acknowledgement and prompting the sender to retransmit the packet. Then in [103], a Batch Mode Multicast MAC protocol (BMMM) was proposed, ensuring the same reliability as unicast by requesting all recipients for acknowledgments (this solution will be assessed in section 5.2.2.1). In practice, as most of the proposed solutions need the standards to be modified, multicast transmissions are generally handled by converting them into as many unicast streams as there are stations to reach. Considering HPAV devices, a unicast conversion is also performed to handle multicast transmissions[(1)]. Yet, if Wi-Fi and PLC networks share a lot of common features, the higher reliability and capacity of the latter [89] makes multicast video streaming a use case much more likely

[(1)] which makes mandatory the integration of IGMP in current PLC devices.

to happen. So, in 2010, the IEEE P1901 specification [22] introduced a multicast tone maps feature in order to simultaneously reach several stations of the network. Now, the standard does not give any direction on how it can be realized in practice, so that the recommendation remains, as in HPAV, to forward a multicast/broadcast stream by proceeding to the unicast conversion of the multicast stream. Yet, as we are going to see in the following, above 3 or 4 stations, this method becomes really costly as the network load severely increases. In this Chapter, we present the gains that can be expected if we use a multicast tone map instead of using the unicast conversion of the stream. The results provided in this Chapter are based on realistic HPAV 2 [25] tone maps, generated in the frequency range $[1.8, 86]$ MHz on PLC channels measured by the HPAV working group. In a second part, the analysis is extended to networks with an increased number of stations, such that the definition of a unique multicast tone map among the links may not be the best choice. In this last part, we assess a solution where several multicast subsets are created instead of a single one.

5.2 The LCG Solution

5.2.1 LCG: PHY Level Analysis

As it was proposed in the P1901 specification, an easy way to improve Multicast/Broadcast communication could be to allow the transmitter to create multicast tone maps. A multicast tone map defines a tone map that is appropriate for transmissions on multiple links of the network, which are originating from the same node (denoted as the source in the following). A known solution to create such tone map, called Lowest Channel Gain (LCG) [113], lies in the computation of an equivalent channel among the K links we want to transmit on. Equivalently, we can directly apply LCG among the K unicast tone maps defined on the K links, respectively, by choosing for the M active subcarriers the lowest modulation order among them (see Fig. 5.2). That way, we ensure the error rate of multicast accesses to remain lower than the error rate of unicast transmissions.

5.2.1.1 PHY Rates Computation

Considering a unicast transmission on link k, the duration of one information bit reads:

$$t_{\text{bit}} = \frac{1}{D_k^{\text{PHY}}}, \tag{5.1}$$

where D_k^{PHY} is the PHY level data rate achieved on link k, which is computed as follows:

$$D_k^{\text{PHY}} = \frac{1}{T_0 + \text{GI}} R_k, \tag{5.2}$$

in which we recall that T_0, GI and R_k denote the duration of an OFDM symbol, the duration of the guard interval and the capacity of the tone map $T_k[m]$, respectively. If the unicast conversion is used to transmit the same information bit to K stations, its duration becomes:

$$t_{\text{bit}} = \sum_{k \in \mathbb{K}} \frac{1}{D_k^{\text{PHY}}}, \text{ with } \mathbb{K} = \{1, .., K\}, \tag{5.3}$$

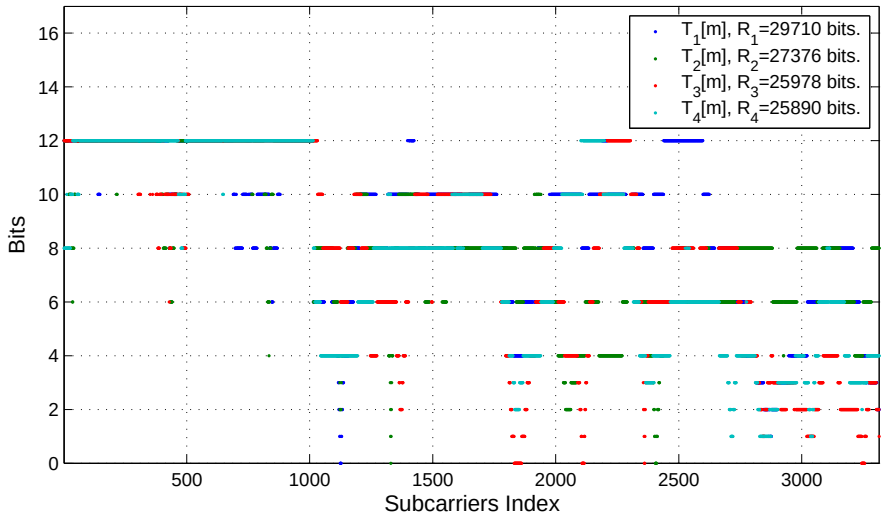

(a)

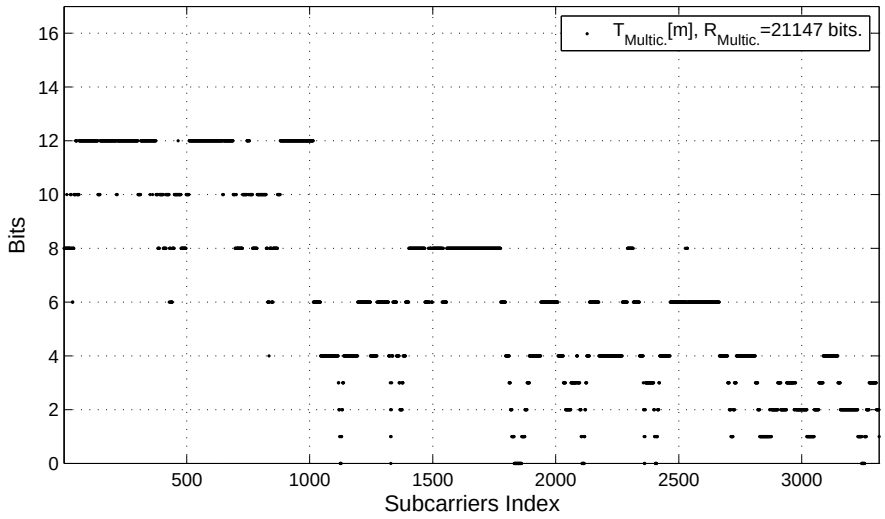

(b)

Figure 5.2: LCG applied among 4 HPAV 2 tone maps: (a) 4 unicast tone maps (b) Multicast tone map after applying LCG.

which, after being inverted, gives us the achieved data rate at the PHY level for multicast transmissions when unicast conversion is used:

$$D_{uniconv}^{\text{PHY}} = \frac{1}{\sum_{k\in\mathbb{K}} \frac{1}{D_k^{\text{PHY}}}} \tag{5.4}$$

$$D_{uniconv}^{\text{PHY}} = \frac{1}{\frac{\sum_{k\in\mathbb{K}} \prod_{p\in\mathbb{K}\setminus\{k\}} D_p^{\text{PHY}}}{\prod_{k\in\mathbb{K}} D_k^{\text{PHY}}}} \tag{5.5}$$

$$D_{uniconv}^{\text{PHY}} = \frac{\prod_{k\in\mathbb{K}} D_k^{\text{PHY}}}{\sum_{k\in\mathbb{K}} \prod_{p\in\mathbb{K}\setminus\{k\}} D_p^{\text{PHY}}} \tag{5.6}$$

Now, if we apply LCG among the K unicast tone maps $T_k[m]$, $k \in \mathbb{K}$ and $m \in \mathbb{M} = \{1, .., M\}$, it results in the definition of a new multicast tone maps $T_{\text{LCG}}[m]$, defined as:

$$T_{\text{LCG}}[m] = \min_{k\in\mathbb{K}} (T_k[m]),\ m \in \mathbb{M}, \tag{5.7}$$

which capacity simply reads $R_{\text{LCG}} = \sum_{m\in\mathbb{M}} T_{\text{LCG}}[m]$, resulting in the following data rate at the physical layer:

$$D_{\text{LCG}}^{\text{PHY}} = \frac{1}{T_0 + \text{GI}} R_{\text{LCG}}. \tag{5.8}$$

where GI is the guard interval duration, that we assume to be fixed to the same value on the K links.

5.2.1.2 Unicast Conversion vs LCG: PHY Level comparison

To compare LCG to the unicast conversion solution, we generate tone maps using the same bit-loading algorithm as presented in section 3.1.3 on page 27. Note that part of this work was used by the HPAV working group to assess the multicast tone map feature for the next release of the HPAV specification (v2.1). Consequently, the generated tone maps are composed of more than 3300 active subcarriers in the frequency range [1.8, 86] MHz. Naturally, the transmitted PSD is limited to -50 dBm/Hz below 30 MHz, and to -80 dBm/Hz beyond that limit. Moreover, we used a colored noise model derived from the work conducted for the OMEGA project [52], depicted in Fig. 5.3, whose PSD follows an exponential decrease with frequency from -100 to -155 dBm/Hz. Concerning the PLC channels, they were directly measured by the HPAV working group during three measurement campaigns, in 3 different houses located in the US, France and Spain, respectively. In each house, all possible communication channels between 5 outlets were measured, such that multicast transmissions can be tested for K=2, 3, or 4 stations to reach. Also, we set the OFDM symbols parameters, such that GI = 5.56 μs and T_0 = 40.96 μs. Finally, to assess the gain brought by the definition of a multicast tone map, we compute a PHY rate improvement factor that simply reads:

$$F^{\text{PHY}} = \frac{D_{\text{LCG}}^{\text{PHY}}}{D_{uniconv}^{\text{PHY}}}. \tag{5.9}$$

In Fig. 5.4 are presented the Cumulative Distribution Function (CDF) distribution of the achieved value of F^{PHY} for K = 2, 3 and 4 stations to reach, respectively. So, with

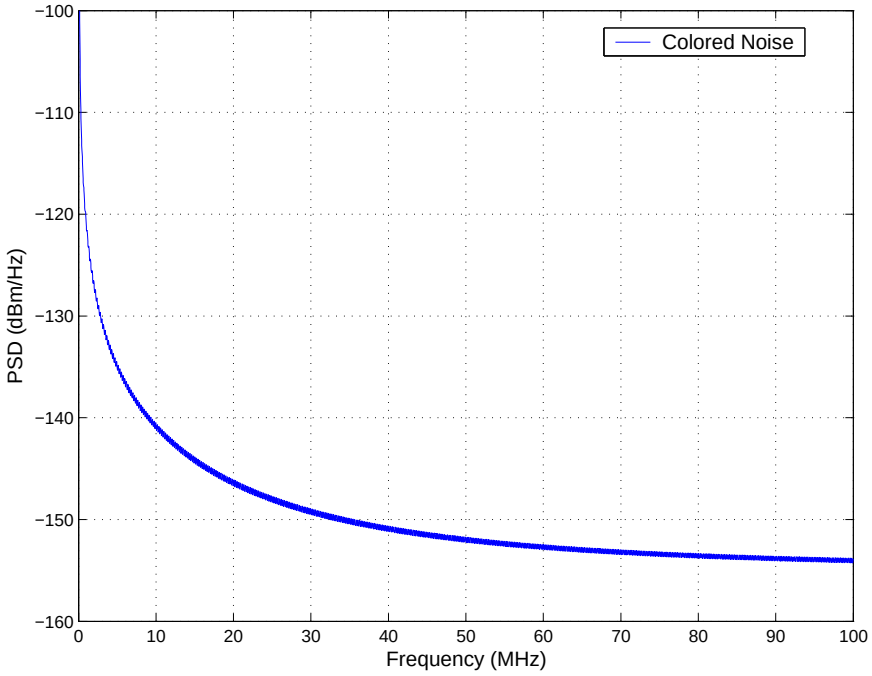

Figure 5.3: Static noise model used for the tone maps generation.

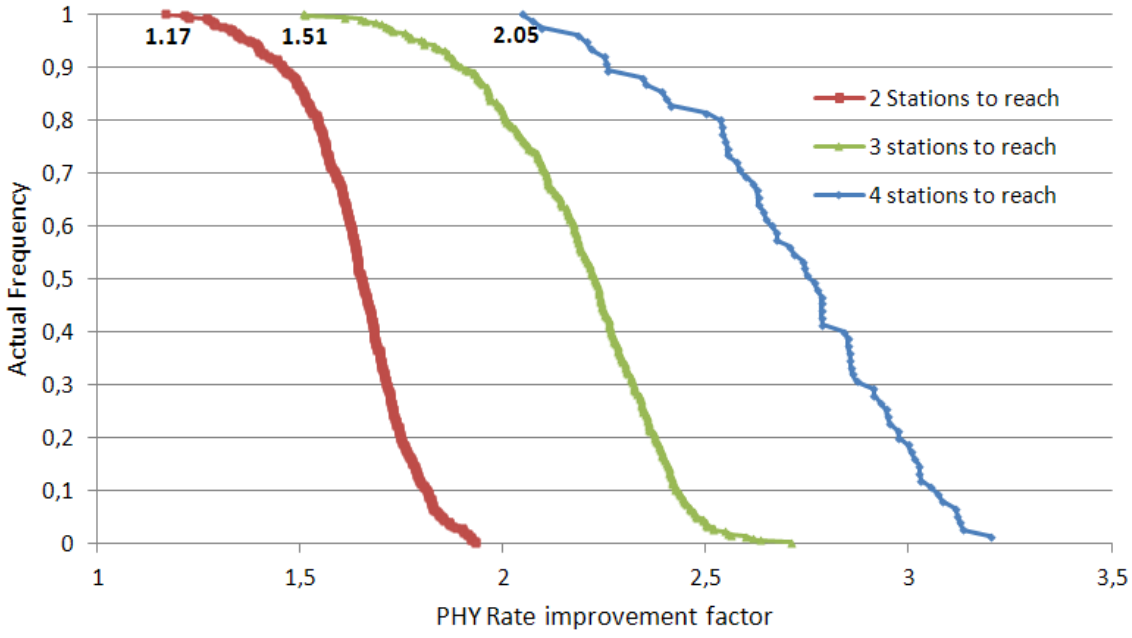

Figure 5.4: Cumulative Distribution Functions of the PHY rate improvement factor ($P(F > X)$), for $K = 2$, 3 and 4 stations to reach.

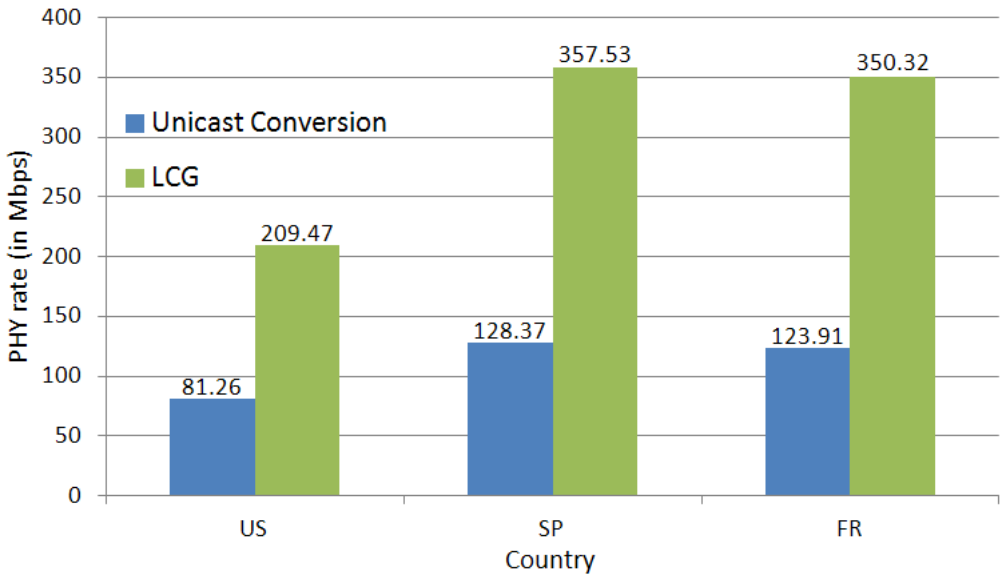

Figure 5.5: Averaged PHY data rate in each one of the 3 countries ($K = 4$).

the 75 different outlets tested as possible sources of a multicast transmission, the $K = 2$, 3, and 4 CDF functions result from the simulation of 450, 300, and 75 different channel combinations, respectively. Naturally, we notice that the data rate improvement increases with K, showing that the cost of the unicast conversion follows the number of stations to reach. Moreover, for all tested PLC channels, LCG always improves the PHY data rate, even if some cases show that the channels may be low correlated, resulting, for the $K = 2$ case, in a minimum improvement of 17% of the data rate. Nevertheless, in the general case, the correlation between channels ensures a massive data rate improvement, such that, if we look at the $K = 4$ curve, thanks to LCG, the achieved PHY data rates are at least doubled.

Looking more in depth to the performance of LCG for the $K = 4$ case, Fig. 5.5 shows a comparison of the two transmission techniques in the 3 countries. The lower multicast data rates achieved in the US may draw our attention, as the results in France and Spain are similar. Actually, two reasons explain this difference: firstly, the measured US channels are, in general, more attenuated than the channels in the other 2 countries. Secondly, we noticed that among the 4 unicast channels linking the transmitter to the receivers, there was often a low attenuated channel in US measures, which is rarely the case with Spain and France PLC channels. So, as the more similar 2 tone maps are, the highest the merging gain will be, it naturally explains the difference between those results. Nevertheless, if we look at Fig. 5.6, we notice that data rates are similarly improved for the 3 countries.

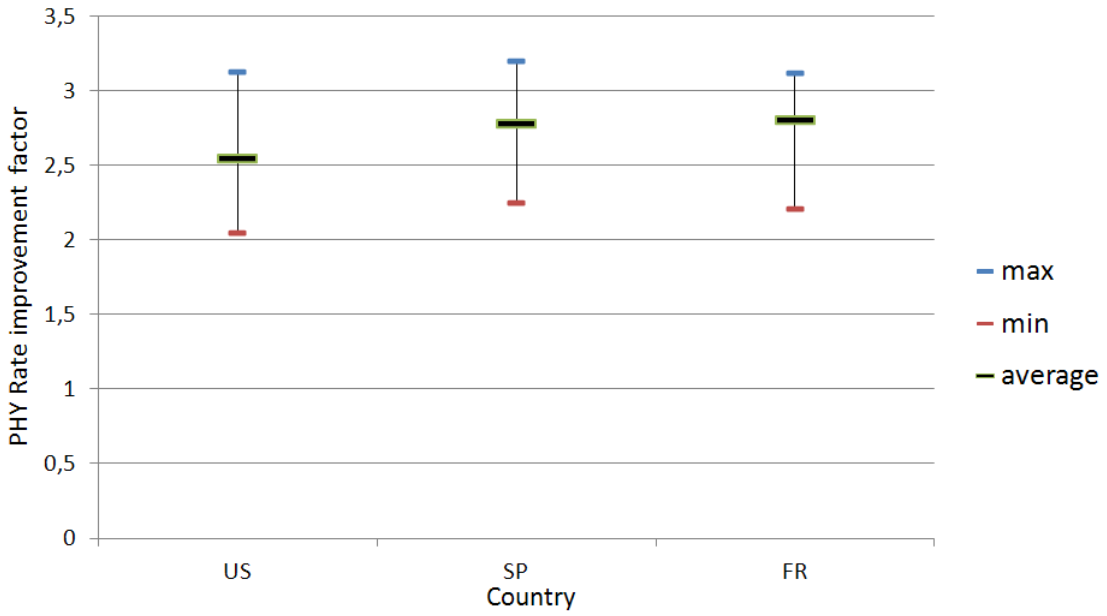

Figure 5.6: Distribution of the PHY rate improvement factor each one of the 3 countries ($K = 4$).

5.2.2 LCG: MAC level Analysis

5.2.2.1 Definition of a Multicast Transmission Scheme

As we have shown in the previous section, enabling the creation of multicast tone maps would greatly benefit to current PLC networks. However, the integration of this new feature in a next release of the HPAV specification would need some functionalities to be added. One of the first issue to be addressed, not the more challenging one though, would be the definition of a new management message to communicate the multicast tone map to the K receivers. Indeed, recalling that in PLC networks, the bit-loading is performed at the receiver side, which then communicates an appropriate tone map to the transmitter, a new management message is needed to transmit the multicast tone map in the other way, from the transmitter to the K receivers. But the major concern we might have about this new feature comes down to the following question: can we ensure the same reliability using a multicast tone map instead of multiple unicast ones? Looking at current HPAV specification, there actually exists a feature allowing "real" multicast transmissions, by the mean of the ROBO mode. Having said that, the reason why we did not introduce this possibility before is because the ROBO mode actually achieves really low data rates, the maximum PHY data rate being limited to 10 Mbps. Consequently, it is only intended to be used for the transmission of critical network management messages, or when there is no appropriate tone map on the link we are transmitting on. Nevertheless, the ROBO mode is interesting because it allows a message to be broadcast to all stations of the network. In this case, as the HPAV transmission scheme allows only one station to acknowledge a

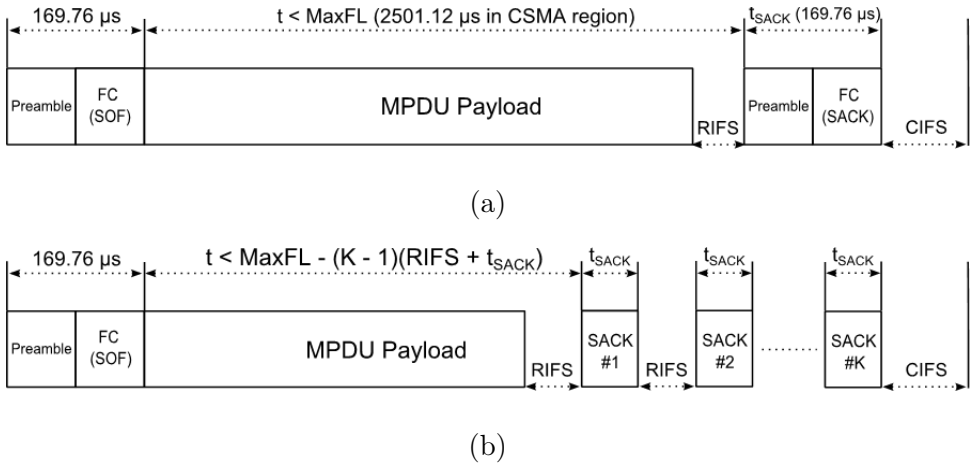

Figure 5.7: Transmission schemes: (a) HPAV unicast [7] (b) HPAV-compliant multicast.

transmission, a "partial acknowledgement" scheme is defined, in which one station in the group serves as a proxy to provide the Response. This solution is actually really close to the Leader-Based ARQ mechanism described in [78], except that HPAV does not allow any other receiver than the proxy to send an ACK. Considering the robustness of ROBO transmissions, this mechanism can be accepted as a satisfactory reliability can still be ensured. However, if we want to use a multicast tone map using the LCG technique, we obviously need the K receivers to acknowledge the transmission to ensure the same reliability as the unicast conversion. So, the problem we are dealing with is exactly the same as the one described in section 4.6, where we have defined an HPAV-compliant OFDMA transmission scheme. As it is shown in Fig. 5.7-(a), the time during which a station can access the medium is limited by the t_{MaxFL} parameter. If keeping a t_{MaxFL} of 2501.12 μs for a multicast frame would theoretically comply with legacy devices, the $(K-1)$ additional acknowledgement frames are part of the whole transmission, so that, as for the OFDMA transmission scheme, we choose to reduce the multicast frame duration by $(K-1)(t_{\text{RIFS}} + t_{\text{SACK}})$ (see Fig. 5.7-(b)). As we are going to see in the following, this decision has a significant impact on the achieved gains.

5.2.2.2 MAC Rates Computation

To assess the MAC level performance, we need to take into account the MAC overhead. As in the previous Chapter, we assume a saturated throughput scenario, meaning that the transmitter has always pending packets to transmit. Consequently, the transmitter always uses the maximum transmission window, limited by the t_{MaxFL} parameter. So, in unicast, the saturated MAC level data rate on link k reads:

$$D_k^{\text{MAC}} = \frac{B_k}{t_{\text{Acc.}}}, \tag{5.10}$$

where B_k is the number of transmitted bits during the access time $t_{\text{Acc.}}$. Considering the transmission of $N_{\text{OFDM}}(t_{\text{pay.}})$ OFDM symbols carrying 520 bytes segments of payload data

using a FEC rate r_{FEC} during $t_{\text{pay.}} = t_{\text{MaxFL}} - t_{\text{RIFS}}$, we have:

$$B_k = 8 \times 520 \lfloor \frac{r_{\text{FEC}} N_{\text{OFDM}}(t_{\text{pay.}}) R_k}{8 \times 520} \rfloor, \tag{5.11}$$

where

$$N_{\text{OFDM}}(t) = \lfloor \frac{t}{(T_0 + \text{GI})} \rfloor \tag{5.12}$$

and

$$t_{\text{Acc.}} = 2 \times t_{\text{PRS}} + \bar{t}_{\text{BO}} + t_{\text{SOF}} + t_{\text{MaxFL}} + t_{\text{RIFS}} + t_{\text{SACK}} + t_{\text{CIFS}}, \tag{5.13}$$

in which t_{PRS} is the duration of one priority resolution symbol (cf. section 2.5.3.1 on page 15); $\bar{t}_{\text{BO}}$ denotes an averaged value of the contention window during the Back-off procedure; t_{SOF} is the duration of the start of frame, which takes into account the synchronization preamble and the frame control symbols; t_{SACK} is the duration of an acknowledgement frame and, finally, t_{RIFS} and t_{CIFS} denote the Response and Contention Inter-Frame Spaces (RIFS and CIFS), respectively. Then, to compute the achieved MAC data rates for multicast transmissions when unicast conversion is used, we apply the formula defined by (5.6), so that:

$$D^{\text{MAC}}_{uniconv} = \frac{\prod_{k \in \mathbb{K}} D^{\text{MAC}}_k}{\sum_{k \in \mathbb{K}} \prod_{p \in \mathbb{K} \setminus \{k\}} D^{\text{MAC}}_p} \tag{5.14}$$

On the other hand, if LCG is used, the transmission scheme defined in Fig. 5.7-(b) leads to the following expression of the MAC data rate:

$$D^{\text{MAC}}_{\text{LCG}} = \frac{B_{\text{LCG}}(K)}{t_{\text{Acc.}}}, \tag{5.15}$$

where

$$B_{\text{LCG}}(K) = 8 \times 520 \lfloor \frac{r_{\text{FEC}} N_{\text{OFDM}}(t_{\text{pay.}} - (K-1) \times (t_{\text{RIFS}} + t_{\text{SACK}})) R_k}{8 \times 520} \rfloor, \tag{5.16}$$

which takes into account the $(K-1)$ new acknowledgement frames reducing the allocated time for payload transmission.

5.2.2.3 Unicast Conversion vs LCG: MAC Level Comparison

In this section, we are going to present simulation results following the same parameters as in section 5.2.1.2, so that we will be able to compare the results at the PHY and at the MAC layers. We define a MAC rate improvement factor that simply reads:

$$F^{\text{MAC}} = \frac{D^{\text{MAC}}_{\text{LCG}}}{D^{\text{MAC}}_{uniconv}}. \tag{5.17}$$

Then, we also need to fix the values of the time parameters introduced in the previous section in order to comply with the HPAV specification. We set: $t_{\text{PRS}} = 35.84\ \mu s$; $\bar{t}_{\text{BO}} = 150\ \mu s$; $t_{\text{SOF}} = 169.76\ \mu s$; $t_{\text{MaxFL}} = 2501.12\ \mu s$; $t_{\text{RIFS}} = 60\ \mu s$; $t_{\text{SACK}} = 169.76\ \mu s$; $t_{\text{CIFS}} = 100\ \mu s$.

In Fig. 5.8 are presented the distribution of the achieved value of F^{MAC} for $K = 2$, 3 and 4 stations to reach, respectively. If these results can be interpreted in a same manner as the PHY level ones, the comparison of the simulation results between the two layers (the

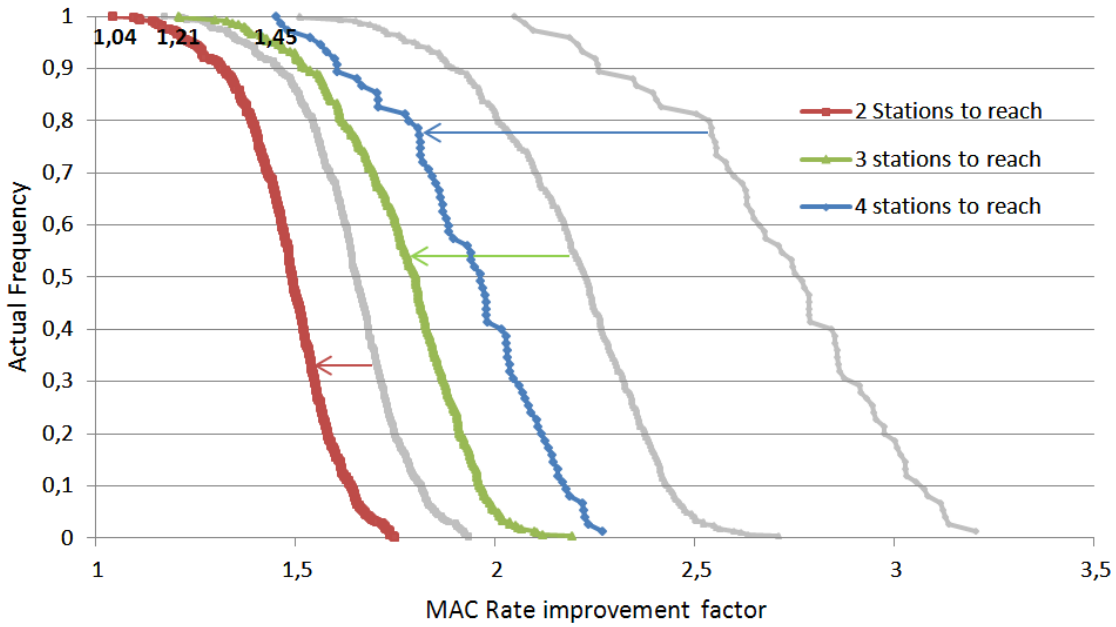

Figure 5.8: Cumulative Distribution Functions of the MAC rate improvement factor ($P(F > X)$), for $K = 2$, 3 and 4 stations to reach.

grey curves present the PHY level CDF) highlights the massive gain reduction induced by the MAC overhead of the transmission scheme defined in Fig. 5.7-(b). Moreover, we can notice that this reduction increases with K. Indeed, as the number of addressed stations increases, the MAC efficiency is worsened. The MAC efficiency can be interpreted as the ratio of time allocated for payload transmission to the total access time. Considering the time parameters set in our simulations, increasing K by 1 reduces the payload transmission window by $100 \times \frac{t_{\text{SACK}}+t_{\text{RIFS}}}{t_{\text{pay.}}} = 9.41$ %.

As in section 5.2.1.2, Fig. 5.9 and Fig. 5.10 detail the performance of LCG for the $K = 4$ case, which provides the worst MAC efficiency. On average, the achieved values of F^{MAC} are reduced by 29 %, in comparison to F^{PHY}. Nevertheless, these results tend to show that LCG still brings a significant improvement of the data rates. However, we may have some concerns on the performance of this new multicast transmission scheme for higher values of K. The next section deals with this particular issue.

5.3 Multicast Transmission Scheme Based on the Creation of Multiple Multicast Subsets

5.3.1 LCG Limitations

In the Chapter dedicated to the study of point-to-multipoint communications, we take advantage of the multiuser diversity between the channels to improve data rates on multiple

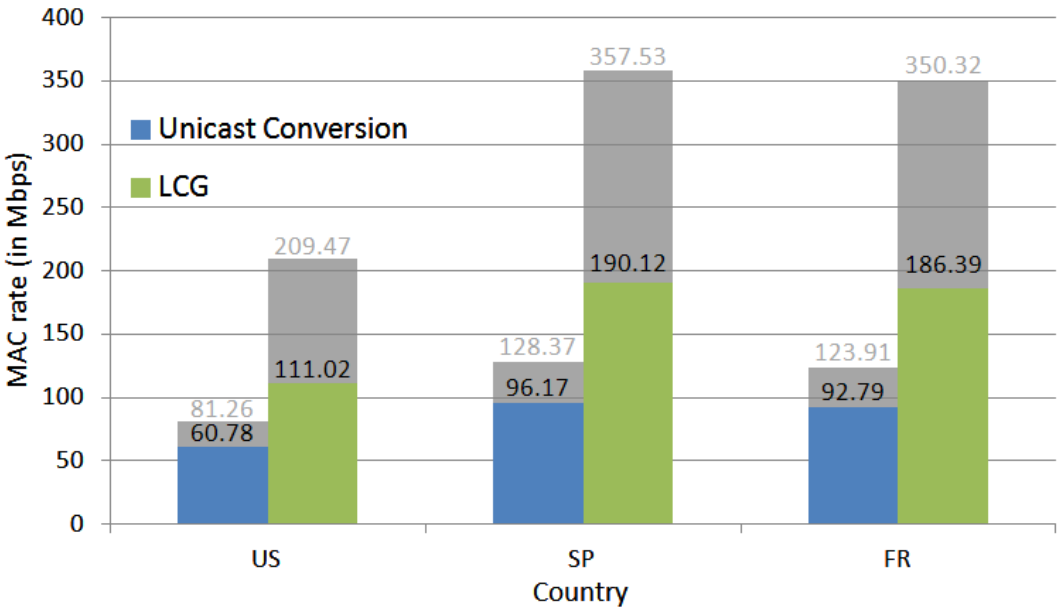

Figure 5.9: Averaged MAC data rate in each one of the 3 countries ($K = 4$).

links, using an OFDMA transmission scheme. Considering multicast transmissions, the higher the multiuser diversity is, the lower is the capacity of the multicast tone map after applying the LCG technique. Moreover, as K increases, as the additional acknowledgement frames reduce the MAC efficiency, so that creating a unique multicast tone map may not be the optimal choice. In the following, we study the opportunity of defining multiple multicast tone maps instead of a single one.

5.3.2 Smart Merging Approach

This section is derived from the work originally presented in [27]. Fig. 5.11 illustrates the case where the definition of more than 1 multicast tone maps provides an higher data rate. Without considering the MAC overhead, we see that of all 3 solutions, this example shows that the creation of 2 multicast tone maps provides the shortest transmission duration. Note that, even if the LCG solution presented in Fig. 5.11-(b) improves the transmission efficiency in comparison to the unicast conversion presented in Fig. 5.11-(a), it is not necessarily the case if we take into account the MAC overhead. Now, to choose which links should be merged into a multicast subset, several parameters need to be taken into account. Among them, there is obviously the number of stations to reach, K, but there is also the overhead inherent to the definition of a new stream (frame headers, inter-frame spaces, signalization induced...). To find the optimal solution, this combinatorial problem needs all possible merging combinations to be tested. To do so, in the case of a transmission to K nodes, it is firstly necessary to look at all possible partitions of the set $\{1, ..., K\}$. Then, for a given partition, $\{1, ..., P\}$, $\{P + 1, ..., Q\}$, $\{Q + 1, ..., K\}$ for instance, where 3 multicast tone maps would be defined, the number of possible merging

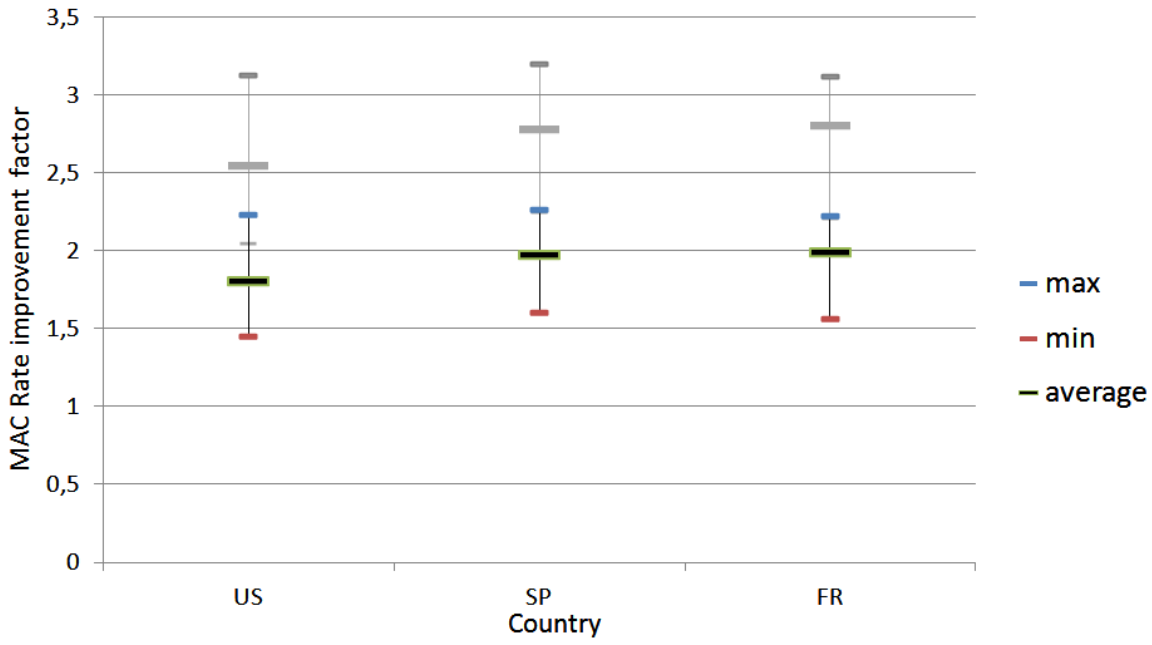

Figure 5.10: Distribution of the MAC rate improvement factor in each one of the 3 countries ($K = 4$).

is equal to $\binom{K}{P} \times \binom{K-P}{Q-P}$. So, it appears that the analysis of all possible partitions can become rapidly very costly in terms of computational resource. So, in the following, we propose an algorithm that quickly finds a sub-optimal partitioning of the K links.

5.3.2.1 Construction of a Fast Tone Map Merging Algorithm

The proposed solution aims at gathering together the K stations into N multicast subsets as the iterations go by so that, for the n^{th} multicast group, we define:

$$R_{\mathbb{L}_n} = \sum_{m \in \mathbb{M}} \min_{p \in \mathbb{L}_n} (T_p[m]), \text{ with } \bigsqcup_{n=1}^{N} \mathbb{L}_n = \mathbb{K}, \tag{5.18}$$

as the capacity of the *n-th* multicast tone map, resulting from the LCG application among the links which indexes are collected in $\mathbb{L}_n$. Then, a given partition of the K links is associated to a multicast data rate that reads

$$D^{\text{MAC}}_{multicast} = \frac{\prod_{n \in \{1,..,N\}} D^{\text{MAC}}_{\mathbb{L}_n}}{\sum_{n \in \{1,..,N\}} \prod_{p \in \{1,..,N\} \setminus \{n\}} D^{\text{MAC}}_{\mathbb{L}_p}}, \tag{5.19}$$

where $D^{\text{MAC}}_{\mathbb{L}_n}$ is the MAC data rate associated to the multicast tone map of capacity $R_{\mathbb{L}_n}$. Then, the inversion of (5.19) gives us:

$$\frac{1}{D^{\text{MAC}}_{multicast}} = \sum_{n \in \{1,..,N\}} \frac{1}{D^{\text{MAC}}_{\mathbb{L}_n}}. \tag{5.20}$$

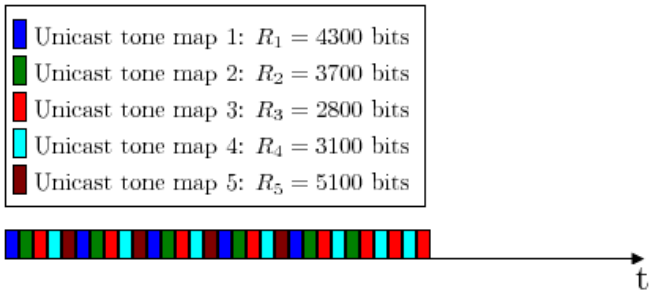

(a)

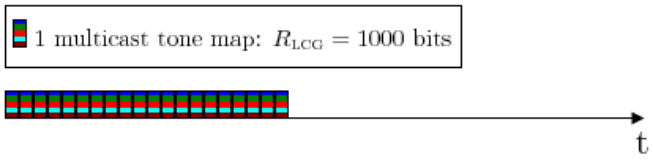

(b)

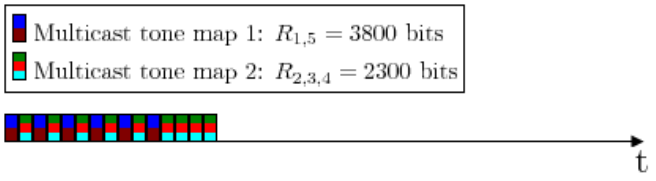

(c)

Figure 5.11: 20000 bits broadcast to 5 stations: (a) by multiplexing 5 Unicast streams, (b) by merging all the tone maps (LCG solution), (c) by creating two merged tone maps.

If we do not take into account the payload segmentation, we can approximate the MAC data rate by multiplying ($D^{\text{PHY}}_{\mathbb{L}_n}$) by the ratio of time allocated for payload transmission as follows:

$$D^{\text{MAC}}_{\mathbb{L}_n} = \frac{t_{\text{Pay.}} - (\text{card}(\mathbb{L}_n) - 1) \times (t_{\text{SACK}} + t_{\text{RIFS}})}{t_{\text{Acc.}}} D^{\text{PHY}}_{\mathbb{L}_n}, \tag{5.21}$$

$$\Leftrightarrow D^{\text{MAC}}_{\mathbb{L}_n} = \frac{t_{\text{Pay.}} - (\text{card}(\mathbb{L}_n) - 1) \times (t_{\text{SACK}} + t_{\text{RIFS}})}{t_{\text{Acc.}}} \frac{R^{\text{PHY}}_{\mathbb{L}_n}}{T_0 + \text{GI}}, \tag{5.22}$$

$$\Leftrightarrow D^{\text{MAC}}_{\mathbb{L}_n} = \frac{1}{C} \left[1 - (\text{card}(\mathbb{L}_n) - 1) \times r_{ACK}\right] R^{\text{PHY}}_{\mathbb{L}_n}, \tag{5.23}$$

where

$$C = \frac{t_{\text{Acc.}}(t_0 + \text{GI})}{t_{\text{Pay.}}} \tag{5.24}$$

is a constant, and

$$r_{ACK} = \frac{t_{\text{SACK}} + t_{\text{RIFS}}}{t_{\text{Pay.}}} \tag{5.25}$$

corresponds to the ratio of time by which the unicast transmission window is reduced each time one station is added in the multicast subset. Then, inserting (5.23) in (5.20) gives us:

$$\frac{1}{D^{\text{MAC}}_{multicast}} = C \sum_{n \in \{1,..,N\}} \frac{1}{\left[1 - (\text{card}(\mathbb{L}_n) - 1) \times r_{ACK}\right] R_{\mathbb{L}_n}}. \tag{5.26}$$

Finally, the transmission efficiency can be assessed using a metric α, proportional to the inverse of the multicast data rate:

$$\alpha = \sum_{n=1}^{N} \frac{1}{\left[1 - (\text{card}(\mathbb{L}_n) - 1) \times r_{ACK}\right] R_{\mathbb{L}_n}}, \tag{5.27}$$

which takes into account the additional MAC overhead induced by the multicast transmission scheme defined in Fig. 5.7-(b). To initialize the merging algorithm, we consider that the multicast stream is transmitted using the unicast conversion, such that:

$$\alpha_{\text{ini}} = \sum_{k=1}^{K} \frac{1}{R_k}. \tag{5.28}$$

Note that R_k exactly follows the same notation as $R_{\mathbb{L}_n}$, with the peculiarity that $\mathbb{L}_n = \{n\}$, $\forall n \in \{1, ..., K\}$. Starting from the initialization value α_{ini}, the method aims at reducing the value of α.

The critical part of the treatment lies in the criterion that will be used to choose the tone maps to merge. Considering the transmission scheme defined in section 5.2.2.1, it obviously appears that the overhead caused by the multiple acknowledgements is the most significant parameter to take into account for the merging decision. Indeed, if K increases, the transmission window reduces and we can easily infer that, above a certain value of K, the creation of multiple multicast subsets will be preferable. Moreover, looking at the expression of α in (5.27), we can write:

$$\alpha \geq \frac{1}{\min_{k \in \mathbb{K}} \left(R_{\mathbb{L}_n} \left[1 - (\text{card}(\mathbb{L}_n) - 1) \times r_{\text{ACK}}\right]\right)}, \tag{5.29}$$

which tends to be an equality if the data rate associated to one multicast subset is much lower than the data rates associated to the other subsets. This result is pretty intuitive as the multicast data rate is naturally limited by the most attenuated channel. Interestingly, this result leads to the definition of a criterion that will help us making the merging decision. Moreover, if the multicast subsets $\mathbb{L}_i$ and $\mathbb{L}_j$ are merged into a single subset, $\forall (i,j) \in \mathbb{K}^2$,

$$\frac{1}{R_{\mathbb{L}_i}\left[1-(\text{card}(\mathbb{L}_i)-1)\times r_{\text{ACK}}\right]}+\frac{1}{R_{\mathbb{L}_j}\left[1-(\text{card}(\mathbb{L}_i)-1)\times r_{\text{ACK}}\right]}, \tag{5.30}$$

originally part of the α computation, is then replaced by:

$$\frac{1}{R_{\mathbb{L}_i\cup\mathbb{L}_j}\left[1-(\text{card}(\mathbb{L}_i)+\text{card}(\mathbb{L}_j)-2)\times r_{\text{ACK}}\right]}. \tag{5.31}$$

As $R_{\mathbb{L}_i\cup\mathbb{L}_i} \leq \min\left(R_{\mathbb{L}_i}, R_{\mathbb{L}_j}\right)\ \forall (i,j) \in \mathbb{K}^2$, we necessarily have:

$$(5.31) \geq \frac{1}{\min_{n\in\{1,..,N\}}\left(R_{\mathbb{L}_n}\left[1-(\text{card}(\mathbb{L}_n)-1)\times r_{\text{ACK}}\right]\right)}. \tag{5.32}$$

From (5.32), it appears that if $\mathbb{L}_i$ or $\mathbb{L}_j$ corresponds to the subset associated to the lowest MAC data rate, so that the lower bound of α, defined in (5.29), will necessarily increase once the two subsets are merged. In order to protect the low capacity subsets, we define the following merging criterion:

$$e_{p,q}=\frac{1}{R_{\mathbb{L}_p\cup\mathbb{L}_q}\left[1-(\text{card}(\mathbb{L}_p)+\text{card}(\mathbb{L}_q)-2)\times r_{\text{ACK}}\right]}, \tag{5.33}$$

assessing the part of α that will change if $\mathbb{L}_p$ and $\mathbb{L}_p$ are merged. Noticing that $e_{p,q}=e_{q,p}$ and setting $e_{p,p}=0$, all the computed values of the criterion are gathered in the matrix E:

$$E=\begin{pmatrix} 0 & e_{2,1} & e_{3,1} & \dots & e_{N,1} \\ e_{2,1} & 0 & e_{3,2} & \dots & e_{N,2} \\ e_{3,1} & e_{3,2} & 0 & \dots & e_{N,3} \\ \vdots & \vdots & \vdots & \ddots & \vdots \\ e_{N,1} & e_{N,2} & e_{N,3} & \dots & 0 \end{pmatrix} \tag{5.34}$$

At each iteration, the choice to merge two tone maps is made by selecting the minimum non-zero value of the matrix E. If this merging leads to an improvement of the transmission efficiency, meaning that the α parameter has been reduced, the choice is validated and the matrix E is updated. To update E, the two merged tone maps are removed and the $e_{p,q}$ values are updated. Then, we pass to the next iteration until the α parameter cannot be reduced anymore. Note that the algorithm presents two possible exits. First, it can converge to a solution where several multicast groups are defined. The second exit corresponds to the definition of a unique tone map shared between all the stations, meaning that the algorithm converged toward the LCG solution. Let us detail more precisely the algorithm (see Fig. 5.12).

Step 1: Initialization

- $\alpha = \alpha_{ini}$;
- $\mathbb{L}_n = \{k\}$, $\forall n \in \{1, ..., K\}$;
- *Compute matrix* E.

Step 2: Merge multicast subsets $\mathbb{L}_i$ and $\mathbb{L}_j$

- *Selection of the pair* (i, j), $i \neq j$, *such that* $e_{i,j} = min\,(E)$;
- $\mathbb{L}_n^{new} = \begin{cases} \mathbb{L}_n, \text{ if } n \notin \{i, j\}; \\ \mathbb{L}_i \cup \mathbb{L}_j \text{ if } n = \min(i, j); \\ \emptyset \text{ if } n = \max(i, j); \end{cases}$
- $R_{\mathbb{L}_n^{new}} = \sum_{m \in \mathbb{M}} \min_{k \in \mathbb{L}_n^{new}} (T_k[m])$;
- *Computation of the new* α *in a temporary variable* $\alpha_{new} = \sum_{n=1}^{K} \frac{1}{R_{\mathbb{L}_n^{new}}}$;

Step 3: Validation

- *If* $(\alpha_{new} >= \alpha)$*:*
  - *elimination of the previously tested* (i, j) *pair by instanciating* $e_{i,j} = e_{j,i} = \infty$;
  - *if* $(\nexists (p, q),\ p \neq q,$ *so that* $e_{p,q} < \infty)$, **end the process** *as all the pairs have been tested;*
  - *Else, go back to* **step 2**.
- *Else, the merging improves the efficiency of the ressource utilization. Continue to* **step 4**.

Step 4: Update parameters

- $\alpha = \alpha_{new}$;
- $\mathbb{L}_n = \mathbb{L}_n^{new}$, $\forall k \in \{1, ..., N\}$;
- *Update* E.

Step 5: Continue or end the process

- *If* $(\exists (p, q),\ p \neq q,$ *so that* $\mathbb{L}_p \neq \emptyset$ *and* $\mathbb{L}_q \neq \emptyset)$, *go back to* **step 2**;
- *Else, the algorithm converged to the definition of a unique multicast subset.* **End the process**.

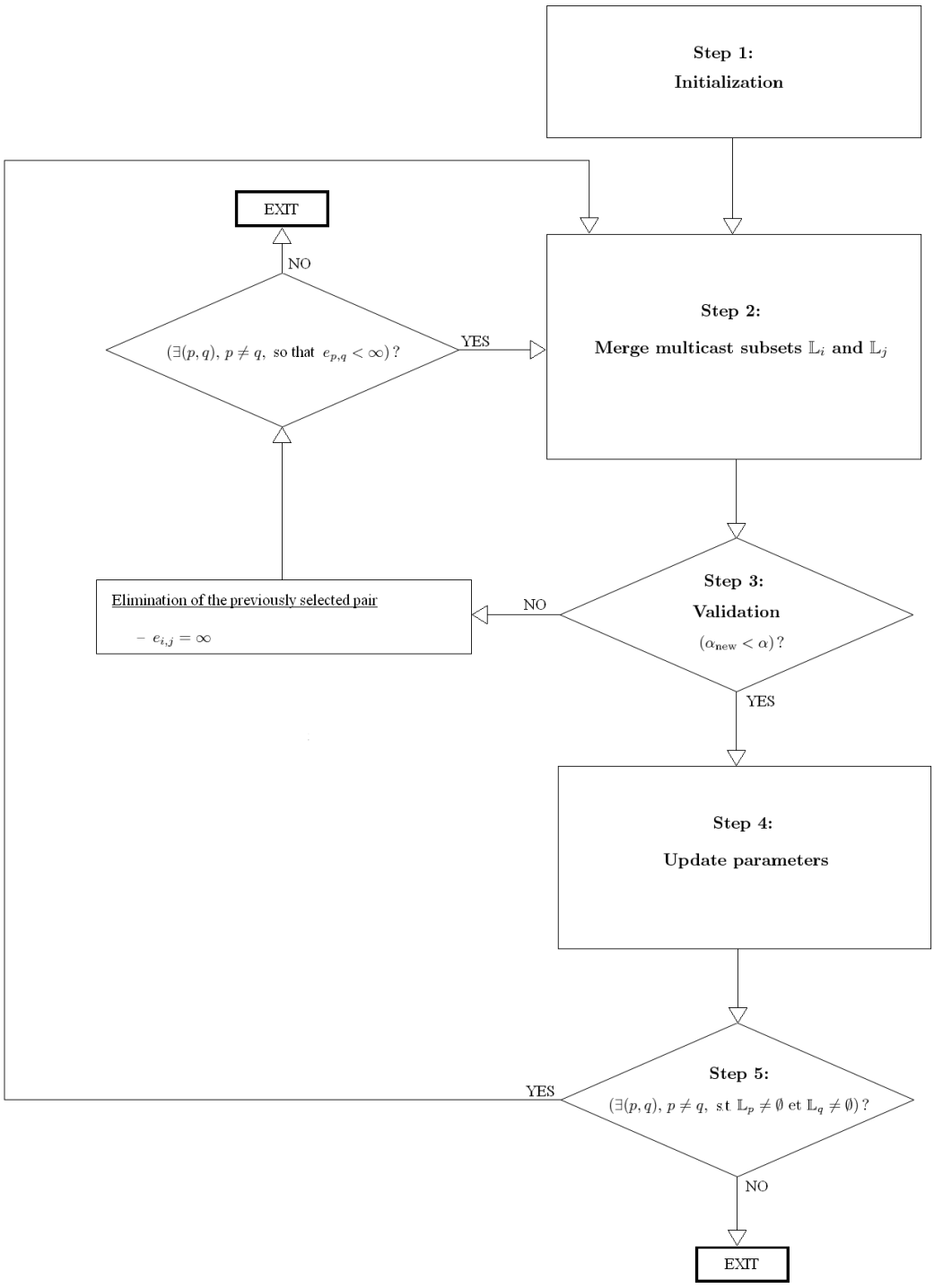

Figure 5.12: Merging Algorithm.

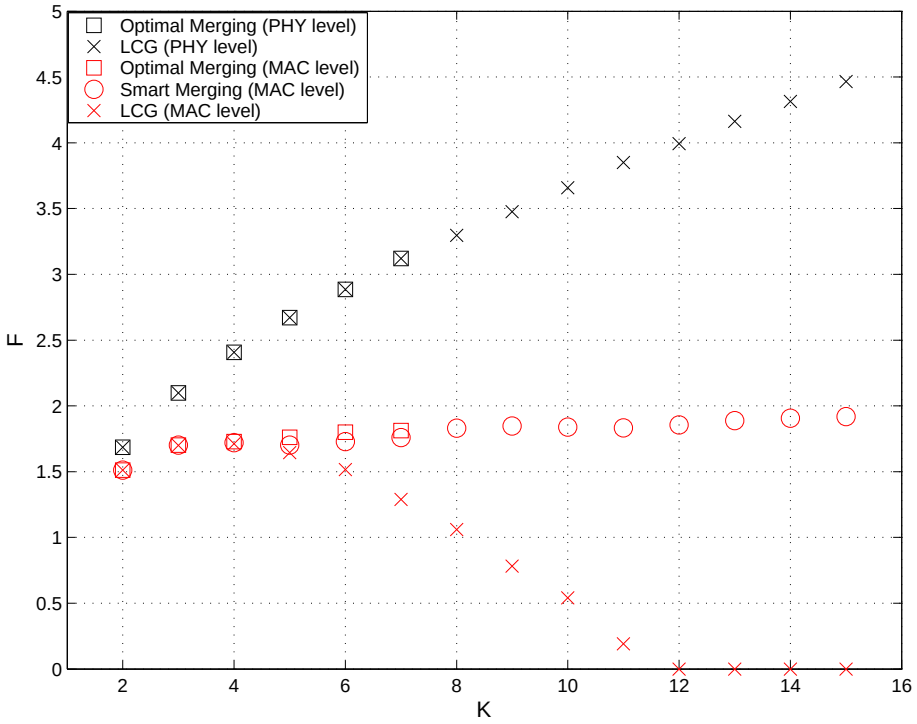

Figure 5.13: Comparison of the rates improvement factor by the smart merging algorithm and by LCG, both at the PHY and MAC layers.

5.3.2.2 Simulation Results

In this section, the merging algorithm is assessed by computing the achieved values of F^{PHY} and F^{MAC} for increasing values of K on various simulated channels. For each simulation run, the unicast conversion, the LCG and the smart merging solutions are tested, by randomly choosing K tone maps in a data base. In order to ensure the singularity of each simulation run and the diversity of the situations, the data base contains 300 uncorrelated HPAV 2 tone maps, generated using 300 simulated static PLC channels realizations belonging either to classes 3, 5 or 7 [107], [106]. To obtain a relevant mean value using the 3 different channel classes, we ensure that each K-tuple combination is tested 100 times. To do so, we use the K-combination with repetitions formula, given by $\binom{n+K-1}{K}$, with $n = 3$. In other words, it means that the $K = 2$ case needs 600 simulation runs and the $K = 15$ case needs 13600 simulation runs. Consequently, it appeared that above $K = 7$, the number of possible solutions becomes too high to obtain the optimal solution. In Fig. 5.13 are gathered the simulation results. We can firstly notice that if the MAC overhead is not considered, LCG appears to the optimal solution, at least until $K = 7$. Moreover, F^{PHY} seems to be linearly increasing above $K = 4$. Note that if we had done simulations for higher values of K, the values of F^{PHY} would be leveling off before starting to decrease, as LCG degrades more and more the capacity of the resulting multicast tone map. Having said that, the most interesting results concern the achieved values of F^{MAC}. Note that we used the exact same values of the time parameters that were used in section 5.2.2.3. These results firstly confirm the massive gain reduction caused by the additional

overhead, firstly observed in section 5.2.2.3 using measured PLC channels. The LCG and the smart merging solutions appear to provide the optimal solution for $K = 2$ and $K = 3$. Then, for $K = 4$, LCG and the proposed algorithm provide the same results, which are slightly lower than the optimal value of F^{MAC}. Above $K = 4$, the improvement factor achieved by LCG starts decreasing with K, and even degrades the transmission efficiency above $K = 8$, in comparison to the unicast conversion. Moreover, as $r_{\mathrm{ACK}} = 0.094$, the transmission window is null over $K = \lceil \frac{1}{r_{\mathrm{ACK}}} \rceil + 1 = 11$, which is confirmed by the null value of F^{MAC} above this limit. However, we can see that the gain provided by the merging algorithm remains pretty close to the optimum, and even slightly increases with K.

5.4 Conclusion

In this study, we have seen that current PLC networks do not optimize the transmission of multicast services. With the popularization of the PLC technology, the multicast issue needed to be addressed. It appears that the definition of multicast tone maps, using the LCG technique, could bring major improvements to PLC networks. Consequently, the integration of this feature in a next release of the HPAV 2 specification is currently under discussion. To keep the same reliability as unicast communications, we assessed the performance of a multiple acknowledgement transmission scheme. It appeared that the additional overhead of this solution imposes to create several multicast tone maps. Now, the merging algorithm presented in this Chapter could satisfactorily respond to this issue. Other analysis would need to be made to evaluate the complexity of the algorithm and its impact on real systems. Now, we are confident that the flexibility in the choice of the criterion combined with programming optimization should lead to a limited complexity, considering the whole system. In the future, it would also be interesting to assess the performance of the leader based solution [78] [44], which has the advantage of adding no overhead to the current unicast transmission scheme. However, this solution needs all segments to be repeated if another station than the leader receives only one erroneous segment. Consequently, a tradeoff has to be made between improving the MAC efficiency, which is done by increasing the transmission window length, and limiting the cost of retransmission on the system throughput, which is done by limiting its duration. This makes this solution much more complicated to assess.

Chapter 6

Conclusion

Broadband Power Line Communications are getting more and more popular for home networking, thanks to the already existing infrastructure and the achievable data rates of current systems. However, looking back in the 2000s, the intense competition between non-compatible solutions has slowed down the adoption of this technology. Fortunately, the release of the IEEE P1901 standard in 2010 has largely been contributing to the stabilization of the market since then. Nowadays, the market is clearly dominated by systems following specifications established by the HomePlug Powerline Alliance, that are the HP 1.0, HPAV 1 and the novel HPAV 2 specifications. Nevertheless, this thesis clearly highlights that these systems could still benefit from significant improvements. In this study, several topics have been tackled to improve broadband PLC networks in a multiuser context. We have firstly addressed the need for more capacity by assessing the benefits of a bandwidth extension of current systems, in association with an alternative modulation scheme. Then, we have proposed novel resource allocation methods that would allow to use more efficiently the limited and shared transmission resource among PLC stations.

In Chapter 2, we have firstly presented the PLC transmission medium that is the in-home power grid. As the PLC channel was obviously not dedicated to support such application in the first place, it is very hostile to broadband communication. Therefore, it needs the most advanced transmission techniques to provide reliability in the delivery of multimedia services. An overview of HPAV networks was conducted, in which we have highlighted some mechanisms that allow to efficiently cope with the harsh transmission medium. We particularly presented the two level MAC-framing process that allows systems to break the dependency between the Ethernet and the HPAV MPDU frame formats. Additionally, this segmentation process allows the network to efficiently react to unexpected events, such as impulsive noise, by only repeating corrupted segments. Moreover, we introduced the two different channel access mechanisms defined by the specification, firstly represented by the contention-based CSMA/CA access technique. However, in spite of the four level access priorities allowed by HPAV CSMA/CA, it can never ensure any QoS guarantee. So, the HPAV specification also defines an optional contention free period, using TDMA, that the CCo can use to schedule dedicated sessions supporting QoS demanding applications such as IPTV.

The multipath nature of the PLC channel, in addition to various sources of interference, have made multicarrier modulation techniques natural candidates for PLC. However, in Chapter 3, we have firstly shown why the classical CP-OFDM is not suited for PLC,

considering the spectral mask every device must comply with. Indeed, because of the radiated power by the electrical grid, PLC systems must refrain from transmitting in multiple narrow notches distributed across the $[1.8, 28]$ MHz frequency range, in order to protect primary applications such as radio amateur. Because of the bad spectral containment of the rectangularly shaped OFDM symbols, HPAV defines a windowing operation which reduces the level of secondary lobes, and consequently limits the number of subcarriers that have to be switched off around notches. However, windowing OFDM symbols reduces the GI in proportion of the Roll-Off interval length, and we highlighted that in the worst channels, a non-negligible interference appears. So, we have established the exact expression of this interference term over a dispersive PLC channel to finely compute the achieved SINR per subcarrier. On the other hand, we have introduced another multicarrier modulation technique: the HS-OQAM modulation. By relaxing the orthogonality condition only to the real field, HS-OQAM offers the possibility to design prototype filters well adapted both to the frequency selective channel and to the transmission mask. Using Frequency selective filters, more subcarriers can be used at notch edges in comparison to windowed OFDM, while still satisfying the PSD constraint imposed by the mask. However, due to the absence of GI, the 1-tap ZF equalizer is generally not sufficient to mitigate interference. So, we have introduced a 3-tap ASCET equalizer, that can be seen as a 3-tap ZF, that efficiently reduces the interference level. We established a generalized expression of the interference and noise terms at the output of ASCET, in order to compute the achievable throughput and the transmission capacity of the HS-OQAM modulation. The comparison between the two schemes was performed both in the HomePlug AV 1 and 2 contexts, where we have shown that HS-OQAM can outperform windowed OFDM, by providing a minimum improvement of 15% in the PHY data rates. However, considering that windowed OFDM has been standardized through IEEE P1901, there is actually little hope to see OFDM/OQAM being chosen for future PLC systems. Yet, considering the CENELEC spectral mask that might be imposed to every PLC device sold in Europe, the performance gap between the two schemes will be even more important.

Thanks to the quasi static nature of the PLC channel, a fine link adaptation can be achieved using bit-loading algorithms. This process, based on an accurate knowledge of the communication channel between two stations, consists in applying independently, for each subcarrier, the appropriate QAM constellation based on the quality of the subchannel on which it is transmitted, resulting in the definition of a dedicated tone map. In Chapter 4, we have emphasized on the fact that the tone maps defined between one station and K other ones highlight a diversity that is not exploited by current PLC networks, as they only work in a TDM scheme. We have shown that this diversity could be efficiently exploited by frequency multiplexing multiple flows, through the definition an OFDMA transmission scheme that could be practically realized in a point-to-multipoint transmission scenario. Considering K tone maps dedicated to each one of the K links we want to simultaneously transmit on, we introduced the tone maps orthogonalization problem. Based on a set of fixed priority coefficients associated to each link, we have demonstrated that this problem could be optimally solved by constructing a concave capacity region between the K links, only using the K tone maps. However, this geometrical approach remains prohibitive in terms of computational complexity. So, we have developed a novel allocation algorithm, called TMSA, that efficiently and quickly distributes the subcarriers among the considered links. This algorithm was then implemented in a PLC network simulator to assess the

actual gain that could be achieved by this new FDM access mode, taking into account constraints of the HPAV specification. Considering a saturated throughput scenario that puts OFDMA at a disadvantage, we were still able to show significant improvement in the data rates, thanks to this novel access method. Then, we have presented this FDM access mode as an additional feature to the current TDM scheme, such that both multiplexing techniques could be cooperatively used by always choosing the most appropriate one. In the future, a fine analysis of the complexity will be necessary to decide whether this OFDMA access mode can be practically realized. A main concern we can have is related to the rate at which the tone maps are changing, as this will impact the actual FDM gain. Moreover, it would be interesting to perform a flow-level analysis of the proposed transmission scheme, using TCP streams. Finally, the comparison between TDM and FDM still needs to be assessed in a non-saturated throughput scenario, where we expect FDM to significantly outperform TDM, as the MAC overhead will be reduced.

Then, in Chapter 5, we have highlighted the broadcast/multicast issue inherent in current PLC networks that arises because of the link adaptation. Indeed, it appears that tone maps isolate stations from one another such that, if a station has to deliver a multicast flow to several stations of the PLC network, it will generally perform a unicast conversion of the stream. The problem comes from the fact that this method wastes the medium, as the message is repeated as many times as there are stations to reach. In this last Chapter, we have assessed the opportunity of defining multicast tone maps, using the LCG technique. A multicast tone map allows to simultaneously communicate with multiple PLC stations, while still complying with each link targeted error rate. From the simulations performed on HPAV 2 channels, the application of LCG among a set of tone maps clearly shows major improvement in the transmission efficiency. However, this statement remains only true from a PHY layer point of view. Indeed, if we want each station to acknowledge its own reception status, it creates an additional overhead that limits the number of stations that can be gathered into a multicast subset. So, we have introduced a smart merging approach that, by simultaneously taking into account this additional overhead and the correlation between tone maps, defines several multicast subsets instead of a single one. This algorithm has shown performance really close to the optimal solution. If the complexity of the algorithm remains to be assessed, we can be confident on the fact that a multicast tone map should not need to be modified too often, as it still remains more robust against errors than the unicast ones, thanks to the LCG principle. As a further study, it would also be interesting to assess the performance of the leader based solution [78], [44], which has the advantage of adding no overhead to the current unicast transmission scheme.

At this point, it appears legitimate to ask us the following question: what is the next step to be taken in the field of broadband PLC networks? The capacity of future HPAV 2 networks, thanks to the bandwidth extension and the introduction of MIMO, should be sufficient to support the growing number of multimedia applications circulating within the home network. However, we cannot ignore the CENELEC spectral mask that could significantly reduce the capacity of PLC networks in Europe. If this mask happened to be validated as it is now defined, it could trigger the need to increase even more the bandwidth of PLC systems. Some people are already thinking of using frequencies above 100 MHz, up to 400 or 500 MHz [60]. In such a case, a whole new Physical layer would have to be defined for this new frequency range. But this new physical layer might not be

desirable for the sake of the in-home PLC market. Indeed, looking back at the evolution of broadband PLC during the last decade, the competition between different solutions had only resulted in slowing down the mass market adoption of this technology. If HPAV or P1901 systems are now massively deployed in Europe, the success of PLC is nothing compared to the one of 802.11 WLAN solutions. If PLC cannot compete with wireless technologies in terms of mobility, this might not be the only reason explaining the gap between the two networking solutions. Indeed, another limitation of PLC concerns the fact that it is never directly implemented in terminal equipments, such as laptops for instance. This could change in the future, but it could mainly depend upon the success of another standard: the IEEE P1905. This new solution, that we have briefly introduced in the first Chapter, aims at taking advantage of every connectivity solution within the home network, wired or wireless, defining an abstraction layer above the technology dependent MAC layers. To have a concrete interest, an increasing number of multiple interface nodes will have to be present in the home network, which is not the case today. So, depending on the number of companies supporting this P1905 standard, this could be the entry point for PLC in users terminal equipments.

Appendix

Appendix A

The ns2-based PLC Network Simulator

General information

For the time being, the simulator only runs in a Unix environment. To work properly, it needs the modified version of ns-2, including the PLC module. To compute statistics on the network traces generated by ns-2, Gawk scripts are used. The interface can also export postscript figures, using the Gnuplot graphic utility.

Core of the simulator

The PLC simulator model [87], based on the version 2.30 of ns-2 [10], was developed in accordance with HPAV and IEEE P1901 specifications. The ns-2 PLC transmission system follows the CSMA-only mode that deploys the CSMA/CA access service. The TDMA access service is not yet available. Thus, as in 802.11-based wireless networks, PLC stations gain access to the medium by using the opportunistic access technique CSMA/CA that separates contending users by defining backoff procedures and uses acknowledgment mechanisms to ensure the delivery of packets and collision detection. Moreover, this access mode allows to prioritize services by defining 4 channel access priorities (CAP), the eight 801.1Q priorities specified by the user being mapped onto these 4 CAP. To closely model the PLC MAC layer as specified in [20], [7], the framing and segmentation processes are also considered. However, unlike the MAC layer, the physical layer in this simulator is modeled quite superficially; it considers only a generalized channel model with channel characteristics like Tone Map, FEC and segment error rate. In fact, modeling the whole communication chain of the PLC physical layer is essential to correctly approach the behavior of PLC networks but, at the same time, this type of modeling increases significantly the complexity of the simulator; simulating seconds of network activity requires hours and hours of computations. Therefore, to improve this simulator, we deploy the PLC channel generator.

To model the PHY layer of PLC networks, a PLC channel generator module is integrated in the software. The creation of this module was only made possible thanks to measurements conducted by Orange Labs in different sites, from the modern apartment

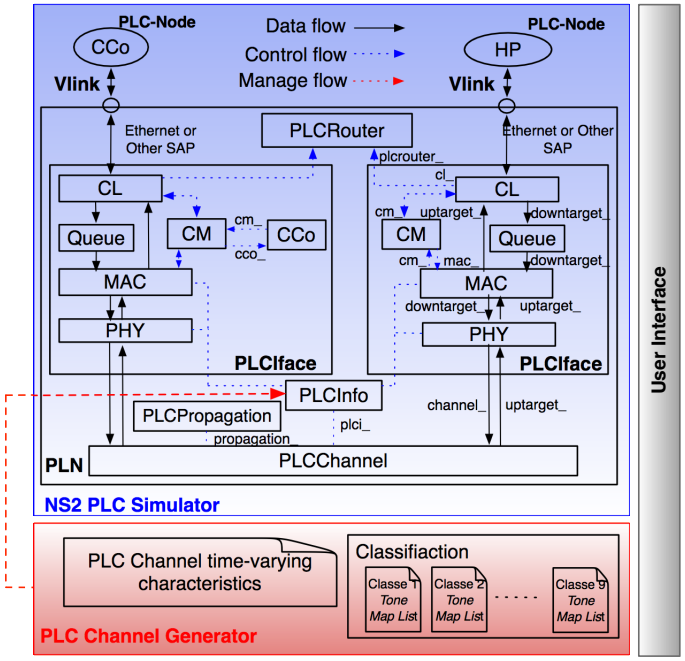

Figure A.1: PLC network simulator Architecture.

to the old countryside house [107]. From this campaign, 144 PLC channels were measured and a statistical analysis was led, resulting in the classification of the channels into 9 different classes, class 1 containing the worst channels (with the lowest transmission capacities) and class 9 the less disturbed ones (with the highest transmission capacities). Finally, this study resulted in the creation of a channel simulator [106], allowing to quickly generate realistic PLC channels, based on the desired channel class and bandwidth. Concerning the noise modeling, we do not use the classical Additive White Gaussian Noise (AWGN) but a colored noise model, also built from a statistical analysis of several measures realized in domestic environments [52]. Based on these realistic channels and noise models, bit-loading algorithms are run to generate adapted tone maps. In Fig. A.2, cumulative distributions functions of HPAV and IEEE P1901 tone maps capacities are plotted with 100 independent channels realizations per class. On this figure, it can be seen that if the transmission capacity of the link naturally increases with the channel class for IEEE P1901 tone maps, HPAV tone maps over classes 6 to 9 channels reach about the same capacities. This can be explained by the fact that, according to this specification, subcarriers cannot carry more than 10 bits per subcarrier, while IEEE P1901 authorizes up to 12 bits. So, in classes 6 to 9 channels, the SNR is high enough on a large majority of the 917 subcarriers so that the maximum of 10 bits is reached. Another reason explaining this difference concerns the PSD limitation to -80 dBm/Hz beyond 30 MHz. Indeed, the IEEE P1901 specification, which extends the HPAV frequency band beyond 30 MHz, has to limit the PSD in the extended band 30 dB under the PSD inside the HPAV band, so that notable differences between the reached SNR for the subcarriers located beyond 30 MHz can be observed with IEEE P1901, whatever the channel class being used. The classification of PLC channels can either be used to define a static quality of the link

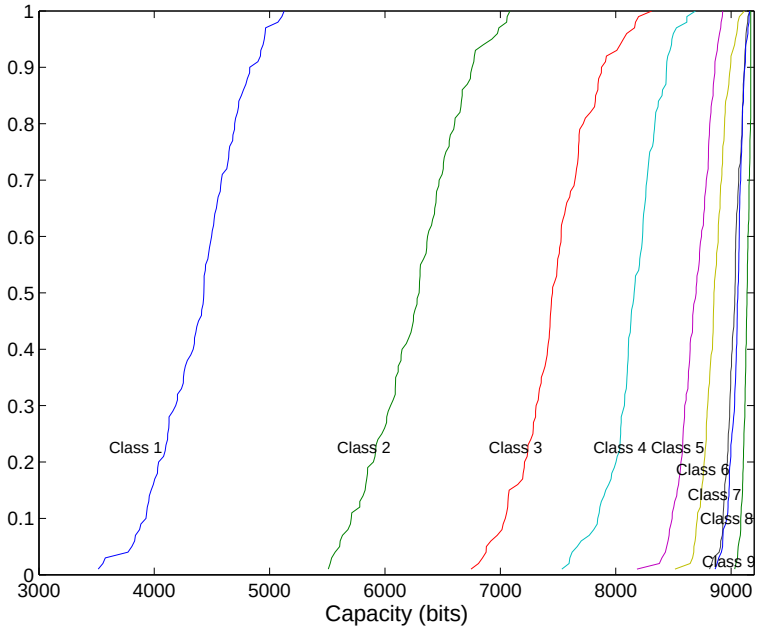

(a)

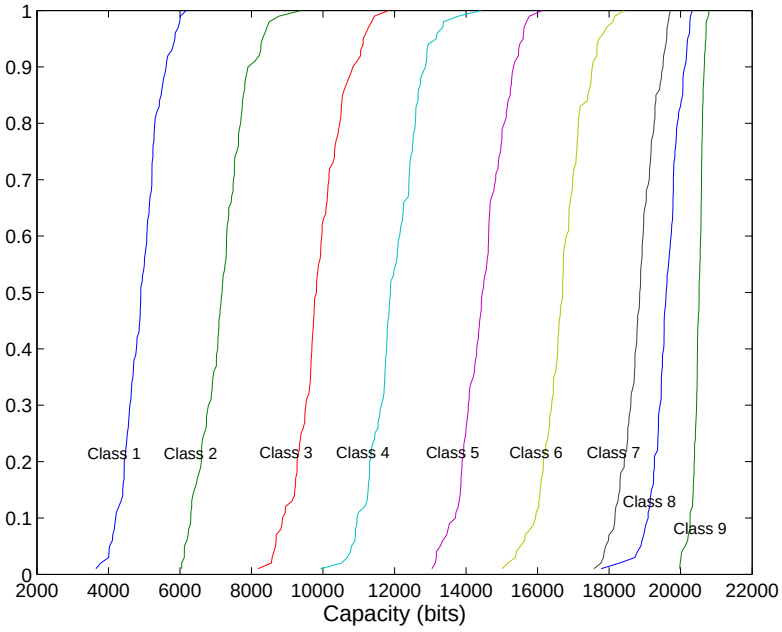

(b)

Figure A.2: Cumulative distribution functions of (a) HPAV and (b) IEEE P1901 tone maps capacities.

to simulate a particular configuration but also to simulate an abrupt change in the PLC

channel characteristics. For example, to take into account an event such as the switching on of a nearby home appliance, we can associate the link to a lower channel class, so that its transmission capacity will be reduced. Therefore, the simulator associates each link of the network to a channel class, parameters that can possibly vary during the simulation.

User Interface

To ease the creation of simulation scenarios and the exploitation of the network traces provided by ns-2, we developed a user interface, written in JAVA. From the main interface, which is described in Fig. A.3, the user can define:

- the number of PLC stations;
- the link qualities between every pair of stations, and potential events that may affect the link quality;
- the streams parameters (target data rate, flow type, duration, priority etc...).

The simulation scenario being defined, the software will run ns-2 simulator by automatically generating the TCL (Tool Command Language) script file needed at input by ns-2. Once the simulation is finished, the ns-2 PLC simulator provides a trace file describing precisely the network activity at the PLC channel level and all levels of the PLC transmission system. This trace file is used for two purposes: on the one hand, it is exploited to compute several statistics about each stream (instantaneous data rate, delay, segment losses). On the other hand, this file can be replayed by the user, the interface displaying the network activity with the desired refresh rate, and also plotting in a "real-time" manner the previously computed statistics.

Validation

To validate the simulator, we compare simulated data rates to the ones retrieved from a real PLC network [114], constituted by devices following the HPAV specification. Considering the ideal conditions in which the measures were done, we assume all communication channels of the simulated HPAV network to be class 9 ones and we set the FEC (Forward Error Correction) rate to 16/21, which is the maximum code rate allowed by the HPAV specification. The network is composed of 5 stations, each of them being able to communicate directly to the others. We place ourselves in an uplink case scenario, which means that transmitting stations contend to gain access to the media and then transmit to the same sink node. In figure A.4, results using 1, 2, 3 and 4 UDP flows are presented, each active station being set to transmit at 30 Mbps. Obviously, on class 9 channels, HPAV networks have no trouble supporting 2 parallel 30 Mbps UDP flows, which is confirmed by the results given by the simulator. Now, as a third flow is defined, the 30 Mbps cannot be reached simultaneously by the 3 transmitting stations, meaning that the network capacity has been reached. This limit is well-shown by the simulator, the behaviors of the simulated and the measured data rates being really similar. With the fourth UDP flow, the per-flow throughput drops even more but again, the simulation results are really close to the measures. In figure A.5, the comparison is made using TCP flows. The first plot shows the HPAV network capacity for TCP, which is around 71 Mbps, which confirmed by the

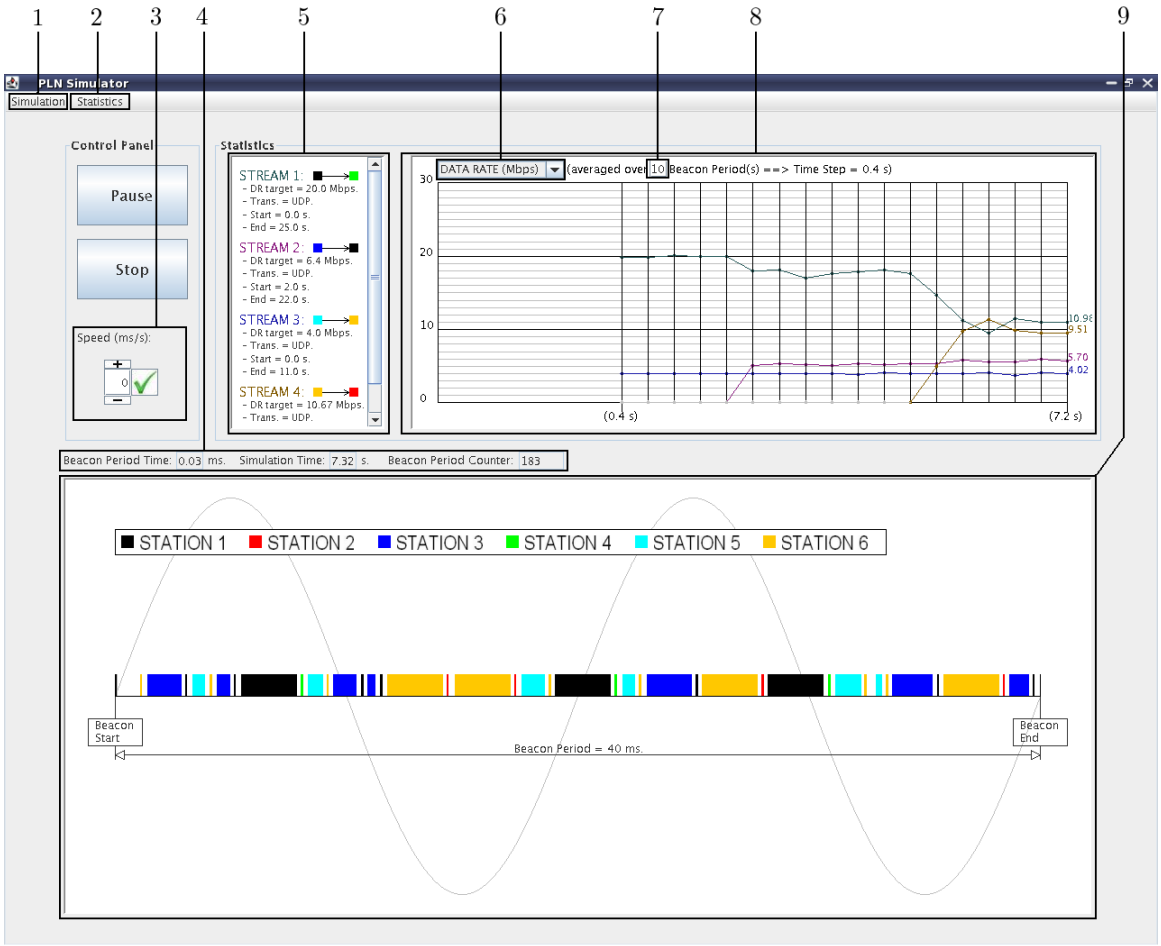

1. Define a new simulation scenario.
2. Export statistics to Gnuplot.
3. Set the refresh rate of the animation.
4. Time informations on the current simulation.
5. Streams legend.
6. Metric to display : data rate, transmission delay, Packet loss (to come), collisions (to come).
7. Adjust time window to average the displayed metric (multiple of 40 ms).
8. Display statistics synchronously with the network activity.
9. Display the network activity during a beacon period (40 ms).

Figure A.3: User interface screen capture.

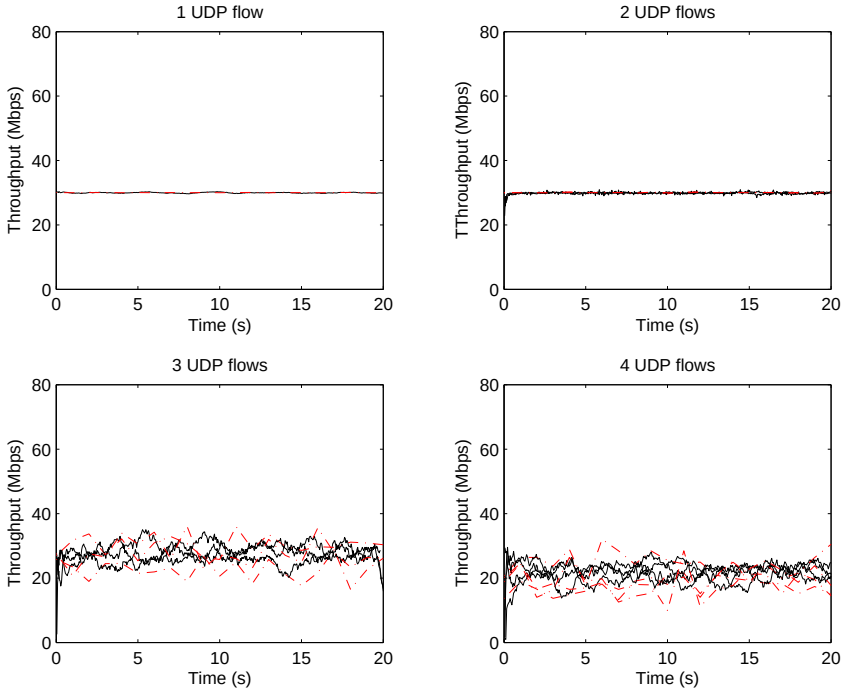

Figure A.4: Comparison between simulated (continuous curves) and measured data rates (dotted curves) for 1, 2, 3 and 4 uplink UDP flows.

results given by the network simulator. Naturally, as additional TCP flows are defined, the per-flow throughput decreases by a factor of n. Yet, we can see that results are slightly pessimistic with 2 and 4 TCP flows, in comparison to the measures. Nevertheless, even if these differences cannot be explained yet, this problem is not relevant in this thesis, considering that only UDP flows were used.

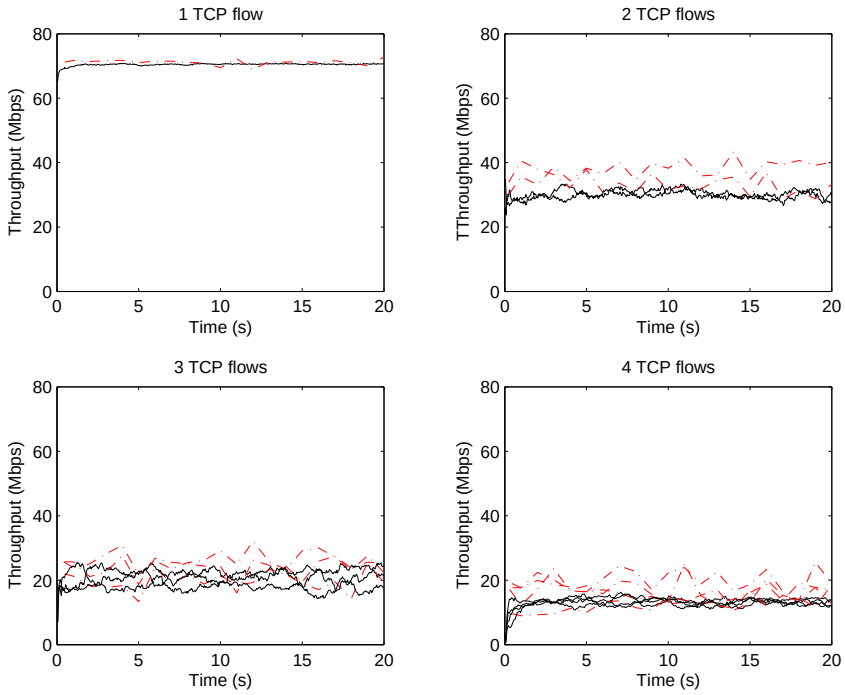

Figure A.5: Comparison between simulated (continuous curves) and measured data rates (dotted curves) for 1, 2, 3 and 4 uplink TCP flows.

Appendix B

Transmission Masks

B.1 North American excluded frequency ranges

Table B.1: North America permanently excluded frequency ranges

Excluded frequency range (MHz)	**Service**
1.80 - 2.00	Amateur Radio Service
3.50 - 4.0	Amateur Radio Service
5.33 - 5.407	Amateur Radio Service
7.0 - 7.30	Amateur Radio Service
10.10 - 10.15	Amateur Radio Service
14.00 - 14.35	Amateur Radio Service
18.068 - 18.168	Amateur Radio Service
21.00 - 21.45	Amateur Radio Service
24.89 - 24.99	Amateur Radio Service
28.00 - 29.7	Amateur Radio Service

B.2 CENELEC excluded frequency ranges

Table B.2: Permanently excluded frequency ranges by CENELEC

Excluded frequency range (MHz)	**Service**
1.80 - 2.00	Amateur Radio Service
2.85 - 3.025	Aeronautical mobile
3.40 - 4.0	Aeronautical mobile: 3.40 - 3.50 Amateur Radio Service: 3.50 - 4.00
4.65 - 4.70	Aeronautical mobile
5.25 - 5.41	Amateur Radio Service
5.48 - 5.68	Aeronautical mobile
6.525 - 6.685	Aeronautical mobile
7.0 - 7.30	Amateur Radio Service
8.815 - 8.965	Aeronautical mobile
10.005 - 10.15	Aeronautical mobile: 10.005 - 10.10 Amateur Radio Service: 10.10 - 10.15
11.275 - 11.4	Aeronautical mobile
13.26 - 13.36	Aeronautical mobile
14.00 - 14.35	Amateur Radio Service
17.9 - 17.97	Aeronautical mobile
18.068 - 18.168	Amateur Radio Service
21.00 - 21.45	Amateur Radio Service
21.924 - 22.00	Aeronautical mobile
24.89 - 24.99	Amateur Radio Service
26.96 - 27.41	CB radio
28.00 - 29.7	Amateur Radio Service

Table B.3: Permanently or dynamically excluded frequency ranges by CENELEC

Excluded frequency range (MHz)	**Service**
2.30 - 2.498	Broadcasting
3.20 - 3.40	Broadcasting
3.90 - 4.05	Broadcasting
4.75 - 5.11	Broadcasting
5.75 - 6.20	Broadcasting
7.20 - 7.70	Broadcasting
9.30 - 9.95	Broadcasting
11.55 - 12.10	Broadcasting
13.55 - 13.90	Broadcasting
15.05 - 15.85	Broadcasting
17.40 - 17.90	Broadcasting
18.90 - 19.02	Broadcasting
21.45 - 21.85	Broadcasting
25.65 - 26.10	Broadcasting

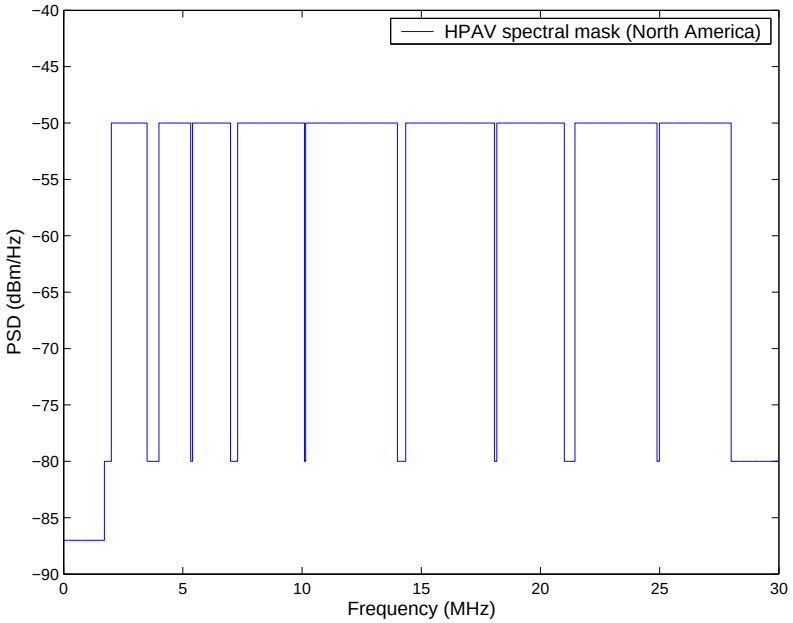

Figure B.1: HPAV Spectral mask.

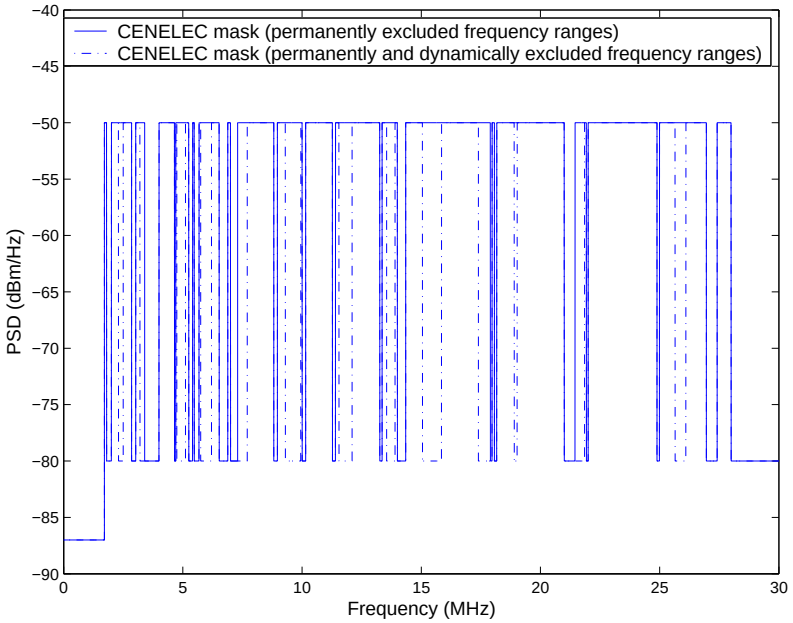

Figure B.2: CENELEC spectral Mask (permanent and dynamic notching).

Appendix C

Some Proofs

C.1 Proof that $E\left[u^2_{m_0,n_0}\right]$ in (3.60) can be written as $(-1)^{n_0}F(m_0)$

$$E\left[u^2_{m_0,n_0}\right] = \sigma_n^2 \sum_{r=-K_e}^{K_e} \sum_{r'=-K_e}^{K_e} e^{(r)}_{m_0} e^{(r')}_{m_0} \int p^*_{m_0,n_0+r}(t) \times p^*_{m_0,n_0+r'}(t)dt \tag{C.1}$$

With the expression of $p_{m,n}(t)$ (see (3.30)) and after some computations we get

$$\begin{aligned} E\left[u^2_{m_0,n_0}\right] &= \sigma_n^2 \sum_{r=-K_e}^{K_e} \sum_{r'=-K_e}^{K_e} e^{(r)}_{m_0} e^{(r')}_{m_0} \\ &\times e^{-j(\phi(m_0,n_0+r)+\phi(m_0,n_0+r')+\pi m_0(r'-r))} \\ &\times A_p[(r'-r)M/2, 2m_0] \end{aligned}$$

Noticing that the phase term can be written as $\Psi^{(r,r')}_{m_0} + \pi n_0$, with

$$\Psi^{(r,r')}_{m_0} = \begin{cases} \frac{\pi}{2}(r+r') + \pi m_0(r-r'+1) \text{ if } \phi_0(m,n) = 0 \\ \frac{\pi}{2}(r+r') + \pi m_0 \qquad \text{if } \phi_0(m,n) = -\pi mn \end{cases} \tag{C.2}$$

and setting $F(m_0)$, independent from n_0 to

$$F(m_0) = \sigma_n^2 \sum_{r=-K_e}^{K_e} \sum_{r'=-K_e}^{K_e} e^{(r)}_{m_0} e^{(r')}_{m_0} e^{-j\Psi^{(r,r')}_{m_0}} \times A_p[(r'-r)M/2, 2m_0] \tag{C.3}$$

we finally have

$$E\left[u^2_{m_0,n_0}\right] = (-1)^{n_0} F(m_0) \tag{C.4}$$

C.2 Proof that $\mathrm{Var}[u_{m_0,n_0}]$ in (3.60) does not depend on n_0

$$\mathrm{Var}[u_{m_0,n_0}] = \sigma_n^2 \sum_{r=-K_e}^{K_e} \sum_{r'=-K_e}^{K_e} e^{(r)}_{m_0} e^{(r')*}_{m_0} \times \int p^*_{m_0,n_0+r}(t) g_{m_0,n_0+r'}(t)dt \tag{C.5}$$

With the expression of $p_{m,n}(t)$ (see (3.30)) and after some computations we get

$$\begin{aligned}\mathrm{Var}[u_{m_0,n_0}] = \sigma_n^2 \sum_{r=-K_e}^{K_e} \sum_{r'=-K_e}^{K_e} & e_{m_0}^{(r)} e_{m_0}^{(r')*} \\ & \times e^{j(\phi(m_0,n_0+r')-\phi(m_0,n_0+r))} \\ & \times A_p[(r'-r)M/2, 0]\end{aligned}$$

Then using the phase function (3.40) we have the following expression, independent on n_0

$$\mathrm{Var}[u_{m_0,n_0}] = \sigma_n^2 \sum_{r=-K_e}^{K_e} \sum_{r'=-K_e}^{K_e} e_{m_0}^{(r)} e_{m_0}^{(r')*} e^{j\Phi_{m_0,0}^{(0,r'-r)}} \times A_p[(r'-r)M/2, 0]$$

Appendix D

Résumé Français du Mémoire de Thèse

D.1 Chapitre 1: Introduction

Dans un marché français de l'accès Internet fortement concurrentiel, l'activité première d'un opérateur de réseaux tel qu'Orange a dû rapidement s'adapter en diversifiant son offre par l'ajout de nouveaux services, tendance qui s'est concrétisée par la démocratisation des offres triple play (Internet+VoIP+TVoIP). Naturellement, un axe majeur de la stratégie de différenciation d'Orange vis-à-vis de ses concurrents s'inscrit dans l'amélioration continue de ses services en enrichissant les contenus proposés. Cependant, en sa qualité d'opérateur historique, le service client constitue un axe majeur de la stratégie de l'entreprise. Aussi, l'assurance d'une bonne qualité d'expérience au niveau du client passe nécessairement par une maîtrise de bout-en-bout de la chaîne de transmission, dont le réseau domestique constitue bien souvent le maillon faible. Une parfaite maîtrise de toutes les solutions de connectivité domestique est donc primordiale pour réussir le pari du meilleur service client. L'augmentation de la capacité du réseau à l'accès pour ses clients Internet, actuellement bénéficiaires d'offres ADSL et, pour certains, dès aujourd'hui éligibles à des offres FTTH (Fiber To The Home), permet de proposer de nombreux services dont certains, tels que la TV HD sur IP, peuvent s'avérer très gourmands en bande passante. Pour diffuser ces services au sein de l'habitation, une solution filaire comme l'Ethernet [16] répond idéalement aux besoins en termes de capacité de transmission. Cependant, du point de vue du client, dont l'environnement domestique est rarement câblé nativement en Ethernet, cette solution est difficilement défendable, l'installation d'un tel réseau entraînant un coût supplémentaire important. À l'heure actuelle, les technologies sans-fil, comme le Wi-Fi [15], permettent de répondre dans une certaine mesure aux cas d'utilisation auxquels elles sont soumises. Cependant, ces solutions sont victimes de leur succès : on peut constater une concentration très importante de points d'accès dans les immeubles qui, par interférences mutuelles, engendre une saturation rapide de ces réseaux [13]. De plus, les mécanismes de QoS mis en place par ces technologies ne permettent pas d'assurer une qualité d'expérience satisfaisante au niveau de l'utilisateur, notamment pour des services tels que la vidéo à la demande. Enfin, les solutions sans-fil ne permettent pas toujours de couvrir les habitations dans leur globalité, en fonction de leurs tailles, mais aussi de l'épaisseur des cloisons. Une solution envisagée pour pallier aux limitations de chaque

technologie prend la forme d'une nouvelle norme: le standard IEEE P1905 [40], qui définit une nouvelle couche réseau au-dessus de la MAC, doit permettre de facilement combiner les différentes solutions de transmission présentes dans l'environnement domestique.

En complément des réseaux WLAN, la technologie des courants porteurs en ligne (CPL) a fait son apparition dans les réseaux domestiques ces dernières années afin de répondre à ces nouveaux besoins. Comme pour les solutions sans-fil, cette technologie présente l'avantage de ne pas nécessiter le déploiement de nouveaux câbles à l'intérieur de la maison, tout en offrant une zone de couverture plus importante. Cependant, les 200 à 500 Mbits/s (maximum théorique au niveau de la couche physique) que sont censés offrir les équipements actuels ne sont pas suffisants pour supporter simultanément des applications gourmandes en bande passante. En effet, les solutions actuelles offrent rarement plus de 80 Mbit/s au niveau IP dans des configurations d'utilisations courantes. De plus, les systèmes CPL actuels ne sont pas plus performants que les technologies sans-fil concernant les mécanismes de Qualité de Service qu'ils intègrent, alors même qu'ils doivent faire face à un milieu de transmission fortement perturbé, dont on peut faire l'analogie, dans une certaine mesure, avec le medium "air" d'un réseau Wi-Fi. Pour prendre l'exemple de France Telecom, les modems CPL vendus actuellement dans les boutiques Orange sont présentés comme un substitut au traditionnel câble Ethernet permettant de relier deux équipements du réseau local. Ces modems CPL, qui suivent la spécification HPAV (la plus répandue), ont pourtant la capacité de transformer le réseau électrique en véritable LAN, supportant la circulation simultanée de plusieurs services concurrents. Cependant, la technique d'accès aléatoire dénommée CSMA/CA, aujourd'hui utilisée pour effectuer le partage de la ressource entre les différents utilisateurs du réseau, ne permet pas d'échapper à des phénomènes de collisions de trames et de saturation du réseau, rendant toute garantie impossible quant au niveau de QoS assurée à des services devant être acheminés sous contrainte(s).

Dans ce contexte, on peut mettre en évidence deux carences majeures des réseaux locaux actuels, à supports filaires ou non, auxquelles il devient urgent de répondre. D'une part, il est nécessaire d'augmenter globalement la capacité de ces réseaux : un problème typique de la couche Physique (PHY) des systèmes. D'autre part, la présence simultanée de flux hétérogènes sur ces réseaux, aux contraintes très différentes (bande passante nécessaire, délais d'acheminement, gigue), nécessite la définition de mécanismes de priorisation plus évolués qu'en l'état actuel des choses. Ces fonctions assurant l'allocation et le partage de la ressource, aussi bien au niveau d'une station qu'entre les différentes stations du réseau, sont implémentées au niveau de la couche MAC des systèmes. Cette thèse vise donc à explorer différentes solutions pour les futurs réseaux domestiques basés sur la technologie des courants porteurs en ligne. L'étude a été menée dans un premier temps au niveau de la couche PHY en vue d'augmenter la capacité globale du réseau. Dans le chapitre 3, nous mettons en évidence les limitations de la modulation windowed OFDM, technique de transmission actuellement utilisée dans les systèmes CPL large bande. Cette solution est ensuite comparée à une modulation alternative, dénommée OFDM Offset QAM (OFDM/OQAM), qui s'avère particulièrement adaptée au contexte des CPL. Cette étude s'est inscrite dans le cadre du projet européen FP7 "OMEGA" [53], et a permis la publication de 3 articles [28], [29], [32]. Le chapitre 4 s'intéresse à la diversité en fréquence entre les différents canaux de transmission dans une configuration de transmission point-à-multipoint. Dans cette partie, nous montrons comment cette diversité pourrait être

efficacement exploitée en définissant un mode d'accès de type OFDMA. Une méthode permettant de diviser de manière optimale le spectre entre les différents canaux de transmission, en faisant l'hypothèse qu'ils sont quasi-statiques, est d'abord présentée. Un algorithme d'allocation sous-optimal est ensuite décrit. Cette dernière solution a été intégrée dans un simulateur de réseau CPL basé sur ns-2, décrit en Annexe A, nous permettant de montrer le gain potentiel que pourrait apporter ce nouveau mode d'accès. Ce chapitre a donné lieu à plusieurs publications et contributions techniques [30], [31]. Enfin, le chapitre 5 aborde le problème de la diffusion broadcast/multicast. L'analyse est d'abord menée sur des canaux CPL mesurés, puis est étendue à des canaux simulés. Dans ce dernier chapitre, nous proposons une méthode itérative permettant d'augmenter les débits en séparant un groupe de stations destinataires d'un même flux broadcast/muticast en sous-groupes de multicast. Ce travail a fait l'objet d'un article [27] et de plusieurs contributions techniques au sein du groupe de travail en charge de l'établissement des spécifications HPAV (toutes les contributions sont listées p. 167). Une conclusion vient finalement clore ce travail de thèse, où nous rappelons les principaux résultats de cette étude, ainsi que les points restés en suspens, puis nous élargissons le champ de cette étude en évoquant brièvement le rôle que pourrait jouer la technologie CPL dans les futurs réseaux domestiques convergents (CDHNs).

D.2 Chapitre 2: La technologie des Courants Porteurs en Ligne pour les transmissions en Large Bande

Le second chapitre est une introduction générale sur le domaine des réseaux CPL large bande. Dans un premier temps, un bref historique rappelle les motivations originelles ayant permis l'avènement de cette technologie. Nous procédons ensuite à une description succincte de l'environnement de transmission que constitue le réseau électrique (canal et sources de bruit). Les mauvaises adaptations d'impédance au niveau des connecteurs électriques confèrent au canal CPL une caractéristique multi-trajet. Ainsi, tout système CPL large bande utilise des modulations de type OFDM, dont l'efficacité n'est plus à prouver sur ce type de canal. Dans cette thèse, nous avons utilisé des modèles de canaux et de bruit coloré basés sur des mesures effectuées sur le terrain, et développés par l'Orange Labs de Lannion [106], [52]. La législation encadrant le niveau des émissions électromagnétiques induites par les équipements CPL n'est pas très claire. Dans notre étude, nous avons utilisé le masque défini par la FCC en Amérique du Nord, représenté sur la Fig. D.1. À l'avenir, ce masque de transmission pourrait être très différent en Europe car une nouvelle norme imposée aux équipements CPL, définie par le CENELEC, sera soumise à un vote de ratification dans les prochains mois. Nous avons également rappelé l'historique des différentes solutions CPL qui sont entrées en concurrence dans les années 2000, dont semble sorti vainqueur le consortium HomePlug, qui édite la spécification HPAV.

Dans cete thèse, nous souhaitions que les solutions développées prennent appui sur les spécifications des systèmes existants. HPAV étant la spécification la plus suivie par les systèmes CPL large bande, nous nous sommes donc attachés à décrire leur fonctionnement. Dans un réseau CPL, il est nécessaire de faire la distinction entre le réseau physique, dont la couverture dépend de la portée du signal transmis, et le réseau logique, qui définit l'ensemble des stations autorisées à échanger entre elles des données de l'utilisateur final. Un système CPL n'intègre que les couches 1 (PHY) et 2 (LLC) du modèle OSI, et est

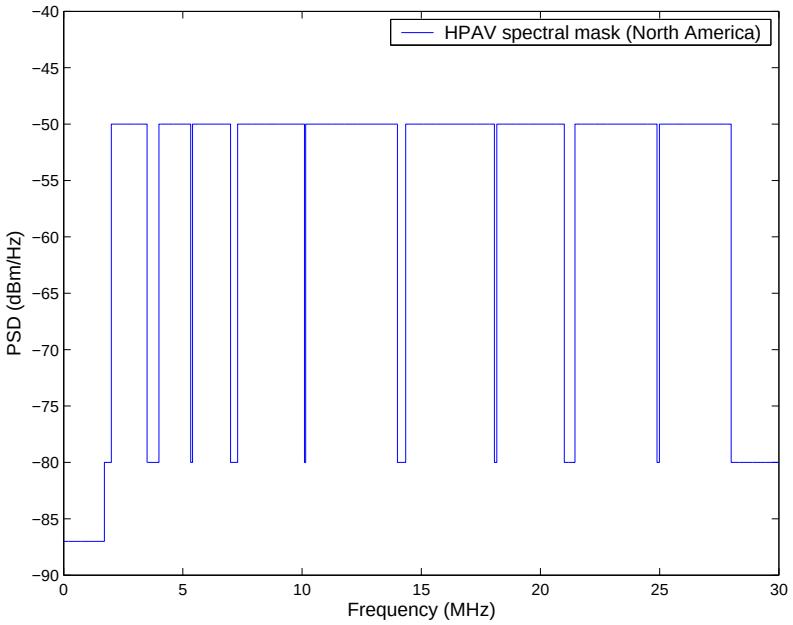

Figure D.1: Masque de transmission défini par la FCC (Amérique du Nord).

généralement utilisé comme un pont entre un réseau Ethernet et le réseau électrique. La couche LLC est divisée en deux sous-couches: les couches de convergence (CL) et de contrôle d'accès au support (MAC). La première reçoit les trames provenant de l'interface Ethernet ou des éventuelles couches supérieures, les classe parmi les connexions actives ou initie éventuellement une demande de connexion pour les paquets n'ayant pu être identifiés. La couche MAC prend en charge le formatage des données avant de les transmettre à la couche physique, et définit les méthodes d'accès au canal. Deux méthodes d'accès permettant le partage de la ressource entre les différentes stations sont définies par la spécification: le CSMA/CA et le TDMA. La première technique, implémentée dans tous les équipements suivant HPAV, est complètement décentralisée. En effet, toute station ayant des données à transmettre peut tenter de prendre l'accès au canal en fixant une fenêtre de temporisation de durée aléatoire. De plus, un mécanisme de résolution des priorités permet de mettre en concurrence uniquement les stations possédant des flux de même priorité à transmettre (la plus élevée), choisie parmi 4 niveaux possibles. A l'inverse, le TDMA est une méthode d'accès centralisée au niveau du CCo (station coordinatrice), qui lui permet d'allouer à une station du réseau un intervalle de transmission exclusif pour l'une de ses connexions, garantissant au service transmis un niveau de QoS préalablement négocié. La trame MAC HPAV est construite en deux étapes. Chaque trame Ethernet est encapsulée une première fois en créant une entête contenant des informations sur la nature et la structure des données transmises, et une séquence permettant de vérifier l'intégrité des données au niveau du récepteur est également calculée. Une seconde étape de formatage des données consiste à segmenter les données appartenant à une même connexion en blocs de taille fixe (512 octets pour les données de l'utilisateur). Ce mécanisme de segmentation a une double utilités: il permet de casser la dépendance entre les longueurs des trames Ethernet reçues et celles des trames émises sur le réseau CPL, mais il permet également de

limiter le coût des erreurs de transmission car seuls les segments erronés sont retransmis. Enfin, les segments ainsi créés sont passés à la couche physique, qui se charge de distribuer le flux binaire selon le "tone map" créé pour le lien concerné par la transmission. Un tone map est une table décrivant les ordres de constellation à utiliser pour chaque sous-porteuse du symbole OFDM, cet ordre étant fixé selon le niveau de l'atténuation locale du canal en fréquence. Les données transmises sont acquittées par le récepteur, qui renvoie une trame informant explicitement l'émetteur des éventuels segments qu'il sera nécessaire de retransmettre.

D.3 Chapitre 3: Analyse de Capacités dans les Contextes des Spécifications HomePlug AV1 et AV2

Dans le cadre du projet européen OMEGA [51], une étude a été menée afin d'étendre la capacité de transmission des réseaux CPL actuels. Nous proposons dans ce chapitre de comparer une modulation multiporteuse à haute efficacité spectrale, dénommée OFDM/OQAM (Offset QAM), à la modulation windowed OFDM, utilisée par les systèmes suivant HPAV. La caractéristique quasi-statique du canal CPL permet aux systèmes une adaptation fine au canal de transmission par l'intermédiaire d'algorithmes dits de "bit-loading", résultant en la construction d'un tone map adapté au lien considéré. Dans notre étude, nous utilisons la forme la plus simple de bit-loading, qui alloue à chaque sous-porteuse l'ordre de modulation le plus élevé permettant de respecter un seuil fixé sur le taux d'erreur symboles (10^{-2} dans le cadre d'OMEGA). Les deux modulations sont comparées dans un premier temps dans la bande utilisée par HPAV 1, s'étendant de 1.8 à 30 MHz, puis la bande est élargie jusqu'à 87.5 MHz, similaire à celle définie par HPAV 2. Dans chaque contexte de simulation, deux métriques sont évaluées. La première, dénommée la "capacité de transmission", correspond au débit binaire qui serait atteint en faisant l'hypothèse d'ordres de modulation à valeurs réelles et non limitées. La seconde métrique calculée est le débit binaire au niveau de la couche physique, où chaque sous-porteuse est associée à un ordre de modulation choisi dans un ensemble discret $\mathbb{E}_{const}$, dépendant de la spécification suivie (ex: HPAV 1, $\mathbb{E}_{const} = \{1, 2, 3, 4, 6, 8, 10\}$).

La modulation définie par la spécification HPAV, dénommée windowed OFDM, est directement dérivée de l'OFDM avec préfixe cyclique (CP-OFDM). Une opération additionnelle de fenêtrage des symboles est néanmoins nécessaire, celle-ci permettant une meilleure localisation fréquentielle des sous-porteuses. Ce traitement permet de limiter le nombre de sous-porteuses devant être éteintes pour respecter le masque de transmission (cf. Fig. D.1). Dans le cas du CP-OFDM classique, si l'intervalle de garde (GI) est plus long que l'étalement en temps du canal, l'interférence causée par les répliques du symbole précédent peut être totalement éliminée, et un simple égaliseur Zero Forcing (ZF) à un coefficient suffit alors à la réception. Cependant, comme le montre la Fig. D.2, l'opération de fenêtrage réduit la longueur de l'intervalle de garde en fonction de la longueur de l'intervalle du facteur de retombée, le "Roll-Off" (RI). Il est donc possible qu'un terme d'interférence non-nul reste présent dans les canaux les plus dispersifs en temps. Le fenêtrage peut donc avoir une influence négative sur la valeur du SINR (rapport signal à bruit plus interférence), métrique utilisée lors de l'opération de bit-loading. Pour calculer de manière précise le SINR par sous-porteuse, nous avons isolé le terme d'interférence qui apparaît lorsque l'étalement temporel du canal dépasse la limite GI−RI. En partant de

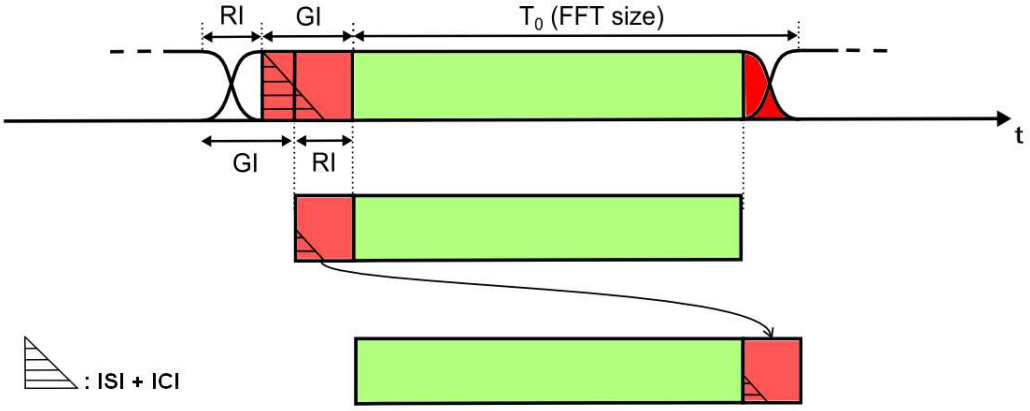

Figure D.2: Pré-traitement effectué au niveau de récepteur avant de démoduler le signal windowed OFDM.

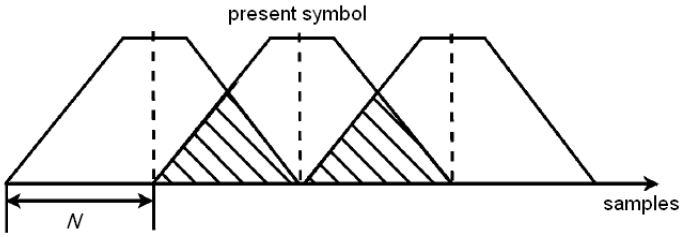

Figure D.3: Recouvrement entre symboles OFDM/OQAM consécutifs [84].

l'expression du signal windowed OFDM en entrée du récepteur:

$$y(t) = \sum_{i=0}^{P-1} h_i \sum_{m=0}^{M-1} \sum_{n=-\infty}^{+\infty} c_{m,n} g(t - nT - \tau_i) e^{j2\pi m F_0 (t-\tau_i)}, \tag{D.1}$$

on peut assez aisément isoler le terme d'interférence, dont l'expression analytique de la puissance au niveau de la sous-porteuse m_0 s'écrit:

$$P_{\mathrm{ISI+ICI}}^{\mathrm{Win}}(m_0) = \sum_{(p^0,q^0)} \sigma_c^2(m_0+p) \left| \sum_{l=0}^{L_h-1} h_l A_{g,f}[-q(M+L_{\mathrm{GI}}) - l, -p] e^{-j\pi(2m_0+p)\frac{l}{M}} \right|^2, \tag{D.2}$$

où p^0 et q^0 signifient $p \neq 0$ et $q \neq 0$; σ_c^2 est la variance des symboles complexes $c_{m,n}$ transmis; L_h et h_l représentent la longueur du canal en nombre d'échantillons et le coefficient associé au $l^{\text{ième}}$ trajet, respectivement, et $A_{g,f}$ est la fonction d'ambiguité croisée entre la fenêtre du symbole windowed OFDM g et la fenêtre rectangulaire de FFT f.

L'alternative que nous proposons au windowed OFDM est la modulation OFDM/OQAM [100], ou HS-OQAM (OQAM avec symétrie hermitienne) dans sa version en bande de base réelle [83]. Dans le cas de l'OFDM classique, la contrainte d'orthogonalité entre

les symboles est imposée dans le corps des complexes. Or, le concept fondamental de l'OFDM/OQAM consiste à limiter cette contrainte d'orthogonalité au corps des réels. Les symboles complexes sont en fait transmis en deux étapes, en séparant les voies en phase et en quadrature d'un délai $\frac{T_0}{2}$, T_0 représentant la durée symbole du système CP-OFDM équivalent. Cette relaxation sur la contrainte d'orthogonalité autorise une plus grande liberté quant à l'allure du filtre de mise en forme des symboles OFDM, qui peut être optimisé selon un critère précis, tel que la sélectivité fréquentielle ou la localisation temps-fréquence. Le recouvrement entre les symboles transmis, illustré sur la Fig. D.3, induit la présence d'un terme d'interférence non-nul. Cependant, les symboles envoyés étant réels, l'imposition d'une quadrature de phase entre les symboles adjacents en temps et en fréquence permet de confiner cette interférence sur la voie orthogonale à celle que l'on souhaite démoduler. L'absence d'intervalle de garde confère à cette modulation une meilleure efficacité spectrale que le système CP-OFDM équivalent. L'absence de GI provoque néanmoins une plus grande sensibilité à la caractéristique multi-trajet du canal vis-à-vis de la modulation CP-OFDM. L'utilisation d'un égaliseur ZF à 1 coefficient pouvant s'avérer insuffisante dans certains cas, nous proposons d'utiliser l'égaliseur ASCET [35] [84], pouvant être vu comme un ZF à 3 coefficients. En partant de l'expression du signal OFDM/OQAM à l'entrée du récepteur:

$$y(t) = \sum_{i=0}^{P-1} h_i \sum_{m=0}^{M-1} \sum_{n=-\infty}^{+\infty} a_{m,n} p_{m,n}(t - \tau_i), \tag{D.3}$$

nous calculons en sortie de l'égaliseur ASCET l'expression analytique de la puissance de l'interférence:

$$P_{\text{ISI+ICI}}(m_0) = \sum_{(p^0,q^0)} \sigma_c^2(m_0 + p) \left[\text{Re}\{e^{j\frac{\pi}{2}(p+q+pq)} A_{m_0}^{(p,q)}\}\right]^2, \tag{D.4}$$

dont les différents termes sont explicités dans la section 3.3.2.2 (p. 42). La puissance du bruit est également exprimée en sortie de l'égaliseur ASCET:

$$\begin{aligned} P_{\text{noise}}(m_0) = \sigma_n^2 &\sum_{r=-1}^{1} |e_{m_0}^{(r)}|^2 A_p[0,0] \\ &+ 2\sigma_n^2 F_\phi(m_0) \text{Im}\{(e_{m_0}^{(1)} - e_{m_0}^{(-1)}) e_{m_0}^{(0)*}\} A_p[M/2, 0], \end{aligned}$$

dont les différents termes sont explicités dans la section 3.3.2.3 (p. 44).

Dans la section 3.4.2.1, nous présentons trois filtres prototypes pouvant être utilisés par la modulation OFDM/OQAM (cf. Fig. D.4). Le premier, dénommé TFL1, est un prototype court de durée T_0 possédant la propriété d'orthogonalité stricte (PR: reconstruction parfaite) et optimisé selon le critère de la localisation temps-fréquence [57]. Dans la thèse de Lin Hao [82], il a été montré que l'interférence inter-porteuse (ICI) est prédominante devant l'interférence inter-symbole (ISI) pour les canaux invariants en temps. Ainsi, il apparaît plus judicieux d'optimiser les prototypes selon le critère de la sélectivité fréquentielle. De plus, la minimisation du niveau des lobes secondaires en fréquence permet de conserver un nombre plus élevé de sous-porteuses en bordure des encoches du masque de transmission (bandes de fréquence interdites à l'émission). Cependant, une bonne sélectivité en fréquence nécessite une longueur minimale de filtre égale à plusieurs fois la durée du

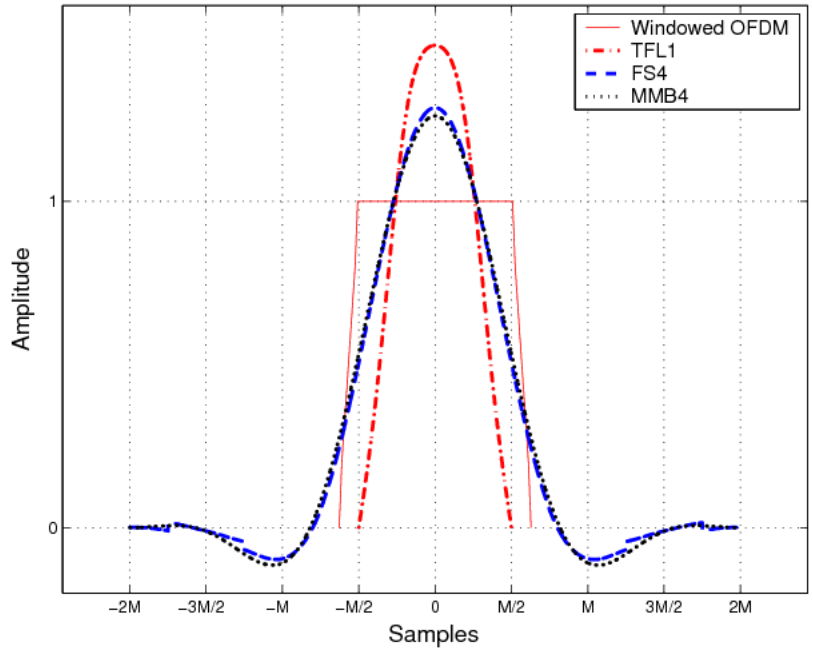

(a)

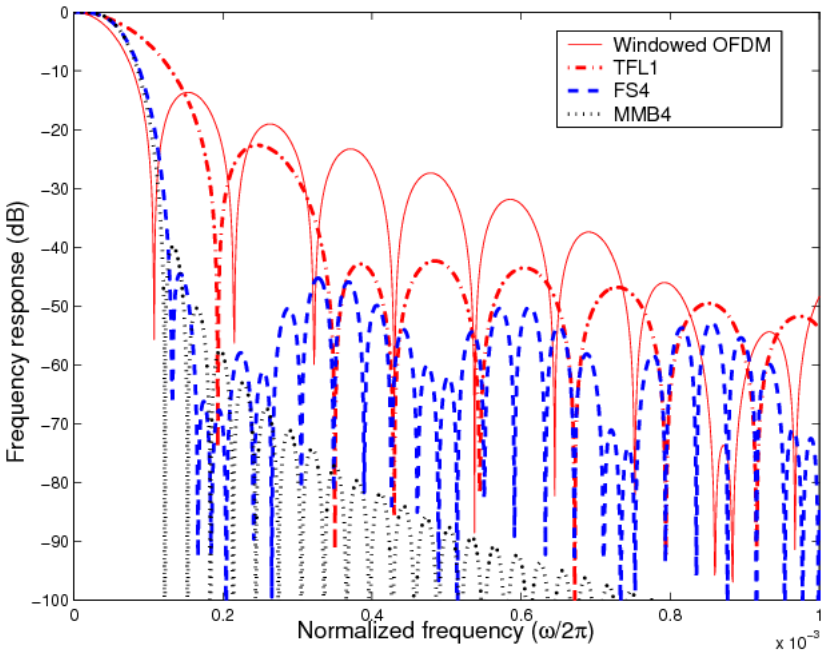

(b)

Figure D.4: Représentation des 3 prototypes étudiés: (a) en temps (b) en fréquence.

symbole OFDM. Ainsi, les deux autres prototypes présentés, optimisés selon le critère de la sélectivité fréquentielle, s'étalent sur une durée $4T_0$. Le premier, dénommé FS4, est un filtre PR et le second, MMB4, est un filtre NPR (reconstruction presque parfaite) proposé dans [88] et [37]. Après une étude comparative entre ces 3 filtres prototypes, nous décidons d'utiliser le filtre FS4 avec un égaliseur ASCET en réception afin de réduire efficacement la composante interférente du signal.

Dans la section 3.4.3, nous comparons les deux systèmes en utilisant 3 types de canaux (bon, moyen et mauvais) générés par le simulateur décrit dans [106], et le modèle de bruit coloré décrit dans [52]. La modulation windowed OFDM est associée à un simple égaliseur ZF à 1 coefficient en réception. L'utilisation du filtre FS4 permet à l'HS-OQAM d'utiliser 970 sous-porteuses dans la bande $[1,8:30]$ MHz tout en respectant le masque nord-américain, alors que le système windowed OFDM doit limiter le nombre de sous-porteuses actives à 917. Dans le cadre d'HPAV 1, au prix d'une complexité légèrement accrue dans le procédé d'égalisation, le système HS-OQAM permet d'atteindre un débit "couche physique" environ 19 % supérieur au système windowed OFDM, quelle que soit la qualité du canal CPL considéré. Dans le cadre d'HPAV 2, où la bande utile s'étend jusqu'à 87.5 MHz, en limitant la puissance d'émission à -80 dBm/Hz au delà de 30 MHz, l'OFDM/OQAM apporte une amélioration de l'ordre de 15 %. Les gains obtenus dans le cadre d'HPAV 2 sont moins élevés que dans la bande [1.8 : 30] MHz car l'extension de bande utilisée ne définit pas de nouveaux encoches. Or, ce sont ces fréquences interdites qui permettent de mettre en avant la meilleure efficacité spectrale de l'OFDM/OQAM, en activant des sous-porteuses additionnelles à leurs frontières. L'écart de performance entre les deux systèmes est d'ailleurs largement accru dans les simulations présentées à la section 3.4.4, où nous utilisons le nouveau masque de transmission défini par le CENELEC pour les équipements CPL vendus en Europe. Sous la contrainte de ce nouveau standard, l'OFDM/OQAM permettrait d'atteindre des débits de transmission de 28 à 40 % supérieurs au windowed OFDM en fonction du nombre de bandes à protéger.

D.4 Chapitre 4: Transmissions en Configuration Point-à-Multipoint dans les Réseaux CPL

En partant du constat que l'activité du réseau CPL est généralement concentrée autour de la station servant de pont vers l'accès internet du domicile, la configuration de transmission point-à-multipoint apparaît très fréquemment. Lorsque cette station particulière, que l'on peut considérer comme le "point d'accès" (AP) du réseau CPL, possède K flux de données en attente de transmission, chacun étant destiné à une unique station parmi K, celle-ci doit effectuer K accès consécutifs au medium afin de communiquer vers chacune d'entre elles. Or, la création de tone maps sur chacun des canaux de transmission fait apparaître une diversité en fréquence entre les utilisateurs qui ne peut être exploitée si le multiplexage des accès s'effectue uniquement en temps. La définition d'un mode d'accès utilisant l'OFDMA permettrait d'exploiter cette diversité multi-utilisateur: cette idée s'avère d'autant plus séduisante qu'elle ne pose pas de grandes difficultés techniques de mise en oeuvre. En effet, si dans la configuration du canal à accès multiple (chaque station possède des données à transmettre), l'accès multiple en fréquence pose de nombreux soucis de réalisation (synchronisation, effet champ proche/champ lointain), ces difficultés disparaissent dans une configuration de liaison descendante (pour prendre une analogie

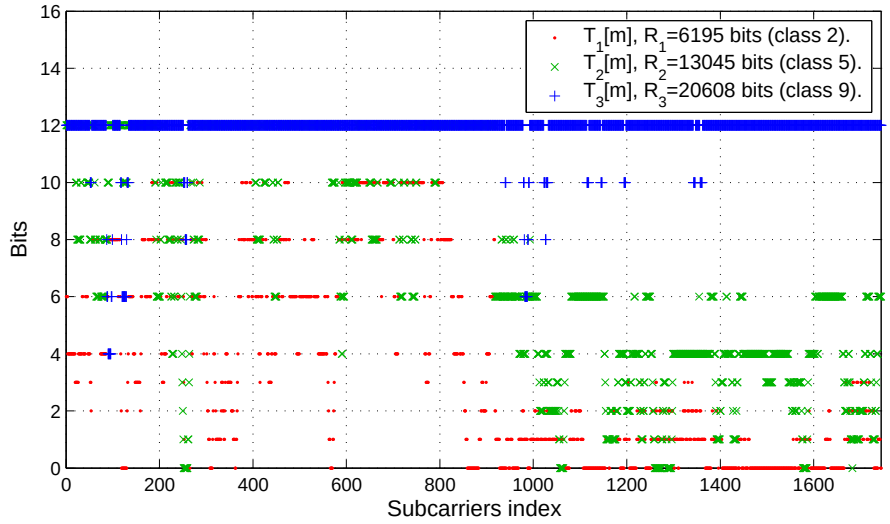

Figure D.5: Tone maps suivant la spécification IEEE P1901 générés sur des canaux de classes 2, 5 et 9, respectivement.

avec le domaine des radio télécommunications). Le problème posé dans ce chapitre consiste à trouver une stratégie pour distribuer les M sous-porteuses du signal OFDM parmi les K canaux sur lesquels l'AP souhaite transmettre.

Dans la section 4.1.3, sous l'hypothèse de canaux quasi-statiques, nous démontrons que le multiplexage en fréquence de K flux permet d'atteindre une capacité de transmission toujours supérieure ou égale à un multiplexage en temps de ces même flux. En effet, si l'on considère une fenêtre de transmission correspondant à la transmission de N symboles OFDM, avec $N = \sum_{k=1}^{K} p_k$ où p_k est le nombre de symboles transmis sur le lien k de capacité

$$C_k = \int_B \log_2(1 + \frac{\mathrm{SINR}_k(f)}{\Gamma}) df, \tag{D.5}$$

on peut démontrer qu'il existe toujours $\{B_k | B_k \in B,\, B \subseteq \mathbb{R}^+\}$, tel que:

$$\begin{cases} \bigcup_{k=1}^{K} B_k \subseteq B \\ \bigcap_{k=1}^{K} B_k = \varnothing \\ C_k^{\perp} \geq \frac{p_k C_k}{N},\ \forall k \in \mathbb{K} \end{cases} \tag{D.6}$$

où $C_k^{\perp} = \int_{B_k} b_k(f) df$, $B_p \cap B_q = \varnothing$, $\forall\ (p,q) \in \mathbb{K}^2$, $p \neq q$. Dans la suite, on définit $\alpha_k = \frac{p_k}{N}$ comme le coefficient de priorité associé au canal k. Le théorème démontré utilisant un formalisme continu, nous trouvons dans la section 4.2.1 une condition minimale permettant d'étendre ce théorème au cas discret, en utilisant des tone maps. En observant les 3 tone maps représentés Fig. D.5, Il est intéressant de noter que deux facteurs viennent influencer le degré de diversité multi-utilisateur. Premièrement, la caractéristique multi-trajet du canal CPL provoque des évanouissements en fréquence dont les positions dépendent du point du réseau à partir duquel le signal est récupéré. Ainsi, l'atténuation constatée à une fréquence précise peut varier significativement en fonction du lien considéré. De plus, si les systèmes CPL peuvent émettre à un niveau de -50 dBm/Hz jusqu'à 30 MHz, le

niveau maximal d'émission descend à -80 dBm/Hz au delà de cette limite. Dans la Fig. D.5, on constate que la limitation de puissance au delà de 30 MHz entraîne un gaspillage de la ressource pour les porteuses situées au delà de cette limite sur le lien 3. En se limitant aux canaux 1 et 3, dont le premier est beaucoup plus atténué que le second, on comprend intuitivement que les sous-porteuses situées dans la première partie du spectre seront préférablement allouées au lien 1, alors que le lien 3 recevra les sous-porteuses situées au-dela de 30 MHz.

Afin de poser le problème d'orthogonalisation des tone maps sous la forme d'un problème d'optimisation sous contraintes, nous effectuons une relaxation continue du problème. Ainsi, on considère que chaque sous-porteuse peut être allouée partiellement à un lien, la contrainte à respecter étant que la somme des allocations partielles d'une porteuse soit unitaire. En considérant K tone maps, chacun étant associé exclusivement à un unique lien de communication et à un coefficient de priorité α_k, nous formulons le problème d'orthogonalisation ainsi:

$$\begin{aligned}
&\text{Maximiser: } \textstyle\sum_{k\in\mathbb{K}} \sum_{m\in\mathbb{M}} w_{k,m} \frac{t_k[m]}{\alpha_k} \\
&\text{Contraintes:- } \textstyle\sum_{m\in\mathbb{M}} \{w_{i,m} \frac{t_i[m]}{\alpha_i} - w_{j,m} \frac{t_j[m]}{\alpha_j}\} = 0,\ \forall\ (i,j) \in \mathbb{K}^2,\ \forall\ m \in \mathbb{M} \\
&\qquad\qquad \text{- } \textstyle\sum_{k\in\mathbb{K}} w_{k,m} = 1,\ \forall\ m \in \mathbb{M} \\
&\qquad\qquad \text{- } w_{k,m} \geq 0,\ \forall\ (k,m) \in \mathbb{K} \times \mathbb{M}
\end{aligned}$$

où $0 \leq w_{k,m} \leq 1$ formalise l'allocation partielle de la sous-porteuse m au lien k. Ce problème d'optimisation est convexe, et peut-être résolu en appliquant les conditions de de Karush-Kuhn-Tucker (KKT). Cependant, le système d'équations résultant nécessite une capacité de calcul trop importante pour espérer obtenir une solution dans une fenêtre de temps raisonnable. Nous développons alors une nouvelle méthode, basée sur une approche géométrique du problème, qui va permettre de converger directement vers une orthogonalisation optimale des tone maps. Nous montrons tout d'abord que le problème d'allocation revient à maximiser la norme d'un vecteur $\vec{R}$ de dimension K, colinéaire au vecteur $(\alpha_1, \alpha_2, .., \alpha_K)$, et dont les composantes correspondent aux fractions de capacité r_k allouées à chacun des K liens. L'idée de cette méthode est de construire itérativement le vecteur optimal, en étendant progressivement les dimensions de l'espace d'allocation. À partir d'une région de capacité concave construite en dimension N, une analyse géométrique de la région résulte en la définition d'une fonction de coût dont la propriété de croissance stricte permet de générer une nouvelle région de capacité concave dans l'espace de dimension $N+1$. La Fig. D.6 illustre la résolution du problème en dimension 3.

Si l'approche géométrique permet de converger vers une orthogonalisation optimale des tone maps, la mise en oeuvre de cette méthode dans un système embarqué n'est pas envisageable. Dans la section 4.5, nous proposons un algorithme d'allocation sous-optimal, dénommé TMSA (Tone Maps Splitting Algorithm), permettant de construire très rapidement des tone maps orthogonaux exploitant efficacement la diversité multi-utilisateur. Afin d'évaluer quel pourrait être le gain apporté par un mode d'accès OFDMA utilisant cet algorithme, nous proposons ensuite un nouveau schéma de transmission permettant de satisfaire aux contraintes des spécifications HPAV et IEEE P1901 (Fig. D.7). Celui-ci in-

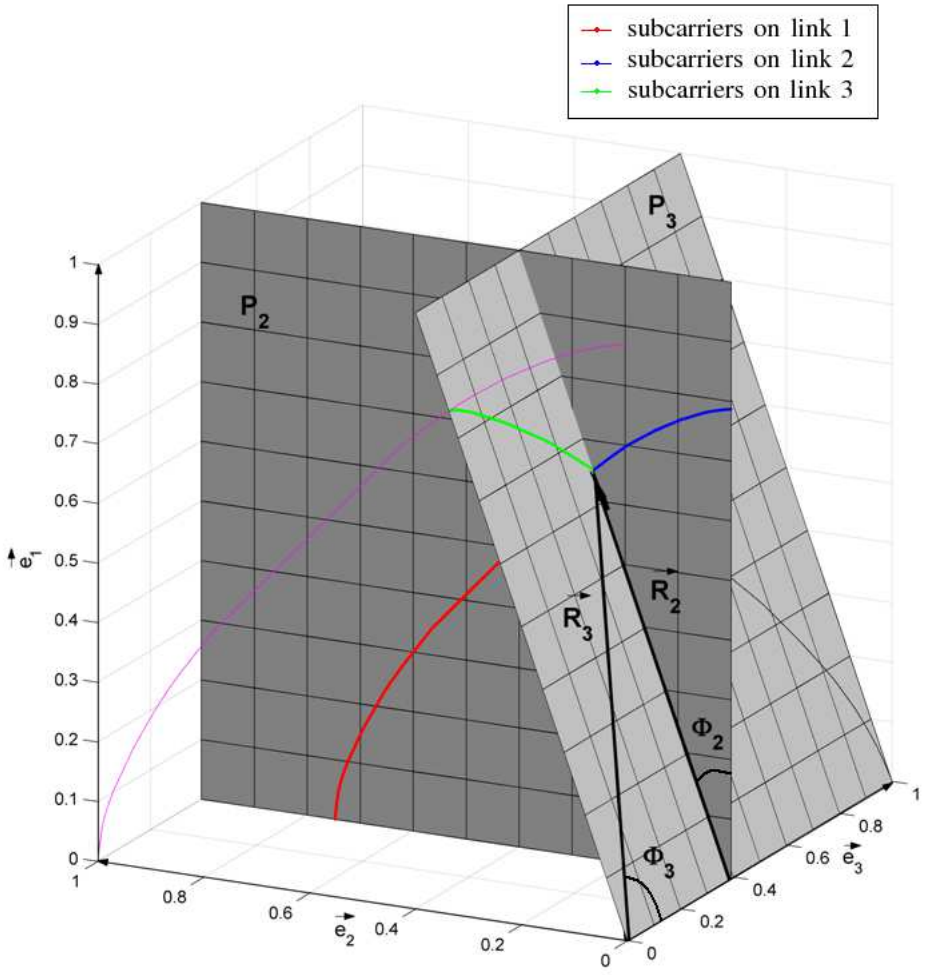

Figure D.6: Région de capacité optimale pour $K = 3$ ($\alpha_1 = 0.5$, $\alpha_2 = 0.2$ and $\alpha_3 = 0.3$).

troduit un mécanisme d'acquittement multiple permettant aux K récepteurs d'informer la station émettrice sur les états des segments reçus. Si le multiplexage en fréquence permet théoriquement de surpasser le simple multiplexage en temps, le respect de la contrainte sur la durée maximale de la fenêtre de transmission ne permet pas de vérifier cette propriété dans tous les cas. En utilisant l'algorithme TMSA dans un simulateur de réseaux CPL, décrit en Annexe A, nous montrons néanmoins des gains sur les débits saturés allant jusqu'à 30 % pour $K = 2$, et 26 % pour $K = 3$. Afin d'éliminer les cas où l'OFDMA dégrade les performances, nous définissons une métrique permettant de choisir, sous l'hypothèse de liens saturés, la solution de multiplexage la plus adaptée.

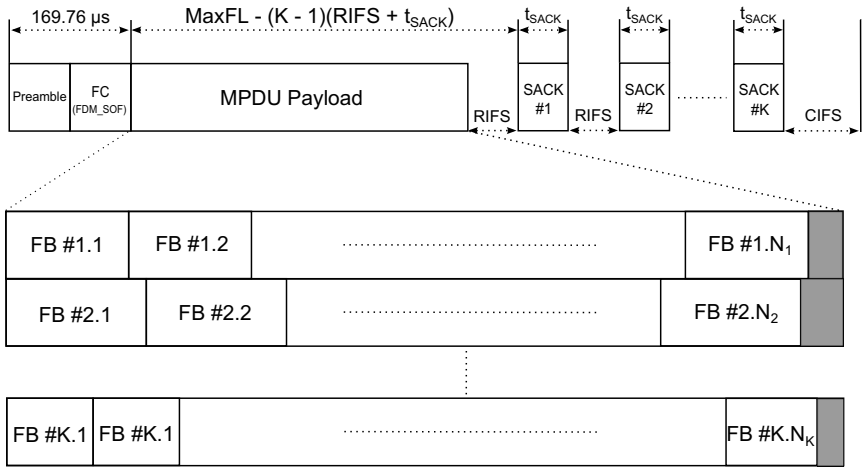

Figure D.7: Modified P1901 payload and acknowledgment frames structures for FDM transmissions.

D.5 Chapitre 5: Diffusion de Flux Multicast dans les Réseaux CPL

Le dernier chapitre de cette thèse s'intéresse au problème de la prise en charge des flux multicast/broadcast dans les réseaux CPL, causé par la création de tone maps adaptés aux liens de communication. En effet, lorsqu'une station souhaite transmettre un même flux de données à plusieurs stations du réseau, les spécifications HPAV [20] et la norme IEEE P1901 [22] recommandent la duplication du flux multicast en K flux unicast, K étant le nombre de stations destinataires. Cette conversion multicast vers unicast induit une charge excessive du réseau que nous cherchons à réduire. Dans un premier temps, nous analysons une solution simple, dénommée LCG (Lowest Channel Gain), qui permet de construire un tone map "multicast" à partir de tone maps "unicast". Ce tone map est obtenu en choisissant simplement, pour chaque sous-porteuse m, l'ordre de modulation le plus faible parmi les K tone maps "unicast". En procédant ainsi, on assure que le seuil limite sur le taux d'erreur est respecté sur tous les liens concernés par la transmission. L'analyse est d'abord menée au niveau de la couche physique, en évaluant le gain sur les débits "couche PHY" apporté par la solution LCG vis-à-vis de la conversion multicast vers unicast. Ces travaux ayant été menés pour le groupe en charge de l'établissement de la spécification HPAV 2, nous avons travaillé sur des canaux CPL réels fournis par le consortium HomePlug, en générant des tone maps dans la bande $[1.8, 86]$ MHz. Dans cette étude, dont les résultats sont résumés en Fig. D.8, nous testons des configurations de réseaux CPL avec 2, 3 et 4 stations destinataires du flux multicast. Avec ces résultats, il apparaît clairement que la définition d'un tone map de multicast pourrait améliorer de manière significative l'efficacité de transmission.

Pour assurer le même niveau de QoS pour les transmissions multicast que pour les transmissions unicast, nous définissons un mécanisme d'acquittement multiple à la manière de la proposition faite dans le chapitre précédent. Ce mécanisme a néanmoins le désavantage de dégrader l'efficacité de transmission au niveau de la MAC. En effet, la fenêtre de

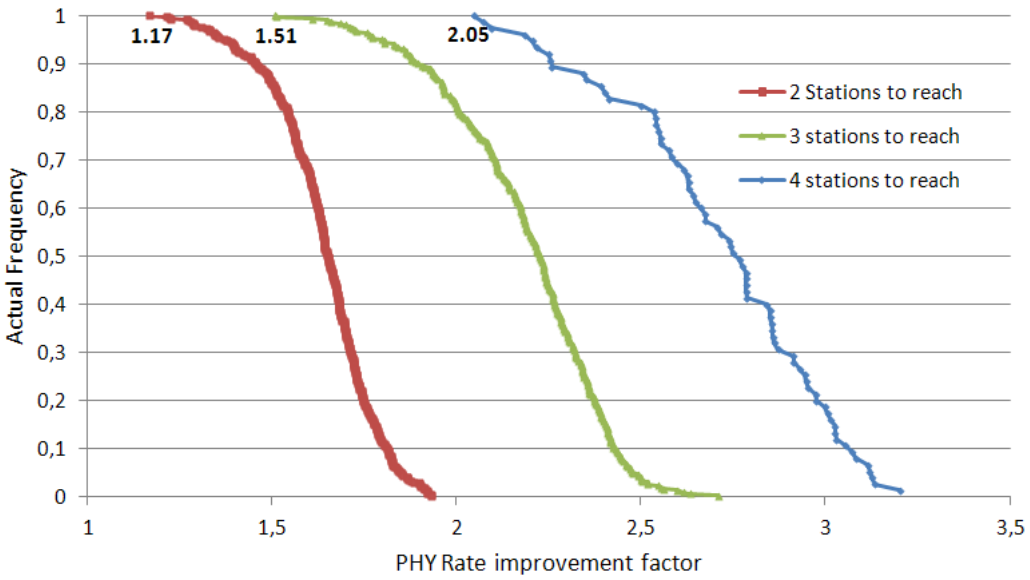

Figure D.8: Fonction de répartition des facteurs de multiplication du débit au niveau de la couche physique($P(F > X)$), pour $K = 2$, 3 et 4 stations destinataires.

---

transmission se réduisant avec le nombre de stations à joindre K, il existe un seuil à partir duquel la définition d'un tone map commun entre les stations à joindre devient moins efficace que la conversion multicast vers unicast. Entre les deux solutions précédemment comparées, une proposition alternative est formulée. Au lieu de définir un unique tone map "multicast" entre les K stations à joindre, l'idée de cette troisième solution est de classer les K stations en N sous-groupes de multicast, chacun étant associé à un tone map multicast construit par l'application de la méthode LCG entre les tone maps du sous-groupe. Ainsi, le problème posé revient à trouver un compromis entre le nombre de stations adressées simultanément, et la durée de la fenêtre de transmission qui se réduit à mesure que ce nombre augmente. Dans la section 5.3.2.1, nous établissons d'abord une métrique α, proportionnelle à l'inverse du débit des transmissions multicast au niveau de la couche MAC:

$$\alpha = \sum_{n=1}^{N} \frac{1}{[1 - (\text{card}(\mathbb{L}_n) - 1) \times r_{ACK}]\, R_{\mathbb{L}_k}}, \tag{D.7}$$

où $\mathbb{L}_n$ contient les indices de stations regroupées dans le $n^{\text{ième}}$ sous-groupe de multicast, r_{ACK} est le paramètre permettant de prendre en compte l'overhead engendré par une trame d'acquittement, et $R_{\mathbb{L}_k}$ est la capacité du tone map associé au $k^{\text{ième}}$ sous-groupe de multicast. Dans un second temps, on définit un critère qui va permettre d'isoler rapidement les sous-groupes de multicast qu'il semble judicieux de fusionner:

$$e_{p,q} = \frac{1}{R_{\mathbb{L}_p \cup \mathbb{L}_q}\, [1 - (\text{card}(\mathbb{L}_p) + \text{card}(\mathbb{L}_q) - 2) \times r_{\text{ACK}}]}. \tag{D.8}$$

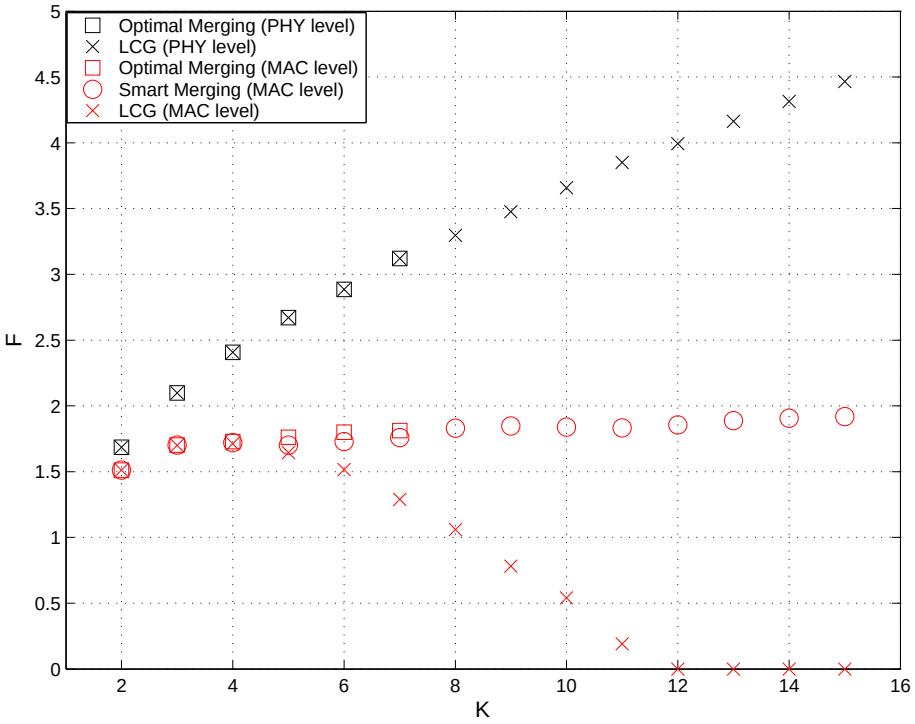

Figure D.9: Comparaison des facteurs de multiplication des débits entre l'algorithme proposé et la solution LCG, aux niveaux des couches PHY et MAC.

Ces deux paramètres permettent alors de construire un algorithme convergeant rapidement vers une partition des K stations en N sous-groupes de multicast, dont les performances sont très proches de la solution optimale (cf. Fig. D.9).

D.6 Chapitre 6: Conclusion

La popularité grandissante des systèmes CPL pour les réseaux domestiques s'explique par les débits atteints par les systèmes actuels, ainsi que par la facilité d'installation du réseau qui ne nécessite pas de déployer de nouveaux câbles. Ce succès était pourtant loin d'être acquis au regard de la concurrence acharnée entre les différents acteurs du domaine dans les années 2000, chacun voulant imposer son propre système. Depuis la finalisation de la norme IEEE P1901 en 2010, on a pu heureusement constater une stabilisation du secteur. A l'heure actuelle, le marché est clairement dominé par des systèmes suivant les spécifications établies par le consortium HomePlug, représentées par les versions HP 1.0, HPAV 1 et bientôt HPAV 2. Dans cette thèse, en abordant la problématique des réseaux CPL dans un contexte multi-usagers, nous avons montré que les performances des systèmes actuels pourraient encore être significativement améliorées. Nous avons premièrement répondu à la problématique de l'augmentation de capacité, en procédant à une extension de la bande utile et en proposant une modulation alternative. Dans une seconde partie, nous avons proposé de nouvelles méthodes d'allocations de ressources permettant de partager de manière plus efficace le milieu de transmission entre les différentes stations du réseau.

Le Chapitre 2 a été introduit par une brève présentation des caractéristiques du canal de communication CPL. Le réseau électrique n'ayant pas été conçu pour supporter un réseau de données, il constitue un milieu très hostile aux transmissions à haut-débits. Il est donc nécessaire de mettre en oeuvre les techniques de transmissions les plus évoluées afin de supporter le transport de services multimedia. Les principes généraux de fonctionnement des réseaux basés sur la spécification HPAV ont ensuite été présentés. En particulier, nous nous sommes attachés à décrire la segmentation à deux niveaux permettant de rompre la dépendance entre les structures de la trame Ethernet et de la trame HPAV. Le mécanisme de segmentation décrit par HPAV s'avère également particulièrement efficace pour lutter contre les perturbations du milieu de transmission, causées notamment par des sources de bruits impulsifs, en ne répétant que les segments erronés. Nous avons ensuite introduit les deux modes d'accès définis par la spécification, en présentant premièrement la technique d'accès opportuniste dénommée CSMA/CA. Si HPAV décrit 4 niveaux de priorité pour l'accès au medium, le mode CSMA/CA ne permet aucune garantie quant au niveau de QoS atteint. Ainsi, la spécification définit un second mode d'accès TDMA garantissant à une station l'accès exclusif au canal. C'est le CCo qui se charge d'allouer une fenêtre de transmission à une station qui souhaiterait, par exemple, transmettre un flux de type IPTV.

Pour lutter efficacement contre les interférences causées par la caractéristique multi-trajet du canal CPL, les modulations multiporteuses s'avèrent particulièrement appropriées. Nous avons néanmoins mis en évidence dans le chapitre 3 que la forme la plus classique de l'OFDM, le CP-OFDM, utilisant une fenêtre rectangulaire, n'apporte pas une réponse satisfaisante en raison du masque de transmission imposé à tout système CPL large bande. En effet, les émissions électromagnétiques induits par les cables électriques imposent aux systèmes de limiter l'émission de leurs signaux à des bandes de fréquences particulières, afin de protéger d'autres applications telles que les radio amateurs. Pour améliorer la localisation fréquentielle des sous-porteuses, les systèmes HPAV procèdent à un filtrage temporel des symboles OFDM permettant d'adoucir la retombée à zéro à leurs bordures. Ce traitement permet d'atténuer fortement le niveau des lobes secondaires en fréquence, limitant ainsi le nombre de sous-porteuses devant être éteintes en bordure des zones interdites à l'émission. Cependant, l'opération de fenêtrage a pour effet de réduire l'intervalle de garde en proportion de la longueur de l'intervalle du facteur de retombée ("roll-off"), et nous avons pu mettre en évidence qu'un terme d'interférence non-négligeable apparaît dans les canaux les plus dispersifs. L'expression analytique de ce terme a été établie afin de calculer précisément la valeur du SINR. Nous avons ensuite introduit une modulation alternative au windowed OFDM: la modulation HS-OQAM. En limitant la condition d'orthogonalité au corps des réels, la modulation HS-OQAM permet de filtrer les symboles émis en utilisant des filtres prototypes adaptés à la fois au canal CPL, sélectif en fréquence, et au masque de transmission. L'utilisation de filtres optimisés selon le critère de la sélectivité fréquentielle permet de conserver un nombre plus important de sous-porteuses actives en bordure des encoches du masque, tout en respectant les contraintes imposées sur le spectre du signal. La modulation HS-OSAM ne définissant pas d'intervalle de garde, un terme d'interférence est néanmoins toujours présent, ce qui rend l'égaliseur ZF à 1 coefficient généralement insuffisant. Un égaliseur légèrement plus complexe, dénommé ASCET et pouvant être vu comme un égaliseur ZF à 3 coefficient, permet quant à lui de réduire de manière significative le niveau d'interférence. Nous avons établi

les expressions généralisées des termes d'interférence et de bruit en sortie de l'égaliseur ASCET, ce qui nous a permis de calculer les capacités de transmission et débits théoriques atteints par l'OFDM/OQAM. Les comparaisons effectuées entre les deux modulations, en considérant à la fois les spécifications HomePlug AV1 et AV2, ont permis de démontrer la supériorité de l'HS-OQAM dans le contexte des CPL, en assurant un gain minimum de 15 % dans les débits vis-à-vis de la modulation windowed OFDM. Cependant, il est nécessaire d'avoir à l'esprit que la standardisation de la modulation windowed OFDM, telle que définie par HPAV, au travers de la norme IEEE P1901, rendra d'autant plus difficile l'adoption d'une solution alternative par les futurs standards CPL. En introduisant en fin de chapitre le nouveau masque de transmission du CENELEC concernant les systèmes CPL, il apparaît pourtant clairement que ce standard pourrait largement contribuer à accentuer l'écart de performance entre les deux solutions de transmission.

Le canal CPL étant quasi-statique, on peut utiliser des techniques de bit-loading qui permettent d'adapter finement la quantité d'information transmise. L'application de ces méthodes nécessite au préalable une connaissance avancée du canal de transmission, par laquelle il devient possible de décider pour chaque sous porteuse l'ordre de modulation optimal, i.e. adapté à la capacité locale du canal. Il en résulte la création d'une table, appelée tone map, listant les constellations allouées sur tout le spectre. Dans le chapitre 4, nous avons tout d'abord mis en évidence la diversité qui apparaît par la définition de tone maps entre une station et K autres stations du réseau. Cette diversité multi-utilisateur n'est actuellement pas utilisée car les accès au canal sont exclusivement multiplexés en temps. Un multiplexage en fréquence des flux permettrait néanmoins de l'exploiter efficacement, ce qui pourrait être réalisé en pratique en définissant un mode d'accès utilisant l'OFDMA. Nous avons alors considéré K tone maps, chacun étant associé à un unique canal de transmission, et nous avons posé le problème d'orthogonalisation des tone maps. En associant chaque lien à un coefficient de priorité, nous avons démontré que ce problème pouvait être résolu de manière optimale par la construction itérative d'une région de capacité concave entre les K liens, en utilisant simplement les K tone maps. Il nous est néanmoins apparu que cette méthode d'orthogonalisation restait trop complexe pour envisager une implémentation dans des systèmes réels. Nous avons alors développé un algorithme sous-optimal, dénommé TMSA, qui permet de distribuer rapidement et efficacement les sous-porteuses entre les différents liens de communication. Cette technique a été intégrée dans un simulateur de réseau CPL, nous permettant ainsi d'évaluer de manière plus réaliste le gain que pourrait apporter ce nouveau mode de transmission, en tenant compte des contraintes imposées par la spécification HPAV. En se plaçant dans une situation de saturation du réseau désavantageant notre solution, nous avons montré des gains significatifs vis-à-vis de l'existant. Enfin, une métrique permettant de prendre une décision quant au mode de multiplexage à privilégier, temporel ou fréquentiel, en fonction du niveau de diversité entre les K tone maps a été définie. À l'avenir, cette étude mériterait d'être complétée par une analyse de la complexité induite par l'intégration de ce nouveau mode de transmission. Une incertitude reste néanmoins présente concernant la fréquence à laquelle les tone maps évoluent, et avec quelle amplitude, car ces paramètres impactent directement le gain réalisé lors de l'orthogonalisation. Il serait également intéressant de procéder à une analyse des performances de cette solution sur des flux TCP. Enfin, les multiplexages en temps et en fréquence des flux pourraient être comparés en deçà du point

de saturation du réseau, où l'utilisation de l'OFDMA devrait permettre une réduction de l'"overhead" au niveau de la couche MAC.

Dans le chapitre 5, nous nous sommes intéressés au problème de la prise en charge des flux multicast/broadcast dans les réseaux CPL. Il apparaît en effet que la création de tone maps exclusifs sur chaque lien de communication conduit aux isolations mutuelles des stations à joindre. En conséquence, une station devant transmettre un flux multicast vers plusieurs stations le dupliquera en autant de flux unicast qu'il y a de stations à joindre. L'application de cette méthode provoque une utilisation excessive de la ressource de transmission, pouvant rapidement conduire à une saturation du réseau. Dans le but d'améliorer la prise en charge de ce type de flux, nous avons tout d'abord évalué le gain qu'apporterait une méthode dénommée LCG, permettant d'obtenir un tone map multicast. Ce tone map peut être utilisé simultanément sur plusieurs liens de communication du réseau CPL car il respecte les seuils de taux d'erreur fixés sur tous les canaux considérés. D'après les résultats de simulation obtenus sur des canaux mesurés par le groupe de travail établissant la spécification HPAV 2, il apparaît clairement que la méthode LCG pourrait améliorer significativement l'efficacité des transmissions multicast. Cependant, cette observation n'est vraie que du point de vue de la couche Physique. En effet, si l'on souhaite que chaque station puisse, indépendamment des autres, acquitter la trame reçue, cela engendre un overhead additionnel qui limite fortement le nombre de stations pouvant être adressées simultanément. Nous avons alors introduit un algorithme procédant à une répartition intelligente des stations en sous-groupes de multicast, tenant compte à la fois de cet overhead additionnel, mais également de la similarité entre les tone maps des stations regroupées. Cet algorithme montre des performances très proches de la solution optimale. À ce jour, la complexité de cette méthode reste à évaluer. Nous pouvons néanmoins émettre l'hypothèse que la plus grande robustesse du tone map multicast vis-à-vis des erreurs de transmission devrait rendre moins fréquente la mise à jour de celui-ci. Dans l'optique d'une étude future, il serait intéressant d'évaluer la solution développée dans [78] et [44], qui a l'avantage de ne pas ajouter d'overhead MAC.

En cette fin de thèse, la question suivante paraît légitime : Quelle pourrait être la prochaine étape à franchir pour les réseaux CPL large bande? Grâce à l'introduction du MIMO dans la spécification HPAV 2, la capacité des futurs réseaux CPL devrait être suffisante pour supporter le nombre grandissant de services multimedia dans l'environnement domestique. Nous ne pouvons cependant pas ignorer la possible introduction du masque CENELEC qui pourrait significativement réduire les performances des systèmes CPL en Europe. Si ce masque de transmission venait à être imposé en l'état aux systèmes actuels, il pourrait être alors utile d'étendre encore la bande de transmission. Certaines études ont par ailleurs déjà été menées afin d'imaginer des systèmes exploitant des bandes de fréquences allant jusqu'à 400, voire 500 MHz [60] : il serait alors nécessaire de définir une nouvelle couche physique pour les fréquences situées au-delà de 100 MHz. Du point de vue du marché des systèmes CPL large bande, cette éventuelle couche physique additionnelle ne serait peut-être pas une bonne nouvelle. En effet, au regard de l'évolution du domaine au cours de la décennie passée, la bataille entre plusieurs solutions concurrentes n'a eu pour effet que de ralentir l'adoption de cette technologie. Aujourd'hui, les systèmes basés sur la spécification HPAV ou le standard IEEE P1901 sont massivement déployés en Europe, mais leur succès n'est rien en comparaison de celui des solutions sans-fil basées sur le standard 802.11. Si cette technologie ne peut tenir la comparaison face aux réseaux Wi-Fi

du point de vue de la mobilité, cette unique raison ne suffit pas pour expliquer l'écart d'adoption entre ces deux technologies de connectivité. Il apparaît également qu'un défaut majeur des systèmes CPL concerne leur absence de tout équipement terminal, tel qu'un ordinateur portable par exemple. Cette situation pourrait évoluer à l'avenir, mais elle sera sûrement le fait d'un autre standard: le standard IEEE P1905. Cette nouvelle norme, que nous avons brièvement introduit dans le premier chapitre, doit permettre de combiner facilement les différentes technologies de communication de l'environnement domestique, filaires ou non, en définissant une nouvelle couche réseau contrôlant les accès aux différentes couches MAC situées en dessous. Ce standard n'aura de réel intérêt que si un nombre grandissant d'équipements connectés dans la maison possèdent plusieurs interfaces de communication de natures différentes. Ainsi, si ce nouveau standard obtient un fort soutien de la part du secteur industriel, il pourrait potentiellement constituer le point d'entrée des interfaces CPL dans des équipements terminaux.

Contributions

Conference papers

- P. Achaichia, M. Le Bot, P. Siohan, "Windowed OFDM versus OFDM/OQAM: A Transmission Capacity Comparison in the HomePlug AV Context," International Symposium on Power Line Communications, ISPLC 2011, Udine, Italy, April 2011.

- P. Achaichia, M. Le Bot, P. Siohan, "An Efficient Technique for Merging Transmissions in a Multicarrier Context," IWCLD 2011, Rennes, France, November 2011.

- P. Achaichia, M. Le Bot, P. Siohan, "Frequency Division Multiplexing Analysis for Point-to-Multipoint Transmissions in Power Line Networks," International Symposium on Power Line Communications, ISPLC 2011, Udine, Italy, April 2011.

- P. Achaichia, M. Le Bot, P. Siohan,"Point-to-Multipoint Communication in Power Line Networks: A Novel FDM Access Method," ICC 2012, Ottawa, Canada, June 2012.

- P. Achaichia, M. Le Bot, P. Siohan, "Potential Impact of the CENELEC Spectral Mask on Broadband PLC Networks," ISPLC 2013, *submitted*.

Journal papers

- P. Achaichia, M. Le Bot, P. Siohan, "OFDM/OQAM: A Solution to Efficiently Increase the Capacity of Future PLC Networks," *Power Delivery, IEEE Transactions on*, vol. 26, no. 4, pp. 2443-2455, Oct. 2011.

- P. Achaichia, M. Le Bot, P. Siohan, "A Geometrical Approach to Construct an Optimal OFDMA Downlink Capacity Region in Broadband PLC Networks," *Communications, IEEE Transactions on*, *submitted*.

Patents

- P. Achaichia, M. Le Bot, P. Siohan, "Procédé de regroupement de stations pour optimiser la diffusion d'un flux multicast/broadcast," 2011.

- P. Achaichia, M. Le Bot, P. Siohan, "Procédé de distribution des sous-porteuses d'un système multiporteuse entre différents liens de communication," 2011.

Technical Contributions

- A. Tonello, S. D'Alessandro, M. Antoniali, M. Biondi, F. Versolatto, A. Maiga, J.-Y. Baudais, F. S. Muhammad, P. Siohan, M. L. Bot, H. Lin, P. Achaichia, G. Ndo, G. Mijic, B. Cerato, S. Drakul, E. Viterbo et O. Isson, "Performance report of optimized PHY algorithms," Deliverable D3.4, FP7 project "OMEGA", June 2010.

- P. Achaichia, M. Le Bot, P. Siohan, "Multicast Tone Maps: Gains to Expect," HPAV face-to-face meeting, Lannion, March 2012.

- P. Achaichia, M. Le Bot, P. Siohan, "FDM to Improve Point-to-Multipoint Communications in Powerline Networks," HPAV face-to-face meeting, Lannion, March 2012.

- P. Achaichia, M. Le Bot, P. Siohan and P.Pagani, "Multicast Tone Maps Performance on Measured PLC Channels," HPAV TWG, April 2012.

- P. Achaichia, M. Le Bot, P. Siohan and P.Pagani, "Multicast Communications: Practical Use Cases," HPAV TWG, May 2012.

Oral presentations

- P. Achaichia, M. Le Bot, P. Siohan, J. Palicot, "Etude et application des systèmes de transmission multi-usagers pour le réseau électrique indoor," Séminaire SCEE, Supélec, Rennes, April 2011.

- P. Achaichia, M. Le Bot, P. Siohan, J. Palicot, "Transmission de données point à multipoint dans les réseaux PLC," Comission Télécom, Supélec, Gif-sur-Yvette, Sept. 2011.

Bibliography

[1] Cisco Visual Networking Index: Forecast and Methodology, 2010-2015. http://www.cisco.com/en/US/solutions/collateral/ns341/ns525/ns537/ns705/ns827/white_paper_c11-481360.pdf.

[2] Devolo website. www.devolo.com.

[3] HD-PLC Alliance website. www.hd-plc.org.

[4] HomePlug AV White Paper. www.homeplug.org/tech/whitepapers/HPAV-White-Paper_050818.pdf.

[5] HomePlug Green PHY White Paper. www.homeplug.org/tech/whitepapers/ HomePlug_Green_PHY_whitepaper_100614.pdf.

[6] HomePlug Powerline Alliance website. www.homeplug.org.

[7] IEEE P1901 working group official website. http://grouper.ieee.org/groups/1901/.

[8] Lea website. www.leacom.fr.

[9] Maxim website. www.maxim-ic.com.

[10] ns-2 home page. http://www.isi.edu/nsnam/ns/.

[11] PHYDYAS project website. http://www.ict-phydyas.org/index.php/camax/page/view?id=21.

[12] Qualcomm Atheros website. www.atheros.com.

[13] The Wireless Security Survey of Paris, 2008. www.rsa.com/solutions/wireless/survey/ WLANPA_WP_1008.pdf.

[14] Universal Powerline Association website. www.upaplc.org.

[15] IEEE Standard for Information Technology- Telecommunications and Information Exchange Between Systems-Local and Metropolitan Area Networks-Specific Requirements-Part 11: Wireless LAN Medium Access Control (MAC) and Physical Layer (PHY) Specifications. *IEEE Std 802.11-1997*, pages i –445, 1997.

[16] Part 3: Carrier Sense Multiple Access With Collision Detect on (CSMA/CD) Access Method and Physical Layer Specifications. *IEEE Std 802.3, 2000 Edition*, pages i –1515, 2000.

[17] *HomePlug Specification.* Version 1.0.1, Dec. 2001.

[18] *Internet Group Management Protocol (IGMP), Version 3.* RFC 3376, Oct. 2002.

[19] IEEE Standard for Local and metropolitan area networks: Media Access Control (MAC) Bridges. *IEEE Std 802.1D-2004 (Revision of IEEE Std 802.1D-1998)*, pages 1 –277, 9 2004.

[20] *HomePlug AV Specification.* Version 1.0.05, Oct. 2005.

[21] *Protocol Independent Multicast - Sparse Mode (PIM-SM).* RFC 4601, Aug. 2006.

[22] *IEEE Standard for Broadband over Power Line Networks: Medium Access Control and Physical Layer Specifications.* Dec. 2010.

[23] IEEE Standard for Local and metropolitan area networks–Audio Video Bridging (AVB) Systems. *IEEE Std 802.1BA-2011*, pages 1 –45, 30 2011.

[24] *Wireless LAN Medium Access Control (MAC) and Physical layer (PHY) specifications: Enhancements for Very High Throughput for operation in bands below 6GHz, IEEE P802.11ac.* Draft 1.0, May 2011.

[25] *HomePlug AV Specification.* Version 2.0, Mar. 2012.

[26] *HomePlug Green PHY Draft Specification.* Version 1.1, Feb. 2012.

[27] P. Achaichia, M. Le Bot, and P. Siohan. An Efficient Technique for Merging Transmissions in a Multicarrier Context. In *IEEE International Workshop on Cross Layer Design*, pages 1 –5, Rennes, France, Dec. 2011.

[28] P. Achaichia, M. Le Bot, and P. Siohan. OFDM/OQAM: A Solution to Efficiently Increase the Capacity of Future PLC Networks. *IEEE Transactions on Power Delivery*, 26(4):2443 –2455, Oct. 2011.

[29] P. Achaichia, M. Le Bot, and P. Siohan. Windowed OFDM versus OFDM/OQAM: A Transmission Capacity Comparison in the HomePlug AV Context. In *IEEE International Symposium on Power Line Communications*, pages 405 –410, Udine, Italy, Apr. 2011.

[30] P. Achaichia, M. Le Bot, and P. Siohan. Frequency Division Multiplexing Analysis for Point-to-Multipoint Transmissions in Power Line Networks. In *International Symposium on Power Line Communications*, Beijing, China, Mar. 2012.

[31] P. Achaichia, M. Le Bot, and P. Siohan. Point-to-Multipoint Communication in Power Line Networks: A novel FDM Access Method. In *International Conference on Communications*, Ottawa, Canada, June 2012.

[32] P. Achaichia, M. Le Bot, and P. Siohan. Potential Impact of the CENELEC Spectral Mask on Current PLC networks, to be submitted. In *IEEE International Symposium on Power Line Communications*, Johannesburg, South Africa, 2013.

[33] K.H. Afkhamie, S. Katar, L. Yonge, and R. Newman. An overview of the upcoming HomePlug AV standard. In *International Symposium on Power Line Communications*, pages 400 – 404, Vancouver, Canada, Apr. 2005.

[34] M. Alard. Construction of a multicarrier signal. Patent WO/35278, 1998.

[35] J. Alhava and M. Renfors. Adaptive sine-modulated/cosine-modulated filter bank equalizer for transmultiplexers. In *European Conference on Circuit Theory and Design*, Espoo, Finland, Aug. 2001.

[36] P. Amirshahi and M. Kavehrad. Transmission Channel Model and Capacity of Overhead Multi-Conductor Medium-Voltage Power-Lines for Broadband Communications. In *Consumer Communications and Networking Conference*, pages 354 – 358, Las Vegas, USA, Jan. 2005.

[37] M.G. Bellanger. Specification and design of a prototype filter for filter bank based multicarrier transmission. In *IEEE International Conference on Acoustics, Speech, and Signal Processing*, Salt Lake City, UT, USA, May 2001.

[38] Bellanger, M. and Renfors, M. and Ihalainen, T. and da Rocha, C.A.F. OFDM and FBMC Transmission Techniques: a Compatible High Performance Proposal for Broadband Power Line Communications. In *IEEE International Symposium on Power Line Communications*, pages 154 –159, Rio de Janeiro, Brazil, Mar. 2010.

[39] E. Biglieri. Coding and modulation for a horrible channel. *IEEE Communications Magazine*, 41(5):92 – 98, May 2003.

[40] M. Brzozowski, S. Nowak, F.-M. Schaefer, R. Jennen, and A. Palo. Inter-MAC - From Vision to Demonstration: Enabling heterogeneous meshed home area networks. In *Proc. IEEE Conference on Electronic Media Technology*, Frankfurt, Germany, Mar. 2011.

[41] G. Bumiller, L. Lampe, and H. Hrasnica. Power line communication networks for large-scale control and automation systems. *IEEE Communications Magazine*, 48(4):106 –113, Apr. 2010.

[42] F.J. Cañete, J.A. Cortes, L. Diez, J.T. Entrambasaguas, and J.L. Carmona. Fundamentals of the cyclic short-time variation of indoor power-line channels. In *International Symposium on Power Line Communications*, pages 157 – 161, Vancouver, Canada, Apr. 2005.

[43] R. Chandra, S. Karanth, T. Moscibroda, V. Navda, J. Padhye, R. Ramjee, and L. Ravindranath. DirCast: A practical and efficient Wi-Fi multicast system. In *IEEE International Conference on Network Protocols*, pages 161 –170, Princeton, USA, Oct. 2009.

[44] H.C. Chao, S.W. Chang, and J.L. Chen. Throughput Improvements Using the Random Leader Technique for the Reliable Multicast Wireless LANs. In *Proc. of the First ICN-Part 1*, volume 2093, pages 708 – 719, Colmar, France, July 2001.

[45] A. Chen, D. Lee, and P. Sinha. Optimizing Multicast Performance in Large-Scale WLANs. In *IEEE International Conference on Distributed Computing Systems*, page 17, Toronto, Canada, June 2007.

[46] R.S. Cheng and S. Verdu. Gaussian multiaccess channels with ISI: capacity region and multiuser water-filling. *IEEE Transactions on Information Theory*, 39(3):773 –785, May 1993.

[47] M.Y. Chung, M.-H. Jung, T.-J. Lee, and Y. Lee. Performance analysis of HomePlug 1.0 MAC with CSMA/CA. *IEEE Journal on Selected Areas in Communications*, 24(7):1411 – 1420, July 2006.

[48] J.M. Cioffi. A Multicarrier Primer. http://www.stanford.edu/group/cioffi/, Sep. 2006.

[49] J.A. Cortes, F.J. Cañete, L. Diez, and J.T. Entrambasaguas. Characterization of the cyclic short-time variation of indoor power-line channels response. In *International Symposium on Power Line Communications*, pages 326 – 330, Vancouver, Canada, Apr. 2005.

[50] T. Cover. Broadcast channels. *IEEE Transactions on Information Theory*, 18(1):2 – 14, Jan. 1972.

[51] Omega Deliverable D2.1. State of the art, application scenario and specific requirements for PLC. http://www.ict-omega.eu/fileadmin/documents/deliverables/Omega_D3.1.pdf, Mar. 2008.

[52] Omega Deliverable D3.2. PLC Channel Characterization and Modelling. http://www.ict-omega.eu/fileadmin/documents/deliverables/Omega_D3.2_v1.1.pdf, Dec. 2008.

[53] Omega Deliverable D3.4. Performance report of optimized PHY algorithms. http://www.ict-omega.eu/fileadmin/documents/deliverables/Omega_D3.4_v1.1.pdf, June 2010.

[54] S. D'Alessandro, A.M. Tonello, and L. Lampe. Adaptive pulse-shaped OFDM with application to in-home Power Line Communications. *Journal on Telecommunication Systems*, Jan. 2010.

[55] Y. Dandach and P. Siohan. Packet transmission for overlapped offset QAM. In *International Conference on Wireless Communications and Signal Processing*, pages 1 –6, Suzhou, China, Oct. 2010.

[56] Y. Dandach and P. Siohan. FBMC/OQAM Modulators with Half Complexity. In *IEEE Global Telecommunications Conference*, pages 1 –5, Houston, USA, Dec. 2011.

[57] M.I. Doroslovački. Product of second moments in time and frequency for discrete-time signals and the uncertainty limit. *Signal Processing*, 67(1), May 1998.

[58] K. Dostert. *Power Line Communications*. Prentice Hall, 2001.

[59] H. Ferreira, L. Lampe, J. Newbury, and T. Swart. *Power Line Communications*. 1st ed. New York: Wiley, 2010.

[60] K. Findlater, T. Bailey, A. Bofill, N. Calder, S. Danesh, R. Henderson, W. Holland, J. Hurwitz, S. Maughan, A. Sutherland, and E. Watt. A 90nm CMOS Dual-Channel Powerline Communication AFE for Homeplug AV with a Gb Extension. In *IEEE International Solid-State Circuits Conference*, pages 464 –628, San Francisco, USA, Feb. 2008.

[61] S. Galli. A simplified model for the indoor power line channel. In *International Symposium on Power Line Communications*, pages 13 –19, Dresden, Germany, Apr. 2009.

[62] S. Galli and T.C. Banwell. Modeling the Indoor Power Line Channel: New Results and Modem Design Considerations. In *Consumer Communications and Networking Conference*, Las Vegas, USA, Jan. 2004.

[63] S. Galli and T.C. Banwell. A Deterministic Frequency-Domain Model for the Indoor Power Line Transfer Function. *IEEE Journal on Selected Areas in Communications*, 24(7):1304 – 1316, July 2006.

[64] S. Galli, H. Koga, and N. Kodama. Advanced signal processing for PLCs: Wavelet-OFDM. In *IEEE International Symposium on Power Line Communications*, pages 187 –192, Jeju Island, Korea, Apr. 2008.

[65] S. Galli, A. Kurobe, and M. Ohura. The inter-PHY protocol (IPP): A simple coexistence protocol for shared media. In *IEEE International Symposium on Power Line Communications*, pages 194 –200, Dresden, Germany, Apr. 2009.

[66] S. Galli, A. Scaglione, and Zhifang Wang. For the Grid and Through the Grid: The Role of Power Line Communications in the Smart Grid. *Proceedings of the IEEE*, 99(6):998 –1027, June 2011.

[67] M. Gotz, M. Rapp, and K. Dostert. Power line channel characteristics and their effect on communication system design. *IEEE Communications Magazine*, 42(4):78 – 86, Apr. 2004.

[68] H. Hrasnica, A. Haidine, and R. Lehnert. *Broadband Powerline Communications Networks*. John Wiley & Sons, 2004.

[69] T. Hayasaki, D. Umehara, S. Denno, and M. Morikura. A bit-Loaded OFDMA for in-home power line communications. In *IEEE International Symposium on Power Line Communications*, pages 171 –176, Dresden, Germany, Apr. 2009.

[70] Y. Hirayama, H. Okada, T. Yamazato, and M. Katayama. Noise Analysis on Wide Band PLC with High Sampling Rate and Long Observation Time. In *International Symposium on Power Line Communications*, pages 142–147, Kyoto, Japan, Mar. 2003.

[71] B. Hirosaki. An Orthogonally Multiplexed QAM System Using the Discrete Fourier Transform. *IEEE Transactions on Communications*, 29(7):982 – 989, July 1981.

[72] Hooijen, O. G. On the Relation between Network-Topology and Power Line Signal Attenuation. In *International Symposium on Power Line Communications*, pages 45 –56, Tokyo, Japan, Mar. 1998.

[73] Myoung-Hee Jung, Min Young Chung, and Tae-Jin Lee. MAC throughput analysis of HomePlug 1.0. *IEEE Communications Letters*, 9(2):184 – 186, Feb. 2005.

[74] S. Katar, M. Krishnam, B. Mashburn, K. Afkhamie, R. Newman, and H. Latchman. Beacon Schedule Persistence to Mitigate Beacon Loss in HomePlug AV Networks. In *IEEE International Symposium on Power Line Communications*, pages 184 –188, Orlando, Florida, Apr. 2006.

[75] S. Katar, B. Mashbum, K. Afkhamie, H. Latchman, and R. Newrnan. Channel Adaptation based on Cyclo-Stationary Noise Characteristics in PLC Systems. In *IEEE International Symposium on Power Line Communications*, pages 16 –21, Orlando, Florida, Apr. 2006.

[76] S. Katar, B. Mashburn, R. Newman, and H. Latchman. GEN01-6: Allocation Requirements for Supporting Latency Bound Traffic in HomePlug AV Networks. In *IEEE Global Telecommunications Conference*, pages 1 –6, San Francisco, USA, Dec. 2006.

[77] M. Kuhn, S. Berger, I. Hammerstrom, and A. Wittneben. Power line enhanced cooperative wireless communications. *IEEE Journal on Selected Areas in Communications*, 24(7):1401 – 1410, July 2006.

[78] J. Kuri and S.K. Kasera. Reliable Multicast in Multi-access Wireless LANs. *Wireless Networks Journal*, 7(4):359 – 369, July 2001.

[79] B. Le Floch, M. Alard, and C. Berrou. Coded orthogonal frequency division multiplex [TV broadcasting]. *Proceedings of the IEEE*, 83(6):982 –996, June 1995.

[80] M.K. Lee, H.A. Latchman, R.E. Newman, S. Katar, and L. Yonge. Field performance comparison of IEEE 802.11b and HomePlug 1.0. In *IEEE Conference on Local Computer Networks*, Tampa, USA, Nov. 2002.

[81] M.K. Lee, R.E. Newman, H.A. Latchman, S. Katar, and L. Yonge. HomePlug 1.0 powerline communication LANs-protocol description and performance results. *International Journal of Communication Systems*, pages 447 –473, Feb. 2003.

[82] Hao Lin. *Analysis and design of multi-carrier systems for power line communications*. PhD thesis, Télécom ParisTech, Nov. 2009.

[83] Hao Lin and P. Siohan. OFDM/OQAM with Hermitian Symmetry: Design and Performance for Baseband Communication. In *International Conference on Communications*, pages 652 –656, Beijing, China, May 2008.

[84] Hao Lin and P. Siohan. Capacity Analysis for Indoor PLC Using Different Multi-Carrier Modulation Schemes. *IEEE Transactions on Power Delivery*, 25(1):113 –124, Jan. 2010.

[85] J. Liu. Current situations of PLC in China (keynote speech). In *IEEE International Symposium on Power Line Communications*, Beijing, China, Mar. 2012.

[86] W. Liu, H. Widmer, and P. Raffin. Broadband PLC access systems and field deployment in European power line networks. *IEEE Communications Magazine*, 41(5):114 – 118, May 2003.

[87] M. Meftah, L. Toutain, D. Ros, and A. Kortebi. ns-2 Model of HomePlug AV PLC Technology. In *SIMUTools*, Barcelona, Spain,, Mar. 2011.

[88] S. Mirabbasi and K. Martin. Overlapped Complex-Modulated Transmultiplexer Filters With Simplified Design and Superior Stopbands. *IEEE Trans. on circuits and systems II: analog and digital signal processing*, 50(8):456–469, Aug. 2003.

[89] R. Murty, J. Padhye, R. Chandra, A. Roy Chowdhury, and M. Welshn. *Characterizing the End-to-End Performance of Indoor Powerline Networks.* Harvard University Technical Report, 2008.

[90] G. Ndo. *Etude et Optimisation de Techniques de Réduction de Bruit Impulsif pour Transmissions Haut Débit sur Lignes à Courants Porteurs en Contexte Résidentiel.* PhD thesis, École Nationale Supérieure des Télécommunications de Bretagne, 2010.

[91] V. Oksman and S. Galli. G.hn: The New ITU-T Home Networking Standard. *IEEE Communications Magazine*, 47(10):138 –145, Oct. 2009.

[92] M. Ouzzif and J. Le Masson. Statistical analysis of the cyclic prefix impact on indoor PLC capacity.

[93] R. Pang, M. Allman, M. Bennett, J. Lee, V. Paxson, and B. Tierney. A First Look at Modern Enterprise Traffic. In *Internet Measurement Conference*, Berkeley, California, Oct. 2005.

[94] H. Philipps. Modelling of powerline communication channels. In *Proc. IEEE International Symposium on Power Line Communications and its Applications*, Lancaster, UK, Mar. 1999.

[95] H. Philipps. Development of a Statistical Model for Power Line Communications Channels. In *International Symposium on Power Line Communications*, Limerick, Ireland, Apr. 2000.

[96] D. Pinchon, P. Siohan, and C. Siclet. Design Techniques for Orthogonal Modulated Filter Banks Based on a Compact Representation. *IEEE Transactions on signal processing*, 52(6):1682 – 1692, June 2004.

[97] B.R. Saltzberg. Performance of an efficient parallel data transmission system. *IEEE Trans. on Comm. Tech.*, 15(16):805–813, Jan. 1967.

[98] M. Schwartz. Carrier-Wave Telephony over Power Lines: Early History [History of Communications]. *IEEE Communications Magazine*, 47(1):14 –18, Jan. 2009.

[99] J. L. Seoane, S. K. Wilson, and S. Gelfand. Analysis of Intertone and Interblock Interference in OFDM when the Length of the Cyclic Prefix is Shorter than the Length of the Impulse Response of the Channel. In *IEEE Global Telecommunications Conference*, Phoenix, Arizona USA, Nov. 1997.

[100] P. Siohan, C. Siclet, and N. Lacaille. Analysis and Design of OFDM/OQAM Systems Based on Filterbank Theory. *IEEE Transactions on Signal Processing* , 50(5):1170–1183, May 2002.

[101] F. Sjoberg, R. Nilsson, M. Isaksson, P. Odling, and P.O. Borjesson. Asynchronous Zipper [subscriber line duplex method]. In *IEEE International Conference on Communications*, volume 1, pages 231 –235 vol.1, Vancouver, Canada, 1999.

[102] A. Skrzypczak, P. Siohan, and J.-P. Javaudin. Application of the OFDM/OQAM Modulation to Power Line Communications. In *IEEE International Symposium on Power Line Communications*, pages 71 –76, Mar. 2007.

[103] M.-T. Sun, L. Huang, A. Arora, and T.-H. Lai. Reliable MAC Layer Multicast in IEEE 802.11 Wireless Networks. *Proc. ICCP 2002*, 2002.

[104] P. Tanguy, F. Nouvel, and P. Maziearo. Power Line Communication standards for in-vehicule networks. In *International Conference on Intelligent Transport Systems Telecommunications*, pages 533 –537, Lille, France, Oct. 2009.

[105] J. T. Tengdin. Distribution Line Carrier Communications - An Historical Perspective. *IEEE Transactions on Power Delivery*, 2(2):321 –329, Apr. 1987.

[106] M. Tlich, A. Zeddam, F.P. Gauthier, and P. Pagani. Wideband Indoor Transmission Channel Simulator for Power Line: WITS Software. *IEEE Transactions on Power Delivery*, 25(2):702 –713, Apr. 2010.

[107] M. Tlich, A. Zeddam, F. Moulin, and F. Gauthier. Indoor Power-Line Communications Channel Characterization Up to 100 MHz-Part I: One-Parameter Deterministic Model. *IEEE Transactions on Power Delivery*, 23(3):1392 –1401, july 2008.

[108] M. Tlich, A. Zeddam, F. Moulin, and F. Gauthier. Indoor Power-line Communications Channel Characterization Up to 100 MHz-Part II: Time-Frequency Analysis. *IEEE Trans. on Power Delivery*, 23:1402–1409, Jul. 2008.

[109] M. Tlich, A. Zeddam, F. Moulin, F. Gauthier, and G. Avril. A broadband Powerline Channel Generator. In *Proc. IEEE International Symposium on Power Line Communications and its Applications*, pages 59–64, Pisa, Italy, Mar. 2007.

[110] A. M. Tonello. Wideband impulse modulation and receiver algorithms for multiuser power line communications.

[111] C.Y. Wong, R.S. Cheng, K.B. Lataief, and R.D. Murch. Multiuser OFDM with adaptive subcarrier, bit, and power allocation . *IEEE Journal on Selected Areas in Communications*, 17(10):1747 –1758, Oct. 1999.

[112] Wei Yu and J.M. Cioffi. FDMA capacity of Gaussian multiple-access channels with ISI. *IEEE Transactions on Communications*, 50(1):102 –111, Jan. 2002.

[113] Seong-Won Yuk and Dong-Ho Cho. Parity-based reliable multicast method for wireless LAN environments. In *Vehicular Technology Conference*, volume 2, pages 1217 –1221 vol.2, Houston, Texas, 1999.

[114] B. Zarikoff and D. Malone. Construction of a PLC test bed for network and transport layer experiments. In *IEEE International Symposium on Power Line Communications*, pages 135 –140, Udine, Italy, Apr. 2011.

[115] M. Zimmermann and K. Dostert. A Multi-Path Signal Propagation Model for the Power Line Channel in the High Frequency Range. In *Proc. IEEE International Symposium on Power Line Communications and its Applications*, Lancaster, UK, Mar. 1999.

[116] M. Zimmermann and K. Dostert. An analysis of the broadband noise scenario in powerline networks. In *Proc. IEEE International Symposium on Power Line Communications and its Applications*, Limerick, Ireland, Apr. 1999.

[117] M. Zimmermann and K. Dostert. A Multipath Model for the Powerline Channel. *IEEE Transactions on Communications*, 50(4):553–559, Apr. 2002.